Development and Investigation of photoswitchable DTE(OMe)-Fluorophore-Conjugates

vorgelegt von

Master of Science

Nandor Ziebart

geb. in Rüdersdorf

von der Fakultät II - Mathematik und Naturwissenschaften
der Technischen Universität Berlin
zur Erlangung des akademischen Grades

Doktor der Naturwissenschaften
- Dr. rer. nat. -

genehmigte Dissertation

Promotionsausschuss:

Vorsitzender: Prof. Dr. Michael Gradzielski

Gutachterin: Prof. Dr. Karola Rück-Braun

Gutachter: Prof. Dr. Bernd Schmidt

Tag der wissenschaftlichen Aussprache: 15.01.2019

Berlin 2019

Die vorliegende Arbeit wurde unter Leitung von Frau Prof. Dr. Karola Rück-Braun in der Zeit von November 2014 bis November 2018 im Institut für Chemie der Fakultät II der Technischen Universität Berlin angefertigt.

Abstract

Photoswitchable modulation of fluorescence became a field of high interest for different applications, as optical devices. The detailed nature of energy- and electron-transfer in conjugates on semiconductor surfaces could lead to a better understanding and future applications in sensors or optoelectronics. Former work group projects showed efficient on-off energy-transfer in photoswitchable DTE-BODIPYs with fluorescent open forms and fluorescence quenched closed forms. Furthermore, a DTE-BODIPY conjugate attached to TiO_2 showed photoinduced electron-transfer in both, open and closed form. Both transfer processes should be improved in new DTE-fluorophore conjugates.

In this thesis, the development of a synthetic access to unsymmetrically substituted DTE(OMe)-fluorophore conjugates, carrying a carboxylic anchor group for future surface attachment is shown. Different photoswitch-fluorophore arrangements of donor-acceptor conjugates were designed, synthesized and investigated. The sophisticated handling of DTE(OMe)s under UV-irradiation exclusion leads to a late-step synthetical formation of the photoswitchable unit. The spectroscopical properties of symmetrical and nonsymmetrically substituted DTE(OMe)s were studied extensively and methods developed and discussed in detail. The literature known spectroscopical DTE(OMe) properties of quantitatively switching between both photoisomers, as well as fatique resistance, were confirmed.

Furthermore, different fluorophores (BODIPYs and BTDs) were designed, synthesized and investigated by their absorption and emission properties. The final conjugates showed unexpected *in-solution* results. The DTE(OMe)-BODIPY conjugate showed the expected energy-transfer process and confirmed the design rules, while BTD-DTE(OMe) hints towards an induced charge transfer (ICT) character in acetonitrile.

Therefore, both DTE(OMe)-fluoropore conjugates were studied for solvatochromic behaviour and investigated for their ground- and excited-state nature. Both BTD- and BODIPY-attached DTE(OMe) photoswitch- conjugates showed small solvent dependency in the absorption and increased dependency in the emission properties, which are stronger in the BTD-conjugate. The BTD-coupled DTE(OMe) showed a new possibility of modulating fluorescence by solvatochromism, which is more pronounced in the open, than in the closed form.

Kurzzusammenfassung

Fotoschaltbare Verbindungen, welche Fluoreszenzmodulation zeigen sind in den letzten Jahrzehnten ein wichtiges wissenschaftliches Thema geworden, z.B. im Bereich der optischen Geräte. Detaillierte Untersuchungen des Energie- und Elektronentransfers in Konjugaten gebunden auf Halbleiteroberflächen können zum tieferen Verständnis im Bereich Sensorik und Optoelektronik führen. Vorangegangene Arbeiten des Arbeitskreises zeigten einen effizienten Energietransferprozess in DTE-BODIPY-Konjugaten mit fluoreszierender offenen und nicht fluoreszierender geschlossenen DTE-Form. Zusätzlich zeigten beide Fotoisomere eines DTE-BODIPY-Konjugats auf TiO_2 fotoinduzierten Elektronentransfer. Beide Transferprozesse sollen in neuen DTE-Fluorophor-Konjugaten gesteigert werden.

In dieser Arbeit ist die Darstellung und Untersuchung von unsymmetrischen DTE-Fluorophor-Konjugaten beschrieben, welche eine Carbonsäurefunktionalität für zukünftige Anbindungen auf Halbleiteroberflächen tragen. Verschiedene Fotoschalter-Fluorophor-Verknüpfungen von Donor-Akzeptor-Konjugaten wurden designed, dargestellt und untersucht. Die anspruchsvolle Handhabung von DTE(OMe)s unter Ausschluss von UV-Strahlung, führte zu einer Syntheseroute, mit Bildung des Fotoschalters in einem späten Reaktionsschritt. Die spektroskopischen Eigenschaften von symmetrischen und asymmetrischen DTE(OMe)s wurden teilweise mit neuen Methoden im Arbeitskreis detailliert untersucht. Die literaturbekannten spektroskopischen Eigenschaften von DTE(OMe)s, quantitatives Schalten zwischen beiden Fotoisomeren, konnten bestätigt werden.

Außerderm wurden verschieden Fluorophore (BODIPYs und BTDs) designed, dargestellt und ihre Absorptions- und Emissionseigenschaften untersucht. Die finalen Konjugate ergaben unerwartete *in-solution* Resultate. Die DTE(OMe)-BODIPY-Verbindung zeigte den erwarteten Energietransferprozess zwischen dem Fluorophor und der geschlossenen Form von DTE(OMe) und bestätigt damit die Designregeln. Für BTD-DTE(OMe) in MeCN hingegen wurden Hinweise auf einen fotoinduzierten Elektronentransfer (ICT) gefunden.

Aus diesem Grund wurden das Solvatochromieverhalten beider DTE(OMe)-Fluorophor-Konjugate untersucht, um den Grund- und angeregten Zustand zu untersuchen. Das BTD-, sowie auch das BODIPY-verknüpfte DTE(OMe)-Konjugat zeigten geringe Lösemittelabhängigkeiten in den Absorptions-, und stärkere Abhängigkeiten in den Emissionseigenschaften, wobei diese stärker in BTD-DTE(OMe) ausgeprägt sind. BTD-DTE(OMe) weist eine neue Möglichkeit der Fluoreszenzmodulation durch Solvatochromie auf. Hierbei zeigt die offene Form eine deutlich stärkere Abhängigkeit, als die geschlossene Form.

Content

Table of Figures

Table of Tables

Abbrevations

abs. – absolute

Abs - absorption

aq. – aqueous

APCI – atmospheric pressure ionisation

BODIPY – Borondipyrromethene

br. – broad

BTD – benzothiadiazole

CF – closed form

DAE – diarylethene

δ – chemical shift

DCE – dichloroethane

DCM - dichloromethane

DEA – diethyl amine

DIA – diisopropylethylamine

DIPEA – diisopropyl amine

DMSO – dimethyl sulfoxide

DTE – dithienylethylene

DTE(Me) – 2,2'-dimethyldithienylethene

DTE(OMe) – 2,2'-dimethoxydithienylethene

ε – molar extinction coefficient

EA – elemental analysis

Emi – emission

EtOAc – ethyl acetate

FRET – Förster resonance energy transfer

HMBC – heteronuclear multiple bond correlation

HPLC – high pressure liquid chromatography

HR-MS – high resoluted mass spectrometry

IR – infrared

ISC – intersystem crossing

iso – isosbestic

λ – wavelength

M – molar

MeCN – acetonitrile

MeOH – methanol

MP – melting point

NIR – near infra-red

NMR – nuclear magnetic resonance

pss – photostationary state

OF – open form

QY – quantum yield

Rf – retention factor

rt – room temperature

TLC – thin layer chromatography

THF – tetrahydrofurane

TMEDA – tetramethylethylenediamine

TMS – trimethylsilyl

UV – ultraviolet

Vis – visible

1 Introduction

1.1 Photochromism

"Photochromism is the reversible transformation of a chemical species between two forms by the absorption of electromagnetic radiation, where the two forms have different absorption spectra" (Figure 1).[1] The term of photochromism (greek *phos* – light, *chroma* – colour) was described firstly by Hirshberg in 1950 for compounds with light induced colour change.[2]

The thermodynamic more stable form defined as A is transformed into B with suitable irradiation. B can be converted back to A thermodynamically (T-type photochromism) or photochemically (P-type photochromism). The photochromic process can be based on E/Z-isomerization, tautomerism, electron-transfer or electrocyclic reaction.

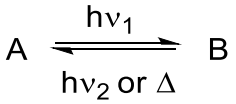

Figure 1: generalized photochromic reaction between two species A and B

In Figure 2, different classes of common photochromic molecules (also photoswitches) are shown. The sometimes strongly different properties (spatial orientation of residues, dipole-moment, conductivity, refractive indices, redox potentials etc.) of the two species are used in several applications.

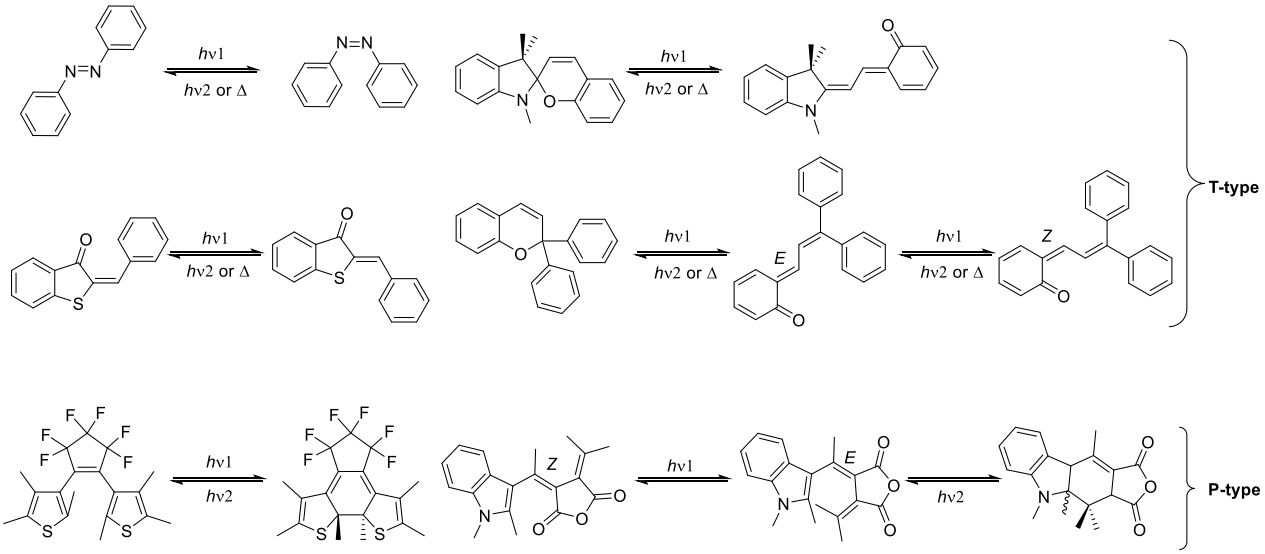

Figure 2: different classes of photochromic molecules.

1.1.1 Diarylethenes

IRIE presented 1982 a class of photoswitches discovered in a polycondensation reaction of stilbene, consistent of two aryl moieties coupled with an ethene bridge.[3] [4] The highest reversibility of these diarylethenes (DAEs) and most stable forms was reached by using thiophenes as aryl rings and by blocking the ethene bridge for E/Z-isomerization by introducing ring structures.

DAE open form (OF) and closed form (CF) are thermally stable and can be usually closed by UV-irradiation (cyclization) and opened (cycloreversion) by visible light. The absorption spectra of the DTE(Me) **1** OF and CF are illustrated in Figure 3. The absorption band of the CF in the visible range allows to convert the diarylethene quantitatively into the OF. In comparison to other photoswitch classes, DAEs are fatique resistant (some DAEs with 10.000 and more cycles are literature known), the conversion of the forms into each other is fast (picosecond range)[5] [6] and several DAEs can be switched in the crystal.[6] [7]

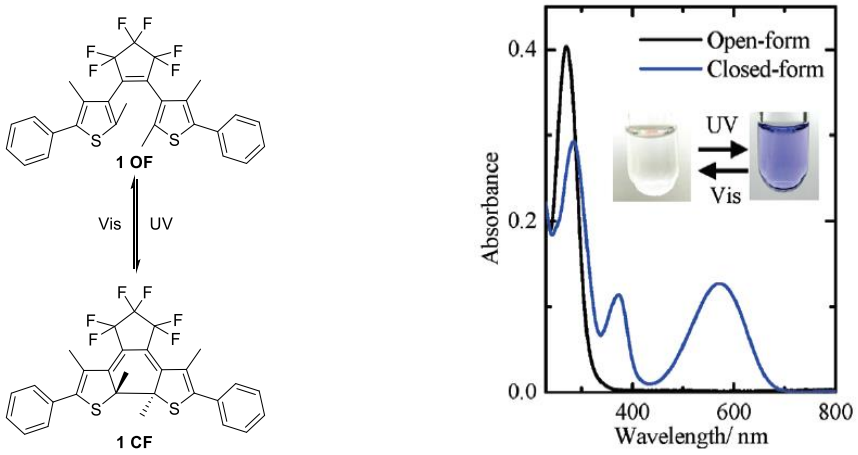

*Figure 3: left: structures of DTE(Me) **1** OF and **1** CF; right: absorption spectra of DTE(Me) **1** OF (black) and **1** CF (blue) in hexane.*[8]

Diarylethenes are an important class of photoswitches with a less-conductive OF and a conductive CF. Therefore different applications (for example electrochemical windows, chemical sensors, organic light-emitting diodes (OLEDs) and organic field-effect transistors (OFETs)) are part of the research nowadays.[9]

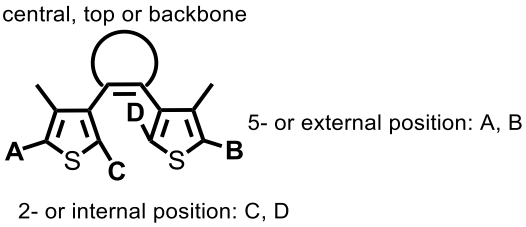

Figure 4: common assignments for the different positions in DTEs.

The different positions around the thiophene units get assigned as internal, external and backbone position in this thesis (Figure 4). In this thesis, to simplify the structures the internal binding angles of 120° towards the methyl- or methoxy-substituents are illustrated in a different manner.

1.1.2 Structure of DAEs

1.1.2.1 Aryl residues

Diarylethenes with furan or thiophene moieties have a lowered ground state energy and a high energy barrier between the isomers OF and CF, resulting in an isomeric stabilization (Figure 5).[10] Phenyl moieties are thermally unstable and convert back into the isomer with the lower ground state energy (OF) over time. Furthermore, the cyclization is facilitated by the highly reduced stabilization energy of the heteroarenes compared to the phenyl unit (Figure 6).

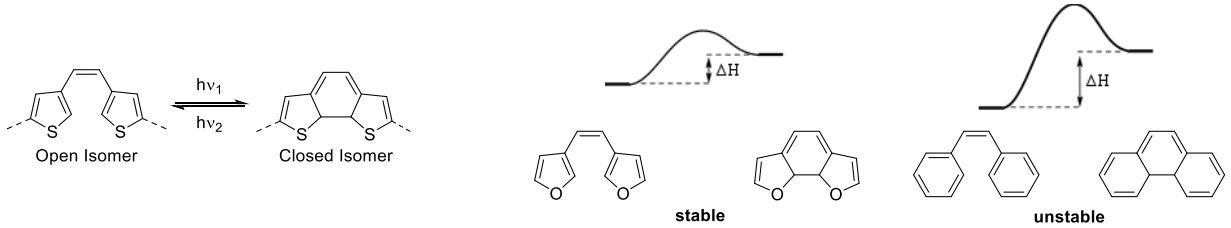

Figure 5: structures of the OF and CF for thiophene-, furan- and phenyl-DAEs; right: scheme of calculated energy barrier for furan- and phenyl-DAEs.[10]

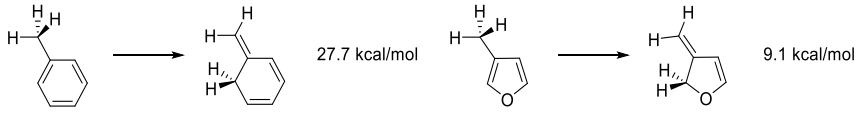

Figure 6: calculated energy barrier for the removement of aromaticity in toluene and methyl-furane structures.[10]

The quantum yields of the cyclization with thiophene units is increased in comparison to the furan DAEs. Nowadays usually thiophenes are used in DAEs, but the substitution pattern of the DAE-structures are still an ongoing research field.

Literature studies of DTEs with unsubstituted thiophene 4-positions showed an increased amount of photodecomposition.[18] To hinder the molecule for undergoing a cyclization reaction with substituents in the 4-position, and to increase the fatigue resistance, methyl groups are used.[19] These lead to a twist between the thiophene- and external attached phenyl-moieties induced by steric repulsion.[11]

1.1.2.2 Backbone of DTEs

The backbone structure of the cyclic bridge-moiety was varied over the last decades for several improvements of the photochromic properties. Different fluorophores for a read-out signal[12], polar maleic imides for biological applications[13] and controlling charge separation[14], ring-size for improvement of quantum yields[15], and others were tested. The absorption band maxima can be hypsochromically shifted by four-membered ring systems, while the value for the quantum yields of the cyclization is facilitated by a six-membered cycle. To have both advantages, five-membered ring systems are common structural motifs in DTEs. Maleic anhydrides show a high bathochromic shift and high polarity which suits applications for lower wavelengths. Nevertheless, the perfluorocyclopentene was discovered to have the highest fatigue resistance, best stability on air, and to improve the switching process through the electron-withdrawing properties on the bridge. Furthermore, the backbone can influence the reactivity (ring-opening or ring-closure) in oxidation- and reduction-processes called electrochromism.[16] While cyclopentene shows a ring-closure in the oxidation process, the perfluorocyclopentene bridge has the opposite behaviour.[17][18] Connected to electron-transfer conjugates, this property can lead to undesired behaviour of the photoswitch.

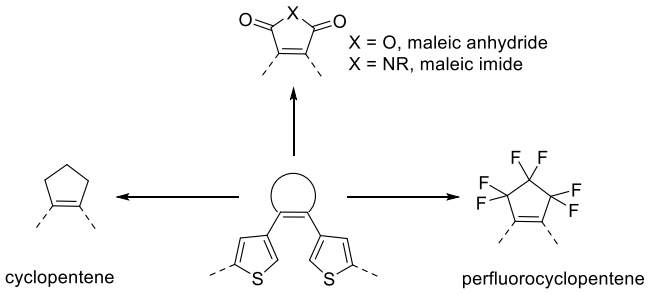

Figure 7: different backbone structures for changing the photochromic properties of DTEs.

In sum, the choice of the backbone of DTEs can help to control or improve the desired properties. In this thesis, the most common perfluorinated backbone is used in all photoswitches.

1.1.3 Cyclization of DTEs

The photochromic properties of DTEs are based on a conical intersection (also molecular funnel or photochemical funnel) in the potential energy surfaces between the excited state and the ground state

and got investigated by ROBB et al. 2003.[19] The conical intersection is the crossing of two potential energy surfaces, where the vibronic couplings are not excluded.

Taking the BORN-OPPENHEIMER approximation into account, the atoms of a molecule can be treated as atom cores exclusively, which are in movement on a potential energy surface. For the most of chemical reactions, this approximation can be used for describing the mechanism of forming new bonds. One of the exclusions from the BORN-OPPENHEIMER approximation is the conical intersection, where the electrons and the cores are interacting.[20] One of the first examples for the conical intersection was butatriene, which showed an unexpected band in the photo electron spectra, which could not be explained by the common JAHN-TELLAR effects.[21]

DTEs in the OF exist in two conformers (the parrallel and the anti-parallel conformation), which can be converted into each other at room temperature in the ms-range (Figure 8).[22] [23] For the photocyclization process, the anti-parallel conformation can undergo the pericyclic reaction with UV-irradiation exclusively, while the parallel conformation is photochemically inactive. The conformers usually have a ratio of 1:1 but can be influenced by steric and/or electronic interactions – sterically demanding residues can increase the ratio of the anti-parallel (photoactive) conformer. Therefore the quantum yields of typical DTEs have a maximum of 0.5.

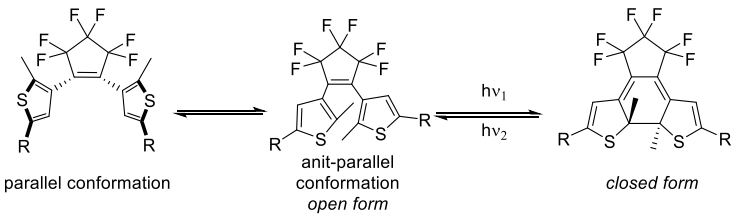

Figure 8: the two conformers of DTE-OF (parallel and anti-parallel) and switching process to the DTE-CF.

With UV-irradiation the OF can not be converted to the CF quantitatively, because the CF absorbs in the UV-range (<350 nm) as well. So a stationary equilibrium is reached, which is called photostationary state (pss). The dynamics to reach the pss are dependent of the intensity of the light, the structure of the molecules and the excitation wavelength extinction coefficient. The product stereochemistry of the electrocyclic reaction can be explained by the WOODWARD-HOFFMANN rules. Thus the thermal reaction of hexa-1,3,5-triene is allowed disrotatoric only, while the photochemically reaction leads to the conrotatoric product.[24] Therefore, the residues in internal position are directed in the opposite direction of the π-plane after the irradiation-induced cyclization. KUCH et al. showed recently the possibility for a disrotatorical *cis*-product by electron transfer in a radical mechanism with a STM (scanning tunnelling microscope) tip.[25][26]

1.1.4 Cycloreversion of DTEs

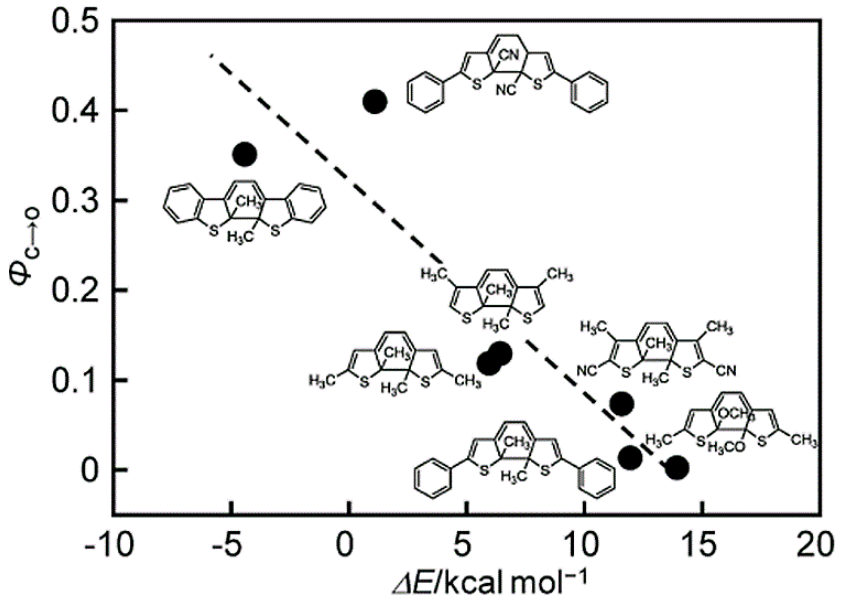

Figure 9: the effect of different functional groups at the internal position in DTEs on the cycloreversion quantum yields.[6]

The quantum yields for the cycloreversion of DTEs are highly dependent of the substitution pattern in internal positions (see Figure 9).[27] After transition of DTE CF ground state (S_0) in the first excited state (S_1), an energy barrier has to be overcome for reaching the conical intersection (CI, Figure 11).[28] This barrier is mainly influenced by the internal substituents directing out of the π-plane in CF. While dinitrile-groups (DTE(CN)) are increasing the QY_{CO} up 0.41, dimethoxy-substituents (DTE(OMe)) lower this value to 0.00013 (see Table 1).

Table 1: effect of the 2-substituents on the quantum yields of cyclization and cycloreversion of DTEs in hexane with right: structure of OF and CF of DTEs with different substituents in 2-position..[27]

R	λ_{max}	QY_{OC}	QY_{CO}
CN	545	0.42	0.41
CH_3	575	0.59	0.015
OMe	625	0.44	0.00013

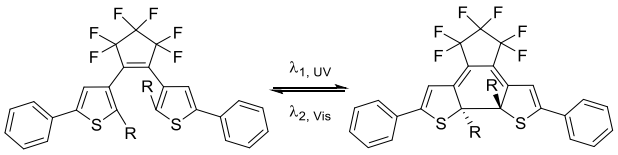

The stepwise dimethoxy-substitution of DTE(Me) **1** reveals the possibility of tuneable cycloreversion quantum yields (Figure 10). Monosubstitution (**2**) lowers QY_{CO} by almost factor 10, while QY_{CO} of

DTE(OMe) **3** is one magnitude lower. Furthermore, the DTE OF and CF absorption bands are red shifted by the stepwise increase of the π-system. While the **1**-**3** OFs show a bathochromic shift of 17 nm from DTE(Me) to DTE(OMe), the DTE CF π-π* absorption bands undergo a red shift of 52 nm from **1** to **3**.

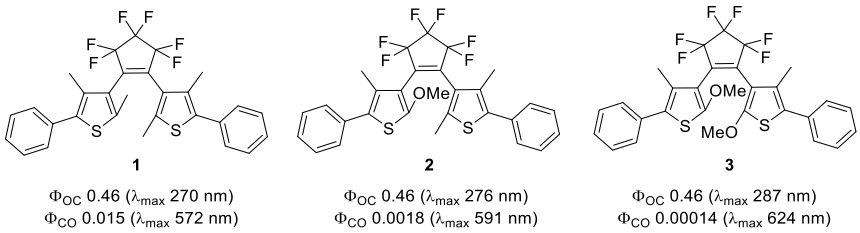

*Figure 10: change of the cycloreversion quantum yield by stepwise introduction of methoxy-groups at the reactive carbon centers from **1** to **3**.*[29]

The ratio of antiparallel to parallel conformation of DTE OFs can be usually determined by NMR spectroscopy, since two signal-sets can be seen at room temperature for OF.[23] This is not possible for DTE(OMe)s, having a sterically less demanding functionality in the internal position, which therefore show only one set of signals in the ^{1}H-NMR spectra at room temperature.[29]

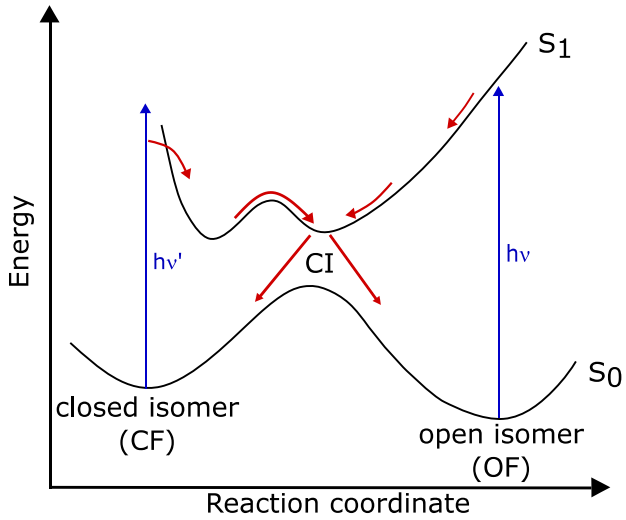

Figure 11: outline of the two reaction paths corresponding to cycloreversion (CF to OF) and cyclization (OF to CF) reactions of diarylethenes.[28]

DTE(OMe)s have a quantitatively pss for the cyclization and the cycloreversion but require very strong light sources. To facilitate and accelerate the ring opening for application of DTE(OMe)s, a pulsed laser can be used for an up to 20.000-times faster reaction.[30] This pulsed photons can lift the electron up to a high S_x

state, where the relaxation stepwise down to the ground state has a chance in each S_X state for the cycloreversion reaction.

In summary, DTE(OMe)s are a good alternative to the extensively used DTE(Me) switches for quantitatively switching with sterically demanding residues.[31] [32] [29] Furthermore, the methoxy-groups could be a good read-out signal in the IR-spectroscopy for following in the future the switching behaviour on surfaces. Nevertheless, the low number of publications focussing on DTE(OMe)s assumes to have a synthetically sophisticated approach towards unsymmetrically substituted conjugates.

1.2 FLUOROPHORES

1.2.1 BODIPYs

Boron-dipyrromethenes (abbr. BODIPY, Figure 12) are strong fluorophores which were discovered in the 1960s by TREIBS and KREUTZER (Figure 12).[33] They usually have a very sharp absorption and emission band and a very small Stokes-Shift due to their small and rigid structure. BODIPYs show a high photochemical and thermal stability, high extinction coefficients, high fluorescent quantum yields (usually >0.8), straightforward synthetic approaches and almost solvent- and pH-independent fluorescence spectra. They are despite their ionic structure relatively nonpolar. Applications of BODIPY-compounds can be found for example in biolabeling and for laser-dyes.[34]

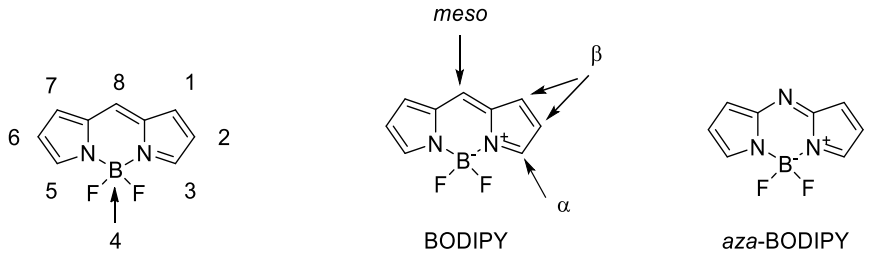

Figure 12: left: IUPAC numbering of the positions; right: indication of the different attachment positions on the BODIPY core.

Since the synthesis of unsubstituted BODIPY is sophisticated and the properties of **7** (Figure 13) were predicted in the literature but not proved until 2008[35], the synthetic approach for methyl-substituted BODIPYs (e.g. **4**) are well known. With increasing the flexibility in the molecule, the Stokes shifts can be influenced (see **5** and **6**). Due to the strong dipole moment of BODIPY, the different position substitutions around the BODIPY-core show various influence on the spectroscopic and energy- and electron-transfer processes. Whereas π-conjugated *α*-and *β*-substituted BODIPYs have a strong mesomeric effect coupling

(α>β)[36], the attachment in *meso*-position is usually preferred for the influence on energy-transfer processes. Common attachment of *meso*-substituted aryl-BODIPYs (Figure 13) with methyl-groups in the *β*-positions are twisted against the π-plane of the BODIPY-core and therefore partly separated from the fluorophore itself. This is obvious in the comparison of the methyl-aryl-BODIPY **9** with aryl-BODIPY **8**, with a blue-shift of 10 nm and the increasing of the fluorescence by factor 3.5. The attachment of π-systems in *β*-position, is furnishing fluorophores that have linear dipole moments and therefore a strong influence on the energy transfer emission properties of the dye.

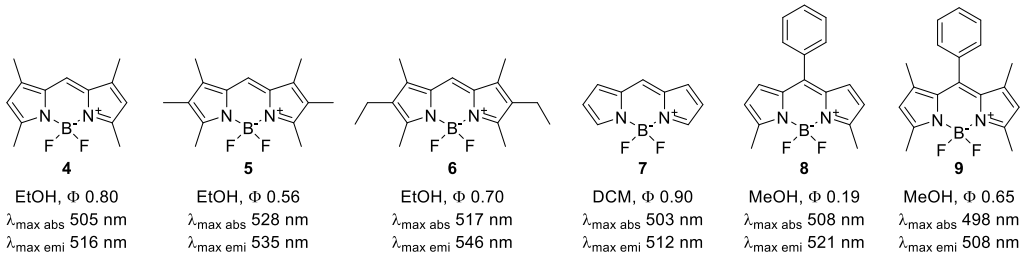

*Figure 13: structure formulas of compounds **4-9** for different substitution pattern around the BODIPY-core and the influence on the spectroscopic properties.*

By exchanging the central methene bridge of BODIPYs to a nitrene bridge, the core-structure gets highly red-shifted in *aza*-BODIPYs (**10** and **11**, Figure 14).[37][38] In combination with an extended π-system through phenyl rings and further π-system extending functional groups, the emission can be red-shifted up to the near infrared region (**12**).

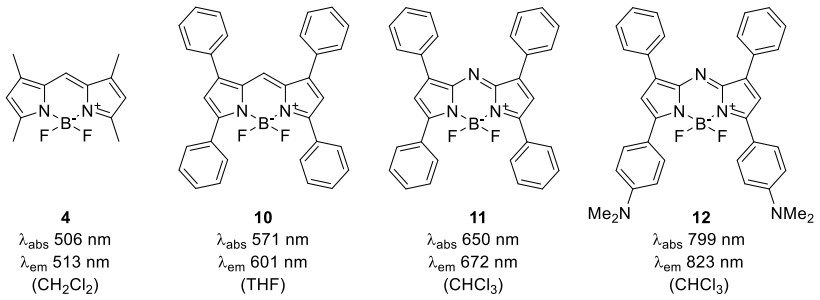

*Figure 14: structures of BODIPYs **4, 10-12** and their spectroscopic properties without and with aza-bridge.*

In our workgroup, the differences between *meso*- and *β*-attachments of photoswitches on BODIPYs were investigated in former projects. [39][40][41] While the *meso*-substituted DTE-BODIPY (Figure 15) conjugate **BODIPY543-DTE-COOH** has a better ratio in the pss in chloroform, which results in a higher fluorescence quenching, the *β*-substituted **BODIPY585BCP** showed a more pronounced signal at the end of the time-

resolved spectroscopy which indicated an electron-transfer process (detailed explanation in chapter 1.5.2). Therefore, in this thesis, only *β*-attached DTE(OMe)-BODIPY conjugates should be synthesized.

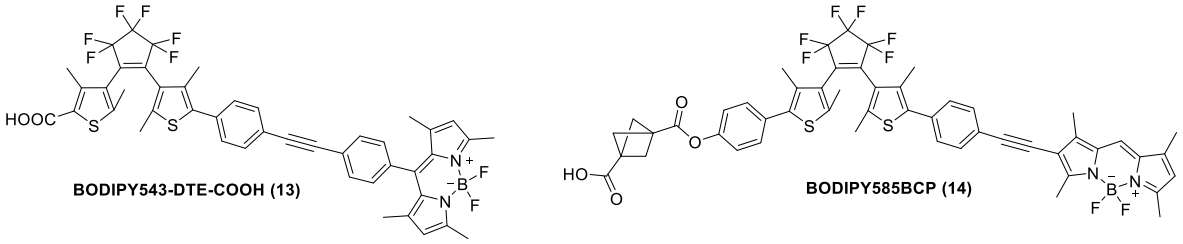

*Figure 15: last generation of DTE-BODIPY conjugates **BODIPY543-DTE-COOH** (**13**) and **BODIPY585BCP** (**14**).*[41]

1.2.2 BTDs

Benzothiadiazoles (BTDs) became one of the most important nuclei of lumincescent compounds in the last decades.[42] The BTD-derivatives have normally desirable characteristics: a) the arene is highly electron-deficient and can be used as electron-carrier in polymeric structures or as electron-acceptor unit in conducting materials; b) they are efficient fluorophores with stacking effects, which is important for the orientation on surfaces but a disadvantage in solution. BTDs show a relatively high reduction potential and electron affinity, therefore they were intensively investigated for the usage in LEDs. BTDs are often used in DSSC-design for increasing the absorption spectra and fine-tuning the redox-potentials of the dyes.[43]

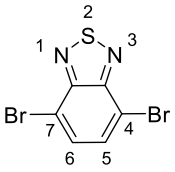

15

*Figure 16: structure formula for 4,7-dibromo 2,1,3-benzothiadiazole **15**.*

The typical starting point for BTD-containing molecules is dibromo-BTD **15** (Figure 16), with two bromo-substituents in 4- and 7-position. The synthesis is discussed in a later chapter (2.2.5.2). An *ortho*-quinoide structure for **15** in solution was assumed after the investigation of **15** in crystal structure. Since quinoides can be treated as closed rings with conjugated double bonds, these structures attached to fluorophores are resulting in dramatic red-shifts of the fluorophores absorption spectra.[42] Furthermore,

the quinoides show a smaller band gap between HOMO and LUMO, which was proven in theoretical studies for BTDs.

Another important property of BTDs is the steric demand of the core structure and the therefore twisted conjugation to attached aryl-moieties (Figure 17). Conducted in donor-acceptor conjugates, this property is assumed to reduce the electron recombination and facilitates the electron transition between donor and BTD, which is desired in for example DSSCs.[44] [43]

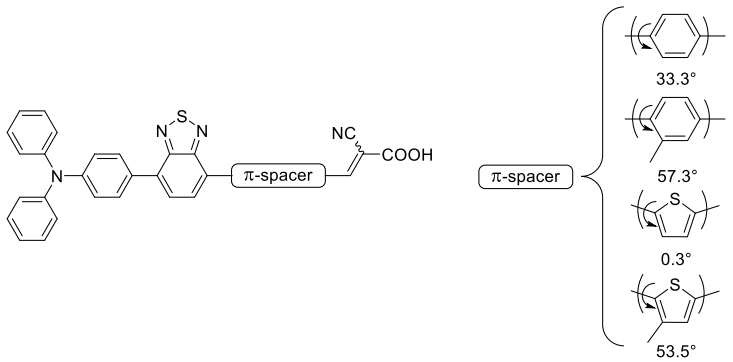

Figure 17: dihedral angle by twisting of the BTD-aryl bond.[44]

In sum, BTDs could be a good alternative to the already used BODIPY-dye structures for their property to be a strong electron withdrawing group and an efficient fluorophore. The effect of the attachment to DTE(OMe)s and switchability of the properties of BTD should be investigated in this work.

1.3 UV/VIS-SPECTROSCOPY

1.3.1 General

If a beam of photons (200-750 nm) hits a homogeneous, isotropic medium the irradiation can be absorbed. Next to reflection and scattering effects the solvent and the molecules in the medium have an influence on the penetrating photons. The absorption of a molecule is based on the excitation of electrons and lead to a transition of electrons in the molecules, normally from the ground state to higher energy states (e.g. HOMO into the LUMO). To absorb a photon, the energetic distance between two states needs to have the same value as the energy of the incoming photon. The conversion of wavelengths λ into corresponding energies *E* of the photon follows Eq. 1, with the PLANCK´s constant *h* and the speed of light *c*.

Eq. 1

$$E = h\nu = \frac{hc}{\lambda}$$

The absorption [dimensionless] of the medium compared with the light intensity follows a linear dependency of the concentration [$mol \cdot L^{-1}$], the way through the medium [cm] and the extinction coefficient [$L/(mol \cdot cm)$] called the LAMBERT-BEER´s law (Eq. 2).

Eq. 2

$$E_\lambda = log_{10}\frac{(I_0)}{(I_1)} = \varepsilon * c * d$$

The dependency was discovered by BOUGER and discussed by LAMBERT and BEER and is valid for monochromatic light and dissolved solutions.[45] The equation does not describe solutions with for example dimerization- or aggregation effects.

The determination of the absorbance of a solution for each wavelength, is called a UV/Vis-spectra. Due to the energy width in the spectra, the signals were named bands. Each band can be correlated with a defined energy transition in the molecules. The absorptions of the solvent are subtracted by a reference spectra. For the comparison of different bands a red-shifted band (shifted to higher wavelengths/lower energy) is called bathochromically shifted. A blue-shifted band (shifted to lower wavelengths/higher energy) is called hypsochromically shifted. A higher intensity is called hyperchrome, a lower intensity hypochrome. For a higher intensity, a lower life-time of the excited state can be predicted.

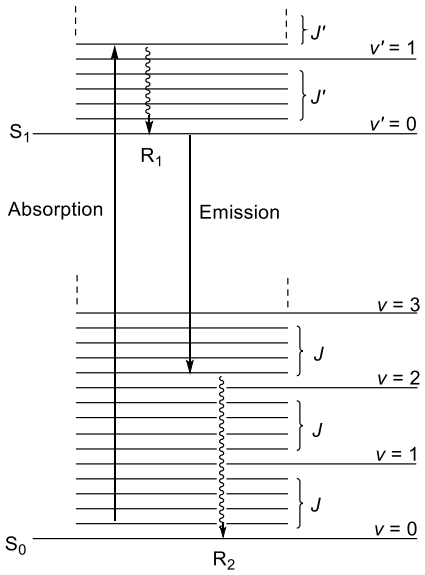

Figure 18: schematic energy-level of a molecule with an excitation-relaxation process.[46]

The molecules are almost quantitatively in the vibrational ground state at $v = 0$ (BOLTZMANN distribution) in different rotational states (J) at room temperature (Figure 18). After excitation from the singlet-state S_0 to a higher singlet-state S_X (*Absorption*), the electron relaxes fast (R_1) into the lowest vibrational excited state $v' = 0$. After the *Emission* step, the molecule relaxes in a second relaxation step (R_2) to the vibrational ground state of S_0. Therefore, energy is released and the emission energy (photon (luminescence, see chapter 1.4.1) or emission heat (vibronic energy)) is lower, than the excitation energy. The possibility to reach a higher vibrational state ($v \neq 0$) in the excited state is dependent of the position in the hypersurface towards the ground state and follows the FRANCK-CONDON principle (the movement of the atomic nucleus (10^{-13} s) is neglectable for electronic transitions (10^{-15} s)). The form of the absorption band for a non-overlapping transition can give a hint of the excitation level nature (Figure 19).

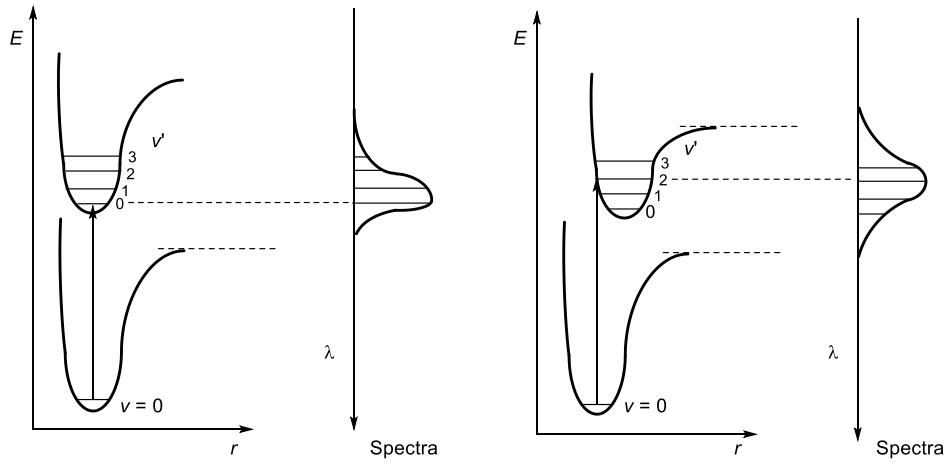

Figure 19: transition probability of an electron and the resulting absorption band form. [46]

The position of an absorption band in an UV/Vis spectra is dependent of the specific excitation energies in molecules and the nature of the transition (energy necessary: σ->σ* > π->π* > n->σ* > n-> π*). Different functional groups have an influence on the absorption of a molecule. Rule of thumb for π-π* transitions, a bigger π-system decreases the HOMO/LUMO-gap and leads to a bathochromic shift. Electron withdrawing groups lowering the energy of the LUMO and electron-rich groups pushing the HOMO to a higher energy level. In both cases, the absorption band gets a bathochromic shift. On the other hand, a break in the π-system by the introduction of non-conjugated moieties or by twisting the molecule (induced by charge separation or sterically), leads to hypsochromic shifts of the absorption band.

In summary, the UV/Vis-spectroscopy allows to investigate the ground state electronic structure of a molecule in dissolved solutions. Therefore the UV/Vis-spectra are often used for the investigation of photoswitches, due to the definition of photochromic molecules to have a different absorption spectra in

the different isomers. This kind of spectroscopy is sensitive (usually 10^{-6}-10^{-4} mol·L^{-1}), non-invasive, fast and easy to reproduce.

1.4 FLUORESCENCE SPECTROSCOPY

1.4.1 General

If an electron gets excited into a higher state S_0 to Sx, the electron has several possibilities to relax back to the ground state as shown in Figure 20. Generally, the emission of light from a substance is called luminescence - in the range of UV-irradiation or visible-light photoluminescence. The direct relaxation from an singlet state S_X to S_0 under emission of radiation is named fluorescence (lifetimes 10^{-9}-10^{-7} s). The intersystem crossing to a lower triplet T_X state and relaxation from T_x to S_0 is named phosphorescence (lifetimes 10^{-3}-10^{2} s). A relaxation back from T_x to S_0 without emission of radiation or by quenching effects is possible. Latter, the excited electron can transfer its energy to another excitable system (inter- or intramolecular, see more in chapter 1.4.2).

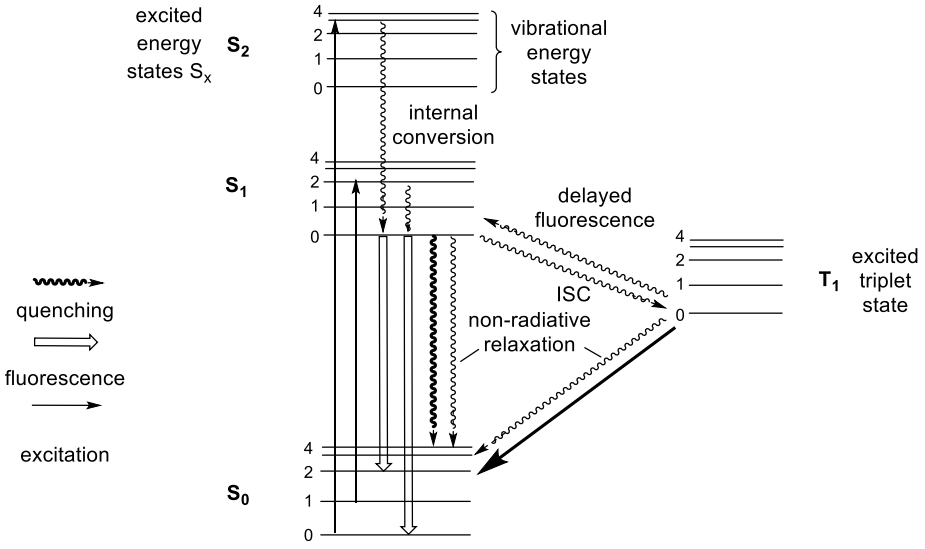

Figure 20: JABLONSKI energy diagram.

Since the time-scale of a fluorescent process is in the range of nanoseconds, the investigation methods are sophisticated in steady-state and transient spectroscopy compared to UV/Vis-investigations.

The detection of fluorescence is usually done by the following spectroscopic method: a light source with a diffraction grating produces an irradiation of a certain wavelength, which is focussed through a cuvette

with a sample. The sample shows luminescence, which is recorded by a detector in 90 ° angle to the irradiation beam to prevent scattered light. The emitted photons of the sample are passed through a grating, which allows to transmit a single wavelength to the detector. The detector is a photo-multiplier (PMT), which produces a quantifiable voltage at each wavelength corresponding to the amount of photons emitted by the sample. By scanning the full wavelength spectra, the characteristic emission of a sample can be recorded. In newer spectrometers, the full spectra is recorded with a CCD.

The emission spectra is usually the mirror image of the absorption spectra, following the probabilities of an electron transition relaxation (Figure 21). Due to the relaxation pathways and vibronic pathways, the emitted photons have a lower energy (higher wavelength), than the excitation irradiation. Therefore the emission spectra is red-shifted and the difference between excitation and maximum of the emission is named Stokes-shift.

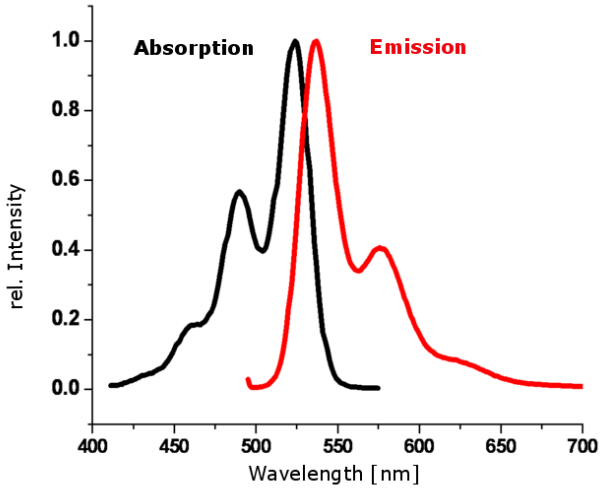

Figure 21: schematic illustration of the mirror image between absorption and emission. (picture from: http://photonicswiki.org/index.php?title=File:Oled1_14_abs-lum-graph.png, 24.01.2019)

1.4.2 Energy transfer

An excited electron of a chromophore is able to transfer its energy to another chromophore without irradiation in a dipole-dipole coupling.[34] This energy transfer is generally divided in the transfer through bonds and the transfer through space. The former is only possible in an intramolecular process and usually with π-coupling of energy donor and energy acceptor, which is called through-bond-energy-transfer

(TBET). The latter can be seen in inter- and in intramolecular processes and requires the overlap of the donor-emission spectra and the acceptor-absorbance spectra. This process is called FÖRSTER-resonance-energy-transfer (also referred to as fluorescence-resonance-energy-transfer, FRET) and the efficiency of the transfer (k_t) is highly dependent on the distance between donor and acceptor (r), the lifetime of the donor (τ_0) and on the FÖRSTER distance (R_0), which is a compound-specific length, when the efficiency of the FRET is 50 % (Eq. 3).

Eq. 3
$$k_t = \frac{1}{\tau_0} * (\frac{R_0}{r})^6$$

After excitation of a donor-electron, relaxation back to the ground state by energy-transfer to an acceptor-electron takes place (Figure 22). Thereupon the acceptor-electron is excited and can relax to the ground state by non-irradiative pathways or luminescence. This process usually takes place in the nanosecond scale. BODIPYs can be used in both, FRET and TBET procecesses.[47] The assignment of the energy transfer nature is sophisticated and will not be part of this thesis.

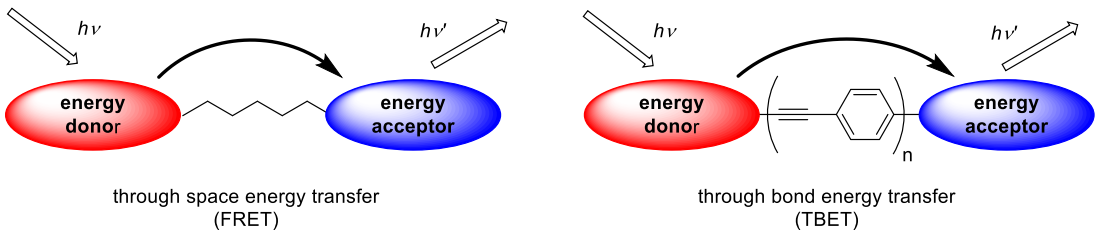

Figure 22: schematical difference between intramolecular FRET and TBET.[47]

On a molecular level, the distance between a donor and an acceptor can be measured indirectly by the quantitative determination of fluorescence and the correlation with the quenching of donor-emission by FRET. Therefore FRET-systems are used in microscopy and biological investigations as molecular ruler.[48]

1.4.3 Environmental effects on the fluorescence spectra

The emission properties of a molecule are highly dependent of the molecules surrounding.[49] Several solvent properties influence the emission outcome of an excited molecule like solvent polarity, viscosity and the rate of solvent relaxation. Furthermore probe conformational changes, rigidity of the local environment, internal charge transfer, proton transfer and excited state reactions, probe-probe interactions and the changes in radiative and non-radiative decay rates (k_{nr}) have an influence on the emission spectra of a sample (Figure 23). Often these effects overlap and the analysis and interpretation of the processes leading to the emission spectra are complex.

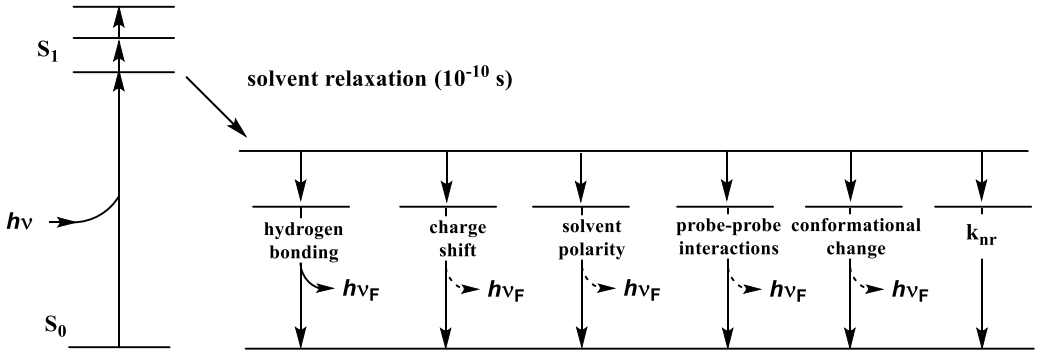

Figure 23: effects of environment on the energy of the excited state.[49]

Usually, the excited state of a molecule has a higher and spatial changed dipole, than the ground state. Therefore the surrounding solvent molecules react with their own dipole via a rearrangement in the local environment. After excitation of a molecule from the ground state to the FRANCK-CONDON state (derived by FRANCK-CONDON principle; nuclei do not move during the time scale of an electronic transition (10^{-15} s)), energy consuming solvent relaxation leads to a relaxed excited state (≈10^{-10} s), which is the origin of the relaxation back (≈10^{-8} s) to the ground state (Figure 24). After energy emission in form of a photon or vibronically, the dipoles of the solvent molecules have to change back to their initial arrangement, causing a further loss of energy. A highly polarized solvent leads to a lower energy of relaxation – a larger Stokes shift.

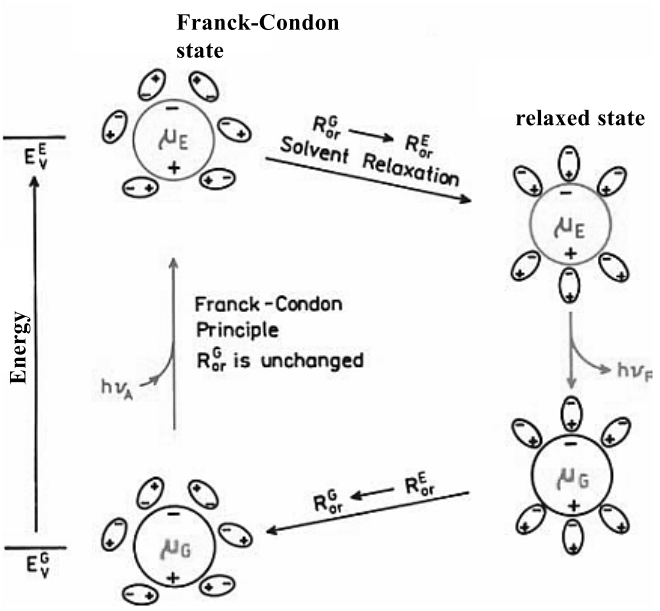

Figure 24: effects of the electronic and orientation reaction fields on the energy of a dipole in a dielectric medium, $\mu_E > \mu_G$. The smaller circles represent the solvent molecules and their dipole moments.[49]

Solvent polarity described by the dielectric constant (ε) is one of the main origins of Stokes shifts and is summarized by general solvent effects. These effects are described by the LIPPERT equation (Eq. 4), which is derived in the time scale of interactions of a fluorescent molecule with the environmental solvent. In the equation $\Delta\bar{\nu}$ is the frequency shift (in cm^{-1}) between absorption and emission, Δf is the orientation polarizability (dependent on ε and the refractive index *n*), *a* is the cavity radius, and μ_E and μ_G are the excited- and ground-state dipole moments, respectively.

Eq. 4
$$hc\Delta\bar{\nu} = hc(\bar{\nu}_A - \bar{\nu}_F) = \frac{2\Delta f}{a^3}(\mu_E - \mu_G)^2 + constant$$

with
$$\Delta f = \frac{\varepsilon - 1}{2\varepsilon + 1} - \frac{n^2 - 1}{2n^2 + 1}$$

Assumptions in these equations are: a) the fluorophore is spherical, b) the fluorophore has no other interactions, than general solvent effects, c) the fluorophore has no polarizability in the ground and excited state and d) the dipole moments of the ground- and the excited-state point in the same direction.

For a first interpretation of general solvent effects LIPPERT-MATAGA plots are often used. The Stokes shifts in cm^{-1} are plotted against the orientation polarizability.

1.5 TIME RESOLVED SPECTROSCOPY

1.5.1 General

For the investigation of fundamental processes of the ground and excited state of a molecule, time resolved spectroscopy can be used. The basic principle of transient absorption spectroscopy is a UV/Vis-spectrometer with a laser light source. The ultrashort laser pulse (150 fs, provided by a laser-amplifier system) gets transformed in a suitable wavelength by different processes (from 775 nm to 520 nm, by a CaF_2-crystal) and separated in an excitation part and a scan part (Figure 25).[41] The scan part is influenced by mirrors for a longer distance and therefore is delayed in reaching the sample, than the excitation pulse. The transmission light of the scan pulse is afterwards recorded and shown as UV/Vis-spectra. By changing the length of the way in small steps, time resolved spectra can be recorded. The limit in the time scale is set by the time of a single laser pulse and the sensitivity of the mirror-positions.

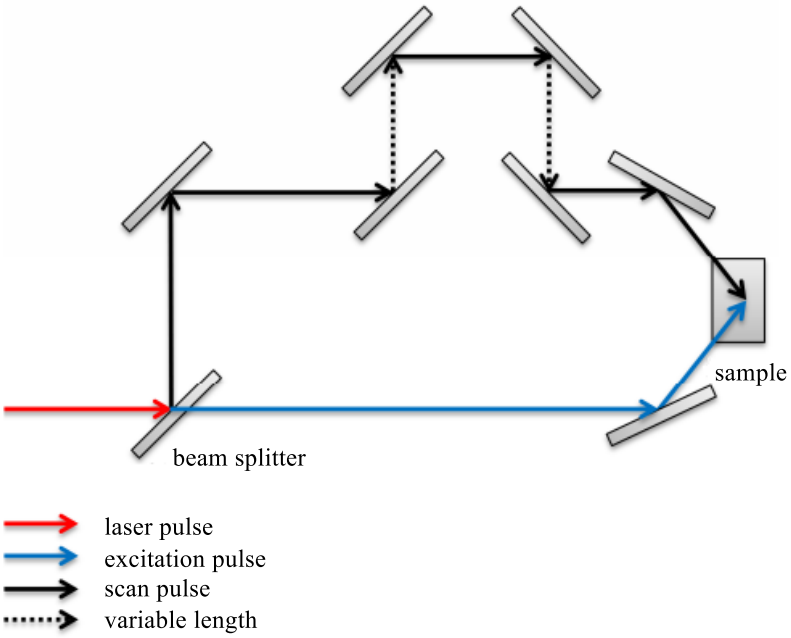

Figure 25: scheme of an excitation-/scan-experiment.

To gain an average reproducible spectra, for each time slice, the spectra gets recorded thousands of times and the sample was moved transversally to the laser beam to minimize degradation by the pump light. Due to the uncertainty principle, the light quantum's energy gets broadened, when it comes to shorter laser pulses. Therefore the excitation at a certain wavelength has a FHWM of >25 nm.

The results of transient absorption spectroscopy of an excited molecule gives detailed insights into structural and electronical changes in ultrashort time frames. The set up and interpretation of the data is sophisticated and complex.

1.5.2 Previous results of transient spectroscopy

This thesis focusses on the development of DTE-fluorophore conjugates carrying an anchor group for the attachment on TiO_2 semiconductor and Al_2O_3 as inert reference system. The systems are investigated in our group in solution-studies for the determination of absorption and emission properties. Investigations on surfaces are aiming the analysation of semiconductor surface impact on the switching- and spectroscopic behaviour, as well as understanding elemental processes of DTE conjugates by using ultrafast transient spectroscopy. The first generation conjugates DTE(Me) **DTE** (**16**) with one anchor group and DTE(Me) **tripod-DTE** (**17**) with a tripodal anchor, shown in Figure 26, were investigated in solution and on TiO_2 surfaces.

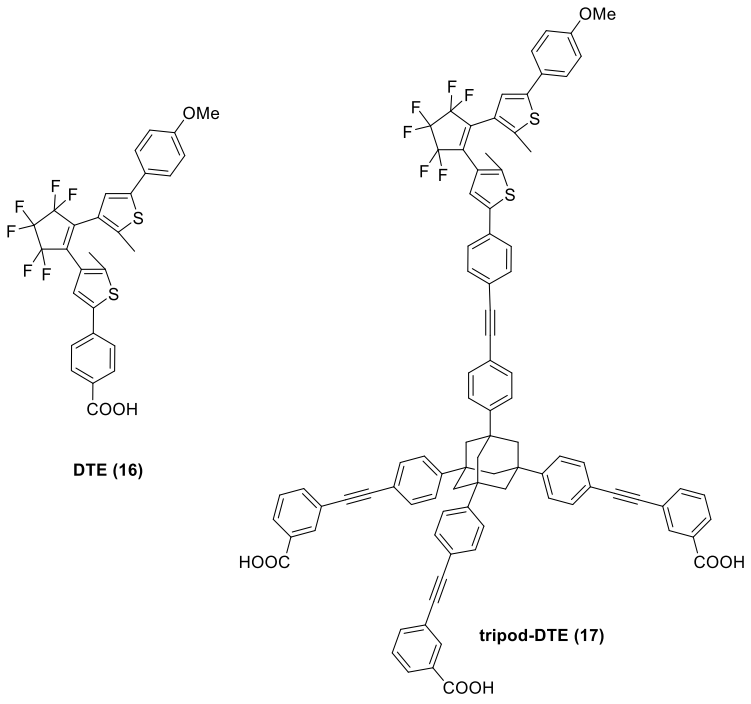

*Figure 26: first generation of DTE(Me)-conjugates **DTE** (**16**) and **tripod-DTE** (**17**) for the investigation on semiconductor surfaces.*[50]

DTE (**16**) CF on TiO_2 showed a photoinduced electron transfer after excitation into the absorption maximum of **DTE** CF at 590 nm, and shortened relaxation times after excitation in comparison to

DTE OF (**16**) in solution.[51][50] The **tripod-DTE** CF (**17**) showed almost no influence after coupling to the surface, which suggests a decoupled conjugate due to the increased linker length.

In the second generation, DTE(Me) was coupled with a BODIPY fluorophore to investigate the energy-transfer between the donor-fluorophore and the acceptor-photoswitch in solution (Figure 27). The compound **BODIPY-DTE** (**18**) should serve as a prototype for future studies of DTE-Fluorophore conjugates with anchor groups on surfaces.

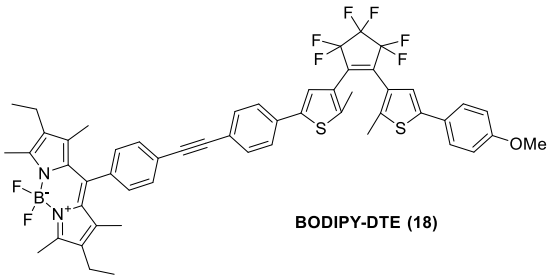

*Figure 27: second generation of DTE-fluorophores **BODIPY-DTE (18)**.[40]*

BODIPY-DTE showed unexpected vibrational coherence with an oscillating signal in the transient spectroscopy in solution.[40] The FRET signature could be observed in an oscillating interval between fluorophore and DTE. The loss of energy by vibronic movements of the molecule resulted in a higher temperature of the surrounding medium. However, **BODIPY-DTE** showed the desired energy transfer properties by remaining reversible switchability.

In the third generation, the DTE-fluorophores **BODIPY543-DTE-COOH** (**13**) and **BODIPY585BCP** (**14**) carrying a carboxylic acid anchor group were synthesized and investigated in solution, on Al_2O_3 and on TiO_2 (Figure 28).[41] Both conjugates could be switched reversibly in solution and showed a FRET signature in **13** CF and **14** CF. Attached to Al_2O_3, both conjugates **13** CF and **14** CF showed faster relaxation to the ground state after excitation. While attached on the semiconductor TiO_2, **13** OF and **14** OF showed an additional relaxation pathway, which was assumed to be a photoinduced electron-transfer. This signal was more pronounced for **BODIPY585BCP**, than for **BODIPY543-DTE-COOH**. In **13** and **14** CFs this signal is still detectable but additional the FRET signature. Since a pure form of CFs could not be reached by UV-irradiation and all processes overlapped in the CF, the nature of the formed cation and the assignment was not clear.

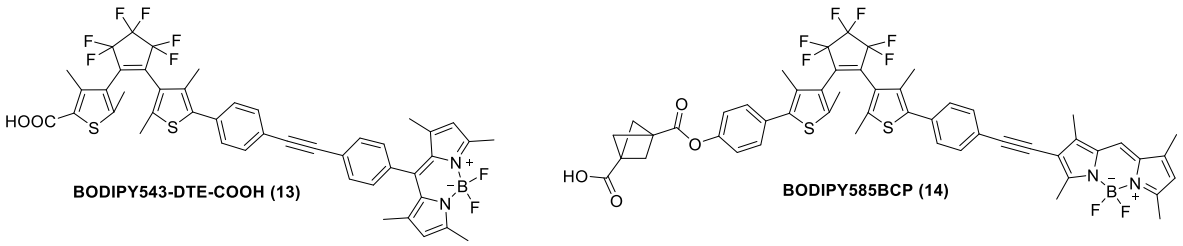

*Figure 28: last generation of DTE(Me)-BODIPY conjugates **BODIPY543-DTE-COOH (13)** and **BODIPY585BCP (14)**.*[41]

A next generation of DTE-fluorophores should fulfill the following requirements: a) quantitative switching for the determination of the excited conjugate processes in both states; b) electron withdrawing properties towards the anchor group, to facilitate the electron-transfer and c) substitution of the BODIPY fluorophore, for determination of the nature of a formed cationic intermediate upon photoinduced electron-transfer, and to improve the stability of the conjugates.

1.6 PHOTOINDUCED INTRAMOLECULAR ELECTRON-TRANSFER

A photoinduced intramolecular electron-transfer is a process of electron movement between a donor (D) and an acceptor (A), which results in a charge separated molecule by the external stimulus irradiation (Figure 29).[52] The resulting charge-separated state of a molecule often differ markedly from the parent ground state in the molecular structure and dipole moment.[53] To reach a charge-transferred state, D and A can twist around a single bond for the lowest frontier orbital overlap (minimum overlap rule) of D and A (90 °) leading to a twisted intramolecular charge transfer (TICT) state with changed energy level, which can be detected by fluorescence spectroscopy.[54] Furthermore, the charge-separated state is able to undergo electron-transfer processes to a) another molecule (intermolecular) or b) redox systems in the direct environment, or c) into surfaces, if the band gap matches the energy of the electron or d) a charge recombination, resulting in the uncharged molecule. The electronic structures of a charge transfer system in the excited state can be usually refered to the ground state of the free radical ion pair of opposite charges (radical anion D^+ and radical cation A^-).[55] Since the possible applications of electron-transfer systems are versatile (for example electronical devices, solar cells, etc.), many approaches and design rules were developed to facilitate the process.

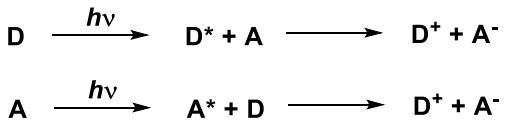

Figure 29: generalized photoinduced electron-transfer between a donor (D) and an acceptor (A).

In general the uncharged system should carry an electron-rich donor (D) and an electron deficient acceptor (A) moiety, which can be both adressed by light for a charge transfer process (Figure 29). In Figure 30 schematically shown is the excitation of an electron of the high lying donor HOMO (or low lying HOMO of the acceptor) to the donor LUMO (acceptor LUMO) and charge recombination. The donor or the acceptor should be able to absorb photons of low energy with a high transition possibility and slow relaxation of the excited electron to the ground state. Furthermore, the acceptor moiety has to be able to stabilize the negative charge for a long lifetime of the charge separated state. Both parts should be electronically connected in a π-system, whereas the distance between both are highly influencing the electron-transfer rate after the external stimulus. A short distance between A and D results in a fast electron-transfer process, but ususally has a high charge recombination rate. Long distances on the other hand, slow down the electron-transfer with the advantage of a low charge recombination rate. In sum, the molecule needs to be designed for the desired application.

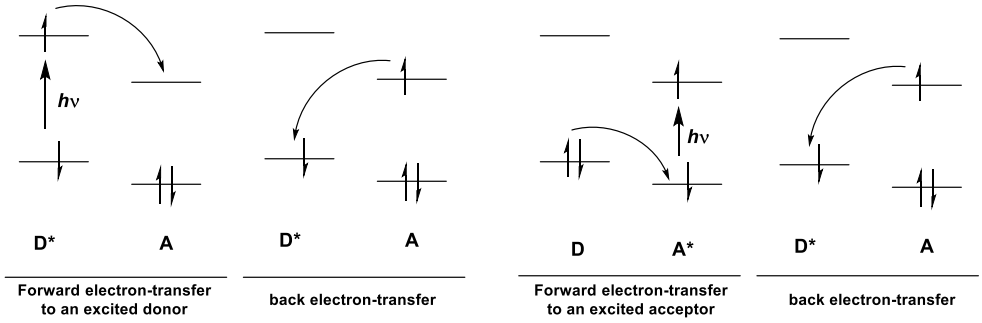

Figure 30: schematical excitation of a donor or acceptor to a charge separated state and charge recombination.[52]

In this thesis, the structure of **BODIPY585BCP** (**15**) synthesized by a former member of our work group should be improved for its electron-transfer ability.[41] The anchor-DTE-fluorophore system **BODIPY585BCP** OF on TiO_2-semiconductor can be assigned generally as a donor-acceptor (D-π-A) system with a thiophene-unit as donor resulting in photoinduced electron-transfer (Figure 31). Upon photoisomerization, the former thiophene donor becomes part of the increased rigidified π-system between the BODIPY-donor and the carboxylic anchor group modulating highly the donor strength. The

overlap of the **BODIPY585BCP** CF π-π* absorption with the BODIPY emission leads to an energy-transfer as competitive process to the electron-transfer.[41]

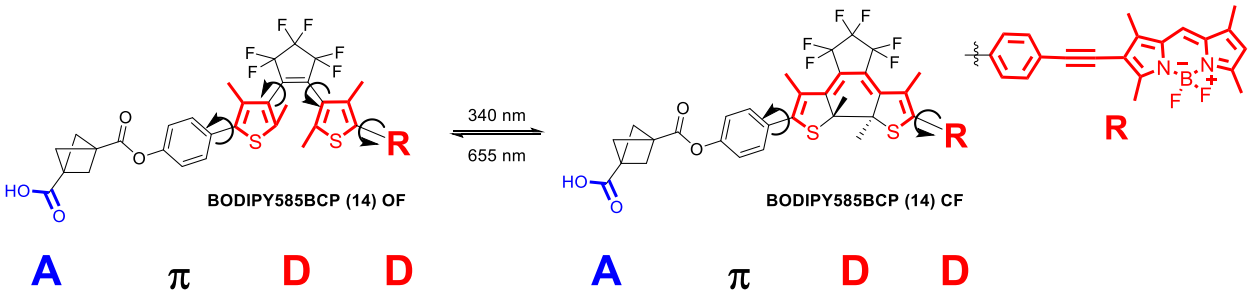

*Figure 31: structures of **BODIPY585BCP** (**14**) OF and CF with electron rich (red) and electron poor (blue) structural motifs.*

D-A system arrangements are of high interest in the field of optoelectronical devices (f.e. dye-sensitized solar cells (DSSCs)). Commonly in DSSCs the fluorophore donor is connected to the TiO_2 acceptor via a π-bridged conjugate in a redox-solution, whereas the length, rigidity[56], torsions in the conjugate[57], type of anchor-group[58] and usage of electron deficient heterocycles[43] in the π-bridge are still part of the ongoing discussion. The redox-solution is often an I^-/I_3^--system in MeCN and the non-coupled systems are often investigated in MeCN solution. Since our systems are investigated attached to the surface on air, a direct transition of DSSC design rules to our application is sophisticated. However, despite the differences for the conjugates in the DSSC application field the photochemical properties of our conjugates will be investigated and compared to literature known design rules for DSSCs.

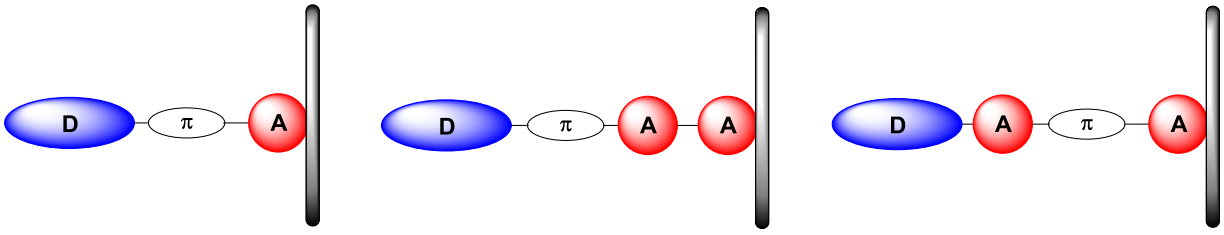

Figure 32: different arrangements of donor-acceptor structures for electron-transfer to a semiconductor surface.

Literature known attachment of a second acceptor between the acceptor of a D-π-A system and the semiconductor surface leads to faster electron transfer with disadvantagous highly increased charge recombination rates from the TiO_2 to the conjugate (Figure 32).[43] A further acceptor in a row between donor (D) and acceptor (D-A-π-A) strongly lowers the HOMO-LUMO gap and therefore red-shifts the absorption of a fluorophore. Furthermore it decreases the charge recombination rates (Figure 32).[43] A DTE-photoswitch with two different photoswitchable conductivity properties can serve as a modulable π-bridge, either between D-A, as well as A-A; or as a donor/acceptor itself by the attachment of electron

rich/deficient functionalities. This switchable unit offers a further possibility for the control of electron-transfer processes by light.

In this thesis, by introducing DTE(OMe) between a BODIPY-donor and benzoic acid acceptor and as a switchable donor unit in a row with a BTD- and a benzoic acid-acceptor two options will be investigated. This should give an insight for the versatile applications of DTE(OMe)s in DTE(OMe)-fluorophore conjugates.

2 General Part

2.1 AIM OF THE THESIS

Starting with the synthesis of the literature known DTE(OMe) **3** (Figure 33) and the development of a flexible synthetic approach to unsymmetrically substituted DTE(OMe) structures. DTE(OMe) **3** needs to be investigated for the spectroscopic properties to confirm literature results and the used methods in our group. Herein a method for the determination of quantum yields and ratio in pss should be developed for DTE(OMe)s.

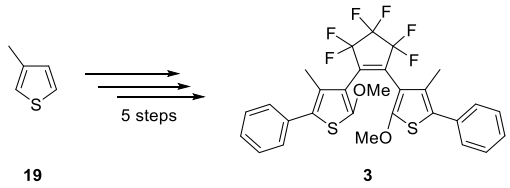

*Figure 33: literature known synthesis of DTE **3** from **19**.[29]*

In the next step, the DTE(OMe)-core structure should be coupled to a BODIPY-fluorophore (Figure 34) and the resulting conjugate **20** should be investigated in solution and compared with the dyads, which were prepared in our work group before. Therefore next to the absorption measurements for DTE(OMe) **3**, emission properties needs to be investigated and a method for the emission characteristics needs to be developed. For the investigation of substituent effects on the spectroscopic properties of the DTE(OMe) photoswitch, the intermediates in the reaction sequence should be analysed.

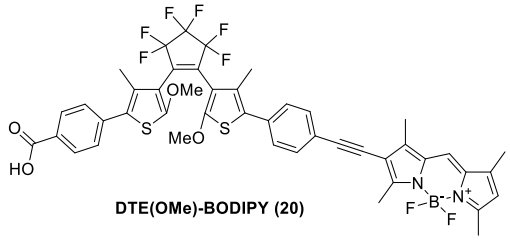

*Figure 34: target DTE(OMe)-BODIPY structure **20**.*

Furthermore, the synthetic approach of a synthetically sophisticated near infra red-BODIPY (**21**) should be investigated together with the spectroscopic and chemical properties of tetramethyl-BODIPY **4** (Figure 35). Moreover the spatial orientation of the last generation of DTE-fluorophore conjugates

(**BODIPY543-DTE-COOH** (**13**) and **BODIPY585BCP** (**14**)) on the semiconductor surface is not clear. For a better understanding of possible electron transfer signature of the BODIPY-cation, the conjugate **22** (BODIPY-stick) should be synthesized and analysed.

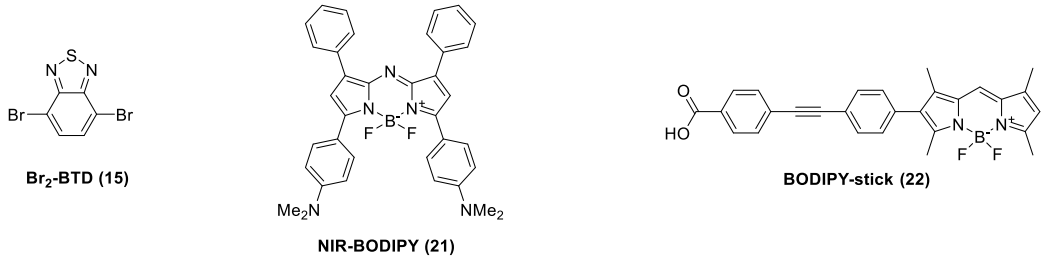

*Figure 35: target structures of left: dibromo-BTD **15**; middle: NIR-BODIPY **21**; right: BODIPY-stick **22**.*

Afterwards the BODIPY fluorophore should be exchanged and the basic properties of new benzothiadiazole(BTD)-dyes should be determined in a stepwise increase of the π-system of BTD **15** and compared to the final BTD-DTE(OME) conjugate **23** (Figure 36). The literature known properties of benzothiadiazoles as acceptor and fluorophore unit should be investigated and compared to the former generations of DTE-fluorophore conjugate **BODIPY585BCP** (**14**, see Figure 28).

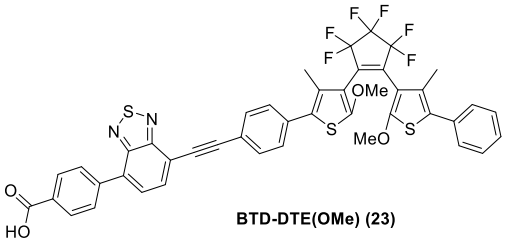

*Figure 36: target BTD-DTE(OMe) -conjugate **23**.*

2.2 SYNTHESIS

2.2.1 The synthesis of DTE(OMe)s

2.2.1.1 Synthetic approach

The synthetic route towards DTE(OMe) **29** is following the approach published by DE MEIJERE et al. (Figure 37).[29] Starting from 3-methylthiophene (**19**) in a lithiation-bromination reaction, the 2-bromo 4-methylthiophene (**24**) is formed. Copper-mediated methoxylation of the arylbromide **24** leads to 2-methoxy 4-methylthiophene (**25**). In a double-bromination step with NBS in tetrachloromethane, the dibromo-thiophene **26** is synthesized. This compound will be the starting point for all the DTE(OMe) conjugates in this thesis.

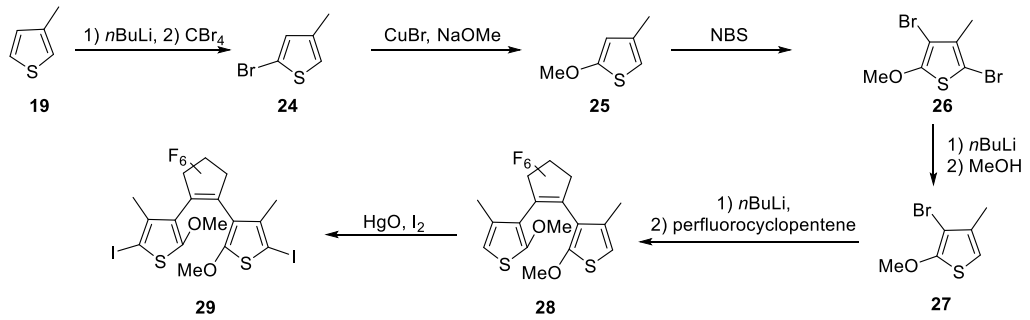

*Figure 37: synthetic approach to the symmetrical diiodo-DTE(OMe) **29** by de Meijere et al..[29]*

With a lithiation-step, the more reactive *ortho*-position to the sulphur in **26** becomes activated and hydrogenated to **27** by quenching with methanol. Via an addition-elimination reaction with the lithiated bromo-thiophene of **27**, DTE(OMe) **28** was synthesized. This DTE(OMe) (**28**) carrying no residues in the external positions is known to show decomposition in photochemical reactions.[59] Both external positions can be substituted by a diiodination-step with mercury oxide and iodine to obtain compound **29**.

2.2.1.2 Synthesis of 2-bromo-4-methylthiophene (24)

Starting with commercially available 3-methylthiophene (**19**) reacting with *n*-butyllithium (activated with TMEDA) functionalizes mainly the 2-position of the thiophene (Figure 38). The further reaction with tetrabromomethane leads exclusively to the desired 2-bromo-4-methylthiophene (**24**). SPINELLI et al. investigated different bromination agents for this reaction, with major side products from multiple bromine additions in different positions.[60] Tetrabromomethane leads exclusively to the mono-

brominated product **24**, which is explained by the bulky agent, which can not approach the positions next to the methyl group for a bromination reaction.

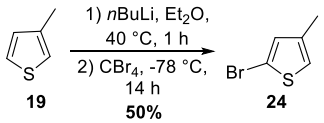

*Figure 38: the bromination of 3-methylthiophene (**24**).*

The work-up of **24** was sophisticated due to the high cryoscopic constant of tetrabromomethane, its property to decrease the boiling point of molecules in the spatial environment. Therefore the purification by fractioned distillation of the product as described in the literature, yielded the product with impurities of CBr_4 (proved by IR and mass-analysis). A bigger batch size/ longer distillation apparatus could avoid these impurities. In the end, the product was purified with flash column chromatography on silica gel with small impurities of the starting material, and the product was stored under argon in the freezer. Nevertheless, the product **24** (colourless oil) showed decomposition over time, so the next reaction step had to be done quickly.

2.2.1.3 Synthesis of 2-methoxy-4-methylthiophene (25)

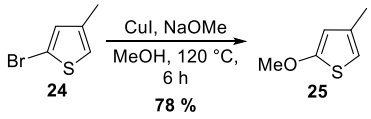

*Figure 39: copper mediated reaction of **19** to the methoxy-thiophene **25**.*

BRAMDSMA et al. investigated 1992 the copper mediated methoxylation of halogene-substituted thiophenes with methanolate (Figure 39).[57] They describe the necessary two equivalents of base for the copper species regeneration in a mechanism shown in Figure 40.[58] The copper(I) bromide needs to be converted to the reactive $Na[Cu(I)(OMe)_2]$-species **30** before coordination with the aryl halogenes to **31**. After an electron shift to form the copper(II)-species **32**, an oxidative addition step into the bromo-thiophene bond forms **33**. A reductive elimination step yields the desired product **25** and a copper(I) species carrying a bromide and a methoxy ligand (**32**). The resulting copper-intermediate **34** can be reactivated with a further methanolate molecule to the starting copper(I)-species **30**. Therefore less than one equivalent copper salt is necessary for the reaction.

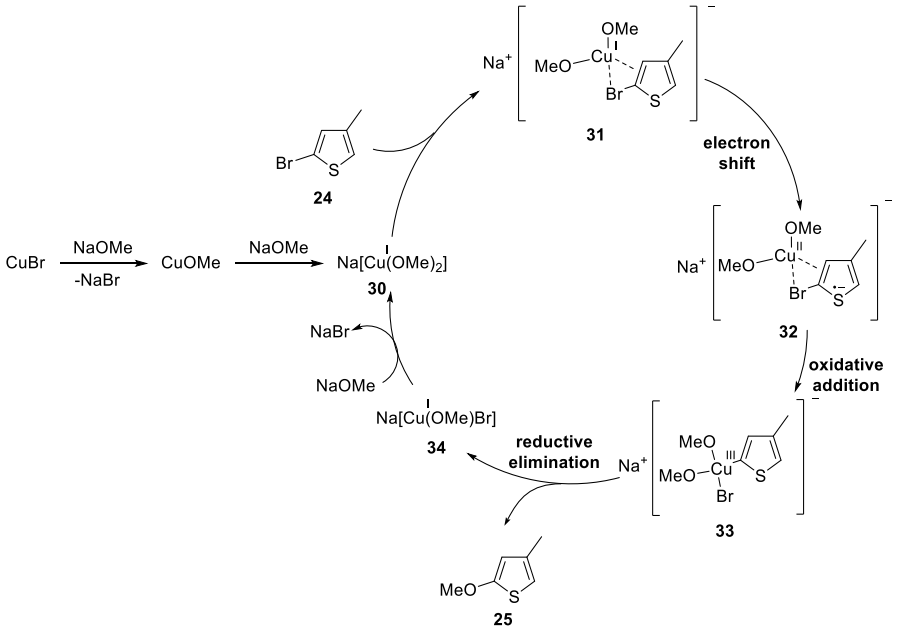

*Figure 40: copper-mediated methoxylation of bromo-thiophene **25**.[61]*

The mechanism is literature discussed with a concerted step for the product formation step between **32** and **30** as well, which seems unusual.[61] The major difficulty in this reaction is the volatility of product **25**. That leads to a loss of product in each work-up step, mainly in the removing of the solvents in *vacuo*. Bigger reaction batches led to higher reaction yields.

2.2.1.4 Synthesis of 2,4-dibromo-5-methoxy-3-methylthiophene (26)

The synthesis of the dibromo-thiophene **26** was done by a two-times nucleophilic aromatic substitution reaction of **25** with *N*-bromosuccinimide with a good yield of 69 % (Figure 41).[29] The product showed rapid decomposition under air and daylight in the fridge. Therefore the compound **26** was stored under argon and exclusion of light in the freezer without any sign of decomposition in 6 month.

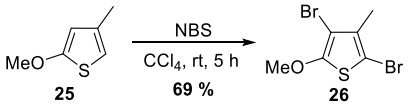

*Figure 41: dibromination of **25** with NBS to **26**.*

Due to the lack of a good commercial availability of tetrachloromethane over the last years and the toxicity, the reaction was tried in different solvents (DCM, MeCN, $CHCl_3$) without any sign of full conversion and a mixture of mono- and dibrominated product (**26**). Literature known low concentration of solved NBS in

CCl_4 and therefore a different reactivity in substitution reactions, could be a reason for exclusive reaction in this solvent.[62]

2.2.1.5 Synthesis of 3-bromo-2-methoxy-4-methylthiophene (27)

Subsequently, the more reactive *ortho*-position of the thiophene **26** was dehalogenated by a lithiation-hydrogenation (quenching of **35** with methanol) sequence in high yields of 83 % (Figure 42). The product **27** needs to be stored under argon in a freezer to avoid rapid decomposition.

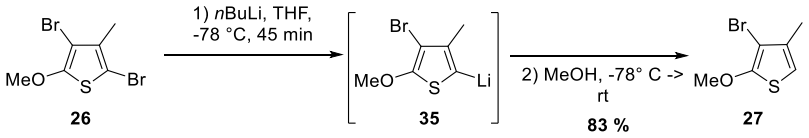

*Figure 42: defunctionalization of **26** to monobromo-thiophene **27**.*

2.2.1.6 Synthesis of 3,3'-(perfluorocyclopent-1-ene-1,2-diyl)bis(2-methoxy-4-methylthiophene) (28)

The combination of two bromothiophenes **27** with the perfluorinated backbone to DTE(OMe) **28** was done with an activation of **27** by *n*-butyllithium, followed by an addition-elimination reaction at the double bond of the highly volatile perfluorocyclopentene (Figure 43). The reaction is literature known to have low reaction yields.[11] [29]

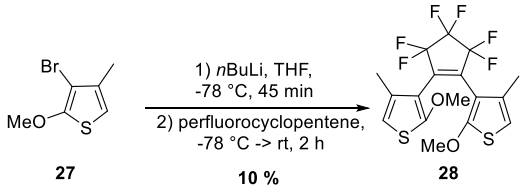

*Figure 43: synthesis of the unsubstituted symmetrical DTE(OMe) **28**.*

A reason could be the quenching of the lithiated thiophene **36** with protons of the acidic *ortho*-position of the thiophenes **27** or the deactivation of the double bond in the backbone of **38**, after the first addition-elimination was successful (Figure 44). The reaction control with TLC showed several products, but only one spot changed the colour under UV-irradiation. Due to the published low yields in different groups over the years for this reaction, an improvement and investigation was renounced.

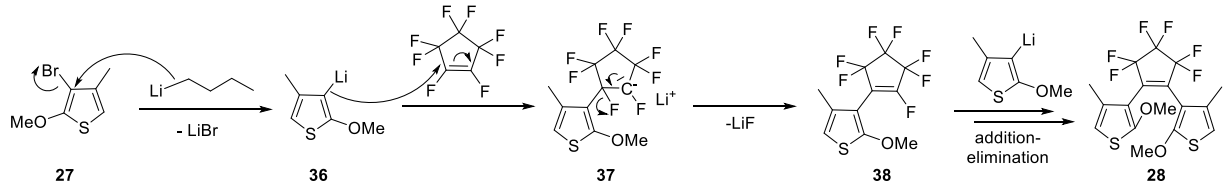

*Figure 44: mechanism of the activation of **27** and coupling with perfluorocyclopentene backbone to DTE(OMe) **28**.*

2.2.1.7 Synthesis of 4,4'-(perfluorocyclopent-1-ene-1,2-diyl)bis(2-iodo-5-methoxy-3-methylthiophene) (29)

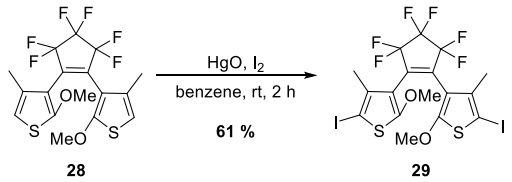

*Figure 45: mercury mediated reaction of DTE(OMe) **23** with iodine to **24**.*

The further diiodination of **28** to **29** was carried out in a mercury-mediated reaction with elemental iodine in good yields of 61 % (Figure 45).[29] The mechanism is an activation step of the iodine (two equivalents) with mercury(II)-oxide (one equivalent) to diiodooxide and mercury iodide (Figure 46).[63] The dioxide exchanges the proton of the thiophenes with an iodo-substituent, which leads finally to the product **29** and formation of water in this reaction. Therefore the used solvent is the hygroscopic benzene. An exchange of the solvent was not investigated due to the subsequently exchange of the synthetic strategy.

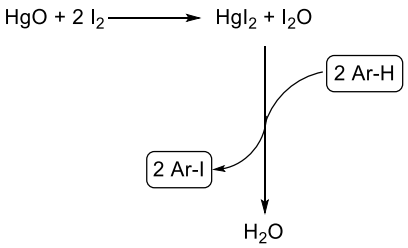

Figure 46: mechanism of aryl iodination with mercury(II)-oxide.[63]

2.2.1.8 Synthesis of ((4-iodophenyl)ethynyl)trimethylsilane (41)

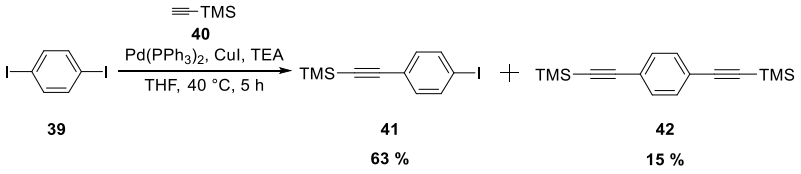

*Figure 47: synthesis of TMS-protected iodo-phenyl-ethinyl **41** and double coupled side product **42**.*

The literature known SONOGASHIRA-coupling of diiodo-benzene **39** with trimethylsilyl-ethyne (**40**) yielded 63 % of the desired product **41** and 15 % of the side product **42** (Figure 47).[64] The diodo-compound **39** was added in excess, because the dropwise addition of the ethyne led to increased byproduct formation. The purification of the product on silica gel is difficult because of the low and comparable polarity of the product **41** and starting material **39**. The product mixture of **39**, **41** and **42** was therefore separated in smaller portions for the flash column chromatography and combined afterwards. The reaction has a literature known moderate yield. SITA et al. described a two-step synthesis of **41** by addition of 1-bromo-4-iodobenzene with (trimethylsilyl)acetylene and halogene exchange with an overall yield of 80 %.[65] This could be an option for future syntheses. The ethyne-aryl-structure of **41** can be assigned as molecular wire, due to the linear orientation of residues and the lack of electronic hindrance in the conjugated π-system.

Kenkichi Sonogashira und Nobue Hagihara published 1975 a new kind of palladium-catalyzed cross coupling reaction of aryl or vinyl halides with alkynes (Figure 48).[66] The textbook description of the reaction involves a catalytic cycle for palladium and one for copper, which are interacting in a transmetallation step.[67] Starting with a palladium(0) species **44** (which can be formed from more stable palladium(II) precatalysts **43**), a coordination to the electron density of the aryl-halogene bond of **45** to **46**, followed by an oxidative addition step with the aryl halide forms the palladium(II) complex **47**. A more electron rich aryl-halogene bond facilitates this step.

The second cycle starts with a coordination of copper(I) on the triple bond of an H-terminated alkyne (**51**). The alkyne **51** is deprotonated by a non-nucleophilic base (often triethylamine) and the copper exchanges the place of the proton to form **52**.

Both cycles are combined by the following transmetallation step, were the copper is exchanged by the palladium(II) to form **48** and the palladium of the halide ligand is exchanged by copper. Therefore the formed copper halide **53** is regained and can react again in the copper cycle. It is still part of the discussion,

if the residues are in *cis* or *trans*-position at the palladium-center in **48** after the transmetallation step. The palladium aryl alkyne **48** undergoes a *cis*/*trans*-isomerization which leads to spatial neighboured aryl and alkyne residues. Both are coupled to the desired product **50** by a reductive elimination step to the coordinated **49** followed by the palladium(0) species **44** regeneration.

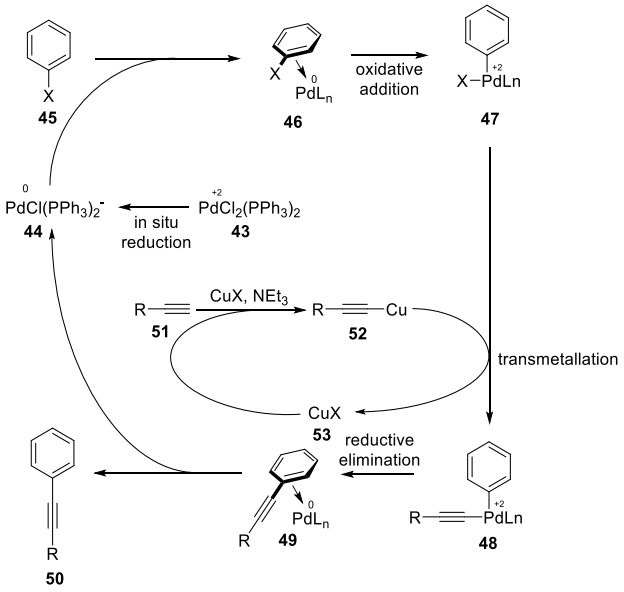

Figure 48: schematical mechanism of a SONOGASHIRA-cross coupling reaction.[67]

A palladium(0) species **58** can be obtained by the reaction of palladium(II) precatalysts **54** with triethylamine (Figure 49).[68] The mechanism starts with a substitution of one ligand of the precatalyst **54** by a triethylamine molecule to **55**, called *σ*-complexation step. One of the hydrogens of **55** in *β*-position is transferred to the palladium (*β*-hydride elimination) and the cationic imine **56** is cleaved. The second ligand of the palladium(II) species **57** and the hydride ligand undergoes a reductive elimination step and the palladium(0) species **58** is formed.

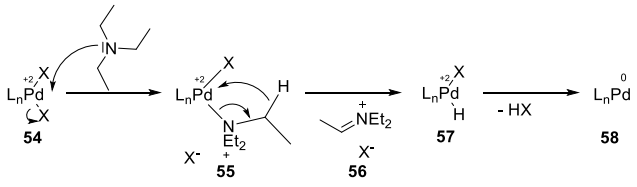

*Figure 49: mechanism of the reduction of Pd(II) **54** to Pd(0) species **58** with triethylamine.[68]*

The diiodo-DTE(OMe) **29** was investigated for a coupling reaction with the molecular wire **41** (Figure 50). The sophisticated activation in a temperature-, concentration- and equivalent-controlled lithiation-step showed several photoswitchable spots on TLC, which could be assigned as protonated mono-lithiation

product, protonated double-lithiation product and non-reacted DTE(OMe) **29**. The following boronation and SUZUKI-coupling (Table 2, mechanism, see 2.2.3.4) were not successful. Three different approaches (Figure 50) did not yield the desired product **59** and unfortunately the access to the diiodo-DTE(OMe) **29** is limited. Therefore, this synthetic approach for unsymmetrically substituted DTE(OMe)s got rejected.

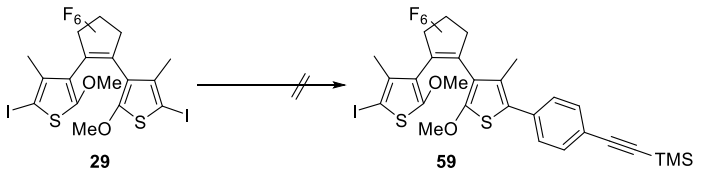

*Figure 50: synthetic approach to unsymmetrically substituted DTE(OMe) **59** starting from diiodo-DTE(OMe) **29**.*

However, this method with brominated-DTE(OMe)s is used by IRIE et al. for different conjugates.[31] [32] The difference to the reaction of **29** to **59** is an already lithiation-inert group on one side of the photoswitch resulting in a single-halogenated DTE exclusively.

*Table 2: investigated conditions for Suzuki-coupling to **59** from diiodo-DTE(OMe) **29**.*

Starting material	Conditions	Product **53**
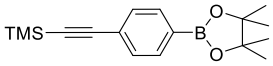	5 mol% $Pd(PPh_3)_4$, Na_2CO_3, THF, 70 °C, 6 h	traces (detectable by mass)
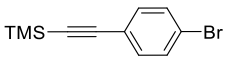	1) *n*BuLi, THF, -78 °C, 1 h; 2) tributylborate; 3) arylbromide, 5 mol% $Pd(PPh_3)_4$, Na_2CO_3, THF, 70 °C, 6 h	no
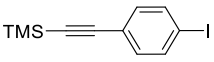	1) *n*BuLi, THF, -78 °C, 1 h; 2) tributylborate; 3) arylbromide, 5 mol% $Pd(PPh_3)_4$, Na_2CO_3, THF, 70 °C, 6 h	no

2.2.2 Synthesis of BODIPY Derivatives

2.2.2.1 Tetramethyl-BODIPY (4)

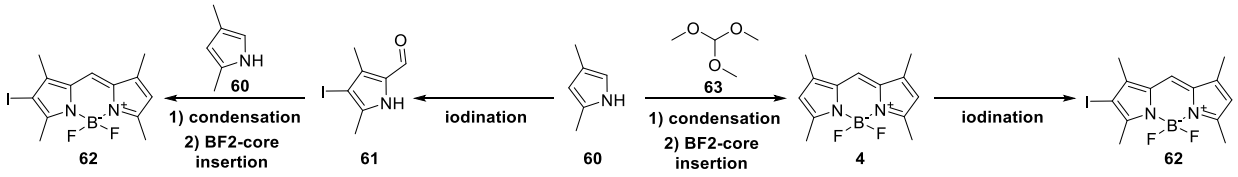

*Figure 51: synthetic approach to mono-iodinated BODIPY **62** from pyrrole **60**..*

The literature known synthesis of mono-halogenated BODIPYs can be done by two main synthetic approaches shown in Figure 51. The starting compound is 2,4-dimethylpyrrole (**60**), which can be coupled to an aldehyde and iodinated to form **61**. An additional condensation reaction with trimethoxymethane

(**60**) and introduction of the BF_2-core forms **62**. This route was used in our work-group by former students. Disadvantage is a further reaction step, which lowers the yield and prolongs the reaction time. Therefore a second route with a condensation reaction to the unsubstituted tetramethyl-BODIPY **4**, core introduction, followed by halogenation to **62** should be investigated.[69]

2.2.2.2 Synthesis 1,3,5,7-Tetramethyl-4,4-4,4-difluoro-4-bora-3a,4a-diaza-s-indacene 4)

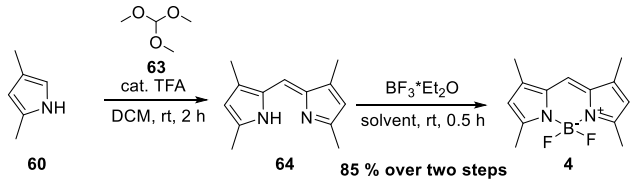

*Figure 52: synthesis of tetramethyl-BODIPY **4** by acid-catalyzed condensation of pyrrole **60**.[69]*

The literature known synthesis of the tetramethyl-BODIPY **4** (Figure 52) starts from 2,4-dimethyl pyrrole (**60**) in an acid-catalyzed condensation reaction with trimethoxymethane (**63**).[69] The trimethoxymethane **63** gets protonated and methanol is formed as a good leaving group (Figure 53). The formed cation intermediate **65** reacts with a pyrrole molecule (**60**) in an electrophilic aromatic substitution reaction via **66** to **67**. A second protonation of the remaining dimethoxymethane moiety of **67** leads to the cationic intermediate **68**, which can undergo an electrophilic aromatic substitution a second time with the pyrrole **60** via **69** to **70**. By a third-time protonation and cleavage of methanol, the methene-bridge is formed in **71** with the mesomeric structure **72**. From the cation **72** by a proton-loss the aromatic dipyrromethene **64** is formed.

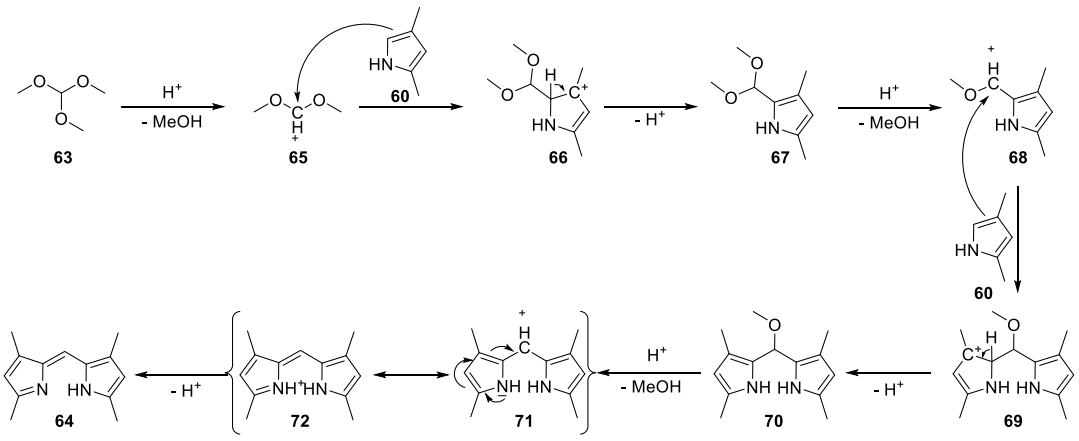

*Figure 53: mechanism of the formation of dipyrromethene **64**.*

The difluoroboron-core is introduced by the treatment of **64** with the non-nucleophilic base triethylamine followed by borontrifluoride etherate. Mechanistically, pyrrole **64** is deprotonated and attacks the boron under the loss of a fluoride substituent to form the chelated tetramethyl-BODIPY **4** in an overall yield of 85 % (Figure 54).

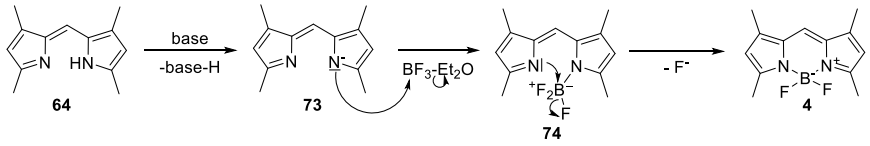

*Figure 54: mechanism of the core-introduction and formation of the tetramethyl-BODIPY **4**.*

2.2.2.3 Synthesis of 5,5-difluoro-2-iodo-1,3,7,9-tetramethyl-5H-5λ⁴4,6λ⁴-dipyrrolo[1,2-c:2',1'-f][1,3,2]diazaborinine (62)

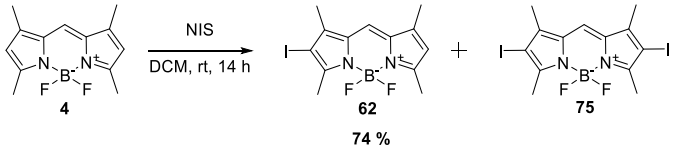

*Figure 55: synthesis of the mono-iodinated BODIPY **62**.*

The synthesis of iodo-BODIPY **62** was done by the treatment of BODIPY **4** with *N*-iodosuccinimide (**76**) in DCM. A disadvantage is the formation of diiodo-BODIPY **75** as a side product. To prevent the second addition on the activated mono-iodinated BODIPY **62**, the concentration is lowered and NIS is dissolved and added dropwise over several hours. The monoiodo-BODIPY **62** could be obtained in 74 % yield.

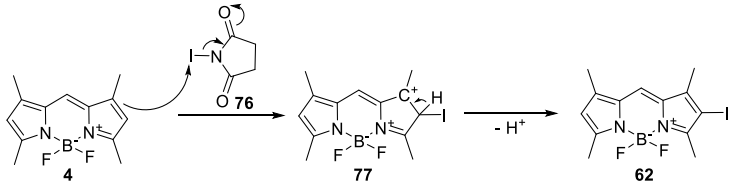

*Figure 56: mechanism of the electrophilic aromatic substitution to the mono-iodinated BODIPY **62**.*

The mechanism is an electrophilic aromatic substitution at the free *β*-position of the BODIPY-core of **4** via **77**. The formed product **62** has an increased electron density in the aryl-system and is therefore preferred for a second addition. The decreased amount of solvent and adding of the NIS in portions led to significantly reduced yield.

2.2.3 BODIPY-stick 22

The synthetic approach for the BODIPY-stick-structure **22** is shown in Figure 57 and starts with the coupling of commercially available methyl 4-iodobenzoate (**78**) with ethinyltrimethylsilane (**40**) in a SONOGASHIRA-cross coupling. The cleavage of the methylester- and trimethylsilane-protecting groups of **79** by base leads to the H-terminated alkyne **80**. The alkyne is coupled to *para*-(iodophenyl)boronic acid (**82**) in a second SONOGASHIRA-cross coupling reaction to form **81**. The boronic acid **81** can be used afterwards for a palladium mediated SUZUKI-cross coupling with the iodo-BODIPY **62** to gain the BODIPY-stick **22**.

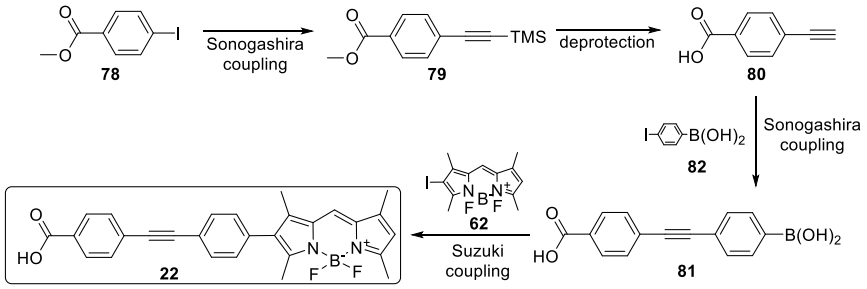

*Figure 57: synthetic approach of BODIPY **22** (BODIPY-stick).*

2.2.3.1 Synthesis of methyl 4-((trimethylsilyl)ethynyl)benzoate (79)

The literature known SONOGASHIRA-cross coupling to the desired aryl alkyne **79** from **78** and ethinyltrimethylsilane is shown in Figure 58.[70] As co-catalyst copper(I) iodide was added and trimethylamine was used to obtain the product **79** in a high yield of 95 %.

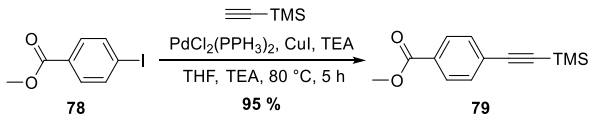

*Figure 58: synthesis of the TMS-protected ester substituted aryl-alkyne **79**.*

2.2.3.2 Synthesis of 4-ethynylbenzoic acid (80)

The cleavage of the TMS- and methylester-protecting groups of **79** to form **80** was done in 2 N aqueous NaOH in high yields of 99 %.[71] The mechanism for the base-induced TMS-cleavage is a nucleophilic substitution reaction, while the base induced ester cleavage follows an addition-elimination mechanism.

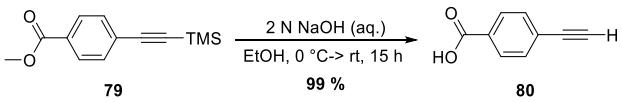

*Figure 59: deprotection of **79** to the H-terminated alkyne **80**.[71]*

2.2.3.3 Synthesis of 4-((4-boronophenyl)ethynyl)benzoic acid (81)

In a second SONOGASHIRA-coupling, the terminated alkyne **80** forms a C-C bond to aryl-boronic acid **82**. A SUZUKI-coupling (mechanism see Figure 62) of two molecules of **82** could be a side reaction of the coupling, but seems to be unlikely due to the mild reaction conditions and the lack of a hydroxide-source.

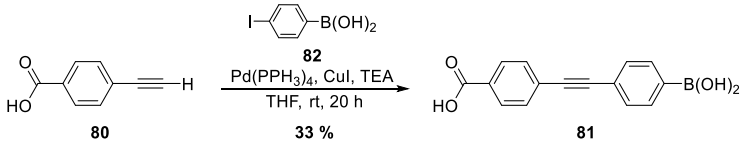

*Figure 60: SONOGASHIRA-cross coupling of **80** with para-iodophenylboronic acid **82**.*

The work-up of the formed product **81** is sophisticated, due to the high polarity of the carboxylic and the boronic acid. Flash column chromatography with acid-saturated silica gel (silica gel was washed several times with EtOAc + 1.0 % acetic acid) was necessary to obtain the product **81** as a mixture of monomer and dimer/trimer (proved by mass spectrometry). Since carboxylic acids often form dimers with themself and boron acids favour trimers in boronic anhydrides, a prediction for the formed species needs to be done by spectroscopy. In the ^{1}H-NMR-spectra (with d_6-DMSO), the broad water peak overlaps with the protons assigned to the boronic acid (see Spectra Appendix 5.1). Since **81** is highly polar, different deuterated solvents were not tried. Therefore, the nature of **81** dimer/trimer was not further investigated. The yield for this reaction is with 33 % low, but acceptable.

2.2.3.4 Synthesis of 4-((4-(5,5-difluoro-1,3,7,9-tetramethyl-5H-5λ⁴,6λ⁴-dipyrrolo[1,2-c:2',1'-f][1,3,2]diazaborinin-2-yl)phenyl)ethynyl)benzoic acid (22)

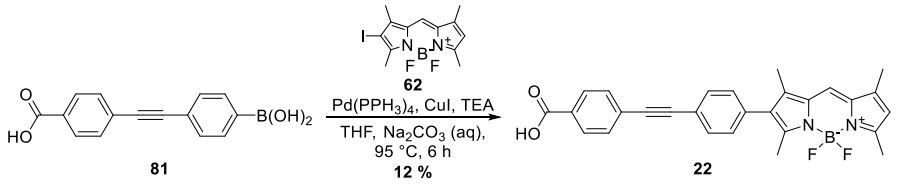

*Figure 61: SUZUKI-cross coupling of **81** with iodo-BODIPY **62** to BODIPY-stick **22**.*

The final coupling to obtain the BODIPY stick **22** is shown in Figure 61 with a low yield of 12 %. The BF_2-core can be cleaved by base.[72] Therefore the reaction was worked-up before the conversion was complete to prevent the formation of core-cleaved BODIPY material.

The mechanism is a palladium mediated cross coupling of organo halides with boronic acid compounds starting with palladium(0) catalyst **83** discovered by Akira Suzuki in 1979 (Figure 62).[73] The palladium catalyst **83** formed by a two times ligand dissociation of $Pd(PPh_3)_4$, inserts in the halide-carbon bond of **84** in an oxidative addition step to obtain the Pd(II) species **85**. The function of the added base in the Suzuki coupling is still not fully understood. One possibility is the activation of the boronic acids by breaking trimerised boroxines. Furthermore, the hydroxyl-ion can exchange the halide in the Pd(II) species **86** and facilitates the following transmetallation step via a four-membered transition state of aryl-palladium with the arylboronic acid. After the transmetalation step a *cis*/*trans*-isomerization has to take place, or a chelating ligand system has to be used for the reaction to bring both coupling partners together in **89**. The C-C bond formation is made by a reductive elimination step and the product **90** is formed, and additionally the Pd(0) catalyst **83** is regained.

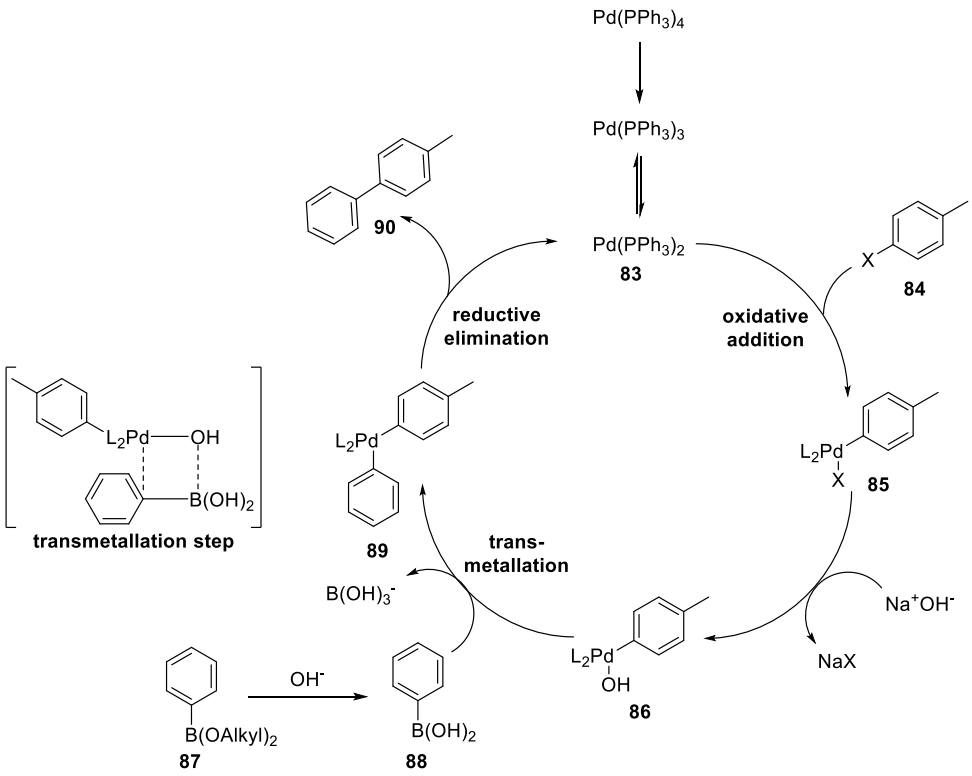

Figure 62: schematical mechanism of a Suzuki-cross coupling reaction.[74]

2.2.4 NIR-BODIPY 21

The *aza*-BODIPY **21** is a literature known NIR emitting dye. The synthesis starts with the *α,β* unsaturated ketone **100** and is described by O'SHEA et al. in 2006 (Figure 63).[38] The starting material was synthesized by a two-step synthesis. Commercially available *N*,*N*-dimethylaniline (**91**) was reacted with acetyl chloride (**92**) and aluminium trichloride in high excess in a FRIEDEL-CRAFTS acylation (Figure 64).[75]

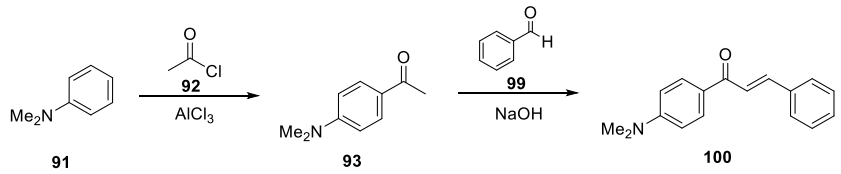

*Figure 63: literature known synthetic access of the α,β-unsaturated ketone **100**.*[38]

2.2.4.1 Synthesis of 1-(4-(dimethylamino)phenyl)ethan-1-one (93)

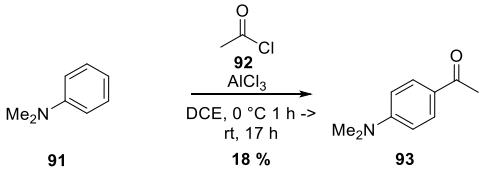

*Figure 64: Synthesis of **93** in a Friedel-Crafts acylation reaction.*

The acyl chloride (**92**) is activated by the Lewis acid $AlCl_3$ to the intermediate **94a-b** and converted to the acyl cation **96a-b** under $AlCl_4^-$ (**95**) cleavage (Figure 65).[76] The electrophilic aromatic substitution in *para*-position of **91** leads to a resonance stabilized intermediate (**97a-c**) until the proton from the reactive carbon of the former arene is abstracted and the aromaticity is regained in **98**. Aqueous work-up leads do the desired aryl-ketone **93**. The dimethyl amine group of **91** leads to the favoured *para*-position for the electrophilic aromatic substitution steps. The *ortho*-positions are sterically hindered by the amine residue. By protonation a meta-directing functional group is formed, which lowers the reaction yield. Furthermore, the yield is lowered by the complex work-up of the product **93**.

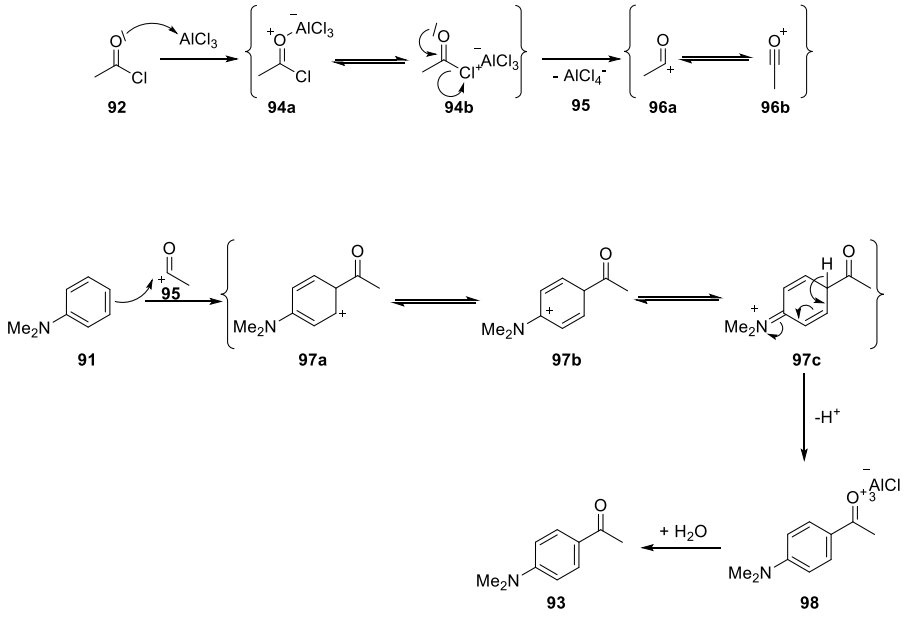

*Figure 65: mechanism of the FRIEDEL-CRAFTS acylation of N,N-dimethylamine **91**.[76]*

2.2.4.2 Synthesis of (E)-1-(4-(dimethylamino)phenyl)-3-phenylprop-2-en-1-one (100)

To obtain the *α,β*-unsaturated ketone **100**, compound **93** was reacted with benzaldehyde (**99**) in a CLAISEN-SCHMIDT condensation reaction (Figure 66).[77] The ketone was dissolved in ethanol and aqueous NaOH, which leads to the desired product **100** in a good yield of 77 %.

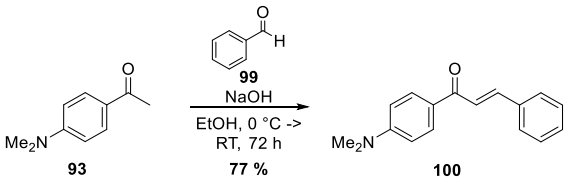

*Figure 66: reaction of dimethylaniline-ketone **93** in a CLAISEN-SCHMIDT condensation reaction to **100**.*

The mechanism is an aldol reaction of **93** and **99** with elimination of the formed hydroxide in an E_{1cB} mechanism.[67] The corresponding deprotonated enolate **101a-b** of the ketone is formed by the base. The enolate attacks the carbonyl function of benzaldehyde (**99**) and forms the aldol adduct **102**. The ketone functionality of **102** is converted to the corresponding enolate **104** by a base-catalyzed deprotonation of the acidic *α*-carbon proton of **103**. The formed anion can eliminate the hydroxy-function to gain the *α,β*-unsaturated product **100**.

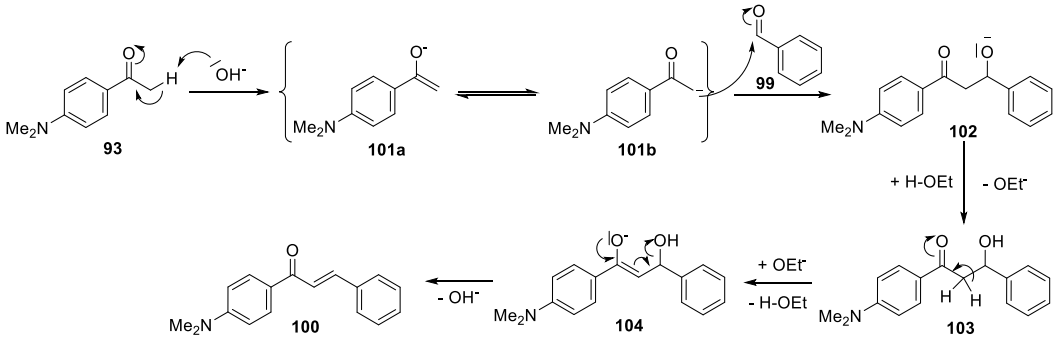

*Figure 67: mechanism of the CLAISEN-SCHMIDT condensation of **98** to **100**.[67]*

2.2.4.3 Synthesis of 1-(4-(dimethylamino)phenyl)-4-nitro-3-phenylbutan-1-one (105)

The next step is an addition reaction of nitromethane to the *α,β*-unsaturated ketone **100** and is published by O'SHEA et al.(Figure 68).[38] The formed anion **109** is stabilized in an enolate structure and forms the desired product after aqueous work-up in high yield of 92 %.

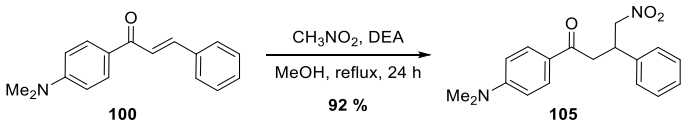

*Figure 68: synthesis of the nitro-ketone **105**.*

The nitromethane (**106**) is deprotonated by the non-nucleophilic base DEA (**107**) to form the resonance stabilized structure **108a-b** (Figure 69). The carbanion of **108a-b** can attack the double bond of **100** in the *β*-position to form the enolate-stabilized intermediate **109**. By aqueous work-up, the desired product **105** is formed.

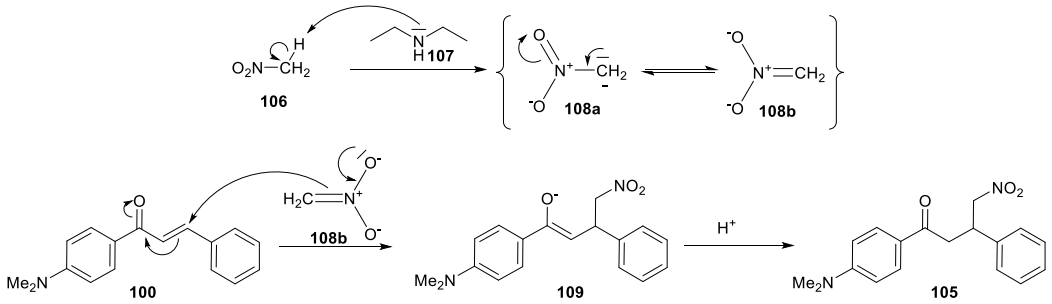

*Figure 69: mechanism of the formation of nitro-ketone **105**.[67]*

2.2.4.4 Synthesis of (Z)-4-(2-((5-(4-(dimethylamino)phenyl)-3-phenyl-1H-pyrrol-2-yl)imino)-3-phenyl-2H-pyrrol-5-yl)-N,N-dimethylaniline (110)

The final step to synthesize the backbone of the NIR-BODIPY **21** starts with a condensation reaction to the pyrrole **115**. After addition of *in situ* formed nitrous acid, a second pyrrole **115** can be coupled and the *aza*-dipyrromethene **110** is formed in a low reaction yield of 24 % (Figure 70).[38]

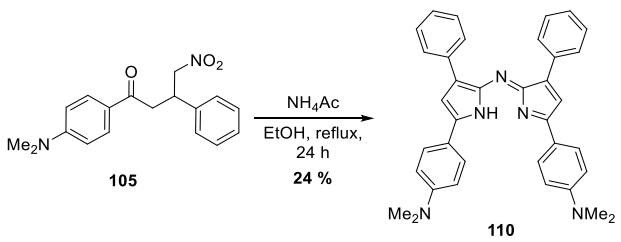

*Figure 70: reaction of the nitro ketone **105** to yield the aza-dipyrromethene **110**.*

The reaction starts with the transformation of the ketone functionality of **105** in an imine group **111** via water cleavage by addition of NH_4Ac to the ketone (Figure 71). The *α*-protons next to the nitro group in **111** are acidic enough to be in an equilibrium with the nitro group as an enamine **112**. The electrophilic addition to the previous formed imine leads to the cyclic structure **113**, which can be attacked by the added base to form the pyrrole **115** after proton loss of **114** to gain aromaticity. The addition of the *in situ* formed nitrous acid in *ortho*-position of the pyrrole **115** forms the nitroso-pyrrole **116**, which loses water after a deprotonation-protonation sequence to form **117**. The regain of aromaticity toward **118** by deprotonation stabilizes the molecule. Supported by protonation of the nitroso-functionality, a second pyrrole of type **115** can attack at the nitroso-nitrogen of **118**, to form the nitroxide **119**. After deprotonation and elimination of the hydroxyl group, the *aza*-dipyrromethene **110** is formed.

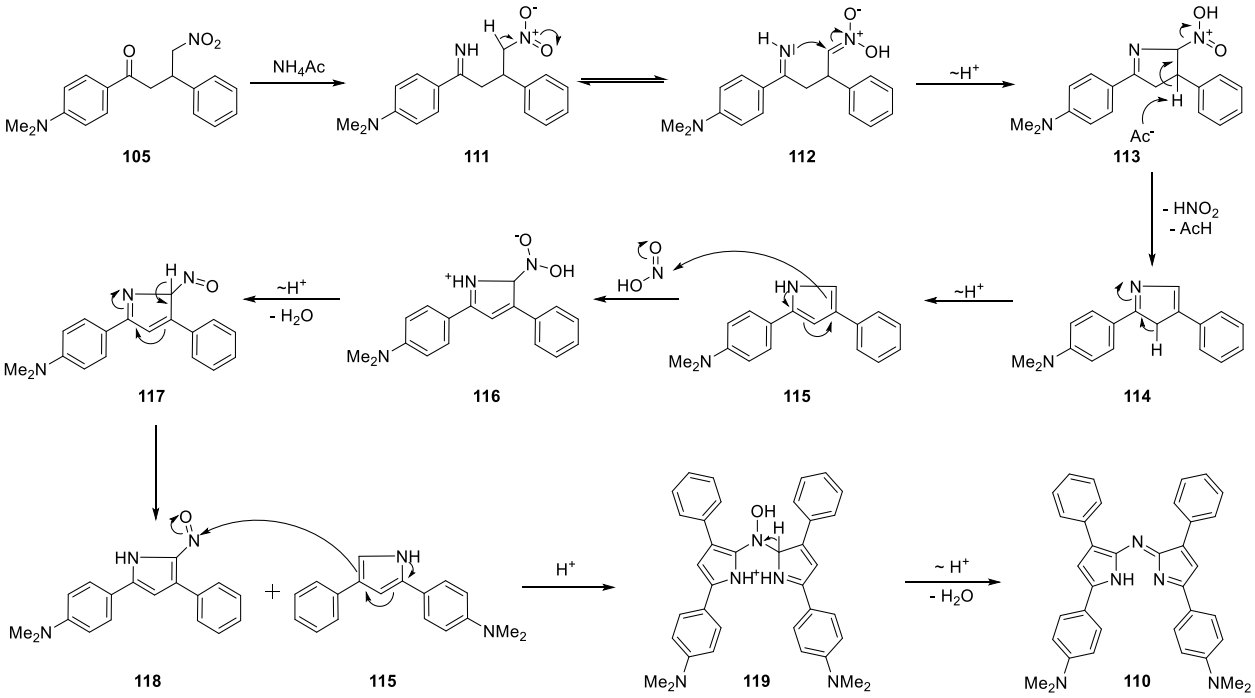

*Figure 71: mechanism of the formation of the aza-dipyrromethene **110**.*

2.2.4.5 Synthesis of 4,4'-(5,5-difluoro-1,9-diphenyl-5H-4λ⁴,5λ⁴-dipyrrolo[1,2-c:2',1'-f][1,3,5,2]triazaborinine-3,7-diyl)bis(N,N-dimethylaniline) (21)

The BODIPY-core of **21** is introduced by the addition of boron trifluoride etherate in the presence of a non-nucleophilic base (DIPEA). After the deprotonation of the pyrrole **110** by the base, the addition of BF_3 and cleavage of a fluorine leads to the desired chelated NIR-BODIPY **21** in a good yield of 84 % (mechanism related to Figure 56).

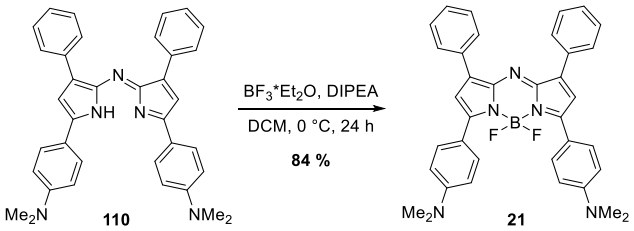

*Figure 72: reaction of aza-dipyrromethene **110** with boron trifluoride to aza-BODIPY **21**.*

2.2.5 Synthesis of BTD Derivatives

2.2.5.1 Synthesis of benzo[c][1,2,5]thiadiazole (121)

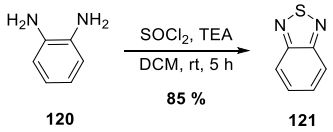

*Figure 73: synthesis of BTD **121** starting from 1,2-phenylendiamine **120**.*

Unsubsituted benzothiadiazole (BTD) **121** can be synthesized by the literature known reaction of *ortho*-phenylene diamine **120** with thionyl chloride (**123**) under basic conditions (Figure 73).[78] After the deprotonation of the starting material amino group **120** to the anionic structure **122**, thionyl chloride (**123**) is attacked and a chloride ion is cleaved to form **124** (Figure 74). Under intramolecular proton exchange to the second amino group of **125** chloride is cleaved to **126** and the former amino group is transformed to a sulfinyl anilin **127**. The second amino group can undergo the same reaction to the double sulfinyl aniline **128**, but both compounds are in equilibrium, and only the mono-NSO compound **127** reacts further in an intramolecular attack of the free electron pair of the amino group with the electrophilic sulphur of NSO to **129**. With a stepwise mechanism of proton transfer, water is cleaved from **131** and the benzothiadiazole **121** is formed.

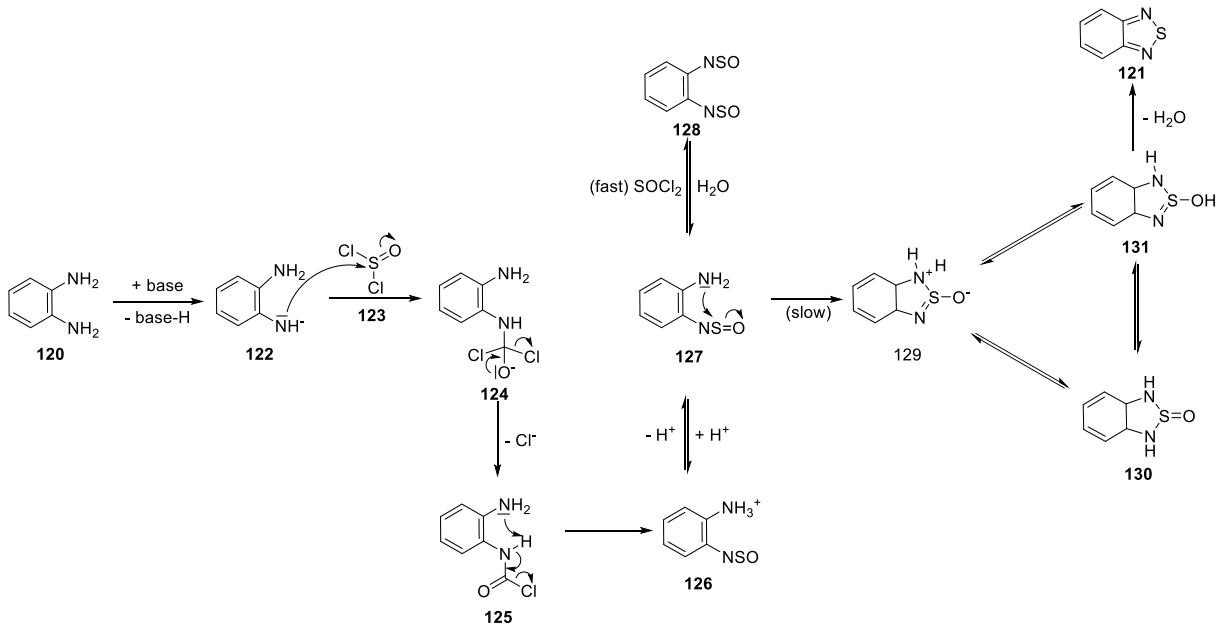

*Figure 74: mechanism of the formation of BTD **121** from **120**.[78]*

2.2.5.2 Synthesis of 4,7-dibromobenzo[c][1,2,5]thiadiazole (15)

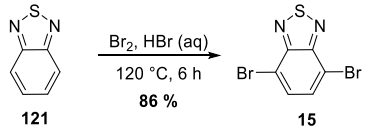

*Figure 75: synthesis of the dibromo-BTD **15**.*

PILGRAM et al. published in 1970 the first synthetic approach for 4,7-dibromo-BTD **15**.[79] Starting from the unsubstituted BTD **121**, the reaction was done in aqueous HBr with bromine under reflux as shown in Figure 75.[42] The bromination step is assisted by a hydrogen bromide molecule, which coordinates on a BTD-nitrogen lone pair and polarizes a bromine molecule (**132**, Figure 76). The loss of aromaticity and the formed cation **133** is stabilized and a bromide ion can combine to form **134**. Proton loss allows to regain the aromaticity to obtain mono-brominated BTD **135**. Repetition of this mechanism yields the double brominated BTD **15**.

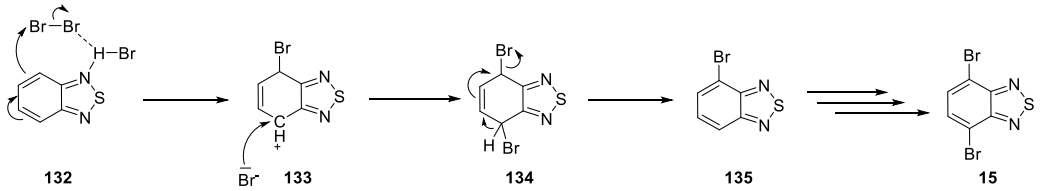

*Figure 76: mechanism of the double-bromination to BTD **15**.[42]*

2.2.5.3 Synthesis of ethyl 4-(7-bromobenzo[c][1,2,5]thiadiazol-4-yl)benzoate (137)

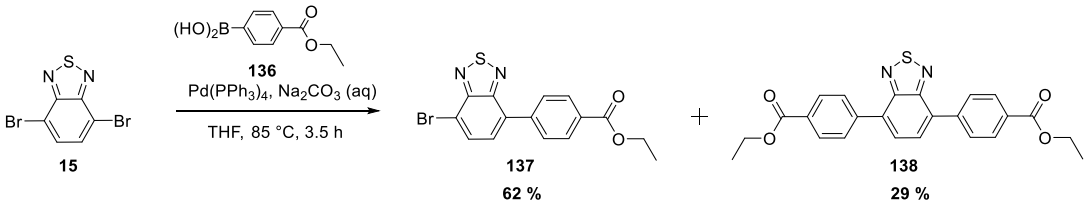

*Figure 77: synthesis of **137** and side product **138**, starting with dibromo-BTD **15**.*

The SUZUKI-coupling of dibromo-BTD **15** with the boronic acid of methyl benzoate **136** yielded **137** in 62 % and the double coupled product **138** in 29 % yield.[80] The desired product **137** is used as BTD-anchor moiety for the final DTE(OMe)-fluorophore conjugate **23**.

2.2.6 Synthesis of DTE(OMe)-Fluorophore conjugates

2.2.6.1 Synthetic approach

Due to the synthetic difficulties in the SUZUKI-couplings of the diiodo-DTE(OMe) **29** another approach was used. Thereby, the dibromo-thiophene (**26**) should be activated by organometallic agents, substituted to boronic acids and then coupled with aryl halides in palladium-mediated cross-coupling reactions (Figure 78). Important to remind in that strategy is to avoid butyllithium-reactive functional groups in the coupled aryls. Otherwise the coupling to perfluorocyclopentene is not possible. Several thiophene-aryl compounds (**139**-**143**) were synthesized with that approach. Due to the aim, finding a general synthetic access for unsymmetrically substituted DTE(OMe)s, the decision was to choose the phenyl-ethinyl compound **142** as starting point for all DTE(OMe)s. Afterwards, the aryl-thiophene **142** should be coupled to the perfluorinated backbone to obtain the working horse molecule **144**.

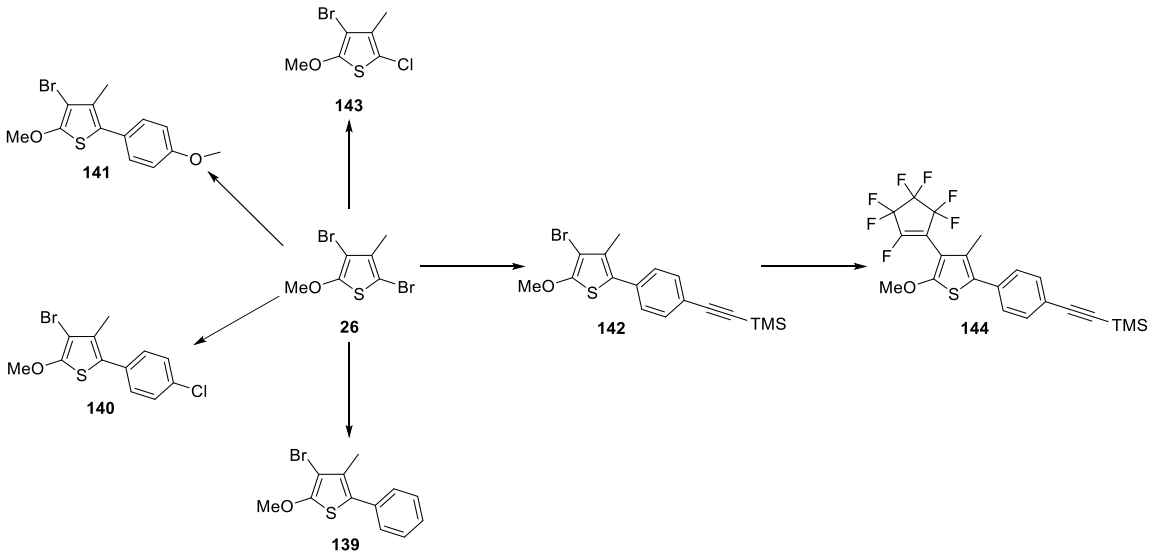

*Figure 78: synthetic approach for the aryl-coupled thiophenes **139-142** and Br-Cl-thiophene **143**, with the subsequently introduction of the perfluorinated backbone for the workhorse molecule **144**.*

For the unsymmetrically substituted DTE(OMe)s the second thiophene-unit is prepared separately, lithiated and coupled to compound **144** to build up unsymmetrically substituted DTE(OMe)-structures **145-148** (Figure 79).

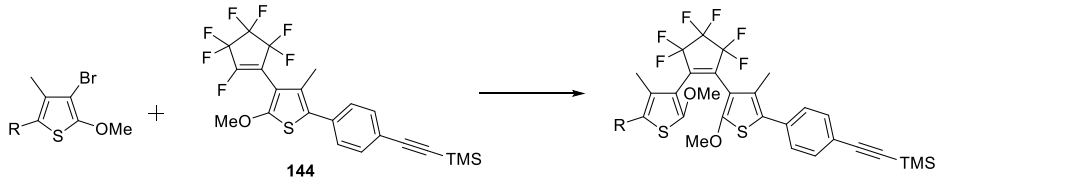

*Figure 79: synthetic approach for unsymmetrically substituted DTE(OMe)s **145-148**.*

To attach different fluorophores, the trimethylsilyl-group of the alkynes **145-148** has to be deprotected and coupled with the BODIPY- (**62**) or BTD-moiety (**137**) afterwards in SONOGASHIRA-coupling reactions (Figure 80).

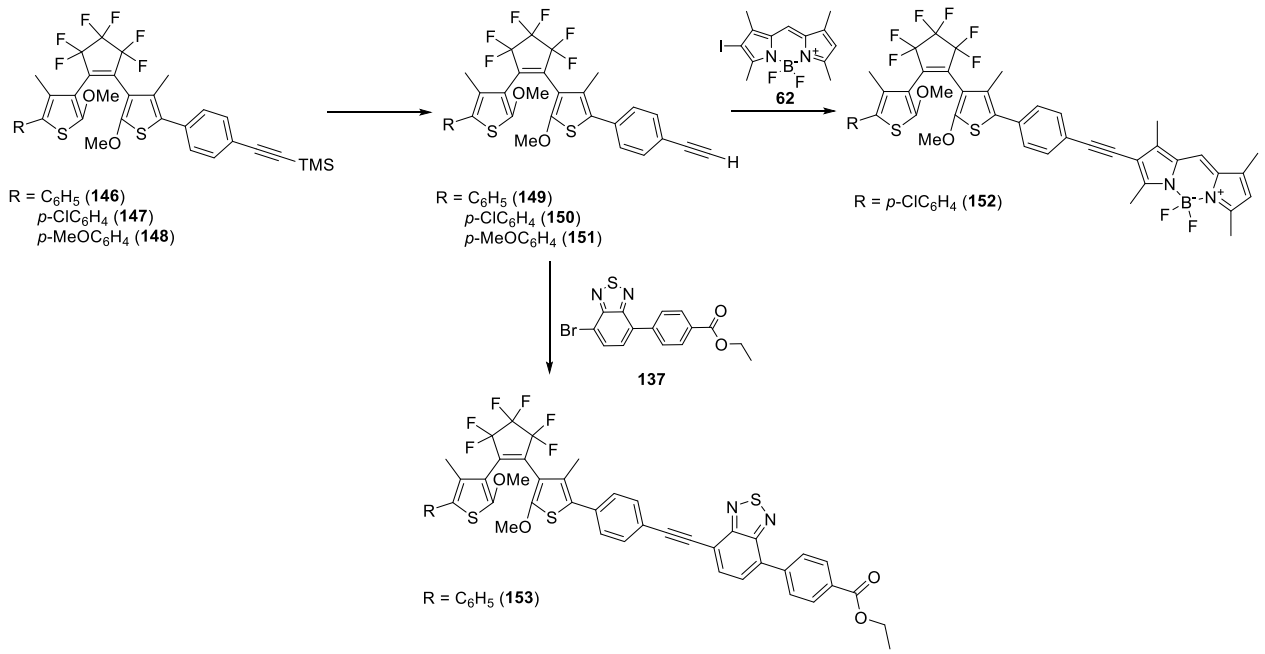

*Figure 80: deprotection of the DTE(OMe)s **146-148** and coupling with fluorophores to DTE(OMe)-BODIPY **152** and benzoate-BTD-DTE(OMe) **153**.*

For the attachment of carboxylic acid groups, a different strategy has to be developed. Herein, the workhorse **144** is coupled with bromo-chloro-thiophene **143** (Figure 78). The chloride in *ortho*-position of **145** is activated and addressable by lithium agents to get converted to the boronic acid (Figure 81). Finally, the boronic acid can be coupled by commercially available aryl-halides in SUZUKI-cross couplings. Deprotection and SONOGASHIRA-coupling with the iodo-BODIPY-fluorophore **62** should give access to conjugates with carboxylic acid groups.

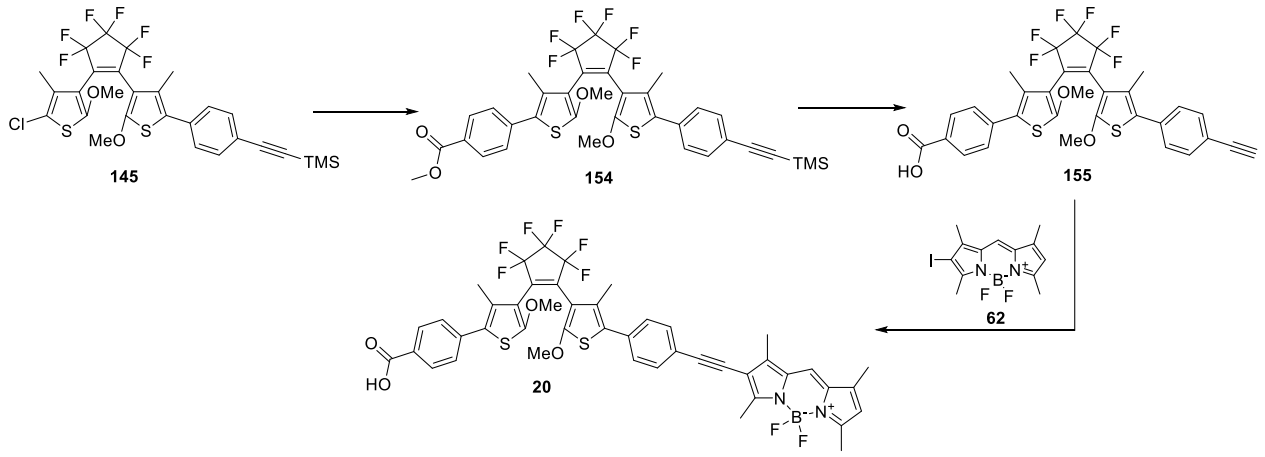

*Figure 81: synthetic approach to DTE(OMe)-BODIPY conjugate **20** with a carboxylic acid anchor group.*

2.2.6.2 Synthesis of ((4-(4-bromo-5-methoxy-3-methylthiophen-2-yl)phenyl)ethynyl)trimethylsilane, 3-bromo-2-methoxy-4-methyl-5-phenylthiophene, 3-bromo-2-methoxy-5-(4-methoxyphenyl)-4-methylthiophene and 3-bromo-5-(4-chlorophenyl)-2-methoxy-4-methylthiophene (139-142)

Due to the similar synthetic approach via a lithiation-boronation-Suzuki-coupling sequence, the synthesis is shown in one figure (Figure 82) Starting from the dibromo thiophene **26** at -78 °C the *ortho*-position of the sulphur in **26** was lithiated and reacted with boronic acid tributyl esters, followed by a SUZUKI-coupling with the different aryl-halides to form thiophene-phenyl **139-142** in moderate to good yields.

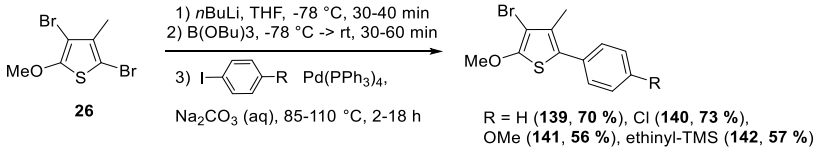

*Figure 82: synthesis of thiophene-aryls **139-142**.*

2.2.6.3 Synthesis of 3-bromo-5-chloro-2-methoxy-4-methylthiophene (143)

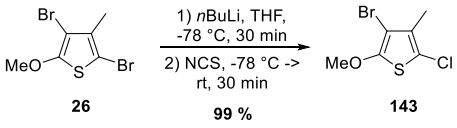

*Figure 83: snthesis of bromo-chloro thiophene **143**.*

The synthesis of the monochlorinated thiophene **143** is done with a lithiation step, followed by the reaction with *N*-chlorosuccinimide in almost quantitatively yield (Figure 83). The product **143** needs to be stored under argon, exclusion of light and in the freezer to avoid decomposition.

2.2.6.4 Synthesis of 4,4'-(perfluorocyclopent-1-ene-1,2-diyl)bis(5-methoxy-3-methyl-2-phenylthiophene) (3)

139 can be lithiated and used in two equivalents for the literature known synthesis of the symmetrical DTE(OMe) **3** (

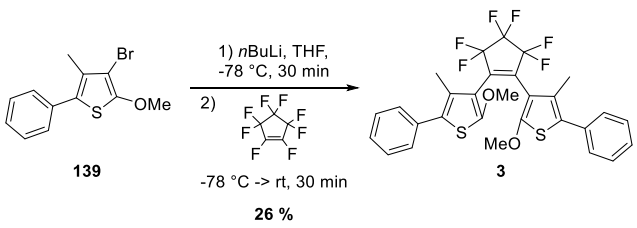

*Figure 84: synthesis of the literature known symmetrical diphenyl-DTE(OMe) **3**.*

2.2.6.5 Synthesis of ((4-(5-methoxy-3-methyl-4-(perfluorocyclopent-1-en-1-yl)thiophen-2-yl)phenyl)ethynyl)trimethylsilane (144)

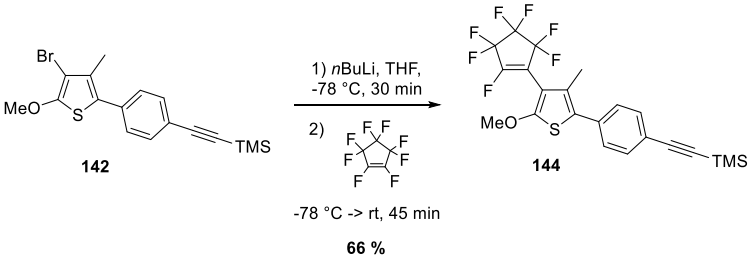

*Figure 85: synthesis of the working horse **144**.*

The introduction of the perfluorinated backbone was done in the same way, as for the symmetrical DTE(OMe)s **28-29** (Figure 85, for mechanism see Figure 44), but with less than one equivalent of bromo-thiophene **142**. The yield is with 66 % moderate and the product **144** can be easily purified by column chromatography on silica.

2.2.6.6 ((4-(4-(2-(5-Residue-2-methoxy-4-methylthiophen-3-yl)-3,3,4,4,5,5-hexafluorocyclopent-1-en-1-yl)-5-methoxy-3-methylthiophen-2-yl)phenyl)ethynyl)trimethylsilans (145-148)

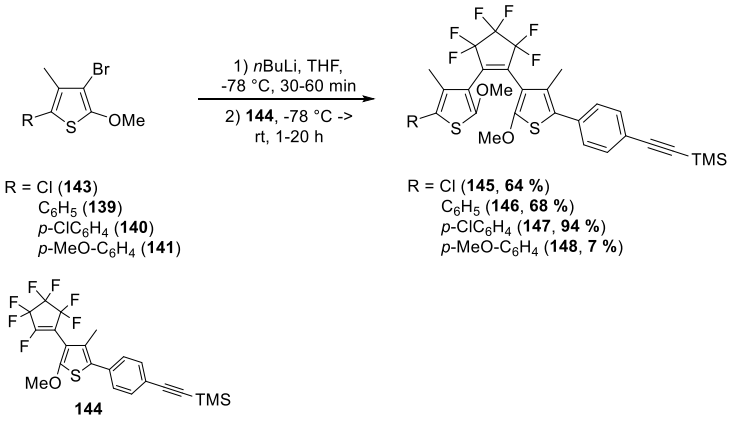

*Figure 86: synthesis of the unsymmetrically substituted DTE(OMe)s **145-148**.*

The synthesis of the unsymmetrically substituted DTE(OMe)s **145-148** starts from the different R-substituted thiophene units **139-141** and **143**, with R = chloro, phenyl, *para*-methoxy-phenyl and *para*-chlorophenyl-substituted (Figure 86). The yield is high for the chloro-substituted compound **147** with 94 %, moderate for phenyl-substituted **146** and chloro-substituted **145** with 68 % and 64 %, respectively, and low for methoxy-phenyl-substituted **148** with 7 %. The low yield of the methoxy-substituted compound

148 can be explained by the sophisticated work-up via column chromatography, since the debrominated starting material (**141**) and the product **148** have almost the same *Rf* value in all tested solvents. The synthesis of the methoxy-substituted compound **148** was canceled, due to the time-consuming reactions and work-up under red-light and the lack of anchor groups for further investigations on surfaces.

2.2.6.7 Synthesis of 2-(4-chlorophenyl)-4-(2-(5-(4-ethynylphenyl)-2-methoxy-4-methylthiophen-3-yl)-3,3,4,4,5,5-hexafluorocyclopent-1-en-1-yl)-5-methoxy-3-methylthiophene, 2-(4-ethynylphenyl)-4-(3,3,4,4,5,5-hexafluoro-2-(2-methoxy-4-methyl-5-phenylthiophen-3-yl)cyclopent-1-en-1-yl)-5-methoxy-3-methylthiophene (149-150)

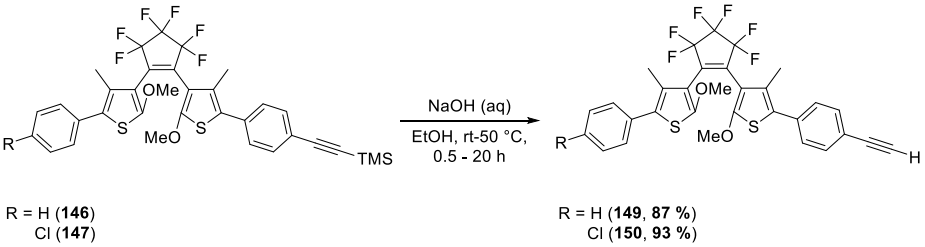

*Figure 87: deprotection of **146** and **147** under basic conditions to yield **149** and **150**.*

The trimethylsilyl-deprotections were done under basic conditions at room temperature for 30 min in high yields of 87 % for **149** and at 50 °C for 20 h with 93 % yield for **150** (Figure 87). The common deprotection method with fluoride-agents was not investigated, due to the already high yields in the easy controllable basic conditions.

2.2.6.8 Synthesis of 2-((4-(4-(2-(5-(4-chlorophenyl)-2-methoxy-4-methylthiophen-3-yl)-3,3,4,4,5,5-hexafluorocyclopent-1-en-1-yl)-5-methoxy-3-methylthiophen-2-yl)phenyl)ethynyl)-5,5-difluoro-1,3,7,9-tetramethyl-5H-5λ⁴,6λ⁴-dipyrrolo[1,2-c:2',1'-f][1,3,2]diazaborinine (152)

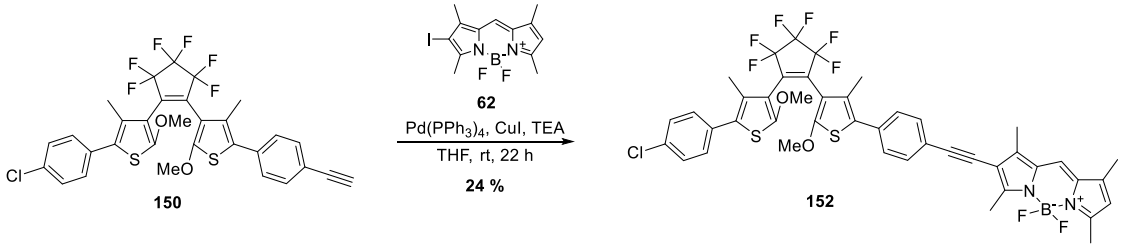

*Figure 88: SONOGASHIRA-cross coupling of **150** with iodo-BODIPY **62** to DTE(OMe)-BODIPY **152**.*

The final SONOGASHIRA-coupling yielded the chloro-DTE(OMe)-BODIPY **152** in a low yield of 24 % (Figure 88). Investigations with different ratios of THF to TEA, higher temperature, longer reaction time, more

catalyst, did not led to more product, but increased the amount of decomposed BODIPY. Since the starting materials **150** and **62** could be received back, the method was not changed in this reaction and further similar reactions were carried out.

2.2.6.9 Synthesis of ethyl 4-(7-((4-(4-(3,3,4,4,5,5-hexafluoro-2-(2-methoxy-4-methyl-5-phenylthiophen-3-yl)cyclopent-1-en-1-yl)-5-methoxy-3-methylthiophen-2-yl)phenyl)ethynyl)benzo[c][1,2,5]thiadiazol-4-yl)benzoate (153)

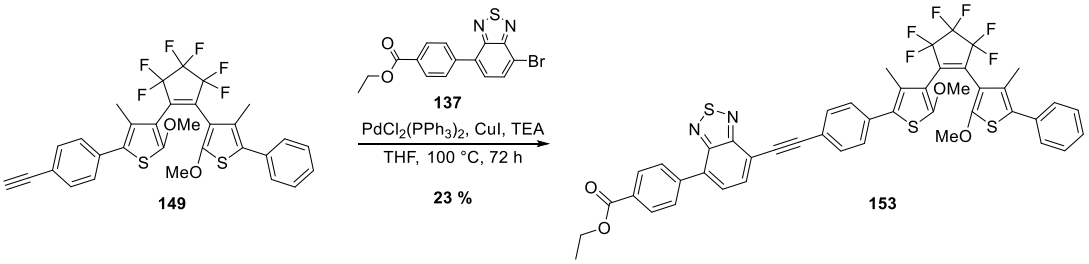

*Figure 89: SONOGASHIRA-cross coupling of **149** with BTD-compound **137** to BTD-DTE(OMe) **153**.*

The Sonogashira-coupling of the DTE(OMe) **149** with the BTD-benzoate **137** yielded the ester **153** of the final BTD-DTE(OME) conjugate **23** in low yield of 23 % (Figure 89). The ester allowed a better purification of the DTE(OMe)-BTD conjugate, than the final carboxylic acid **23** and its dimeric aggregate. Therefore, several purification steps with cholumn chromatography were done.

2.2.6.10 Synthesis of 4-(7-((4-(4-(3,3,4,4,5,5-hexafluoro-2-(2-methoxy-4-methyl-5-phenylthiophen-3-yl)cyclopent-1-en-1-yl)-5-methoxy-3-methylthiophen-2-yl)phenyl)ethynyl)benzo[c][1,2,5]thiadiazol-4-yl)benzoic acid (23)

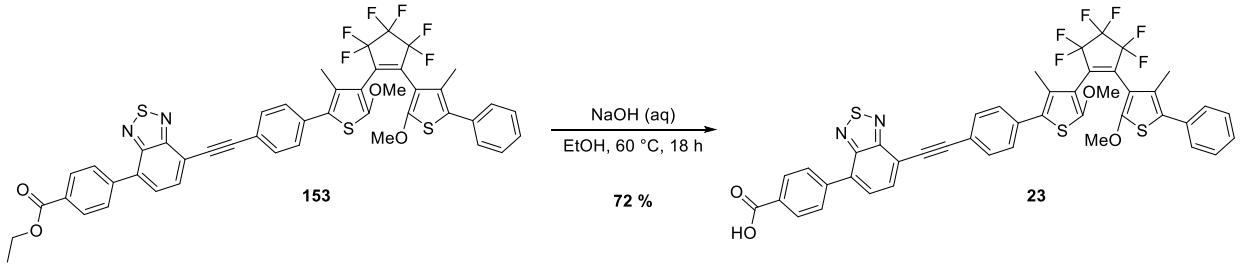

*Figure 90: ester-cleavage of BTD-DTE(OMe) **153** to the final compound **23**.*

The ester cleavage of benzoate-BTD-DTE(OME) **153** to **23** was done under basic conditions with NaOH in ethanol (Figure 90). The yield is moderate with 72 % for this kind of reactions. Because of the low amount of the starting material **153**, the reaction conditions were not optimized further.

2.2.6.11 Synthesis of methyl 4-(4-(3,3,4,4,5,5-hexafluoro-2-(2-methoxy-4-methyl-5-(4-((trimethylsilyl)ethynyl)phenyl)thiophen-3-yl)cyclopent-1-en-1-yl)-5-methoxy-3-methylthiophen-2-yl)benzoate (154)

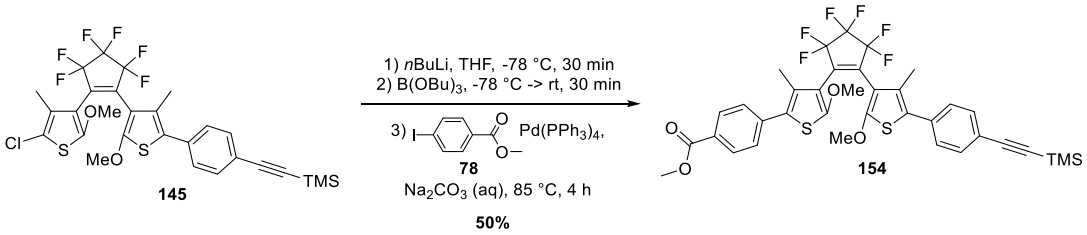

*Figure 91: arylation of DTE(OMe) **145** in a SUZUKI-cross coupling to **154**.*

The chloro-functionality of the DTE(OMe) **145** can be lithiated and converted to a boronic acid with tributyl boronic acid ester. Further SUZUKI-cross coupling with *para*-iodo benzoate **78** led to the DTE(OMe) **154** in moderate yield of 50 % (Figure 91). The temperature and time control of this reaction was important, since the lithiated thiophene of **145** can cleave the TMS-groups, if kept to long before quenching with the boronic acid ester.

2.2.6.12 Synthesis of 4-(4-(2-(5-(4-ethynylphenyl)-2-methoxy-4-methylthiophen-3-yl)-3,3,4,4,5,5-hexafluorocyclopent-1-en-1-yl)-5-methoxy-3-methylthiophen-2-yl)benzoic acid (155)

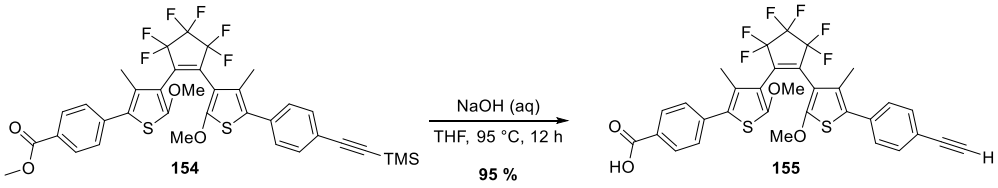

*Figure 92: deprotection of the **154** TMS- and the methyl ester groups under basic conditions to obtain DTE(OMe) **155**.*

The deprotection of the methyl ester and trimethylsilyl group of **154** was done under basic conditions with NaOH in THF. Heating for 12 h at 95 °C yielded the free ethinyl and carboxylic acid (**155**) group with high yield of 95 % (Figure 92). Because of the difficult work-up of **155** for the next steps due to the high polarity of the carboxylic acid, an orthogonal deprotection should be considered for future syntheses. Cleavage of the TMS-group with fluorination agents like TBAF, or similar reactants would allow to couple the fluorophore and DTE(OMe), and facilitates the purification of the ester. Disadvantage of this strategy is the base labile BODIPY-core, which could be cleaved under nucleophilic base-like conditions employing

NaOH. Because of the low amount of starting material, a further investigation of this strategy was renounced.

2.2.6.13 Synthesis of 4-(4-(2-(5-(4-((5,5-difluoro-1,3,7,9-tetramethyl-5H-5λ⁴,6λ⁴-dipyrrolo[1,2-c:2',1'-f][1,3,2]diazaborinin-2-yl)ethynyl)phenyl)-2-methoxy-4-methylthiophen-3-yl)-3,3,4,4,5,5-hexafluorocyclopent-1-en-1-yl)-5-methoxy-3-methylthiophen-2-yl)benzoic acid (20)

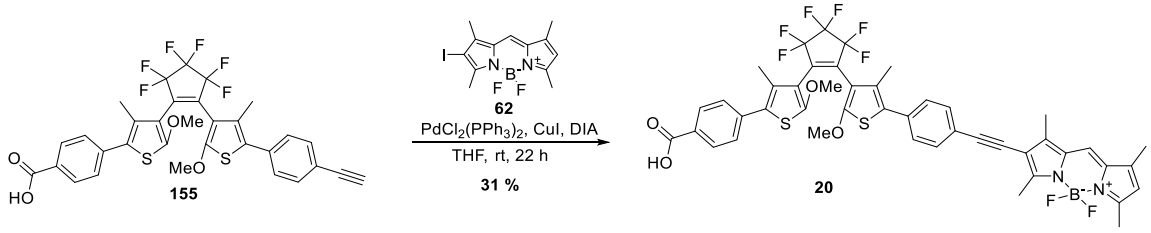

*Figure 93: SONOGASHIRA-cross coupling of DTE(OMe) **155** with iodo-BODIPY **62** to DTE(OMe)-BODIPY **20**.*

The final SONOGASHIRA-cross coupling to the DTE(OMe)-BODIPY **20** was done under the already investigated conditions (Figure 93). Again, an increase of the yield (31 %) was not possible by changing the conditions and due to the low amount of starting material, the strategy of getting back the reactants **155** and **62** in the purification step was not changed.

2.3 DETERMINATION OF THE RATIO OF OF TO CF IN THE PHOTOSTATIONARY STATE

If both photoisomers of the DTE absorbs at the excitation wavelength, a fully conversion of one form into the other is not possible (see chapter 1.1.3). The ratio in the equilibrium is called photostationary state (pss). The predicted ratios of pss in DTE(OMe)s for the cyclization is almost quantitatively, due to the neglectable cycloreversion quantum yield of the CF. The pss for the ring-opening (cycloreversion) is quantitatively in almost all common DTEs, because of the exclusive absorption of the π-π* absorption band of DTE CF in the visible range.

To determine the ratio in the pss, several quantitative analytical techniques can be used, since both photoisomers are thermally stable. The ratio can be determined by analytical HPLC at the isosbestic point, column chromatography (or preparative TLC) and by comparison of the weight of both isomers under light exclusion or by NMR measurements. Since chromatography on silica requires greater amount of substance

and the error bar in NMR measurements is high at low concentrations, due to the signal to noise ratio, HPLC analysis is the most common method for the pss ratio determination.

Therefore, the different polarities of the photoisomers are used to separate the OF from CF, and to integrate their ratio in the UV/Vis-trace at the isosbestic point. In DTE(Me)s the polarity is highly different between the open and the closed-form, based on the formation of a increased π-system in the cyclization step. In the case of DTE(OMe)s, the methoxy-substituents are part of the π-system in the open form and become pushed out of the π-plane in the CF by changing the reactive center from sp^2- to sp^3-hybridization. Therefore, the difference in the polarity is smaller, which requires a sophisticated gradient in the HPLC analysis for approximatively base-line separated peaks.

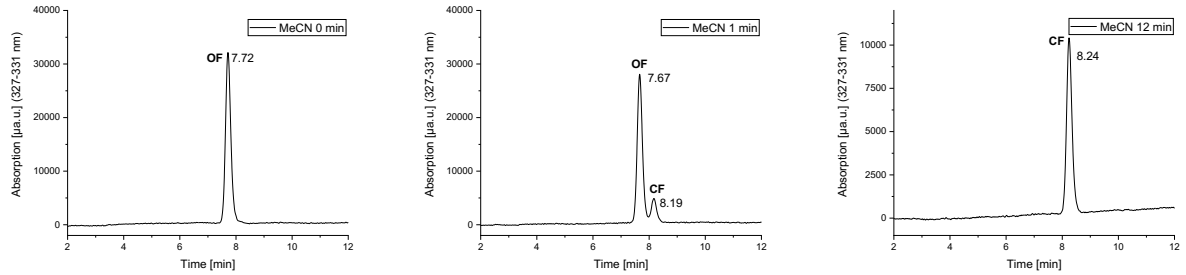

*Figure 94: example chlorophenyl-DTE(OMe) **150** left: start spectra (RT: 7.72 min), middle: after 1 min irradiation (RT: 7.67 and 8.19 min); right: after 12 min irradiation (RT: 8.24 min); MeCN/H_2O (+0.1% HCOOH) 90:10 to 100:0 in 10 min, 0.3 mL/min, detection wavelength 321-331 nm, irradiated with 345 nm LED.*

The UV/Vis-trace of the measurements points out clearly the pure absorption spectra of DTE(OMe) **150** OF and CF, furnishing via integration a ratio of 100:0 (DTE(OMe) **150** CF:OF) in the pss. The mass trace shows the desired molpeak for the molecule in small amount, but in general, the mass spectra of the DTE(OMe) CFs are difficult to receive, based on the low ability of DTE(OMe) CF to ionize.

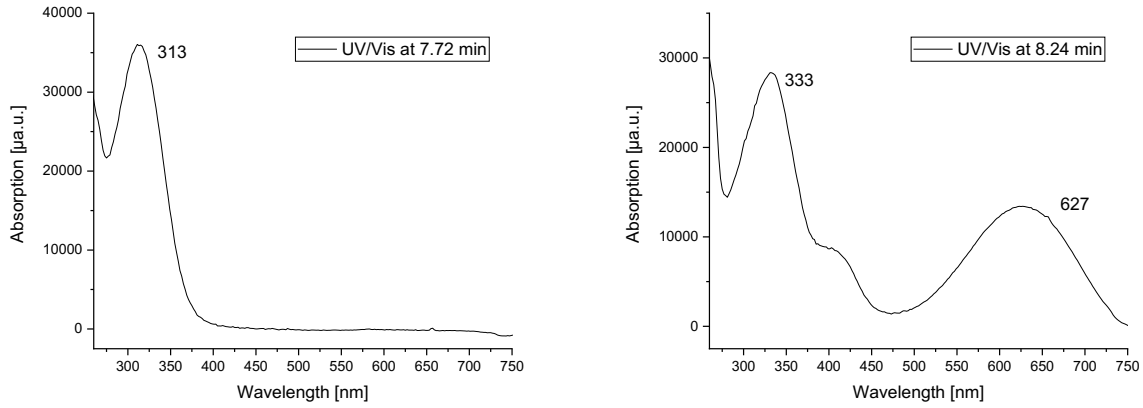

*Figure 95: UV/Vis-spectra via diode-array detector of chlorophenyl-DTE(OMe) **150** in HPLC, left: 0 min irradiation with 345 nm LED in MeCN, (RT: 7.72 min), right: 12 min irradiation with 345 nm LED in MeCN (RT: 8.24 min).*

The results of the determinations for the ratio analysis by HPLC are shown in Table 3. Details for each compounds are shown in the spectra appendix (5.2). A further more nonpolar photoswitchable HPLC peak in DTE(OMe)s with carboxylic anchor group indicates the formation of dimers by aggregation. However, caused by the low ionization in the used mass spectrometry methods the double mass of the monomers are not visible.

Because of the results of quantitatively switching, for further calculations, both photoisomers are assumed to be pure DTE(OMe) OF or CF in the pss. For diiodo-DTE(OMe) **29** the ratio in the pss was not determined, due to the decomposition of the compound under UV irradiation.

*Table 3: ratio of OF to CF in the pss of DTE(OMe)s **20**, **23**, **28**, **145**, **148-150** after irradiation with 345 nm LED in MeCN.*

Compound	**3**	**150**	**148**	**145**	**149**	**20**	**23**
Ratio in pss (CF:OF)	100:0	100:0	decomposition	100:0	100:0	100:0	98:2

2.4 UV/Vis-Spectroscopy

2.4.1 UV/Vis-spectrometer and irradiation

The used spectrometer for the absorption spectra are a *Shimadzu* UV-1601 and an *Avantes* AvaSpec Dual-channel Fibre Optic Spectrometer, equipped with the AvaLight-DH-S-BAL light source (further details, see 4.1.1.6). While UV-1601 used a light beam focused with mirrors, the Avantes spectrometer uses an optical fibre. Optical fibres are highly sensitive to bending, heating up and the permeability is wavelength dependent. In Figure 97, the absorption of the used optical fibre is shown in comparison to the wavelength. High-energy irradiation is almost completely absorbed, therefore this technique is not usable for deep-UV investigations below 170 nm.

The measurements were carried out inside a 10 mm cuvette (Quartz, SUPRASIL, Hellma Analytics). The used cuvettes show a broad permeability from deep UV- (200 nm) up to the IR-region (3000 cm^{-1}) with a transmission of almost 0.9 (Figure 96).

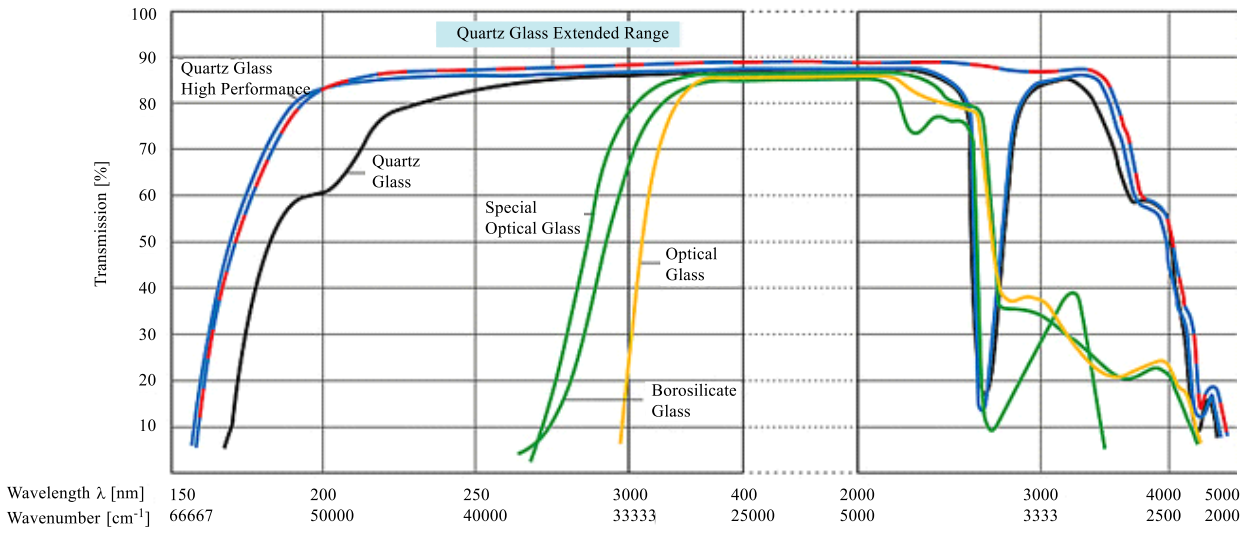

Figure 96: transmission of quartz glass cuvettes (spectra from Hellma Analytics).

The *Avantes* spectrometer records a single UV/Vis spectrum in less than a second (100 spectra stacked, with 2.0 ms integration time) and is therefore faster and more sensitive than the *Shimadzu* spectrometer. Since the used light source is strong enough to switch the DTE(OMe)s during the measurements, a grey

filter (NDUV510B - OD 1.0, transmission spectra, see Figure 97) was used. The grey filter absorbs around 90 % of the incoming light and is made of fused silica substrate.

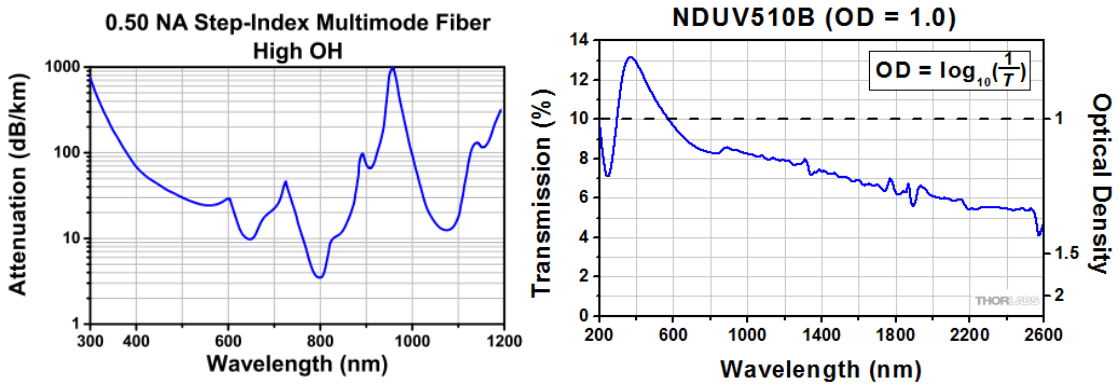

Figure 97: left: attenuation-spectra for the used optical-fibre FP1000URT (spectra from Thorlabs); right: transmission-spectra of the used grey filter (spectra from Thorlabs).

A disadvantage of the filter is the warm-up of the optical element in front of the light source, therefore changing the transmission properties. A cooling fan was set-up but a change in the spectra over time was still visible. Therefore in this thesis, the switching by the measurement was decreased with the usage of a physical shutter and by short time measurements. In the future, a separate filter holder in the fibre optical line would be a better option.

To protect the optical fibres for bending while sample exchange, all flexible parts were strengthened by composite pipes, which are fixed to an aluminium-frame (2, Figure 98). Furthermore, the warm-up of the sample (8) was avoided by connecting the cuvette holder to a temperature control unit (attached to a copper metal plate, 6 + 7) and compressed air tube (9) for cooling while irradiating with LED (5). The mixing was ensured by a self-build external magnetic stirrer (4) below the copper metal plate. Further reduction of bending in the system could be avoided by integrating the whole system in a (for example) perspex box.

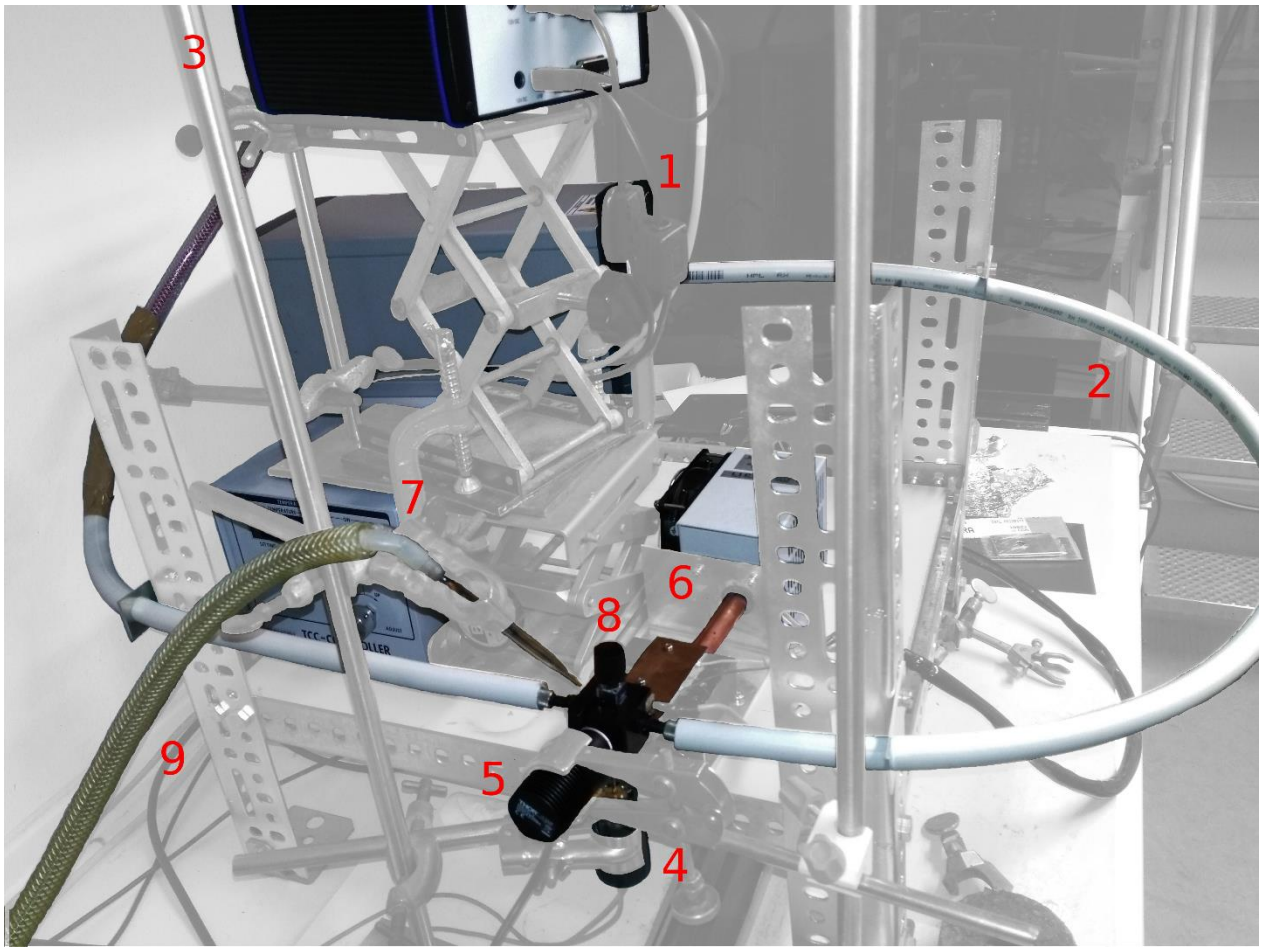

Figure 98: UV/Vis-spectrometer set up with 1) light source; 2) optical fibre in composite pipe; 3) detector; 4) magnetic stirrer; 5) LED; 6) heating-/cooling-unit; 7) temperature control unit; 8) cuvette holder with sample (equiped with stirring bar); 9) pressed air.

For the usage of the *Shimadzu* spectrometer, the sample was irradiated on an optical bench. The irradiation in the ultraviolet region (326 nm, 2.0 mW/cm^2) was made with a high-pressure mercury lamp (200 W, 200 HBO, *Osram*) and a suitable filter. The infrared irradiation heating was reduced by a water-cooled infrared-filter, focused and directed through a cuvette made of quartz-glass equipped with a magnetic stirring bar. For the *Avantes* spectrometer, the irradiation was produced by using LEDs from Thorlabs. The half-widths of these LEDs are higher, the emission spectra is not symmetrical (emission spectra, see Figure 158), but the light sources are cheap (300-800 nm), reproducible, easy to handle and the lifetime for the LEDs are up to >100.000 h. The availability of those LEDs over the last decades made them highly interesting for all light-applications.

The visible irradiation for the sample preparation to use the *Shimadzu* spectrometer (edge filter, >500 nm, 8.3 mW/cm^2) was produced by a xenon lamp (1000 W, 1000 XBO, *Osram*) and an edge filter, since the quantum yields of DTE(OMe)s are so low (determination of quantum yields, see 2.4.4). The visible

irradiation times for the cycloreversion of DTE(OMe)s are still up to 3 h with the usage of the xenon lamp with edge-filter, while the irradiation times with suitable LED (632 nm, 250 mW/cm^2) for the *Avantes* spectrometer-measurements is less than 1 h.

Table 4: light intensities of the LEDs in different distances (d).

LED	*d* (Photometer ↔ LED)	
	< 1 cm [$\frac{mW}{cm^2}$]	2 cm [$\frac{mW}{cm^2}$]
345 nm	11	2.0
632 nm	250	190

Light intensities were determined by using a Photometer *International Light* IL-1400. The intensities were measured directly (distance <1 cm) and through a scheme (representative to the irradiation in the cuvette holder; distance ~2 cm) and are listed in Table 4. The intensities are highly depending on the angle between photometer and LED.

2.4.2 Set-up for NMR-irradiation

The invention of thin optical fibres in reproducible qualities and the amount of usage in applications nowadays, gives possibilities of introducing those fibres into a NMR-spectrometer. Next to irradiation the whole UV/Vis-irradiation and detection can be transferred into the sample by optical fibres.[81] Advantages using NMR-irradiation technique is the clear assignment of different isomers of the photoswitch and the temperature control up to 170 K (solvent dependent). Disadvantages are the higher concentration (10^{-4} M) in comparison to UV/Vis (10^{-5} M), the long recording time (5-15 s for a single spectra) and no possibility of sample stirring.

In our work-group, the development for fast measurements in deep-cooled samples is important for the investigation of ultrafast switches (napthopyrans, hemithioindigos, azobenzoles (Figure 2)) with thermal relaxation pathways and short thermal life-times. Literature known set-ups for these kind of irradiations were adapted and introduced in our group-techniques.[82]

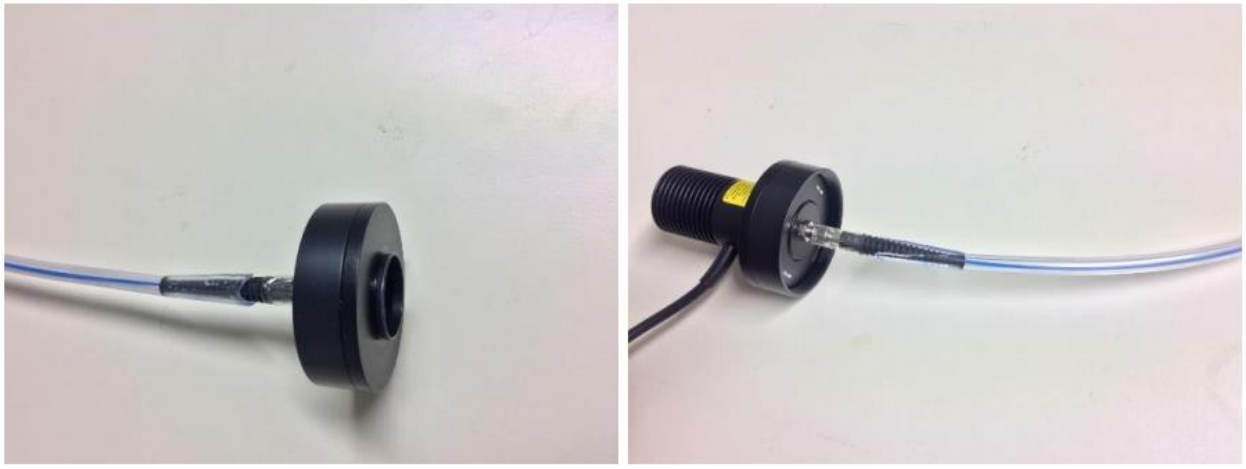

Figure 99: set-up for an irradiation through an optical-fibre by LEDs (pictures from PhD Thesis of Marina-Vlacjić).

A 6 m optical fibre was attached to the Thorlabs LEDs by using different adapters (*Thorlabs*) for a reproducible input of the irradiation in the fibre. Since a LED is not a point source, the coupling to a fibre with as low as possible intensity loss is challenging. For the reproducibility the distance and the angle between the fibre and the light source has to be kept constant. The supplier of the LEDs offers therefore adapters with screw threads for the attachment of optical elements to the LEDs (Figure 99).

The fibre was protected against breaking by coating into rubber tubes. The plastic cover of the fibre was removed for 5 cm and the tip of the fibre, going into the NMR-tube, was sand-blasted for roughening the glass tip (Figure 100). In the end, a reproducible light intensity could be generated which was dispersed by the roughened fibre. The tip was attached to a NMR-tube insert made from quartz-glass with an absorption <300 nm and placed into the NMR-tube with the sample. The tube was stacked into a spinner equipped with a brass ring (*rototec-spintec GmbH*) to protect the NMR-machine from broken glass tubes by a broken connection of the fibre to the glass. The sample was carefully inserted in the NMR-machine and the measurement was started. The important avoiding of magnetic material surrounding the NMR-machine was ensured by the length of the optical fibre.

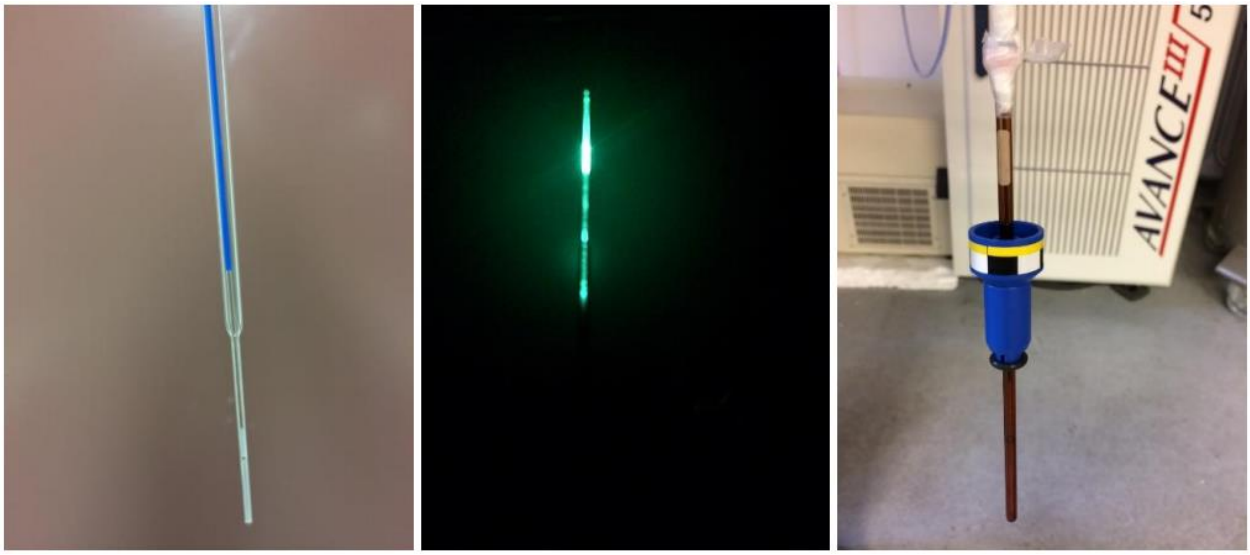

Figure 100: self-made set-up for an in-situ irradiation of a NMR-sample; left: sandblasted tip in the coaxial insert; middle: 505 nm LED light through the optical fibre; right: brown-glass NMR tube connected to the insert and the fibre attached with a NMR-spinner (pictures from PhD Thesis of Marina-Vlacjić).

The light intensity dropped by factor >0.99 for UV-irradiation, therefore a stronger 365 nm LED was attached to the fibre. Based by the low sensitivity of the cyclization reaction of DTE(OMe)s in the 365 nm range, this technique is not suitable for DTE(OMe) investigations. First investigations (*para*-methoxyphenyl-DTE(OMe) **148**) led to switching times of >6 h for cyclization in a 10^{-4} M concentration in $CDCl_3$ with 345 nm LED (7 µW/cm^2, change of the NMR-spectra see Spectra Appendix 5.2). In the future, stronger light-sources in the range of <350 nm will allow the analysis of the switching process of DTE(OMe)s with NMR-technique. Connected with the possibility of UV/Vis-recording *in situ*, this tool could give a powerful insight in molecular processes.

2.4.3 Extinction coefficients

The molar extinction coefficient is an intrinsic property of how strong a chemical species absorbs light at a given wavelength. The unit is $\frac{L}{mol*cm}$ and the value is dependent of the solvent, the temperature and the used wavelength. The value can be determined by plotting the absorption of a solution at a given wavelength against the concentration (Lambert-Beer, Eq. 2). The slope of the resulting line is the extinction coefficient.

For the determination of the extinction coefficients in this thesis, all compounds were measured in three different concentrations and plotted in the described way.

2.4.4 Quantum yields

If a light quantum with a suitable energy is absorbed by a molecule, an isomerization or chemical reaction can be induced. The possibility of a photon causing a single transformation of the molecule is called quantum yield.

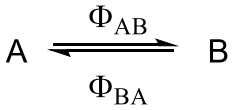

Figure 101: two-state system with interconversion by two different energies.

For a two-species transformation (A to B and *vice versa*, Figure 101) without thermal relaxation, the quantum yield can be determined by using the formula for the initial slope method:[83]

Eq. 5
$$\frac{dA^{obs}(t)}{dt} = -1000 * I_0 * \left(1 - 10^{-A'(0)irr}\right) * l * \varepsilon_B^{obs} * \Phi_{AB}$$

The change of the observed absorption A^{obs} (in DTEs the change of the visible range CF band) over the time correlate with: a) the molar intensity of the light source I_0 and its absorption by the sample at the irradiation wavelength $A'(0)irr$ (with $A'(0)irr = c_A \cdot l \cdot \varepsilon_A$), b) the length of the light through the sample l in cm, c) the extinction coefficient at the observation wavelength ε_B^{obs} and d) with the quantum yield of the

photoisomerization Φ_{AB}. Due to the unit conversion from the standard units, a correction factor of 1000 is used. The cuvettes are normed to 1.0 cm, therefore the length can be shortened as well.

This calculation involves a known starting concentration and the change of the observed absorption can be directly assigned to one of the species. Furthermore the equation is only applicable when the back reaction at the irradiation wavelength is neglectable and the absorption at the irradiation wavelength is the same over the whole observation period and independent of the formed species.

These criteria have been met in the first 10 % of the conversion, which gives the name for the method. The calculations in detail for the investigated DTE(OMe)s can be followed in chapter Appendix Calculations 5.3.

The error bars for the quantum yields are high, due to errors in the weighting of the sample (5 %), signal-to-noise ratio for infinitesimal short time slice (min 5 %), mixing of the sample by fast stirring, distribution or aggregation of CF or OF, reproducibility of light intensity (10 %) and the switching by the light source of the spectrometer itself.

Modern machines are able to separate the irradiation-beam and count the number of photons by a reference subtracted by the number of photons absorbed in the sample. A simple plotting of absorption over time shows an exponential function, where the slope in the beginning is the quantum yield of the photoisomerization. Those quantum yield determination machines are used for DTEs frequently in asian groups. To my knowledge this kind of machines (Shimadzu QYM) are not available on the european market.

2.4.5 Spectra of DTE(OMe)s 3, 29, 145, 147-149 and 155

2.4.5.1 Symmetrical DTE(OMe)s

The investigation of spectroscopical properties of unsymmetrically substituted DTE(OMe)s is sophisticated due to the overlap of the residues in the absorption spectra. Therefore, all synthesized DTE(OMe)s were measured for a better understanding of different structure motifs influence on the position and form of the absorption bands, the extinction coefficients and the quantum yields in the switching process. The absorption spectra after different irradiation times are presented in the UV/Vis-spectra appendix (chapter 5.2). Herein the position of the band-maxima and differences between DTE(OMe) OF and CF are discussed.

Starting from the literature known symmetrical DTE(OMe)s diiodo-DTE(OMe) **29** and diphenyl-DTE(OMe) **3** (Figure 102), diiodo-DTE(OMe) **29** was analysed with the *Shimadzu* spectrometer and irradiated with a Mercury and Xenon lamp for 326 nm and a >500 nm (edge filter, for details, see 4.1.1.6)., while DTE(OMe) **3** was investigated with the *Avantes*-spectrometer with 345 and 632 nm LEDs.

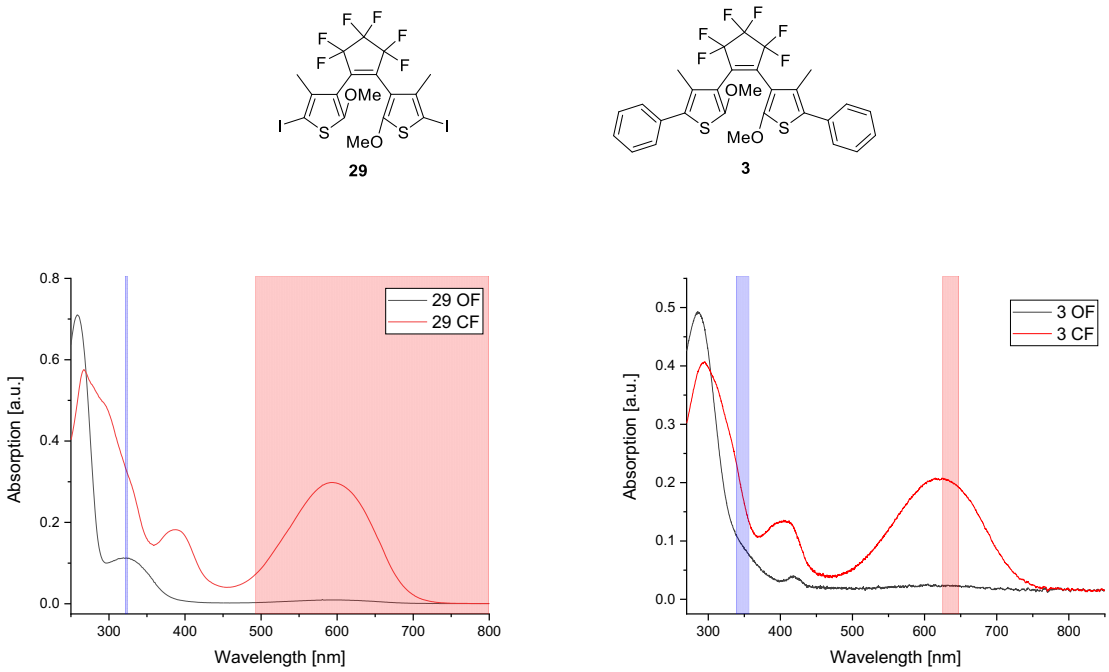

*Figure 102: top: structures of diiodo-DTE(OMe) **29** and diphenyl-DTE(OMe) **3**; bottom: left diiodo-DTE(OMe) **29** 4.0·10^{-5} M in MeCN absorption spectra of OF (grey) and CF (red). OF irradiated at 326 nm (blue area, 2.0 mW/cm^2). CF irradiated with >500 nm (red area, 8.3 mW/cm^2); right: diphenyl-DTE(OMe) **3** 1.8·10^{-5} M in MeCN absorption spectra of OF (grey) and CF (red). OF irradiated at 345 nm (blue area, 2.0 mW/cm^2). CF irradiated with 632 nm (red area, 250 mW/cm^2).*

DTE(OMe) **29** and **3** OFs show a dominant absorption band at 259 nm and 286 nm respectively. This region usually can be assigend to thiophene and phenyl-absorption. A further red-shifted absorption band with low extinction can be assigned for lower singlet transition (S_0->S_1). With UV-irradiation into the thiophene- and phenyl-moiety absorption band, the DTE(OMe) **29** and **3** CFs are formed. A broad absorption band in the visible part of the spectra around 600 nm increases, which can be assigned as DTE(OMe) π-π* absorption. Furthermore, the absorption bands below 300 nm decrease, with an increase for the lower energy absorption band around 400 nm. This behaviour is typical for DTEs. Due to the smaller π-system, the absorption bands of diiodo-DTE(OMe) **29** are hypsochromically shifted and the extinction coefficients are lowered in OF and CF. The back reaction (cycloreversion/ring-opening), was done with visible irradiation to excite the DTE(OMe) CF π-π* absorption band only. Since diiodo-DTE(OMe) **29** showed decomposition over several irradiation cycles under 345 and 365 nm irradiation (see spectra appendix 5.2),

quantum yields were not determined. However, since diiodo-DTE(OMe) **29** was the first DTE(OMe) compound synthesized in our group, we were interested about the IR signature of the two photoisomers of **29** (OF and CF) for future read-out applications on surfaces (see Spectra Appendix 5.2). Usually the IR differences of symmetrical unsubstituted DTE isomers are not well separated. Nevertheless, the two photoisomers of **29** can be easily distinguished by IR-spectroscopy, based on the differences for the methoxy-groups.

The pss ratio of diphenyl-DTE(OMe) **3** CF:OF in MeCN under 345 nm irradiation was determined to be 100:0 (spectra appendix 5.2). The literature known diphenyl-DTE(OMe) **3** quantum yields (QY_{OC} $4.6 \cdot 10^{-1}$, QY_{CO} $1.3 \cdot 10^{-4}$) in MeCN with UV-irradiation of 313 nm and visible irradiation of 575 nm are higher, in comparison to the determined values (Table 5).[29] DE MEIJERE et al. described photodecomposition for DTE(OMe) **3** within UV-irradiation, which could not be confirmed in our measurements with 345 nm irradiation in five switching cycles (see spectra appendix 5.2). An irradiation into the absorption band maxima would increase the QY, but increases photodecomposition at the same time. Therefore all UV-irradiations were carried out with the 345 nm LED.

*Table 5: absorption properties (λ_{max}, ε and λ_{iso}) and cyclization (QY_{OC}) and cycloreversion quantum yields (QY_{CO}) of DTE(OMe) **29** and **3** in MeCN.*

Compound	Open form		Closed form		
	λ_{max} [nm] (ε [10^4 L/(mol·cm)])	QY_{OC}[ac]	λ_{max} [nm] (ε [10^4 L/(mol·cm)])	QY_{CO}[bc]	λ_{iso} [nm]
29	259 (1.78), 325	-	270 (1.44), 389, 594 (0.75)	-	270
3	286 (2.74), 417	$1.5 \cdot 10^{-1}$	292 (2.25), 405, 624 (1.16)	$1.1 \cdot 10^{-4}$	303

λ_{max}: absorption maxima, QY_{OC}: cyclization quantum yield, QY_{CO}: cycloreversion quantum yield, ε: extinction coefficient

[a] Irradiated with 345 nm. [b] Irradiated with 632 nm. [c] Determined using the initial slope method.

In sum, the literature reported absorption properties of DTE(OMe)s **3** in MeCN were confirmed.[29] The maximum of the diphenyl-DTE(OMe) **3** CF is with 624 nm red-shifted compared to the diphenyl-DTE(Me) **1** with 572 nm, the QY_{OC} of DTE(Me) and DTE(OMe) is similar but the cycloreversion is highly unfavourable by excitation with visible light, resulting in the expected low QY_{CO}. Diphenyl-DTE(OMe) **3** showed a nearly quantitatively ratio in the pss for both OF and CF and fatique resistance over five switching cycles .

2.4.5.2 Nonsymmetrically substituted DTE(OMe)s

The next step is the investigation of the unsymmetrically substituted DTE(OMe)s. Therefore the chloro-DTE(OMe) **145**, *para*-benzoate-DTE(OMe) **155**, *para*-chlorophenyl-DTE(OMe) **147**, *para*-methoxyphenyl-DTE(OMe) **148** and phenyl-DTE(OMe) **149** were compared with each other. The first investigated

DTE(OMe) of this series is *para*-methoxyphenyl-DTE(OMe) **148** using the *Shimadzu* spectrometer from 250-800 nm with irradiation via mercury and xenon lamp with suitable filters. A repetition of the measurements with the *Avantes* set-up was not made.

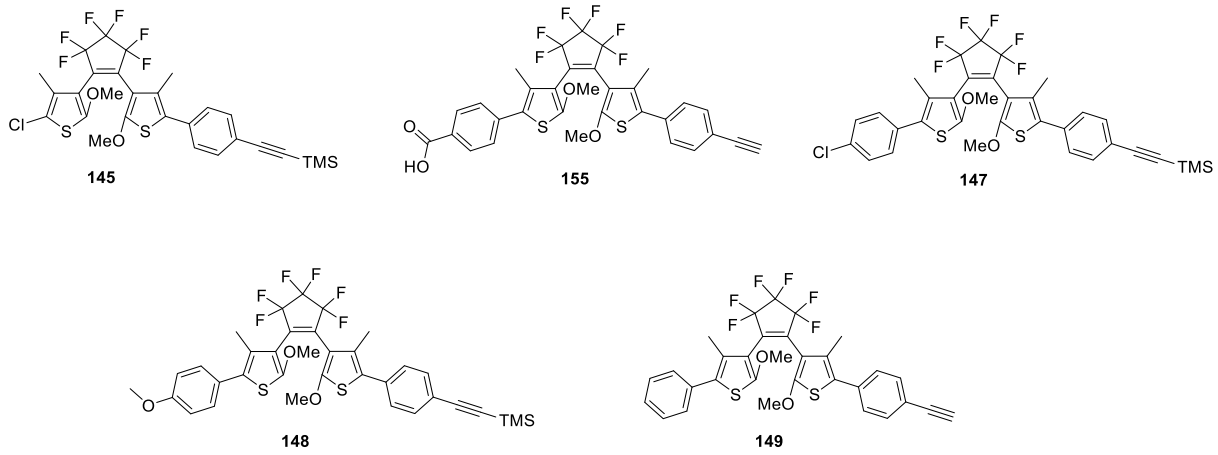

*Figure 103: structures of unsymmetrically substituted DTE(OMe)s **145, 147-149, 155**.*

In general, the absorption spectra of the unsymmetrically substituted DTE(OMe)s **145**, **147-149**, **155** in MeCN show the same absorption band pattern as the symmetrical DTE(OMe)s **3** and **29** with exception of no visible band around 400 nm for methoxy-phenyl-DTE(OMe) **148**. A red-shifting trend of the absorption bands around 310 nm in the order of **148**<**147**<**145**<**155**<**149** for the DTE(OMe) OFs is observable. The decreased π-system of chloro-DTE(OMe) **145** OF shows an exceptional red-shifted absorption band, which is literature known for chloro-DTE(Me) and could be explained by a push-pull interaction (see Figure 104).[17]

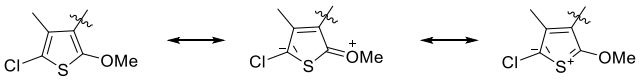

*Figure 104: resonance structures of the chloro-methoxy-thiophene moiety in DTE(OMe) **145**.*

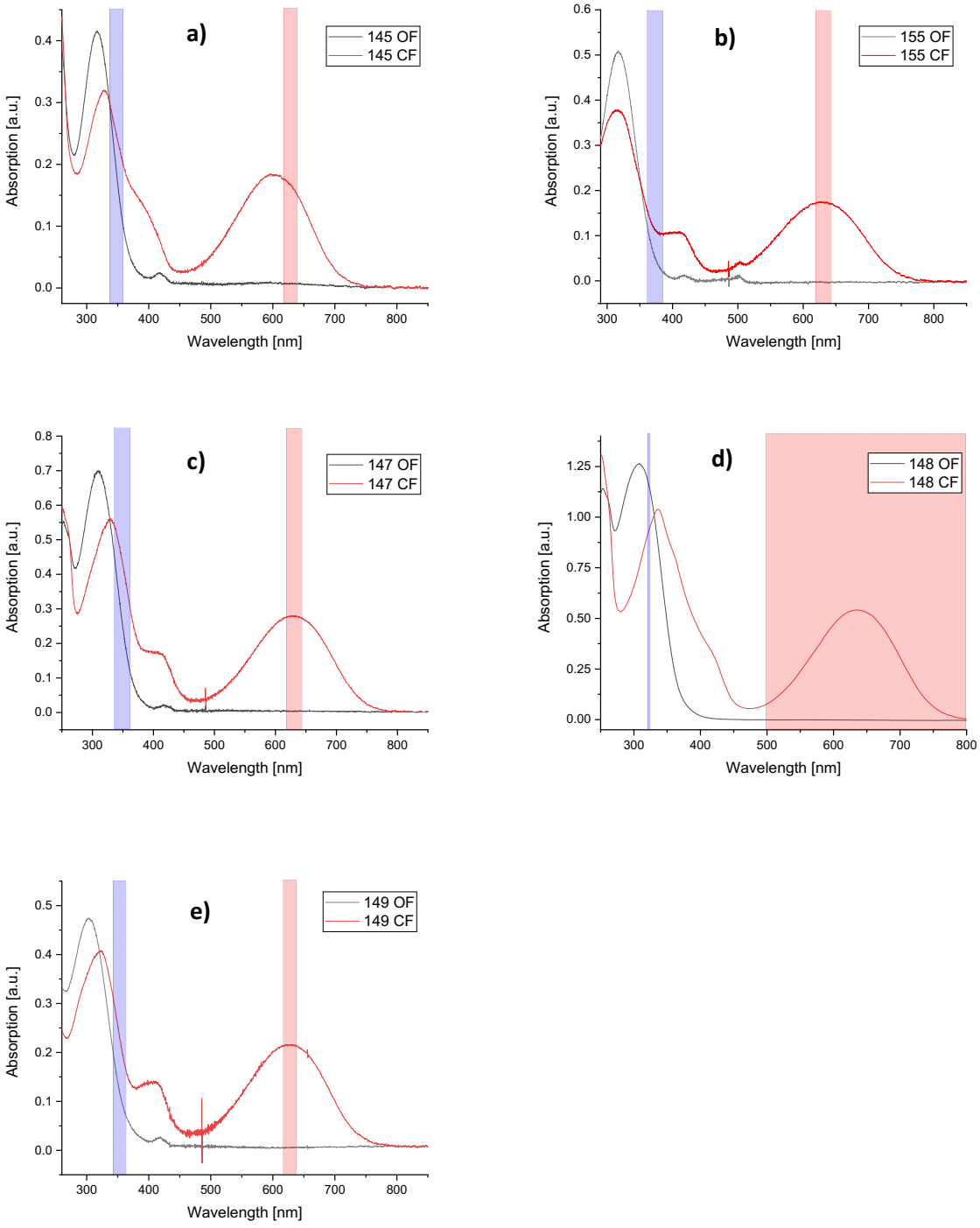

*Figure 105: absorption spectra with irradiation range (cyclization 345 nm blue, cycloreversion 632 nm red) in MeCN; a) chloro-DTE(OMe) **145** with $1.8 \cdot 10^{-5}$ M, b) benzoic acid-DTE(OMe) **155** with $1.8 \cdot 10^{-5}$ M, c) chlorophenyl-DTE(OMe) **147** with $1.8 \cdot 10^{-5}$ M, d) methoxyphenyl-DTE(OMe) **148** ($4.1 \cdot 10^{-5}$ M) with blue (326 nm) and red (>500 nm) irradiation, e) phenyl-DTE(OMe) **149** with $1.8 \cdot 10^{-5}$ M.*

The bathochromic trend for the π-π*absorption band >600 nm of the DTE(OMe)s **145**, **147-149**, **155** CF with increasing π-system in the order of **145**<**149**<**155**<**147**<**148**. This correlates with the size of the π-systems. The extinction coefficients show the smallest values for chloro-DTE(OMe) **145** and the highest for chlorophenyl-DTE(OMe) **147** and are comparable with the symmetrical DTE(OMe) **3** with respect to the increasing π-system (exception chlorophenyl-DTE(OMe) **147**). Upon photoisomerization, the extinction in the phenyl- and thiophene-region is decreased, based on the change of conjugation in the system. All compounds are quantitatively switchable in MeCN (exception methoxy-phenyl-(DTE(OMe) **148**, which was cyclized with higher energy irradiation (326 nm) and showed photodecomposition (see Spectra Appendix 5.2)) with similar quantum yields for the cyclization with 345 nm and the cycloreversion process with 632 nm. The cycloreversion quantum yields are decreased compared to the symmetric diphenyl-DTE(OMe) **3**.

*Table 6: absorption properties (λ_{max}, ε and λ_{iso}) and cyclization (QY_{OC}) and cycloreversion quantum yields (QY_{CO}) of DTE(OMe) **145**, **147-149**, **155** in MeCN.*

Compound	Open form		Closd form		λ_{iso} [nm]
	λ_{max} [nm] (ε [10^4 L/(mol·cm)])	QY_{OC}[ac]	λ_{max} [nm] (ε [10^4 L/(mol·cm)])	QY_{CO}[bc]	
145[ab]	317 (2.31), 417(s)	$2.0 \cdot 10^{-1}$	326 (1.78), 391 (s), 600 (1.02)	$7.1 \cdot 10^{-5}$	337
155[ab]	317 (2.82)	$1.4 \cdot 10^{-1}$	315 (2.10), 411, 629 (0.97)	$4.4 \cdot 10^{-5}$	352
147[ab]	310 (3.88), 416 (s)	$1.2 \cdot 10^{-1}$	329 (3.11), 403, 630 (1.55)	$3.1 \cdot 10^{-5}$	329
148[d]	308 (3.09)	-	336 (2.54), 409 (s), 636 (1.32)	-	331
149[ab]	304 (2.63), 416 (s)	$1.9 \cdot 10^{-1}$	323 (2.25), 405, 629 (1.20)	$5.6 \cdot 10^{-5}$	320

λ_{max}: absorption maxima, QY_{OC}: cyclization quantum yield, QY_{CO}: cycloreversion quantum yield, ε: extinction coefficient

[a] Using 345 nm LED. [b] Using 632 nm LED. [c] Determined via initial-slope method. [d] Using 326 nm and >500 nm irradiation.

Noticeable is a minor blue-shift of the aromatic absorption range between 317 nm in DTE(OMe) **155** OF and 315 nm in **155** CF. Usually, with extending of the π-system, this absorption range shows a bathochromic shift from DTE(OMe) OF to CF.[30] The biggest red-shift was observed for methoxyphenyl-DTE **148** and the biggest blue-shift in this thesis from 310 nm (OF) to 296 nm (CF) was observed for BTD-DTE(OME) **23** (see Figure 106).

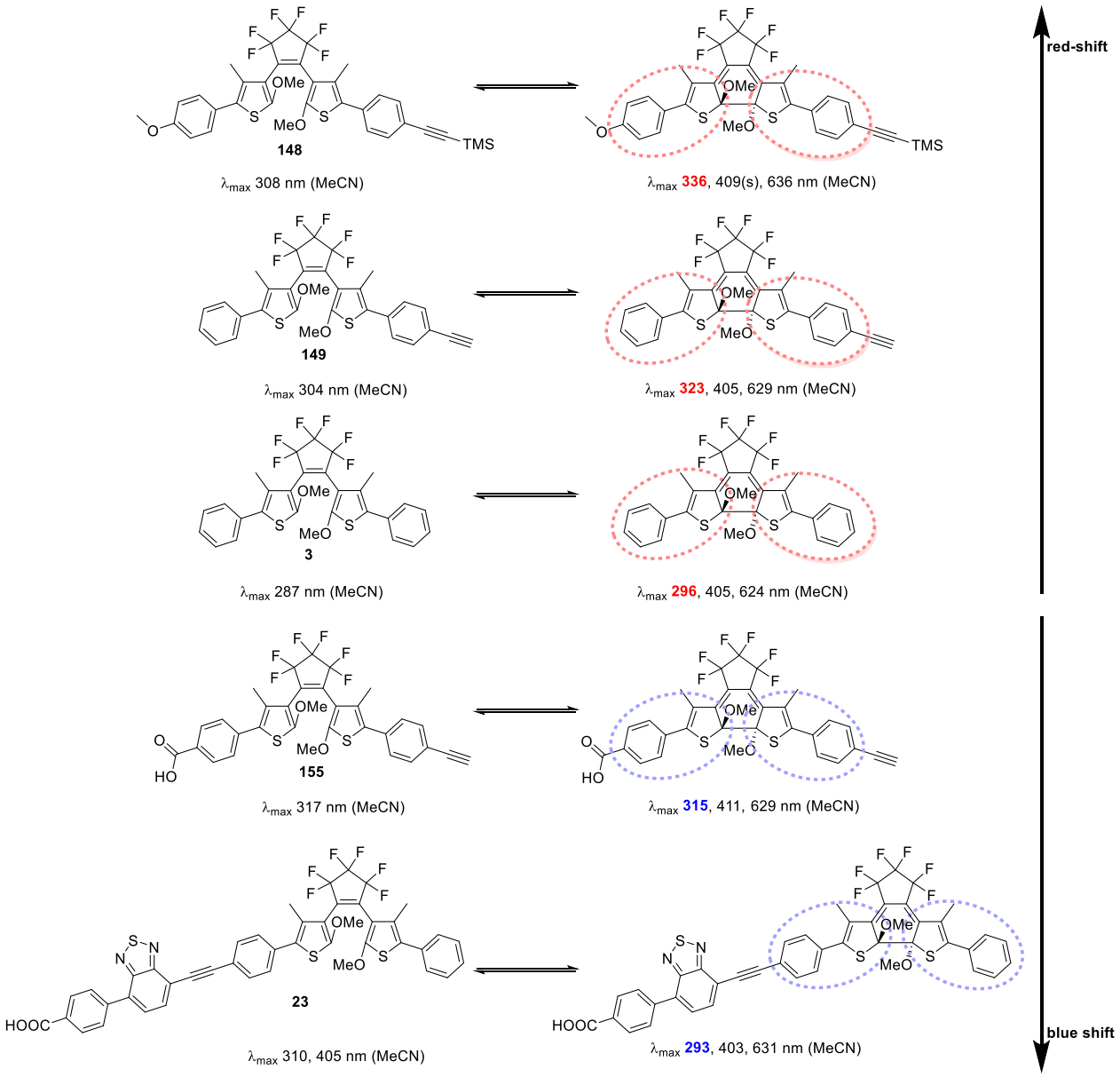

*Figure 106: absorption behaviour of **3, 148-149, 155, 23** OFs and CFs.*

Several published DTEs show the same behaviour, which is not remarked in the literature to the best of my knowledge.[84] All literature known compounds with that behaviour carry a strong electron-withdrawing residue. For a further discussion of this behaviour see chapter 2.6.3.

In sum, the absorption properties of unsymmetrically substituted fully conjugated DTE(OMe)s are influenced by the electronical nature (inductive effects (+I, -I) and resonance effects (+M, -M)) of the attached residues. In DTE(OMe) OFs, an increase in the π-system does not necessarilly show linear dependent bathochromic shifts of the absorption. In DTE(OMe) CFs on the other hand, the absorption spectra show high correlation between the π-system increase and the bathochromic shifts.

2.4.6 Spectra of BODIPYs 4, 156, 62 and 22

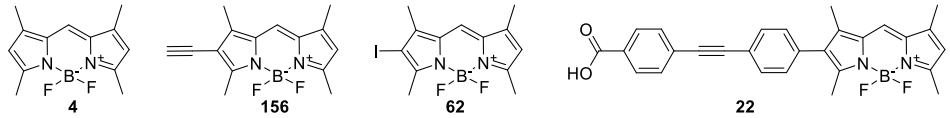

*Figure 107: structures of BODIPYs **4**, **156**, **62**, **22**.*

The literature discussed tetramethyl-BODIPY **4** was analysed by UV/Vis-spectroscopy (Figure 108). A very sharp blue shouldered absorption band at 501 nm with high extinction is visible, which is literature assigned as S_0->S_1 transition band (Table 7) with a hypsochromic shoulder (from vibrational 0-1 transition).[85] A further small absorption band at 361 nm is assigned to higher singlet transitions (S_0->S_2).

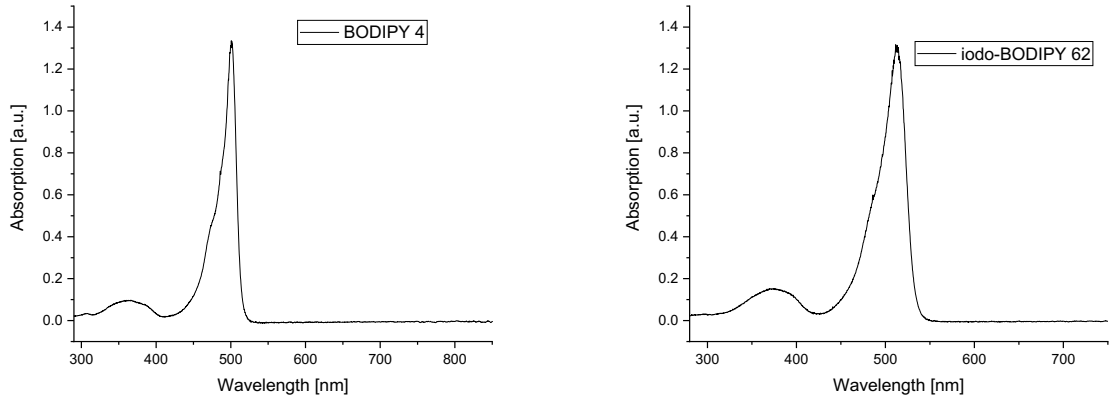

*Figure 108: absorption spectra of left: tetramethyl-BODIPY **4** ($2.0 \cdot 10^{-6}$ M) in MeCN; right: iodo-BODIPY **62** ($1.8 \cdot 10^{-5}$ M) in MeCN.*

With the attachment of iodine in **62** in *β*-position on the BODIPY core, the absorption band pattern stay similar to the BODIPY **4** but a bathochromic shift of 12 nm is observable. Since iodine increases the π-system, and facilitates further relaxation pathways, the extinction coefficient is decreased and the bands appear broadened (see 2.5.3).

With a π-system elongation by an ethinyl-moiety in **156** at the *β*-position of tetramethyl-BODIPY **4** the S_0->S_1 transition band shifts bathochromically by 15 nm. Furthermore, the extinction coefficients are highly lowered, which would hint to a higher degree of flexibility in the molecule. Direct attachment of π-conjugated systems decreases the HOMO/LUMO-gap/ red-shifts the absorption. The synthesis and investigation of ethinyl-BODIPY **156** was part of the diploma thesis of Fanny Schröder in our work group .

With the further enlargement of the π-system in the BODIPY-stick **22**, the main band of BODIPY at 515 nm is bathochromically shifted by 14 nm compared to tetramethyl-BODIPY **4** and a further absorption band at 309 nm appears. Furthermore, the fine-structure of the BODIPY-unit is broadened and the extinction coefficient is compared to tetramethyl-BODIPY **4** lowered by factor 0.33. The absorption band of BODIPY-stick **2** located at 515 nm shows almost no influence of the carboxylic acid tolan on the BODIPY core.[86] The additional broad absorption band at 309 nm indicates the tolan chromophore.

*Table 7: Spectroscopic absorption properties of BODIPYs **4**, **62**, **156** and, **22** in MeCN.*

Compound	λ_{max} [nm]	$\varepsilon_{\lambda max}$ [10^4 L/(mol·cm)]
4	361, 501	8.14 ($CHCl_3$)
62	374, 513	7.33 (MeCN)
156	376, 516	5.78 (MeCN)
22	309, 393, 515	2.67 (MeCN)

λ_{max}: absorption maxima, ε: extinction coefficient

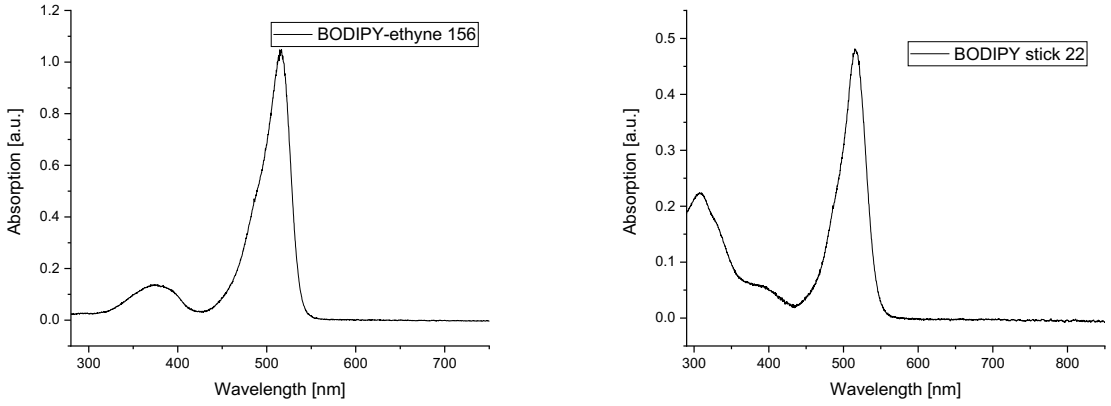

*Figure 109: absorption spectra of left: BODIPY-ethyne **156** with $1.8 \cdot 10^{-5}$ in MeCN; right: BODIPY-stick **22** with $1.8 \cdot 10^{-5}$ M in MeCN.*

Conclusively, with the enlargement of the BODIPY π-system and tune of the flexibility of structures for a suitable π-conjugation, the absorption spectra of BODIPYs can be designed. Attachment of an iodine- (**62**) or ethinyl-unit (**156**) on the *β*-position of BODIPY **4** red-shifts the absorption with simultaneous decrease of the extinction coefficients (Table 7). With the introduction of twisted units in **22**, the expected bathochromic shift of the BODIPY unit can be weakend despite the π-system is highly enlarged. The increase of the BODIPY π-system by attachment of an ethinyl-phenyl unit to the desired DTE(OMe)-BODIPY conjugate **20** (Figure 110), is expected to result in a rigid flattened phenyl-ethyne-BODIPY structure with a further bathochromic shift and moderate extinction of the BODIPY absorption band.

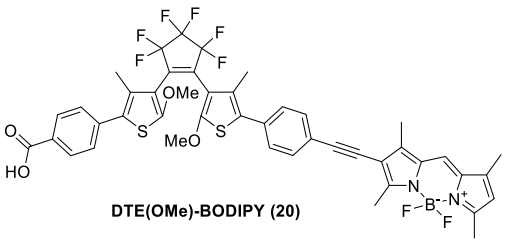

*Figure 110: target DTE(OMe)-BODIPY structure **20**.*

2.4.7 Spectra of NIR-BODIPY 21

The structure is used for the synthetic approach for near infrared BODIPYs to determine the nature of energy transfer in the conjugate, since a FRET-transition would not be possible with no overlap of emission spectra of BODIPY and absorption spectra of the DTE(OMe) CF. The synthesis and analysis of **21** was part of the bachelor thesis of Marta Späth.

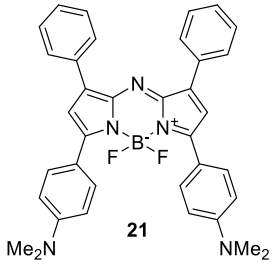

*Figure 111: structure of NIR-BODIPY **21**.*

The absorption spectra of the literature known compound **21** was investigated in toluene and chloroform. In toluene, the BODIPY typical absorption band at 798 nm was detected with a further band at 545 nm with a broad hypsochromic shoulder and an absorption band around 321 nm. NIR-BODIPY **21** carries two dimethylamino groups resulting in pH-sensitivity. A measurement in chlorofom, with small acidic traces leads to three different absorption spectra over time (Figure 112).

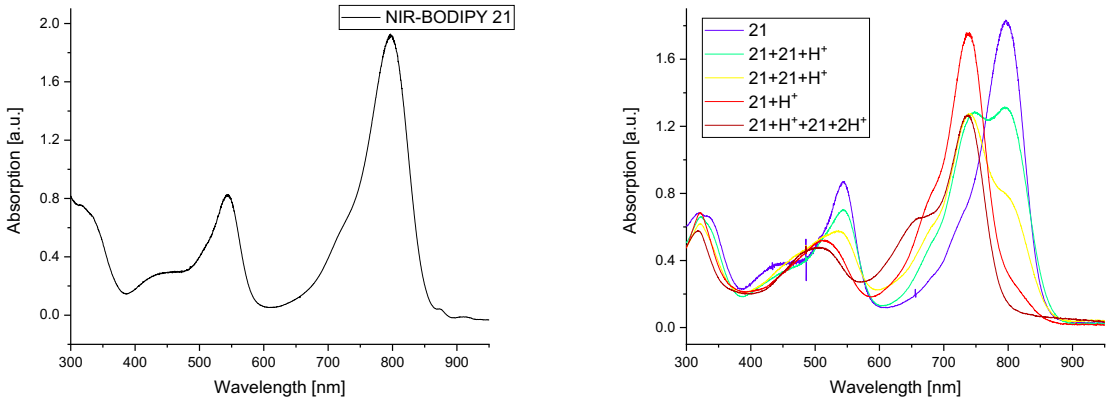

*Figure 112: absorption spectra of NIR-BODIPY **21** in left: toluene; right: in $CHCl_3$ over time with different acid content and resulting protonation grade.*

The two dimethylamino groups can be protonated by the acid traces in the solvent. Therefore, the spectra transforms over time in three distinguishable spectra (21, 21+H^+, 21+2H^+). The pure double-protonated form (21+2H^+) was not achieved in the solvent and since the compound **21** and the pH-behaviour is literature known, further investigations were not carried out. The spectra are similar to the published data, therefore the investigation for a synthetic approach of a near infra-red *aza*-BODIPY is finished.

For future attachment of *aza*-BODIPYs to DTEs, chromophores without pH-dependency should be used. Herein additional electron rich functional groups could tune the fluorescent donor properties.[87]

2.4.8 Spectra of BTDs 15, 137 and 157

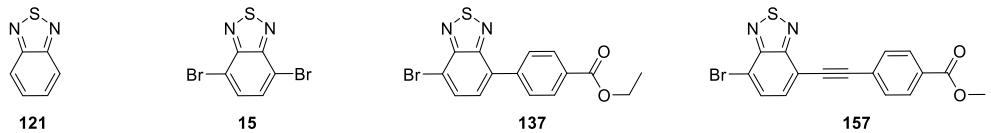

*Figure 113: structures of BTD-moieties **121**, **15**, **137** and **157**.*

BTDs are known for their strong electron-withdrawing property. But they are good fluorophores, with high fluorescence quantum yields.[88] To investigate the position of the absorption bands and their influence on the absorption spectra of DTE(OME)-fluorophore conjugates, a stepwise investigation of BTDs was made. Since unsubstitued BTD **121** shows visible fluorescence around 367 nm after excitation at 312 nm, and phosphorescence around 571 nm, dibromo-BTD **15** is the starting point for the investigation.[89]

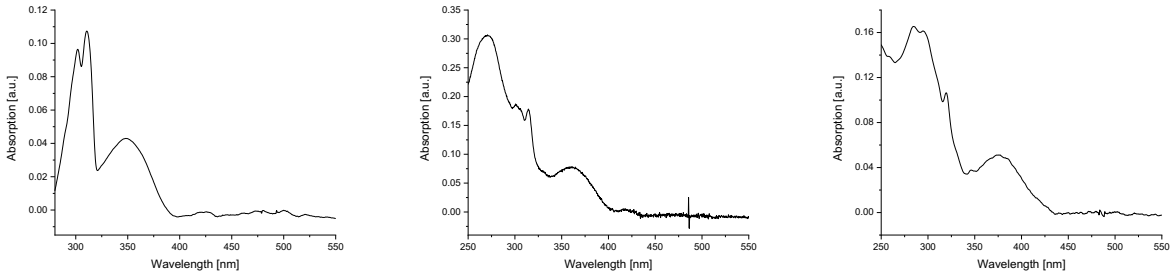

*Figure 114: absorption spectra in MeCN ($1.5 \cdot 10^{-5}$ M) of left: Br-BTD-Br **15**, middle: Br-BTD-benzoate **137**, right: Br-BTD-ethyne-benzoate **157**.*

The absorption spectra of dibromo-BTD **15** shows a double band in the aromatic range around 300 nm and a broadened band at 350 nm with small extinction coefficient (Figure 114). The compound becomes fluorescent when excited at 350 nm (see chapter 2.5.4). This band is assigned to be the π-π* absorption band for the BTD compound and is used to follow the increased π-systems for the next compounds. For the addition of benzoic acid to the BTD-core in **137**, the absorption is bathochromically shifted by 12 nm, while the extinction is almost doubled. Furthermore, the aromatic-region is highly increased with a maximum at 270 nm bearing a bathochromic shoulder. The direct attachment of *para*-benzoic acid to BTDs in **137** leads to a twist of 33°.[57] With the introduction of an ethinyl-unit between the benzoic acid and the BTD in **157**, the broad π-π* absorption band gets further red-shifted by 13 nm with a decrease in extinction coefficient and the appearance of two UV-bands around 290 nm. For BTD-ethyne-benzoate **157** the twist between BTD and benzoate disappears, the structure is flattened and the π-system enlarged, resulting in the observed red-shift with increased conjugation compared to BTD-benzoate **137**. This compound was synthesized in the diploma thesis of Fanny Schröder.

*Table 8: absorption properties of BTDs **15**, **137** and **157** in MeCN.*

Compound	$\lambda_{Abs,max}$ [nm]	$\varepsilon_{\lambda max}$ [10^4 L/(mol·cm)]
15	302, 311, 350	0.29
137	270, 362	0.52
157	285, 295, 375	0.34

λ_{max}: absorption maxima, ε: extinction coefficient

The stepwise investigation of the BTD structures **15**, **137** and **157** and their increase showed the expected behaviour in the absorption spectra. However, literature known addition of both donor and acceptor moieties will lead to strong fluorophoric compounds which are often highly polarized by charge separation.[90] [91] Therefore, the π-attachment of BTD-benzoic acid to the DTE(OMe) is assumed to show interesting spectroscopic properties.

2.4.9 Spectra of DTE(OMe)-BODIPYs 20 and 152

The new DTE(OMe)-fluorophore conjugates **20** and **152** (Figure 115) should be compared to the spectroscopic properties of **BODIPY585BCP** (**14**) (Figure 116). Compound **14** was synthesized by Peng Guo in our work group and investigated by him, Kerstin Mayer and Diana Liebmann in MeCN. **BODIPY585BCP** OF was cyclized by irradiation with a mercury lamp (HBO 200 W) and a 340 nm filter (HW 10 nm, 2.26 mW/cm^2). The cycloreversion was done with a Xenon lamp (XBO 1000 W) and a 655 nm filter (HW 10 nm, 36.7 mW/cm^2). Reversible switching in MeCN with a ratio of 60:40 for CF:OF in the pss was determined.

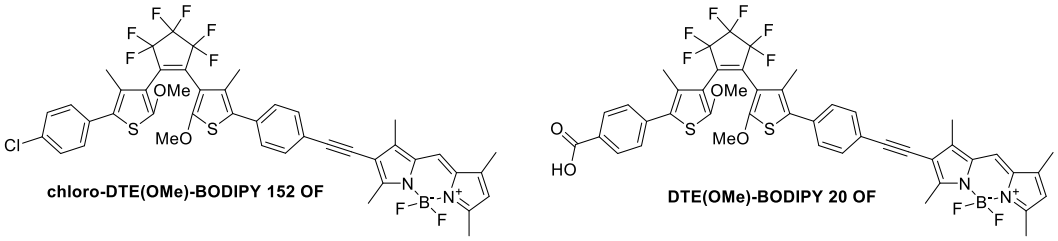

*Figure 115: structures of DTE(OMe)-BODIPY conjugates **152** and **20**.*

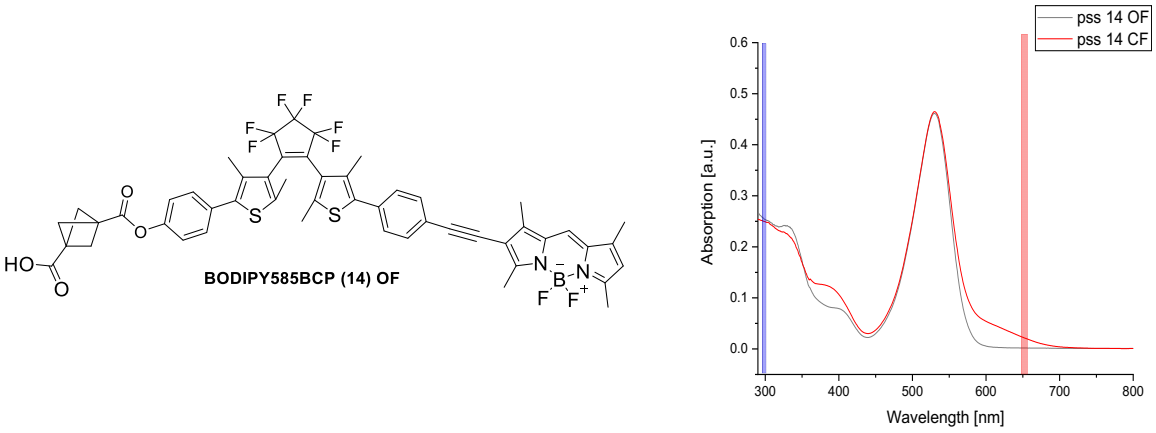

*Figure 116: left: structure of **BODIPY585BCP** (**14**) OF; right: absorption spectra of **BODIPY585BCP** (**14**) OF (red) and CF (blue) (1.3·10^{-5} M in MeCN), irradiation at 300 nm (blue area) and 655 nm (red area).*

By the exchange of the BCP-linker in **BODIPY585BCP** with chloro (**152**) or benzoic acid (**20**), a more pronounced D-A system is expected. Together with the exchange of the DTE(Me) to DTE(OMe), a

batchochromic shift of the π-π* absorption band of the CF is additionally expected. Due to the dramatically decrease of the cycloreversion quantum yield from DTE(Me) to DTE(OMe), for the pure OF and CF absorption spectra and the pss spectra significant differences are expected. The attachment of the BODIPY fluorophore to the DTE(OMe)s **155** (Figure 92) and **150** (Figure 87) increases the π-system and is therefore expected to red-shift the absorption of the conjugated systems in comparison to DTE(OMe) **3**. Furthermore, the BODIPY unit is able to serve as an electron withdrawing group, as well as a donating group.[92][93] Therefore, with the chloro- or benzoic acid substituents, a D-A structure can be formed, with a π-broken form in the OFs and a π-bridged form in the CFs (for further discussion about the structure-property-relationsship see chapter 2.6.3).

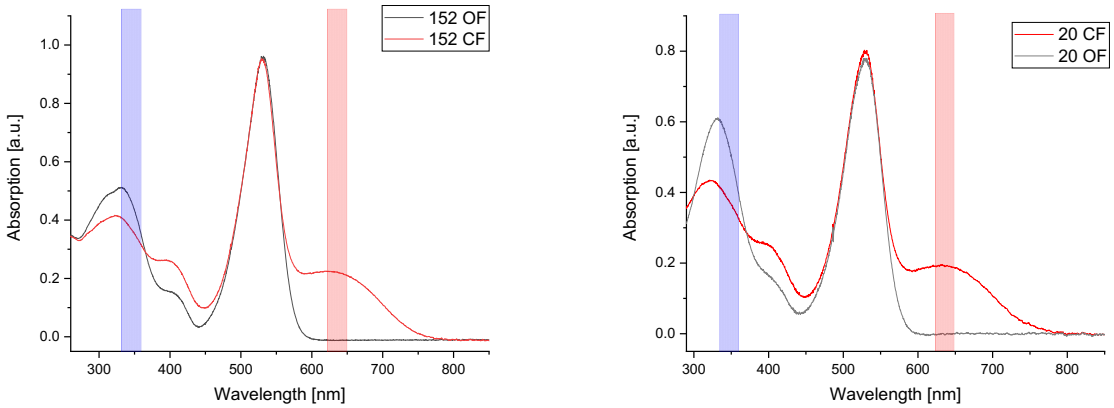

*Figure 117: left: absorption spectra of DTE(OMe)-BODIPY **152** OF and CF ($2.1 \cdot 10^{-5}$ M in MeCN); right: absorption spectra of DTE(OMe)-BODIPY **20** OF and CF ($1.8 \cdot 10^{-5}$ M in MeCN) with UV irradiation (blue area) and visible light irradiation (red area).*

Due to the attachment of BODIPY in chloro-DTE(OMe) **152** and benzoate-DTE(OMe) **20** the typical sharp BODIPY absorption band around 530 nm appears next to the typical DTE(OMe) absorption bands. Furthermore, the extinction of the absorption band around 400 nm is increased (Table 9). The OF of both conjugates **152** and **20** show almost the same absorption band positions with different extinctions. Benzoic acid-DTE(OMe)-BODIPY **20** CF has a red-shifted π-π*absorption band, caused by the increased π-system and the higher acceptor strength. The bathochromic shift of the BODIPY unit from 516 nm to 530 nm indicates the increased π-system, comparing **20** to the blue-shifted ethyne-BODIPY **156** (516 nm) or the blue-shifted BODIPY-stick **22** (515 nm, see chapter 2.4.6). DTE(OMe)-BODIPY **20** OF shows a sharper and higher absorption coefficient in the thiophene and phenyl region (**152** OF $2.4 \cdot 10^4$ L/(mol·cm) vs. **20** OF $3.4 \cdot 10^4$ L/(mol·cm)) indicating an increasing of conjugation. In the CFs the difference in extinction of the thiophene- and phenyl-region (≈320 nm) is decreased, which hints to a more comparable structure after

ring-closure and decreased conjugation especially for **20** CF. Upon photoisomerization from OF to CF, both conjugates show a small blue-shift in the thiophene-phenyl-region around 300 nm, which is unusual for DTE-systems, since the CFs have an enlarged π-system (for further discussion see chapter 2.4.5).[30] In comparison to **BODIPY585BCP** OF and CF, the spectra are red-shifted, due to the enlargement of the π-systems with the methoxy-groups at the DTE unit. Since the absorption of DTE(OMe)s CF are red-shifted, but the BODIPY-moiety (≈530 nm) is almost identical to **BODIPC585BCP**, a π-separation between both moieties can be assumed for compounds **152** and **20**.

*Table 9: absorption properties (λ_{max}, ε and λ_{iso}) and cyclization (QY_{OC}) and cycloreversion quantum yields (QY_{CO}) of DTE-BODIPY **152** and **20** in MeCN.*

Compound	Open form		Closed form		
	λ_{max}[nm] (ε [·10⁴ L/(mol·cm)])	QY_{OC}[a]	λ_{max}[nm] (ε[·10⁴ L/(mol*cm)])	QY_{CO}[a]	λ_{iso} [nm]
BODIPY585BCP (14)	330, 396(s), 531	-	326(s), 381, 531, 598(s)	-	352
152	331 (2.43), 404(s), 531(4.57)	-	322(1.97), 396(s), 531(4.57), 631(1.07)	-	365
20	331(3.39), 401, 530(4.31)	$1.3 \cdot 10^{-2}$	321(2.41), 401(s), 530(4.44), 636(1.08)	$5.1 \cdot 10^{-5}$	369

λ_{max}: absorption maxima, QY_{OC}: cyclization quantum yield, QY_{CO}: cycloreversion quantum yield, ε: extinction coefficient

[a] Determined by using the initial slope method.

The chloro-phenyl DTE(OMe)-BODIPY **152** shows decomposition of almost 15 % of the BODIPY-band in MeCN and in $CHCl_3$ under both UV- (345 nm) and visible light (632 nm) irradiation (see Figure 118). The same result was found under longer wavelength irradation with 360 nm in MeCN. However, chloro-DTE(OMe)-BODIPY **152** is only a precursor for the synthesis of DTE(OMe)-BODIPY conjugates with a chloro-functionality for transition metal-mediated couplings in the future.

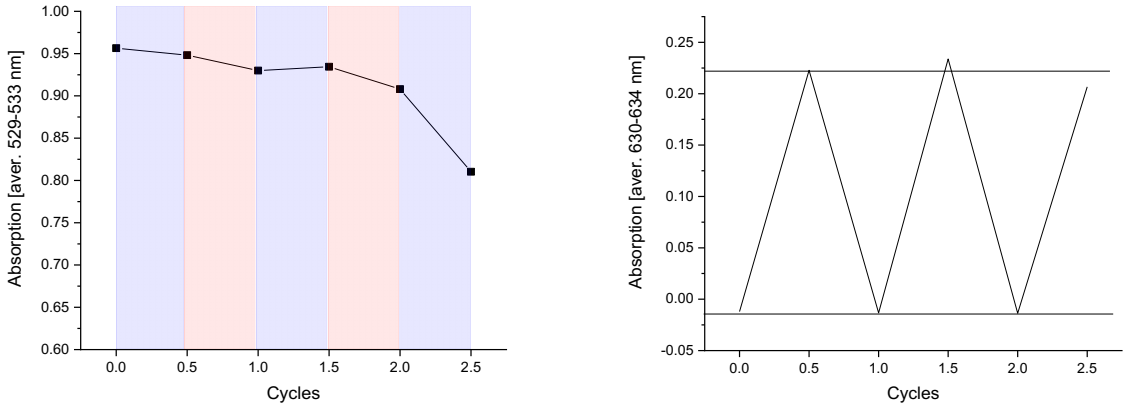

*Figure 118: left: fatique resistance of the chloro-DTE(OMe)-BODIPY **152** BODIPY absorption-band (531 nm) changes over 2.5 switching cycles in MeCN; right: DTE(OMe) **152**-CF absorption-band (632 nm) changes over 2.5 switching cycles.*

Conjugate benzoic acid-DTE(OMe)-BODIPY **20** does not show decomposition over three switching cycles in MeCN (see spectra appendix 5.2). Furthermore, the quantum yields for cyclization with $1.3 \cdot 10^{-2}$ and cycloreversion with $5.1 \cdot 10^{-5}$ are comparable with literature known DTE(OMe)-fluorophore systems.[31] The quantitatively pss ratio of 100:0 for DTE(OMe)-BODIPY **20** CF:OF under 345 nm irradiation in MeCN was determined by HPLC analysis (see Spectra Appendix 5.2).

Conclusively, the attachment of tetramethyl-BODIPY **4** to chloro-phenyl-DTE(OMe) **150** and benzoate-DTE(OMe) **155** resulted in two photoswitchable DTE(OMe)-fluorophore conjugates **152** and **20**. While chloro-DTE(OMe)-BODIPY **152** showed disadvantageous photodecomposition under UV- as well as visbile light-irradiation, the benzoic acid-DTE(OMe)-BODIPY **20** (for the rest of the thesis DTE(OMe)-BODIPY **20**), designed for the attachment on surfaces, shows the desired properties of fatique resistance and quantitatively switching behaviour.

2.4.10 Spectra of BTD-DTE(OMe) 23

The substitution of the BODIPY with a BTD acceptor unit offers several structural possibilities. Keeping the fluorophore in the same order, as it is for DTE(OMe)-BODIPY **20**, a A-π-D-A (carboxylic acid(A)-phenyl(π)-DTE(OMe)(D)-BTD(A)) motif would be created. Since these structures could lead to competitive charge separation away from the semiconductor surface, this option was rejected. Another possibility is the direct attachment of the carboxylic acid group to the BTD, followed by the attachment of

both units to the DTE(OMe), which would lead to a D-A-A structure. Such structures are literature known for highly increased charge recombination rates on semiconductor surfaces (see chapter 1.6). Therefore, the attachment as shown in Figure 119 was chosen, with a benzoic acid group combined with BTD-DTE(OMe) resulting in BTD-DTE(OMe) **23** as a D-A-π-A type structure.

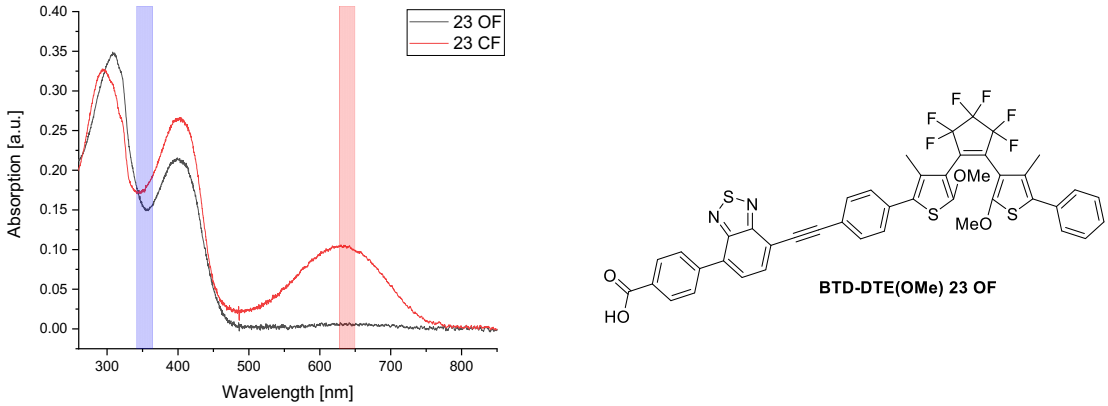

*Figure 119: right: structure of BTD-DTE(OMe) **23** OF; left: absorption spectra of BTD-DTE(OMe) **23** OF (red) and CF (black) ($1.8 \cdot 10^{-5}$ M in MeCN), irradiation at 345 nm (blue area) and 632 nm (red area).*

The most obvious change in the absorption spectra of BTD-DTE(OMe) to the former DTE(OMe)-BODIPY is the better separation of the bands around 300 nm, next to the BTD-absorption band around 400 nm and the absorption band of BTD-DTE(OMe) **23** CF around 630 nm. Furthermore the phenyl-thiophene absorption range around 300 nm is blue-shifted again for CF compared to OF by 17 nm, with decreasing extinction coefficients (for discussion see chapter 2.6.4). The quantum yields are with $3.3 \cdot 10^{-2}$ for the cyclization and $7.7 \cdot 10^{-5}$ for the cycloreversion reaction in the same range, as they are for DTE(OMe)-BODIPY conjugates **152** and **20**. The conjugate did not show any decomposition in three switching cycles (see spectra appendix 5.2). The ratio in pss for BTD-DTE(OMe) **23** CF:OF in MeCN was determined by HPLC analysis to be 98:2 (see chapter 2.3).

*Table 10: spectroscopic properties of BTD-DTE(OMe) **23** OF and CF in MeCN.*

Compound	Open form		Closed Form		λ_{iso} [nm]
	$\lambda_{Abs,max}$ [nm] (ε [10^4·L/(mol·cm)])	QY_{OC}[a]	$\lambda_{Abs,max}$ [nm] (ε [10^4·L/(mol·cm)])	QY_{CO}[a]	
23	310(2.11), 405(1.23)	$3.33 \cdot 10^{-2}$	293 (1.78), 403 (1.43), 630(5.48)	$7.73 \cdot 10^{-5}$	343

λ_{max}: absorption maxima, QY_{OC}: cyclization quantum yield, QY_{CO}: cycloreversion quantum yield, ε: extinction coefficient

[a] Determined by using the initial-slope method.

BTD-DTE(OMe) **23** carrying a substituted fluorophore, which is an acceptor moiety between carboxylic acid and DTE(OMe)-switch shows the desired fatique resistance and almost quantitative switching in MeCN. The fluorophore band is well separated from the π-π* DTE(OMe) CF absorption band which is advantegous for adressing the fluorophore without exciting DTE(OMe), espacially in comparison to the DTE(OMe)-BODIPY conjugates. This could help for the assignment of the different conjugate moieties in time-resolved spectroscopy. The compound shows unexpected solvatochromic absorption and emission properties, which are analysed in the next chapter.

2.5 FLUORESCENCE SPECTROSCOPY

2.5.1 Fluorescence spectrometer – calibration and correction

All fluorescence spectra were recorded on a *Hitachi* F-4500 equipped with a R3788 photomultiplier. Since the measured spectra intensity is highly wavelength dependent, which is caused by a high decrease in the photomultiplier sensitivity for longer wavelengths, and the light source emission intensities. Therefore, several corrections need to be done, for the determination of true emission spectra and the comparison with literature data.[94]

Machine intern corrections:

Wavelength accuracy: can be done by the spectrometer itself with an inaccuracy of ±2.0 nm. The measured accuracy for this thesis is 0.5 nm related to the characteristic Xe-emission line at 450.1 nm.

Signal to Noise ratio: the S/N ratio should be as high as possible. Typical values are around 200; the used spectrometer has 300, which is excellent for this kind of spectrometer.

Detector sensitivity: The photomultiplier has a good detection in the blue area of the visible spectra and gets less effective by decreased photon energy towards red. Therefore, the real emission spectra of a compound is red-shifted relative to the measured spectra. Figure 120 shows the efficiency of the photomultiplier for the full detectable wavelength range.

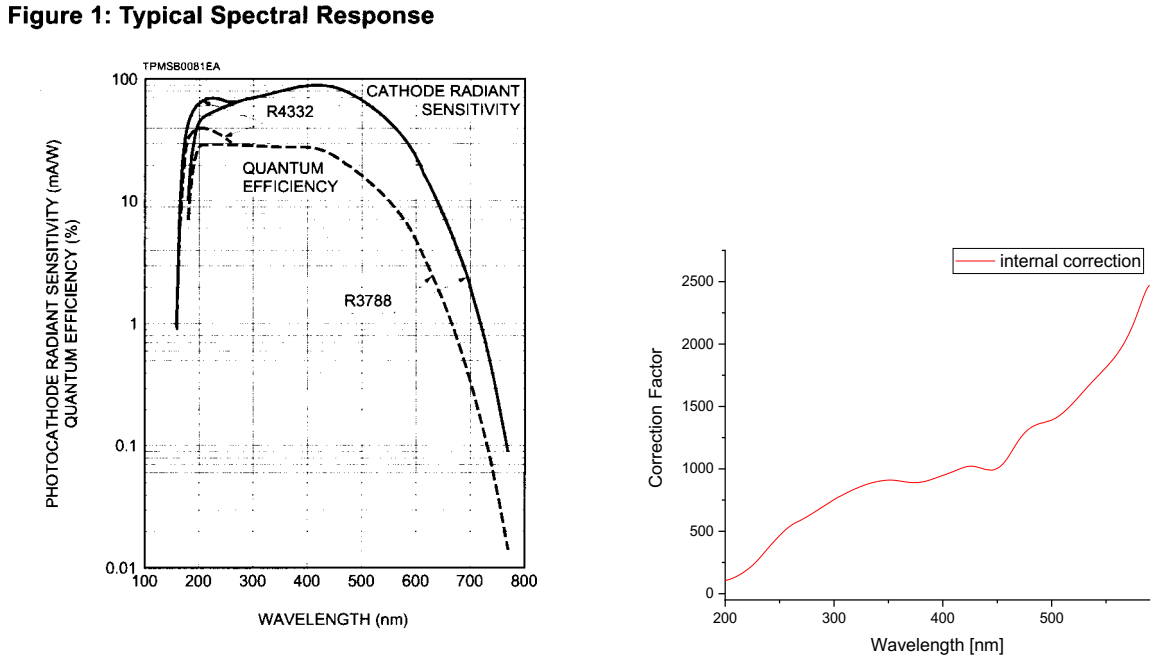

Figure 120: left: photomultiplier sensitivity for 200-800 nm (spectra from supplier); right: callibration factor curve for the Hitachi F-4500.

The used R3788 detector is sensitive up to 740 nm (Figure 120, left), but since the original delivered detector has a range to 600 nm only, the intern calibration function (Figure 120, right) of the spectrometer is designed for corrections between 200-600 nm. BTD-DTE(OMe) **23** CF shows an emission spectra in DCM with a red-shouldered band around 485 nm (Figure 121, upon excitation at 407 nm). With the correction and normalization, the real spectra is red shifted and shows a broad red-shifted shoulder.

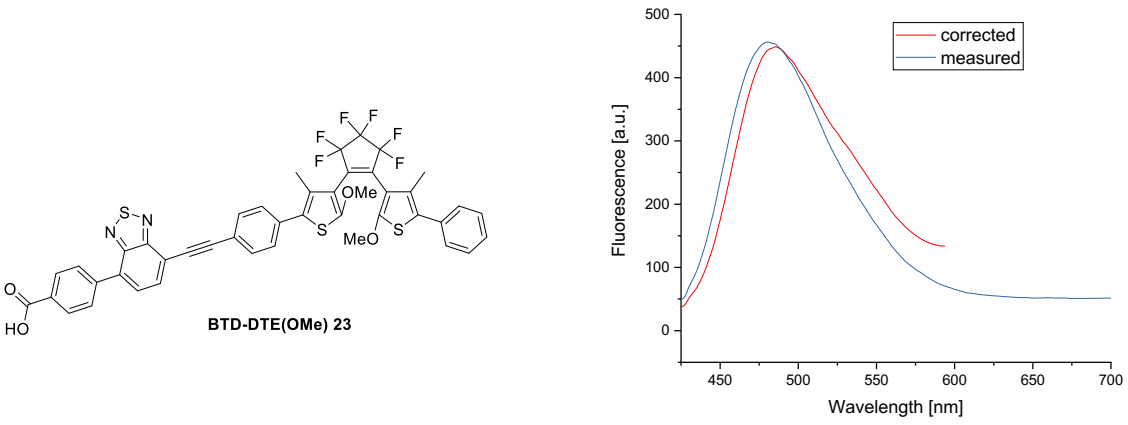

*Figure 121: Measured and corrected spectra of BTD-DTE(OMe) **23** CF ($1.8 \cdot 10^{-5}$ M) in DCM.*

The correction of the BTD-DTE(OMe) **23** OF is more difficult, since the excitation into the absorption maximum of the OF at 407 nm emits in the orange range above 600 nm, and therefore full integration of the curve is not possible with the used spectrometer set-up. Thus, the comparison of our emission results, was corrected by a correction-curve determined by the difference of our spectra with the measurement of a calibrated spectrometer. This was established by the Wachtveitl group and calibrated with an emission correction tool of the supplier.[41] With the expected spectra fully corrected and the measured spectra, a correction-curve can be calculated.

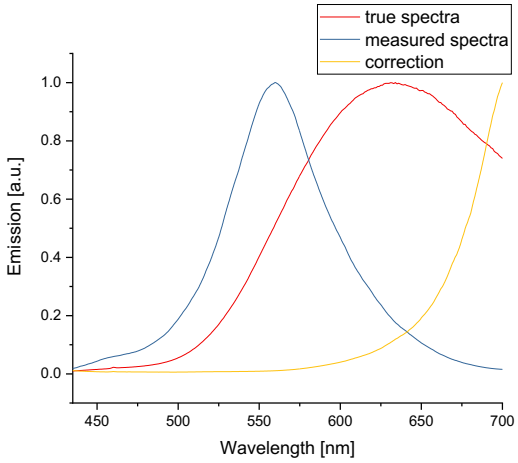

*Figure 122: emission spectra of BTD-DTE(OMe) OF **23** ($1.8 \cdot 10^{-5}$ M) in DCM (λ_{exc} 407 nm); blue (measured spectra), red (true spectra), yellow (correction-curve).*

All measured fluorescence spectra were corrected with the correction-curve from 425-700 nm and normalized. In this thesis, only corrected spectra are shown and discussed.

2.5.2 Fluorescence quantum yields

The fluorescence quantum yield (φ_{Fl}) describes the amount of the photons after an excitation process, which are emitted. Hereby, the measured absorbance of a molecule at the excitation wavelength (λ_{exc}) in different concentrations is plotted against the associated integrals of the emission spectra.

Since the “real” emission-spectra is difficult to obtain, the direct measurement of quantitative emission needs fluorescence standards. An Ulbricht-sphere or the comparative method is therefore often used. The comparative method can be applied in measuring a literature known dye in the sample emission range and with the same spectrometer settings, as used for the sample.[95] Plotting the absorbance against the

fluorescence area, the quotient of the different slopes of the plotted line for the dye and the sample is the fluorescent quantum yield (Eq. 6).

Eq. 6
$$\Phi_{Fl} = \Phi_{\mathrm{Fl,R}} \frac{\mathrm{m} * \mathrm{n}^2}{\mathrm{m_R} * \mathrm{n_R^2}}$$

For this method, several concentrations need to be measured per sample to avoid scattering, aggregation and packing effects. In this thesis the compounds are compared with standards in the same wavelength range (BODIPY (4) ≈500 nm[85], Rhodamine 101 ≈600 nm[96]). Broader emission characteristics will have an error in the fluorescence quantum yields with the used method. For an interim result, φ_{Fl} can be determined by the same method with only one concentration, named single-point method.

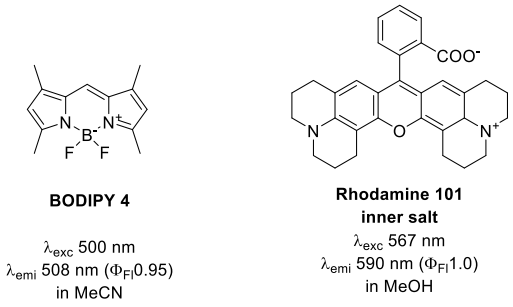

*Figure 123: structures and spectroscopic properties of the fluorescence standards BODIPY (**4**) and Rhodamine 101 inner salt.*

2.5.2.1 Fluorescence standards

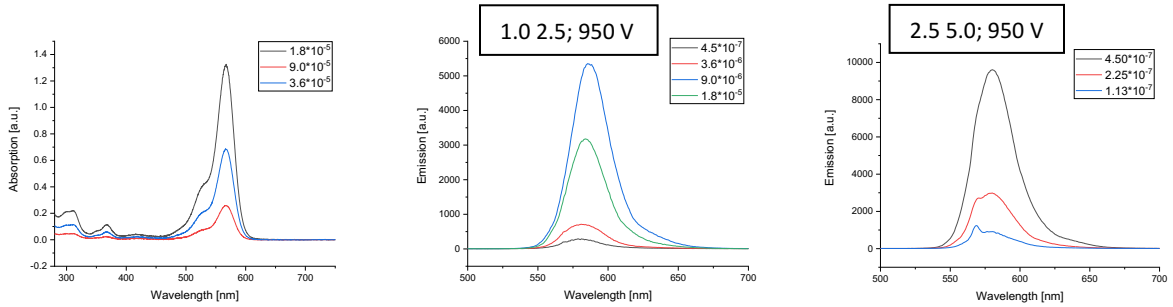

Figure 124: left: absorption spectra of Rhodamine 101 inner salt in MeOH with different concentrations; middle: emission spectra of Rhodamine 101 (λ_{exc} 567 nm) with the spectrometer settings in the box; right: emission spectra of Rhodamine 101 with the spectrometer settings in the boxes.

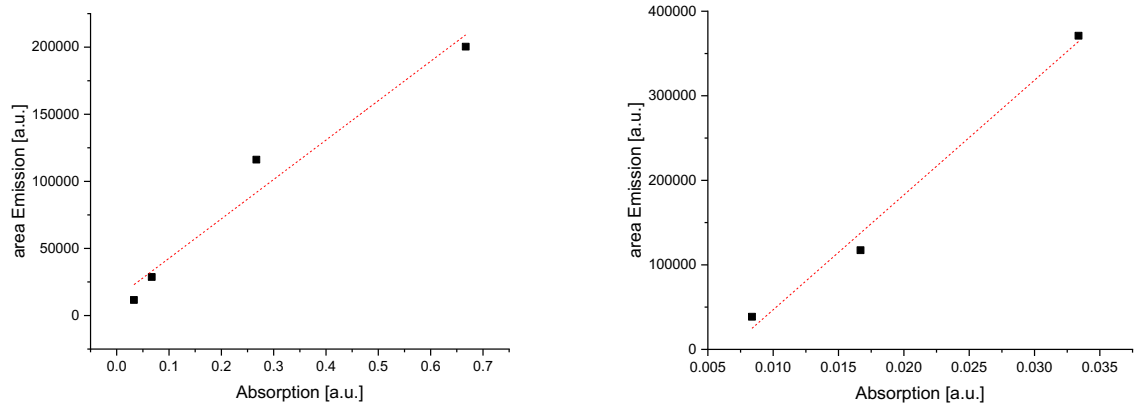

Figure 125: absorption-area emission plots for Rhodamine 101 as standard in the comparative method.

In Figure 124 left, the absorption of Rhodamine 101 inner salt in MeOH shows a linear increase in extinction in the measured concentration range. Because of the high fluorescence sensitivity, the samples were dissolved up to 10^{-7} M in MeOH and measured with the different spectrometer settings. The determined values for Rhodamine 101 as fluorescence standard from absorption spectra in Figure 124 and absorption-emission plots in Figure 125 are presented in Table 11.

The same method was done for tetramethyl-BODIPY **4**. The DTE(OMe)-BODIPY conjugates **20** and **152** showed highly decreased fluorescence. Therefore the standard **4** hat to be diluted up to 10^{-11} M in MeCN to avoid detector saturation. The following values for the quantitative fluorescence were determined by the single-point method.

*Table 11: determined extinction coefficients, and calculated spectroscopic values for Rhodamine 101 inner salt and BODIPY **4** as fluorescence standards.*

compound	ε [10^4 L/(mol·cm)] (λ_{Exc} [nm])	Slope (m_R) Abs. vs. area Emi. A	Slope (m_R) Abs. vs. area Emi. B	Slope (m_R) Abs. vs. area Emi. C	Slope (m_R) Abs. vs. area Emi. D	solvent
Rhodamine 101 inner salt	7.41 (567)	$2.94 \cdot 10^{5}$ [a]	$1.36 \cdot 10^{7}$ [a]	$1.76 \cdot 10^{7}$ [b]	-	MeOH
BODIPY 4	8.14 (501)	$4.08 \cdot 10^{7}$ [b]	$1.30 \cdot 10^{9}$ [b]	$1.71 \cdot 10^{10}$ [b]	$5.14 \cdot 10^{6}$ [b]	MeCN

Spectrometer settings slid widths Exc. Emi. and PMT voltage; A: 1.0 2.5 950 V; B: 2.5 5.0 950 V; C: 5.0 5.0 950 V; D: 5.0 5.0 700 V;
[a] Determined with the comparative method. [b] Determined with the single-point method.

2.5.2.2 Example: Determination of φ_{Fl} for DTE(OMe)-BODIPY OF and CF

For the determination of ϕ_{Fl} for DTE(OMe)-BODIPY **20** OF and CF, the absorption and area emission was measured and plottet in Figure 126.

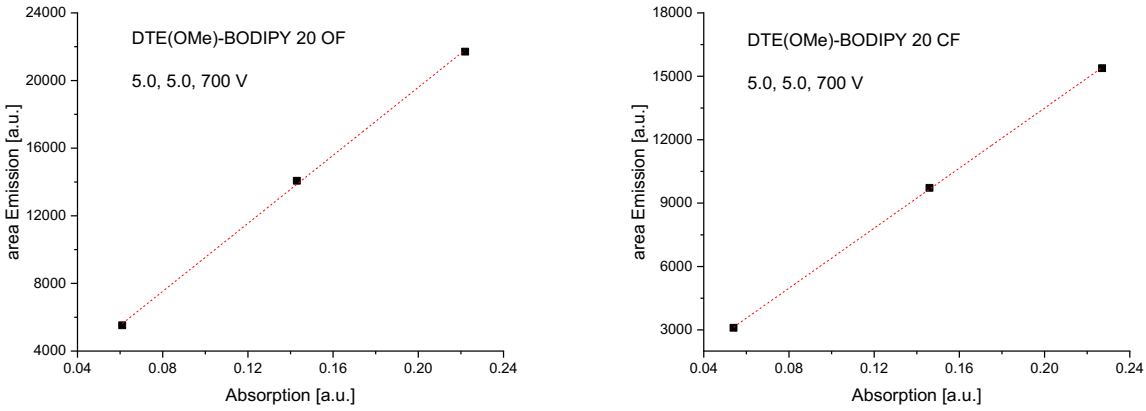

*Figure 126: absorption-area emission plots for DTE(OMe)-BODIPY **20**, left: OF, right: CF.*

The slope of DTE(OMe)-BODIPY OF ($m = 1.01 \cdot 10^5$) and CF ($m = 7.10 \cdot 10^4$) was inserted in Eq. 6. The refractive index can be cancelled out by the measurement in the same solvent and $\varphi_{Fl,R}$ is literature known to be 0.95 in MeCN. ϕ_{Fl} (DTE(OMe)-BODIPY **20**OF) = $1.87 \cdot 10^{-2}$ and ϕ_{Fl} (DTE(OMe)-BODIPY **20** CF) = $1.31 \cdot 10^{-2}$ were calculated.

All further quantitative fluorescence measurements and calculations are listed in the appendix (Calculation Appendix 5.3). Fluorescence quantum yields determined by the comparative method usually have an error of 10-15 %.

2.5.3 Spectra of BODIPYs 4, 62, 156 and 22

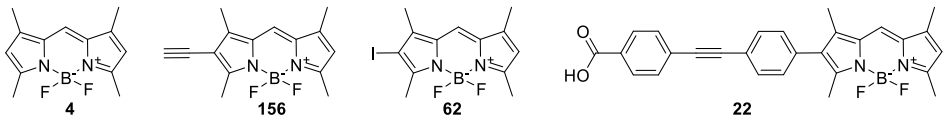

*Figure 127: structures of BODIPYs **4, 156, 62, 22**.*

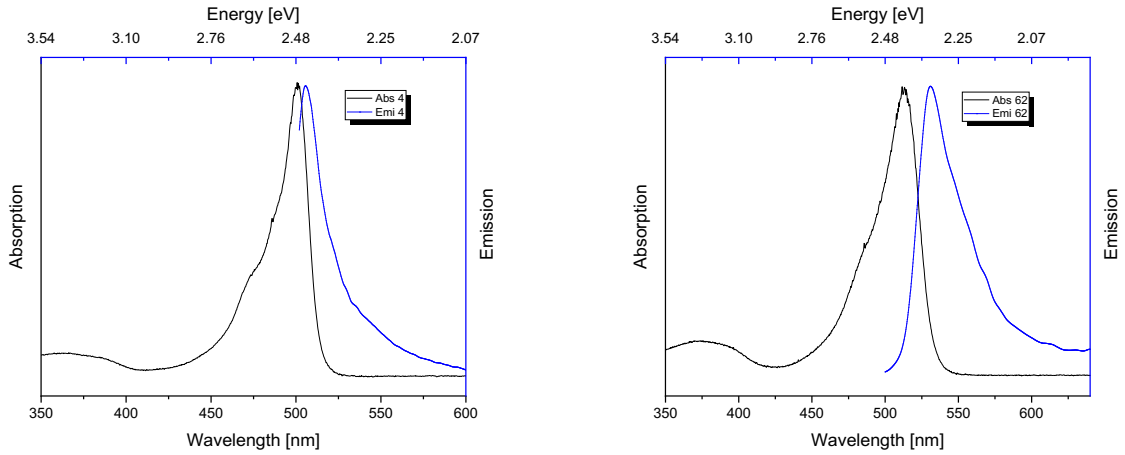

*Figure 128: absorption (black) and emission (blue) spectra of left: BODIPY **4**; right: iodo-BODIPY **62** in MeCN.*

The emission spectra of excited tetramethyl-BODIPY **4** (λ_{Exc} 500 nm, Figure 127) shows a dominant emission peak at 508 nm, with a bathochromic shoulder. Tetramethyl-BODIPY **4** is literature known to have a uniquely small Stokes shift.[85] The rigid structure of the core leads to almost no vibronic loss of energy between excitation and relaxation. Fluorescence quantum yields are almost quantitatively ($9.5 \cdot 10^{-1}$ in MeCN) and well analyzed in different solvents in the literature.[85] Therefore, compound **4** was taken as standard for the comparison with other BODIPY-containing molecules.

With the introduction of an iodine in *β*-position, the emission spectra of iodo-BODIPY **62** (λ_{Exc} 513 nm) has a broadened mayor emission band located at 531 nm with a red-shifted shoulder. Atoms like bromine and iodine are well known for the facilitation of forming triplet-states after excitation. This effect is called heavy-atom effect and is based on the highly localized positive charge and mass in the core of atoms with high atomic number.[97] With the attachment of a single iodine to the core structure, the quantum yield for fluorescence is decreased dramatically ($3.6 \cdot 10^{-4}$) and the Stokes shift is increased to 18 nm. Triplet-states should be avoided for the development of the conjugates due to their reactivity with oxygen, which is disadvantegous for the transient measurements on air (see 1.5.1).

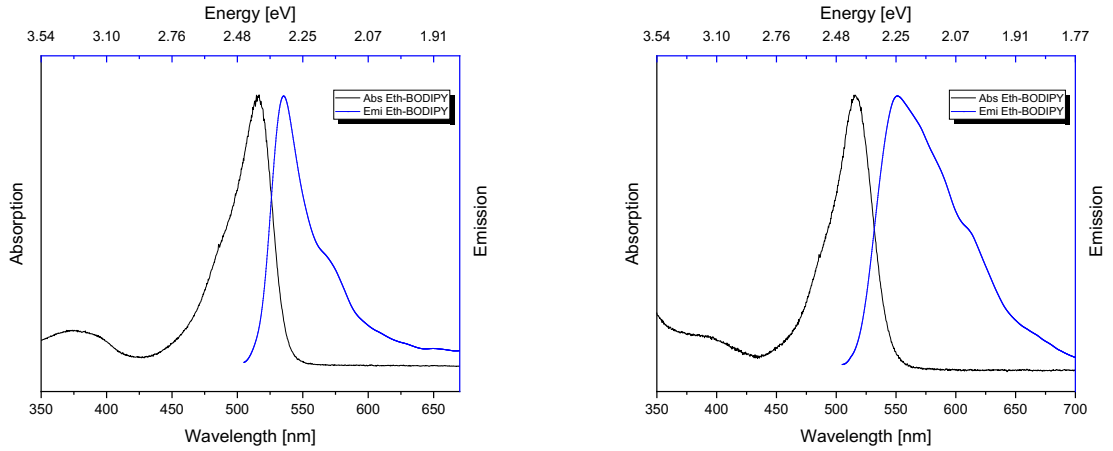

*Figure 129: absorption (black) and emission (blue) spectra of left: ethyne-BODIPY **156**; right: BODIPY-stick **22** in MeCN.*

With the extension of the π-system in ethyne-BODIPY **156** by the attachment of an ethinyl unit, the main emission band (λ_{Exc} 516 nm) located at 535 nm reveals a further increased Stokes shift of 29 nm. The fluorescence quantum yield was not determined in this thesis. The BODIPY-stick **22** shows a more pronounced red-shifted shoulder of the dominant emission band at 551 nm with a 35 nm Stokes shift. The BODIPY stick has a reduced quantum yield of $2.1 \cdot 10^{-2}$, which is a hint for different relaxation pathways.[97]

*Table 12: emission properties of BODIPYs **4**, **62**, **156** and **22**.*

Compound	λ_{Exc} [nm]	$\lambda_{Emi,\ max}$ [nm]	Δν [nm]	ϕ_{Fl}
4	500	508	8	0.95
62	513	531	18	0.000363[a]
156	516	535	29	n.d.
22	516	551	35	0.0213[a]

λ_{Exc}: excitation wavelength, λ_{Emi}: emission maxima, Δν: Stokes shift, ϕ_{Fl}: fluorescence quantum yield

[a] Determined by using the single-point method and BODIPY **4** as standard.

The emission property measurement of the tetramethyl-BODIPY modifications leading to iodo-BODIPY **62**, ethyne-BODIPY **156** and the BODIPY-stick **22** confirmed the literature known design rules for emission properties of BODIPYs (Table 12).[36] For further increased Stokes shifts, several design rules are literature known (e.g. attachment of dialkylamines).[98] Directly attached iodine in iodo-BODIPY **62** opens a further triplet involved relaxation way, which increases the Stokes shift and lowers dramatically the fluorescence quantum yield, while shifting the absorption and emission bathochromically. The increased π-system of ethyne-BODIPY **156** has an even more pronounced red-shift in absorption and emission spectra. An increased Stokes shift indicates the loss of energy in the excited state, which is the highest in the investigated BODIPY systems for the BODIPY-stick **22** with an already twisted phenyl unit attached to the

BODIPY core (Figure 130). This increased Stokes shift together with a small fluorescence quantum yield in the BODIPY-stick **22** shows the possibility for different relaxation pathways (for example twisted intramolecular charge transfer (TICT)) in the D-π-A system. The small changes in the absorption band maxima of **22** compared to tetramethyl-BODIPY **4**, indicate a π-separation of the BODIPY donor to the π-system.

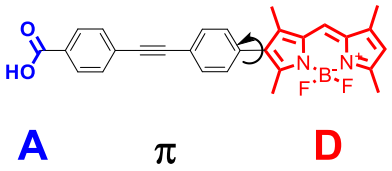

*Figure 130: structure of BODIPY-stick **22** with electron rich (red) and electron poor (blue) structural motifs.*

2.5.4 Spectra of BTDs 15, 137 and 157

BTDs are strong fluorophors with high quantum yields.[99] Due to their strong electron withdrawing behaviour 4,7-attached π-conjugated residues become often polarized or charged, and the molecules are frequently described as stacking, which dramatically reduces the fluorescence. Unsubstituted BTD **121** shows almost no fluorescence in the visible range.[89] Since BTD **137** was chosen to be incorporated in a bigger π-system, the dibrominated BTD **15** was investigated as starting point.

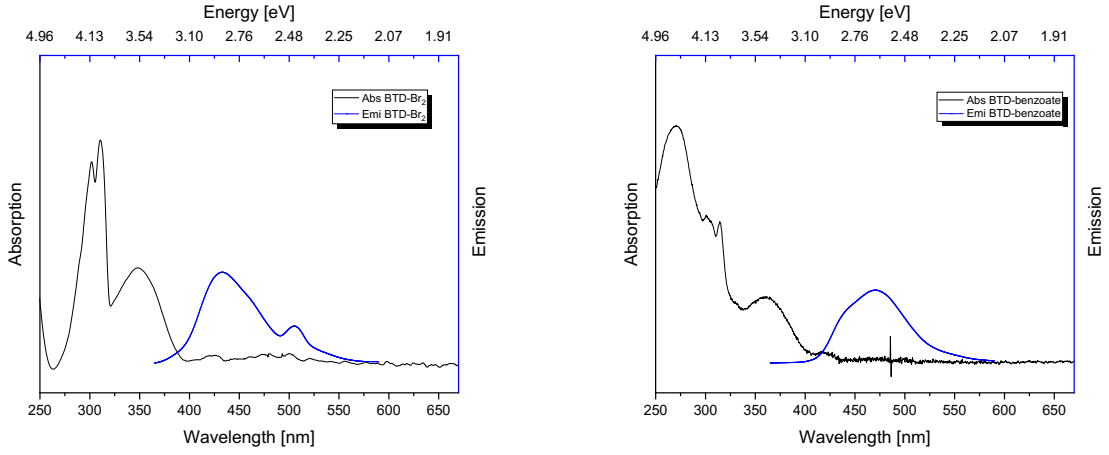

*Figure 131: absorption (black) and emission (blue) spectra of left: dibromo-BTD **15**; right: benzoate-BTD **137** in MeCN.*

The emission spectra of dibromo-BTD **15** (λ_{Exc} 350 nm) has two emission band maxima with a main band at 433 nm and a smaller band at 510 nm (Figure 131, structure see Figure 133). The unsubstituted BTD **121**

excited at 312 nm emits at 367 nm fluorescence and at 571 nm phosphorescence.[89] Therefore, the second emission band of BTD **15** located at 510 nm could be assigned as additional radiative relaxation. The emission properties of dibromo-BTD **15** are not decribed in the literature. A triplet-formation by the heavy-atom effect of the two bromo-substituents is thinkable, which could explain reduced fluorescence quantum yield and next to the major emission band the further red-shifted smaller emission band.

The exchange of one bromo-substituent by a benzoate moiety leads to Br-BTD-benzoate **137** with only one broad emission band and a hypsochromic shoulder (λ_{Exc} 362 nm) centered at 471 nm. The BTD-benzoate structure motif is known to be twisted, which opens further pathways to relaxation by vibronic movements.[57]

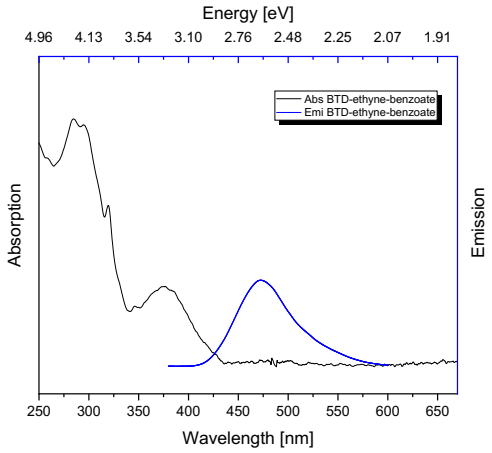

*Figure 132: absorption (black) and emission (blue) spectra of BTD-ethyne-benzoate **157** in MeCN.*

With the insertion of an ethinyl unit between BTD and benzoate of **137** to form **157**, the emission band, shown in Figure 132 is bathochromically shifted and located at 474 nm (λ_{Exc} 375 nm). The repulsion between the BTD core and the phenyl-ring is lowered and the molecule flattened, which leads to a sharper emission band. The Stokes shift is decreased between BTD-benzoate **137** and BTD-ethyne-benzoate **157** by 10 nm. This indicates a rigidified structure and leads to more efficient fluorescence with low solvent dependency. The determination of fluorescence quantum yields of the BTDs **15**, **137** and **157** is not part of this thesis.

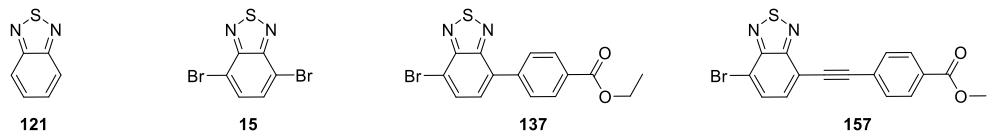

*Figure 133: structures of BTD-moieties **121**, **15**, **137** and **157**.*

*Table 13: emission properties of BTDs **15**, **137** and **157** in MeCN.*

compound	λ_{Exc} [nm]	$\lambda_{Emi,max}$ [nm]	Δν [nm]
15	350	433, (510)	83, (160)
137	362	471	109
157	375	474	99

λ_{Exc}: excitation wavelength, $\lambda_{Emi,\ max}$: emission maxima, Δν: Stokes shift

The emission investigation of a stepwise BTD π-system increase shows the bathochromic shift of the emission band correlating with enlargement of conjugation (Table 13). While the two-band structure of **15** is a hint of another emissive relaxation pathway, this second band could not be clearly observed in **137** and **157**. The twisted structure **137** has a higher Stokes shift, than the rigidified structure **157**, which shows the energy loss by vibronic movements of **137**, a property which should be solvent dependent. The combination of directly attached benzoate at ethyne-phenyl-BTD, expanded by a further DTE(OMe) donor in the designed BTD-DTE(OMe) D-A-π-A structure, the BTD-acceptor is expected to show more pronounced red-shifts in absorption and emission spectra. The bathochromic emission of the BTD fluorophore towards the absorption region of the DTE(OMe) CF π-π*band (centered at 630 nm) is crucial for the desired energy-transfer, and will be further discussed in chapter 2.6.4.

2.6 SOLVATOCHROMISM

2.6.1 General

Solvatochromism is the solvent-dependent change of chromophore properties. Since a molecule is electronically (dipole) and conformationally (viscosity) influenced by the solvent, the necessary energy for absorption and the emitted energy can be changed.[100] The phenomena are complex and can be influenced by various effects in the direct surrounding of the molecules (see Figure 23 in chapter 1.4.3).[101]

For the investigation of solvatochromism, the dielectric constant (ε), Reichardt values (E_T^N), the polarity index or the orientation polarizability (Δf) can be compared with absorption/emission properties. For DTEs the viscosity is also important for the conformational antiparallel and parallel interconversion.[102]

Table 14: solvent properties ordered with increasing orientation polarizability (Δf) values.

Solvent	Δf (ε, n)[a]	Polarity index[b]	ε[c]	E_T^N [d]	viscosity[e]
Hexane	-0.0014	0.1	1.88	0.009	0.30
Toluene	0.013	2.4	2.38	0.099	0.56
Dioxane	0.02	5.27	2.60	0.124	1.18
MTBE	0.1161	2.4	2.25	0.164	0.36
EtOAc	0.201	4.4	6.02	0.228	0.42
DCM	0.219	3.1	8.93	0.303	0.41
DMSO	0.263	7.2	47.2	0.444	1.99
MeCN	0.305	5.8	36.6	0.460	0.37
MeOH	0.309	5.1	32.7	0.762	0.54

a from [103] b from [104] c from [105] d from [106] e from Sigma Aldrich website (10.09.2018, sigmaaldrich.com).

In this thesis the emission and absorption properties of DTE(OMe)-BODIPY **20** and BTD-DTE(OMe) **23** in different solvents are compared to the Δf values of the solvents (Table 14). Therefore, the properties are listed in the order of increasing Δf in Table 15-18.

2.6.2 Sample preparation and measurements

In this chapter **DTE(OMe)-BODIPY 20** and **BTD-DTE(OME) 23** are shortened to **DTE(OMe)-BODIPY** OF and **DTE(OMe)-BODIPY** CF, as well as **BTD-DTE(OMe)** OF and **BTD-DTE(OMe)** CF for a better readability. The photochromic properties of **BTD-DTE(OMe)** OF, **BTD-DTE(OMe)** CF, **DTE(OMe)-BODIPY** OF and **DTE(OMe)-BOPDIPY** CF in different solvents were studied in diluted solutions ($1.8 \cdot 10^{-5}$ M, exception: **BTD-DTE(OMe)** in toluene $9.0 \cdot 10^{-6}$ M, and **DTE(OMe)-BODIPY** in hexane (concentration not determined), Spectra Appendix 5.2). The results of this chapter are part of a publication.[107]

2.6.3 Solvatochromism of DTE(OMe)-BODIPY

DTE(OMe)-BODIPY in both forms (OF and CF) was investigated in five different solvents from nonpolar (hexane) to polar solvents (MeCN), and aprotic to protic solvents (MeOH). The change of absorption spectra under UV- and visible light illumination are shown in the spectra appendix (chapter 5.2), while the main-characteristics of the absorption and emission spectra are listed in Table 15 and Table 16,

respectively. The concentration, and therefore ε and ϕ of **DTE(OMe)-BODIPY** OF and CF in hexane could not be determined because of solubility issues.

*Table 15: photochromic properties of **DTE(OMe)-BODIPY** OF and CF in different solvents.*

Solvent	Open form		Closed form	
	$\lambda_{Abs,max}$ [nm] ε[10^4L/(mol·cm)]	QY_{OC}[ac]	$\lambda_{Abs,max}$ [nm] ε[10^4L/(mol·cm)]	QY_{CO}[bc]
Hexane	331, 408, 540	-	323, 404, 536, 630	-
EtOAc	331 (4.00), 406, 532 (5.16)	$8.64 \cdot 10^{-2}$	314 (2.49), 398, 532 (5.33), 631 (1.67)	$5.97 \cdot 10^{-5}$
DCM	337 (3.44), 405, 537 (4.33)	-	-	-
MeCN	331 (3.33), 401, 530 (4.28)	$3.3 \cdot 10^{-3}$[a]	321 (2.33), 401, 530 (4.39), 636 (1.05)	$5.20 \cdot 10^{-5}$[b]
MeOH	324 (2.11), 407, 531 (3.00)	$2.53 \cdot 10^{-2}$	326 (1.61), 400, 530 (3.16), 627 (1.00)	$6.70 \cdot 10^{-5}$

$\lambda_{Abs,max}$: absorption maxima, QY_{OC}: cyclization quantum yield, QY_{CO}: cycloreversion quantum yield, ε: extinction coefficient

[a] Under irradiation with 345 nm light. [b] Under irradiation with 632 nm light. [c] Determined by using the initial slope method.

Figure 134 shows the typical photochromic behaviour of **DTE(OMe)-BODIPY** in the investigated solvents, e.g. MeOH. The absorption and emission spectra in the other solvents of different polarity are included in the spectra appendix 5.2.

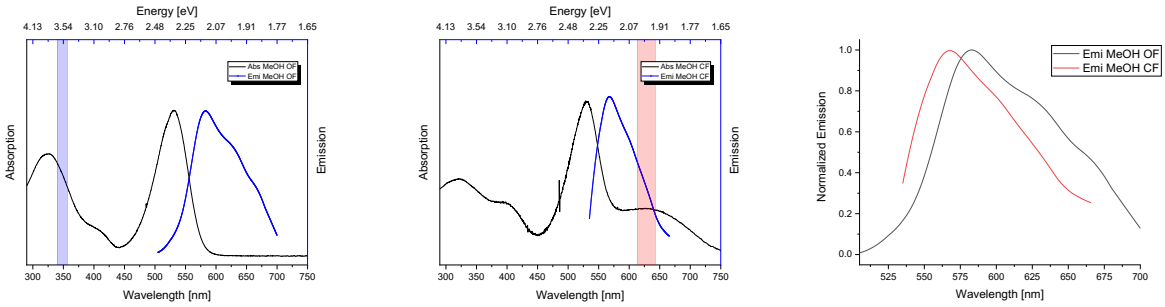

*Figure 134: **DTE(OMe)-BODIPY** in MeOH ($1.8 \cdot 10^{-5}$ M); left: absorption and emission spectra of **DTE(OMe)-BODIPY** OF (λ_{Exc} 531 nm) with irradiation at 345 nm (blue); right: absorption and emission spectra of **DTE(OMe)-BODIPY** CF (λ_{Exc} 530 nm) with irradiation at 632 nm (red).*

Upon photoisomerization of **DTE(OMe)-BODIPY** OF to CF with 345 nm LED irradiation, the main absorption band around 330 nm was 8-10 nm blue shifted in the investigated solvents and showed decreased extinction. Furthermore, a small (0-4 nm) blue-shift of the π-π* BODIPY band (≈535 nm) with similar extinction decrease was observable. The π-π* absorption band of **DTE(OMe)-BODIPY** CF appears (≈630 nm) and the extinction around 400 nm increased upon photoisomerization. All switching processes were reversible in the investigated solvents, with exception of DCM, **DTE(OMe)-BODIPY**, which showed

decomposition under both UV- and visible irradiation. The cleavage of the BF_2 BODIPY-core by acid traces in DCM could be assumed. The absorption spectra of **DTE(OMe)-BODIPY** OF and CF show only a minor solvent influence (Table 15, Spectra Appendix 5.2). A negative solvatochromism of the BODIPY-fluorophore band (≈535 nm) in **DTE-BODIPY** OF and CF with increasing solvent polarity by 10 nm from hexane to MeCN is observed next to a decrease of extinction coefficients. In **DTE(OMe)-BODIPY** CF the DTE(OMe) absorption band around 630 nm shows minor positive solvatochromism, but also a decrease of extinction coefficients. Both trends can be assigned to different twisting behaviour of the **DTE(OMe)-BODIPY** OF and CF structures in solvents with higher polarity (Figure 135). In **DTE(OMe)-BODIPY** OF the electron rich donor (BODIPY) and electron deficient acceptor (carboxylic acid) are separated, and both moieties are stabilized by polar solvents leading to a less π-conjugated more twisted conjugate with small negative solvatochromism. In **DTE(OMe)-BODIPY** CF on the other hand, the increased π-system, followed by flattening of the conjugate leads to a D-D-π-A system which undergoes solvent polarity stabilization and shows small positive solvatochromism. Trends are difficult to determine for **DTE(OMe)-BODIPY** OF and CF, because of the low amount of data points. Therefore, a data analysis was not done but do not seem to be important.

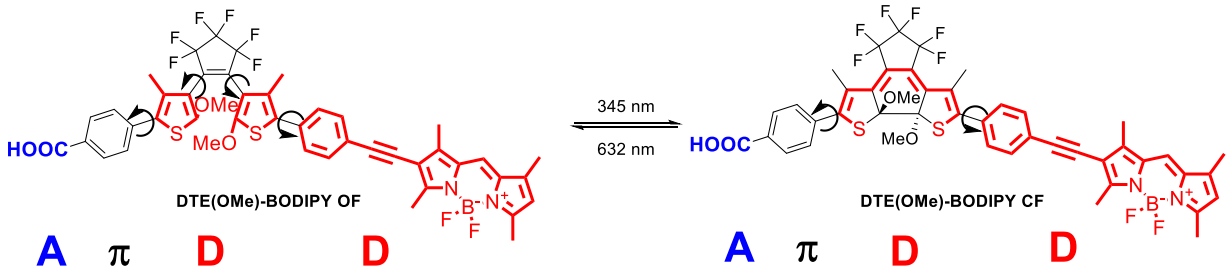

*Figure 135: structures of **DTE(OMe)-BODIPY** OF and CF with electron rich (red) and electron poor (blue) structural motifs.*

2.6.3.1 Emission

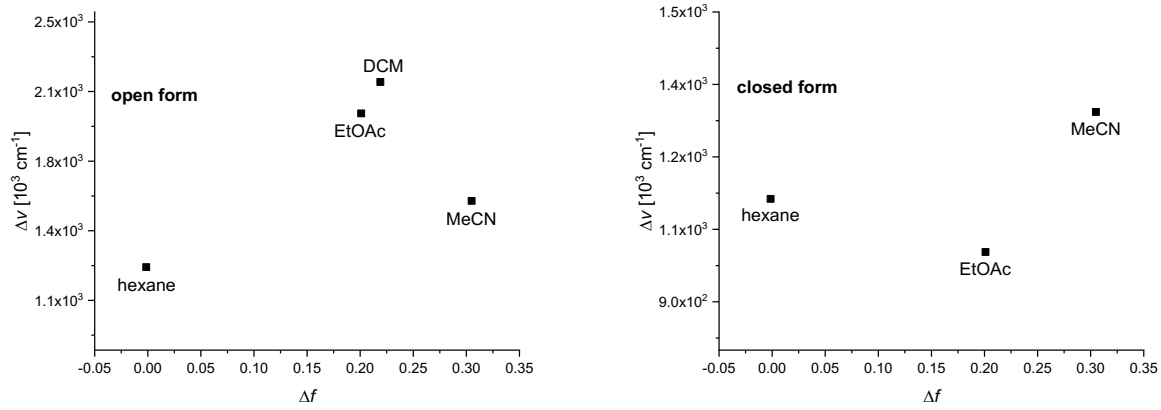

*Figure 136: LIPPERT-MATAGA plots of **DTE(OMe)-BODIPY**, left: OF; right: CF.*

Upon exitation at the π-π* absorption band maximum of the BODIPY unit (≈535 nm), **DTE(OMe)-BODIPY** OF and CF showed fluorescence. Since DTE(OMe) CF showed absorption at the excitation wavelength of the BODIPY moiety, exclusive excitation of the BODIPY fluorophore was not possible. The emission spectra of **DTE(OMe)-BODIPY** OF showed a minor solvent dependency with Stokes shifts of 37-70 nm from hexane to DCM, as shown in the Lippert-Mataga plot in Figure 136 (Table 16, Spectra Appendix 5.2). The **DTE(OMe)-BODIPY** CF had almost no solvent dependent emission bands with Stokes shifts of 30-39 nm.

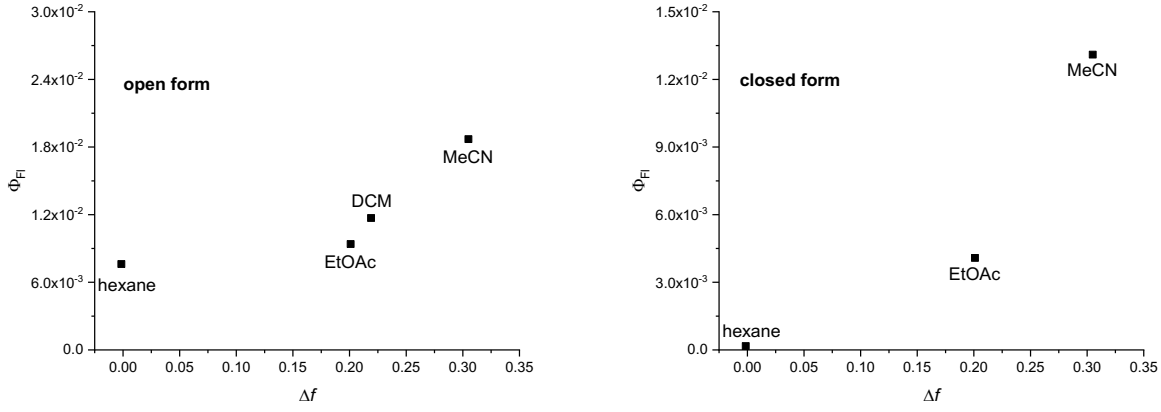

*Figure 137: fluorescence quantum yields versus normalized polarization for **DTE(OMe)-BODIPY** in different solvents, left: OF; right: CF.*

DTE(OMe)-BODIPY OF and CF in the investigated solvents show different behaviour in the emission quantity (Figure 137 and Table 16). With increasing Δf for **DTE(OMe)-BODIPY** OF, the fluorescence quantum yields (ϕ_{Fl} OF) are increased from 0.8% in hexane to 2 % in MeCN. On the other hand, **DTE(OMe)-BODIPY** CF shows a stronger increase of ϕ_{Fl} CF with 0.02% in hexane to 0.13% in MeCN, but altogether a clearly visible fluorescence quenching. This behaviour results in a decreased fluorescence on-off modulation by energy transfer (ϕ_{Fl} CF/ ϕ_{Fl} OF) of 0.02 in hexane up to 0.70 in MeCN. Since the emission bands of **DTE(OMe)-BODIPY** OF and CF are not well separated, the emission signals of both isomers can not be used as read-out signal for exclusively one photoisomer.

*Table 16: emission properties of **DTE(OMe)-BODIPY** OF and CF in different solvents..*

Solvent	Open form				Closed form				
	λ_{Exc} [nm]	$\lambda_{Emi,\ max}$ [nm]	Δν [nm/cm^{-1}]	ϕ_{Fl}[a]	λ_{Exc} [nm]	$\lambda_{Emi,\ max}$ [nm]	Δν [nm/cm^{-1}]	ϕ_{Fl}[a]	$\frac{\Phi_{Fl}\ (CF)}{\Phi_{Fl}\ (OF)}$
hexane	540	578, (630)	38/1217	$7.62\cdot10^{-3}$	536	570	34/1113	$1.70\cdot10^{-4}$	0.022
EtOAc	532	595	63/1990	$9.39\cdot10^{-3}$	532	562, (607)	30/1003	$4.08\cdot10^{-3}$	0.43
DCM	537	607	70/2148	$1.17\cdot10^{-2}$	-	-	-	-	-
MeCN	533	581	48/1550	$1.87\cdot10^{-2}$	530	569	39/1293	$1.31\cdot10^{-2}$	0.70
MeOH	531	583	52/1679	$2.24\cdot10^{-4}$	530	568	38/1262	$7.21\cdot10^{-5}$	0.32

λ_{Exc} : excitation wavelength, $\lambda_{Emi,\ max}$: emission maxima, Δν: Stokes shift, ϕ_{Fl}: fluorescence quantum yield

[a] Determined by the comparative method with tetramethyl-BODIPY and Rhodamine 101.

2.6.3.2 Conclusion

In **DTE(OMe)-BODIPY**, the photoswitchable central DTE(OMe) OF or CF donor modifies the π-conjugation between the carboxylic acid acceptor and the BODIPY donor, leading to two different systems **DTE(OMe)-BODIPY** OF and **DTE(OMe)-BODIPY** CF with distinctive solvent dependent behaviour. The conformational geometrical change in **DTE(OMe)-BODIPY** OF together with the twisting at the external phenyl units, leads to a flexible structure which shows lower π-conjugation with increased solvent polarity in the ground state and small positive solvatochromism for the excited state. On the other hand, the rigidified D-D-π-A structure of **DTE(OMe)-BODIPY** CF (Figure 135) leads to small positive solvatochromism in the ground state and almost no solvent dependent changes in the excited state with clearly visible energy transfer. In sum, the two photoisomers of **DTE(OMe)-BODIPY** show distinguishable absorption and emission spectra with generally small solvent dependency. The on-off fluorescence modulation is highly solvent dependent with almost quantitative fluorescence quenching in hexane to lower quenching in

MeCN indicating energy-transfer in the conjugate. A stronger donor substituting tetramethyl-BODIPY or acceptor substituting the carboxylic acid could increase the difference and solvent effects of the two photoisomers.

2.6.4 Solvatochromism of BTD-DTE(OMe)

BTD-DTE(OMe) OF and CF was investigated in eight different solvents from nonpolar (toluene) to polar solvents (MeCN) and aprotic to protic (MeOH). The change of absorption spectra under UV- and visible light illumination are shown in the spectra appendix (chapter 5.2), while the main-characteristics of the absorption and emission spectra are shown in Table 17 and Table 18, respectively.

2.6.4.1 Absorption Spectra

Figure 138 shows the typical photochromic behaviour **of BTD-DTE(OMe)** in an aprotic solvent, e.g. MTBE. The absorption and emission spectra in the other solvents of different polarity are included in the spectra appendix information 5.2.

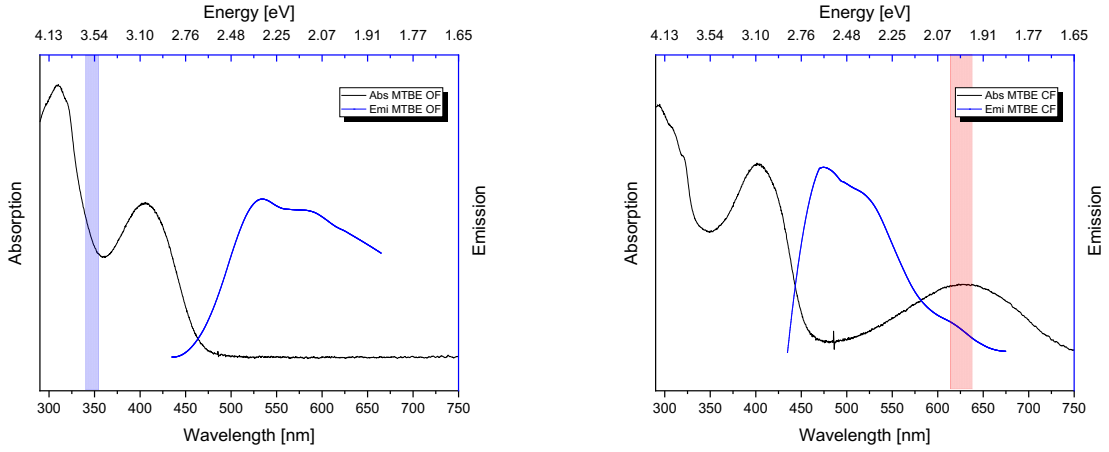

*Figure 138: **BTD-DTE(OMe)** in MTBE ($1.8 \cdot 10^{-5}$ M); left: absorption and emission spectra of **BTD-DTE(OMe)** OF (λ_{Exc} 404 nm) with irradiation at 345 nm (purple); right: absorption and emission spectra of BTD-DTE(OMe) CF (λ_{Exc} 405 nm) with irradiation at 632 nm (red).*

In all solvents the open form **BTD-DTE(OMe)** OF shows the characteristic DTE(OMe) absorption band around 310 nm for the excitation of phenyl and thiophene units.[108] The band around 405 nm of **BTD-DTE(OMe)** OF can be mainly related to the absorption band of the benzothiadiazole (BTD) unit and shows a large 45 nm red-shift compared to Br-BTD-benzoate **137** indicating a highly enlarged π-system. Despite the maxima of **BTD-DTE(OMe)** OF in different solvents are around 310 nm (Table 17), all solutions

were irradiated at longer wavelength of 345 nm with a LED to avoid decomposition.[29] Therefore, the wavelength for the ring closure reaction is not ideal, which is also observable by the decreased ring closure quantum yields of one decimal power reported in Table 17.[32] The ratio of CF:OF was 98:2 in MeCN and 94:6 in MeOH for **BTD-DTE(OMe)** at pss (345 nm) as determined via HPLC measurements (see 5.2), and therefore the conjugate **BTD-DTE(OMe)** is treated herein as a quantitative two-state system for all solvents.[109]

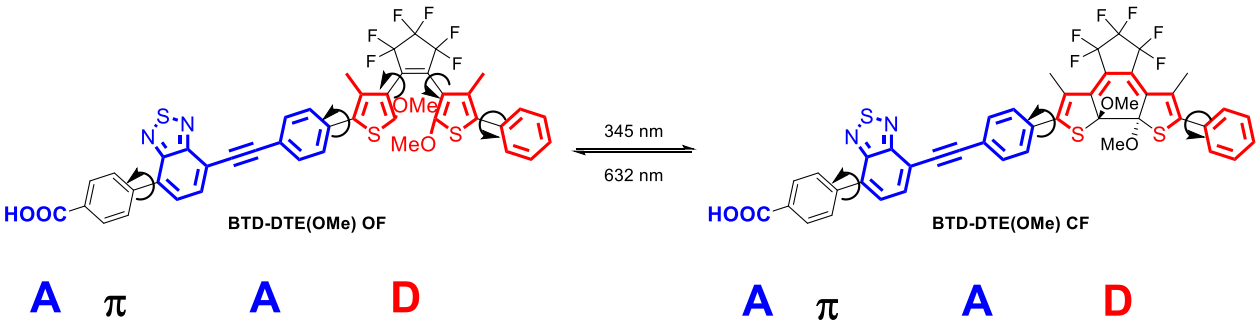

*Figure 139: structures of **DTE(OMe)-BODIPY** OF and CF with electron rich (red) and electron poor (blue) structural motifs.*

Upon photoisomerization from OF to CF, the absorption band of **BTD-DTE(OMe)** at 310 nm shows a decreased ε, a blue shift of 10-17 nm, and a bathochromic shoulder in all solvents, except DMSO (Table 17). The behaviour of a blue shifted thiophene and phenyl region from OF to CF is not typical for DTE(OMe)[30], but already described in the literature for DAEs with strong electron withdrawing residues in push-pull arrangements.[84] We assume that the geometrical change of the molecule between OF and CF is responsible for these observations (Figure 139).[109] A polarized structure in the ground state for **BTD-DTE(OMe)** OF between the BTD acceptor and the methoxy-thiophene donor is observed. Conceivable is a spreading of the push-pull interaction between the electron deficient benzoate-BTD moiety and the electron rich phenyl-thiophene part connected by an ethinyl bridge in the anti-parallel conformation of **BTD-DTE(OMe)** OF. But a distinction of the parallel and anti-parallel conformer is difficult for DTEs with perfluorosubstituted backbone.[110] Upon photoisomerization, the highly increased π-system of **BTD-DTE(OMe)** CF with simultaneous decreased thiophene donor strength by losing the conjugation to the methoxy-group, leads to a rigidified DTE(OMe) structure and different twists in the D-A-π-A system.The benzothiadiazole (BTD) absorption band around 405 nm of **BTD-DTE(OME)** OF is also slightly blue shifted (1-5 nm) upon photoisomerization to the **BTD-DTE(OMe)** CF. The observed hyperchromic change of this band can be related to the increased conjugation of the DTE(OMe) CF π-system.[30] Generally, the extinction coefficient of $\lambda_{Abs,max}$ **BTD-DTE(OMe)** OF (≈310 nm) shows a trend of decreased values in polar solvents (factor 2.3 between MeCN and MTBE, Table 17). The main π-π* absorption band of the DTE(OMe)

unit of **BTD-DTE(OMe)** CF is located around 630 nm and shows a small solvent dependency (628-642 nm), besides decreased ε values observed upon switching from non-polar solvents to solvents with high polarity (factor 1.9 between MeCN and MTBE, Table 17). The hypochromic behaviour of **BTD-DTE(OMe)** OF and CF in solvents with increased polarity can be related to polarized or conjugated ground state structures.[111] The cycloreversion for **BTD-DTE(OMe)** from OF to CF was done with 632 nm LED irradiation. The switching process is reversible in all investigated solvents. In sum, small solvent dependency of **BTD-DTE(OMe)** OF and CF on $\lambda_{Abs,max}$ plus the high decrease in ε values is an indication of a polarized or conjugated ground state of both photoisomers, with higher pronounced effects in **BTD-DTE(OMe)** CF.

The literature known dependency between the increasing polarity of a solvent with the decreasing QY_{OC} of DTE units is not visible, probably caused by the non-ideal irradiation to avoid photodegradation (Table 17).[112] [5] The QY_{OC} does not change significantly for **BTD-DTE(OMe)** OF in the investigated solvents, but has the highest value in toluene ($9.5 \cdot 10^{-2}$) and the lowest value in DMSO ($8.5 \cdot 10^{-3}$). Both values correlate with the most red shifted DTE absorption (most flattened) for **BTD-DTE(OMe)** OF in toluene (314 nm), and the most blue shifted DTE absorption (most twisted) in DMSO (287 nm). However, besides solvent polarity, also solvent viscosity is influencing the ring closure reaction, due to effects on the conversion rate of antiparallel and parallel conformation, which was not investigated further in the current study.[102] However, the cycloreversion is less dependent on the solvent viscosity than the cyclization reaction. This is attributed to the very rapid reaction taking place in the time region shorter than the diffusion motion of the solvent.[102] The QY_{CO} has the highest value in DCM ($2.8 \cdot 10^{-4}$) and the lowest in MTBE ($3.3 \cdot 10^{-5}$), which is comparable with the literature values for DTE(OMe) systems with increased molecule size.[32] A drop down in cycloreversion quantum yield for DTE systems with increased push-pull character is literature known.[84] An oberservable decrease of QY_{CO} could be a hint for a higher polarization of the conjugate in the investigated solvent.

*Table 17: photochromic properties of **BTD-DTE(OMe)** OF and CF in different solvents.*

Solvents	Open form		Closed form	
	$\lambda_{Abs,max}$ [nm] (ε [10^3·L/(mol·cm)])	QY_{OC}[ac]	$\lambda_{Abs,max}$ [nm] (ε [10^3·L/(mol·cm)])	QY_{CO}[bc]
Toluene	314 (32.2), 412 (18.9)	$9.53 \cdot 10^{-2}$	304 (28.9), 408 (22.2), 642 (7.56)	$9.63 \cdot 10^{-5}$
Dioxane	313 (30.0), 407 (18.9)	$4.16 \cdot 10^{-2}$	297 (27.2), 404 (22.6), 639 (8.89)	$9.04 \cdot 10^{-5}$
MTBE	310 (37.8), 405 (21.7)	$2.00 \cdot 10^{-2}$	293 (35.6), 404 (27.2), 631 (10.6)	$3.33 \cdot 10^{-5}$
EtOAc	309 (28.4), 405 (16.1)	$2.67 \cdot 10^{-2}$	293 (25.0), 401 (19.5), 632 (6.95)	$9.80 \cdot 10^{-5}$
DCM	311 (25.0), 407 (13.9)	$4.67 \cdot 10^{-2}$	299 (22.8), 403 (17.2), 633 (4.67)	$2.75 \cdot 10^{-4}$
DMSO	287 (43.4), 408 (19.5)	$8.47 \cdot 10^{-3}$	287 (44.5), 407 (23.9), 642 (9.23)	$4.38 \cdot 10^{-5}$
MeCN	310 (21.1), 405 (12.3)	$3.33 \cdot 10^{-2}$	296 (17.8), 403 (14.3), 630 (5.48)	$7.73 \cdot 10^{-5}$
MeOH	309 (31.7), 405 (19.5)	$2.63 \cdot 10^{-2}$	293 (30.0), 404 (23.3), 628 (9.45)	$7.70 \cdot 10^{-5}$

λ_{max}: absorption maxima, QY_{OC}: cyclization quantum yield, QY_{CO}: cycloreversion quantum yield, ε extinction coefficient

[a] Under irradiation with 345 nm light. [b] Under irradiation with 632 nm light. [c] Determined by using the initial slope method.

2.6.4.2 Emission

Upon excitation at the π-π* absorption band maximum of the BTD unit (≈405 nm), **BTD-DTE(OMe)** OF and CF showed fluorescence. The absorption band of the BTD moiety overlaps with the π-π* absorption band of DTE(OMe) in **BTD-DTE(OMe)** CF. **BTD-DTE(OMe)** OF and CF were always excited in the maximum of the BTD-unit (see Table 17). Therefore, excitation around 405 nm excites the DTE(OMe) unit with a low transition propability as well. A switching of **BTD-DTE(OMe)** OF and CF with λ_{Exc} is neglectable due to the higly decreased cycloreversion quantum yields of the CF and the smaller extinction coefficient of OF in the 400 nm range. Using the comparative method for the determination of quantitative emission, the simultaneous excitation of BTD and DTE leads to smaller determined ϕ_{Fl} values for **BTD-DTE(OMe)** CF. The emission maxima in **BTD-DTE(OMe)** OF show positive solvatochromism, while the emission maxima in **BTD-DTE(OMe)** CF show solvent interactions but only a small visible trend (see Figure 140 and Table 18).

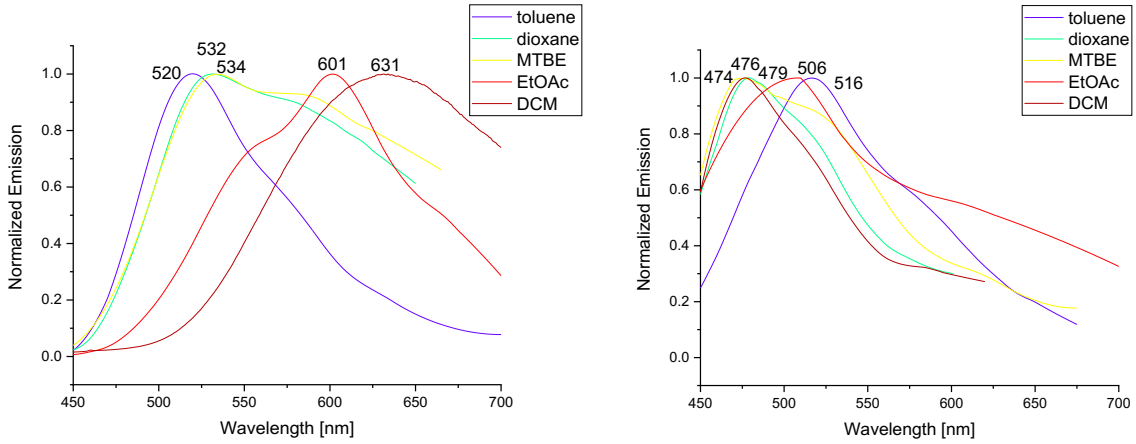

Figure 140: emission spectra of left: ***BTD-DTE(OMe)*** *OF; right: BTD-DTE(OMe) CF.*

The emission bands of **BTD-DTE(OMe)** OF (Figure 3, left) are located between 520-631 nm, and show a broad shoulder towards red, which is less pronounced for **BTD-DTE(OMe)** CF (Figure 3, right) with blue shifted maxima of 474-522 nm. The data of both photoisomers in DMSO and MeOH are presented in the spectra appendix 5.2. While the emission band of **BTD-DTE(OMe)** OF in different solvents overlaps with the long wavelength absorption band of the DTE(OMe) unit of **BTD-DTE(OMe)** CF (exceptions: **BTD-DTE(OMe)** in toluene, DMSO and MeOH shows highly decreased shifts from $\lambda_{Emi,OF}$ to $\lambda_{Emi,CF}$), the emission band maxima of CF in different solvents is located between the absorption of the fluorophore around 400 nm and the absorption of the DTE(OMe) around 630 nm. This results in a read-out possibility for the isomerization of **BTD-DTE(OMe)** OF to CF and vice versa, by following the fluorescence signal at the two different emission maxima of both photoisomers. The difference in the bathochromic emission signal shift of the two isomers follows the order of toluene<MTBE<dioxane<EtOAc<DCM, with 4 nm in toluene up to 155 nm in DCM.

The emission spectra for **BTD-DTE(OMe)** OF in MeCN (Figure 141) shows two bands located at 499 nm and the >600 nm range, which could hint to two different excited states with different energies, and strongly hints to a photoinduced twisted intramolecular charge transfer (TICT) state.[57] The prove of a TICT-state of **BTD-DTE(OMe)** OF in MeCN is not part of this work. However, the emission spectra of **BTD-DTE(OMe)** CF in MeCN shows only one maximum at 485 nm.

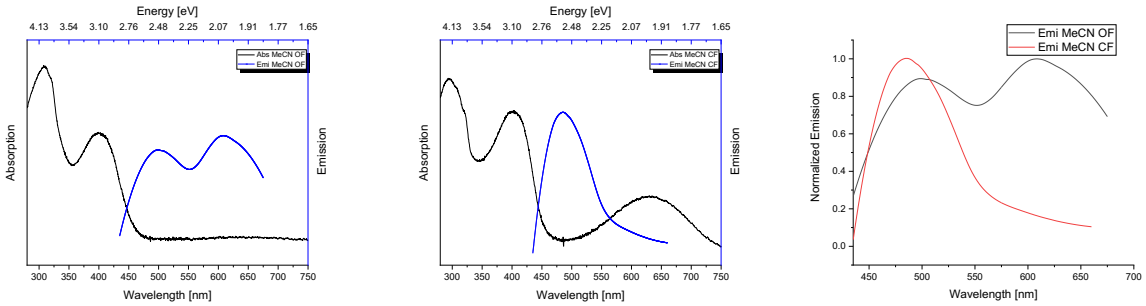

*Figure 141: absorption (black) and emission (blue) spectra of **BTD-DTE(OMe)** in MeCN; left: OF; middle: CF; right: emission spectra of OF (black) and CF (red).*

The Stokes shifts of **BTD-DTE(OMe)** OF in aprotic solvents with different polarity were correlated with the orientation polarizability ($\Delta f(\varepsilon,n)$) of these solvents (Figure 142). The Lippert orientation polarizability function Δf can be calculated**,** which describes the solvent dependency of the Stokes shift for a compound.[49] The plot only considers general solvent effects, for example it does not include hydrogen bonding or other quenching effects, e.g. energy-transfer processes (see chapter 1.4.3). The line fit for **BTD-DTE(OMe)** OF shows a large positive slope with increased Stokes Shifts from non-polar to polar solvents. The plot hints toward a high change in the dipole moment with TICT in MeCN observed upon excitation from the ground state to the excited state of **BTD-DTE(OMe)** OF.

The Stokes Shifts of **BTD-DTE(OMe)** CF are with 73-108 nm comparable to the emission of BTD-fluorophores **137** and **157** (2.5.4), and the Lippert-Mataga plot slope shows a minor dipole moment change upon photoexcitation (Figure 142). Therefore, the excited state of **BTD-DTE(OMe)** CF can be assumed as being of low polarization.

BTD-DTE(OMe) OF in DMSO has an exceptional small Stokes shift of 76 nm and is next to MeOH the only investigated solvent with a bathochromic shift of the emission band upon photoisomerization. This hints to a different excited state in the two solvents. DMSO has the highest viscosity with P = 1.99 causing different behaviour of conformational and twisting movement in the molecule. MeOH can interact with the carboxylic acid and the BTD moieties by H-bridging. Both are therefore excluded in the plots for the investigation of general solvent effects. The highly blue shifted emission maxima of **BTD-DTE(OMe)** OF in toluene can be explained by π-π interactions, with stabilization of photoinduced polarization in the excited state.

*Table 18: emission properties of **BTD-DTE(OMe)** OF and CF in different solvents.*

Solvent	Δf[a]	Open form			Closed form			$\frac{\Phi_{Fl}\ \mathrm{OF}}{\Phi_{\mathrm{Fl}}\ \mathrm{CF}}$
		$\lambda_{Emi,max}$ OF[b] [nm]	Δν [nm/ cm^{-1}]	ϕ_{Fl}[c]	$\lambda_{Emi,max}$ CF[b] [nm]	Δν [nm/cm^{-1}]	ϕ_{Fl}[c]	
Toluene	0.013	520	108/5041	$8.63\cdot10^{-3}$	516	108/5130	$2.91\cdot10^{-4}$	0.034
Dioxane	0.02	532	125/5773	0.80	479	85/3876	$1.10\cdot10^{-3}$	0.001
MTBE	0.116	534	129/5965	0.58	474	70/3655	$6.09\cdot10^{-4}$	0.001
EtOAc	0.201	601	196/8052	0.38	506	105/5175	$6.28\cdot10^{-4}$	0.002
DCM	0.219	631	224/8722	0.27	476	73/3805	$2.52\cdot10^{-3}$	0.009
DMSO	0.263	484	76/3849	$2.77\cdot10^{-5}$	522	115/5412	$1.03\cdot10^{-3}$	37.2
MeCN	0.305	499, 608	94, 204/8243	$9.22\cdot10^{-6}$	485	82/4195	$8.78\cdot10^{-5}$	9.52
MeOH	0.309	509	104/5044	$1.82\cdot10^{-4}$	511	107/5183	$2.09\cdot10^{-4}$	1.15

Δf: orientation polarizability, $\lambda_{Emi,max}$: emission maxima, Δν: Stokes shift, ϕ_{Fl}: fluorescence quantum yield

[a] *Δf* from [103] [b] For $\lambda_{Exc} = \lambda_{Abs,max}$ (BTD). [c] Determined by the comparitive method with tetramethyl-BODIPY and Rhodamine 101.

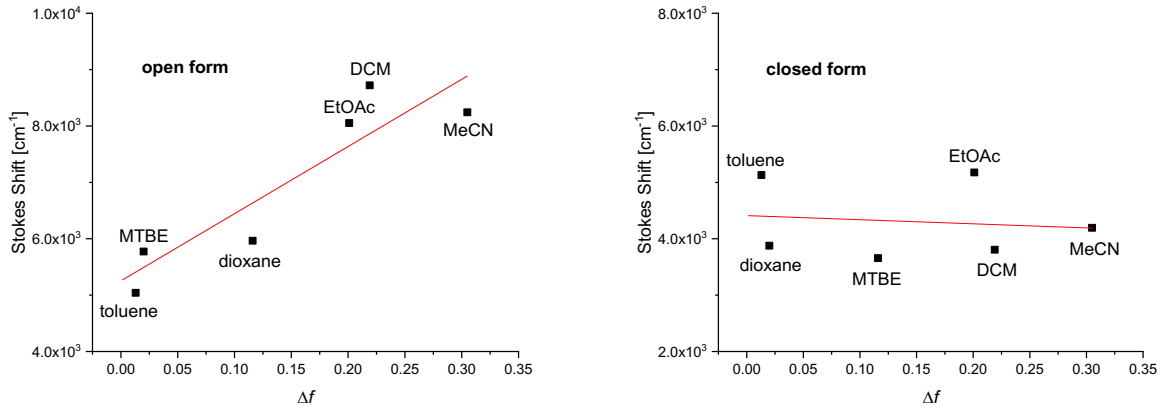

*Figure 142: LIPPERT-MATAGA plots (Stokes shifts, Δf), left: **BTD-DTE(OMe)** OF, right: **BTD-DTE(OMe)** CF.*

Fluorescent quantum yields of **BTD-DTE(OMe)** OF strongly depend on the solvent polarity: in less polar solvents, these values are dramatically increased (Table 2, from $9.2\cdot10^{-6}$ in in MeCN up to 0.6 in MTBE and 0.8 in dioxane). The change of the fluorescence quantum yield by rising Δ*f* for **BTD-DTE(OMe)** OF is shown in Figure 143 and shows a negative slope. With the comparative method, ϕ_{Fl} OF in MeCN could not be determined precisely due to the double band emission from 450-700 nm, but it is highly increased, which indicated a further TICT relaxation pathway for **BTD-DTE(OMe)** OF in MeCN.

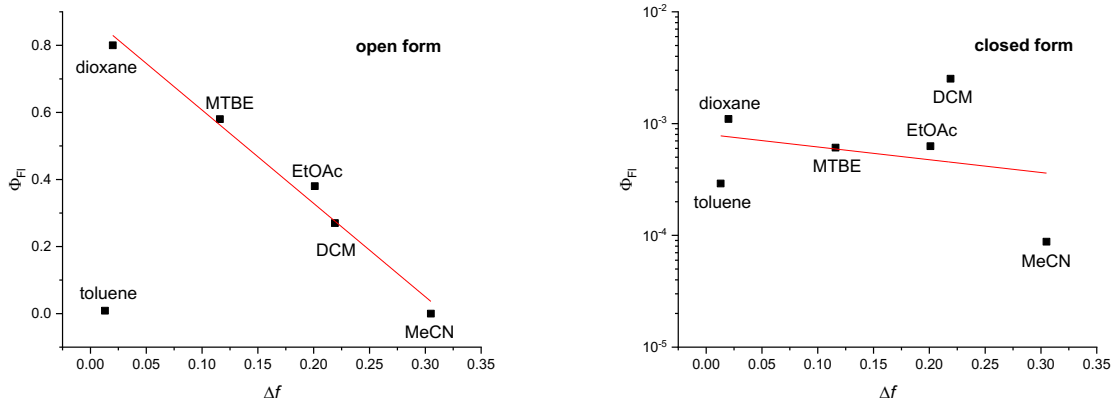

*Figure 143: dependence of orientation polarizability and fluorescence quantum yield of **BTD-DTE(OMe)** in different solvents; left: open form; right: closed form.*

Toluene with a fluorescence quantum yield of $8.6 \cdot 10^{-3}$ is a special solvent due to the ability of π-system stabilization by π-π interactions.[112] Starting from MTBE with high ϕ_{Fl} OF (0.8) the trend is almost linear and drops down for MeCN ($9 \cdot 10^{-6}$). For the **BTD-DTE(OMe)** CF almost no trend is visible, indeed the ϕ_{Fl} strongly differs between various solvents, but is generally rather small (10^{-3}-10^{-5}).

Solvents with $\Delta f < 0.26$ (DMSO) show a significant higher ϕ_{Fl} for **BTD-DTE(OMe)** OF compared to **BTD-DTE(OMe)** CF. Therefore, we define them as normal modulators (toluene, MTBE, dioxane, EtOAc, DCM). Solvents with $\Delta f > 0.26$ (DMSO) show lower emission for **BTD-DTE(OMe)** OF than for **BTD-DTE(OMe)** CF – they are inverse modulators (DMSO, MeCN, MeOH). The highest modulation value (ϕ_{Fl} CF/ϕ_{Fl} OF) have dioxane (0.001) and DMSO (37.2), whereas MeOH has almost the same ϕ_{Fl} for **BTD-DTE(OMe)** OF and CF, which could be caused by a different behaviour of **BTD-DTE(OMe)** in protic solvents.

2.6.4.3 Conclusion

In **BTD-DTE(OMe)**, the donor moiety in the carboxylic acid(A)-phenyl(π)-BTD(A)-methoxy-thiophene(D) structure can be reversibly switched between electron rich in **BTD-DTE(OMe)** OF to electron poor in **BTD-DTE(OMe)** CF. A significant difference in the emission behaviour in solvents of different polarity between **BTD-DTE(OMe)** OF and **BTD-DTE(OMe)** CF were shown, whereas the emission energy could be suitable as a read-out signal for the assignment of the two photoisomers. While the OF shows a strong positive solvatochromism with 76-224 nm Stokes shift with a TICT state in MeCN and almost linear decreased ϕ_{Fl} from nonpolar to polar solvents, CF showed solvent dependency for Stokes shifts (70-115 nm) and quantum yields, but smaller trends. This leads to a two-state switchable system, with

expected on(OF)-off(CF) emission modulators for less polar solvents and unexpected off(OF)-on(CF) emission modulation for polar solvents. With time-resolved studies in solution and on TiO_2 in the future, the investigation of the excited state of **BTD-DTE(OMe)** should give an insight of the elemental processes in the conjugate.

BTD-DTE(OMe) compared to **DTE(OMe)-BODIPY** shows a highly different behaviour in the solvent dependency of the emission properties. A stronger stabilization by the surrounding solvent molecules leads to a broad wavelength range of the **BTD-DTE(OMe)** OF emission bands with moderate to high Stokes shifts. With the higher Stokes shifts of BTD fluorophores compared to BODIPY, a further fluorescence read-out possibility can be used in future applications.

3 Summary and Outlook

In this thesis, the development and investigation of photoswitchable DTE(OMe)s π-coupled with BODIPY- and BTD-fluorophores as energy- and electron-transfer conjugates were shown. The spectroscopical analysis by UV/Vis-/ and fluorescence-spectroscopy of the stepwise synthesized conjugates allowed an insight of molecular ground and excited state behaviour of the conjugates.

3.1 BODIPYs

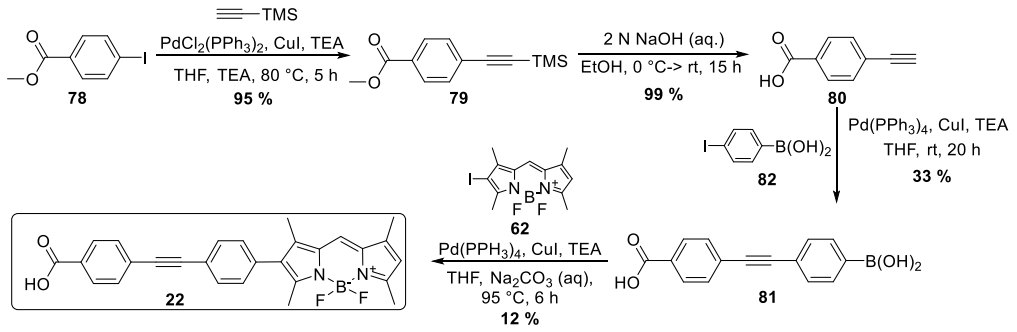

*Figure 144: four-step synthesis of BODIPY-stick **22**.*

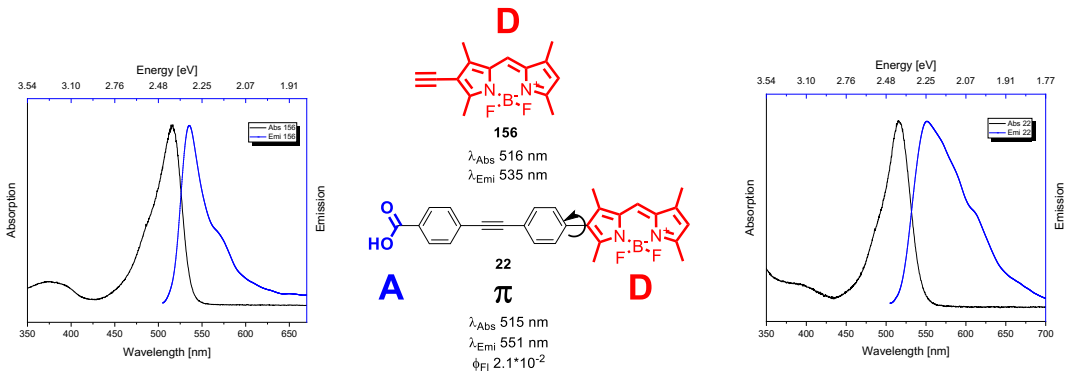

*Figure 145: middle: structures of synthesized BODIPYs **156** and **22** with absorption (black) and emission (blue) spectra of left: **156** and right: **22**.*

The BODIPYs **156** and **22** (Figure 144) were synthesized and spectroscopically investigated (Figure 145). The π-twisted BODIPY-stick **22** shows a D-π-A structure, a moderate Stokes shift and small fluorescence quantum yield. BODIPY-stick **22** attached on a TiO_2-surface in the future, will serve as a fluorophore-conjugate for the time resolved investigation of the BODIPY-cation formation. Furthermore, a NIR-BODIPY (**21**) was synthesized and the literature known highly bathochromic shift of the absorption by the

introduction of an *aza*-bridge in the BODIPY-core, as well as the synthetic access was confirmed. *Aza*-BODIPYs show larger Stokes shifts and bathochromic shifted absorption and emission properties. They could replace the tetramethyl-BODIPY unit (**4**) in the future.

3.2 BTDs

Furthermore, BTDs **15**, **137** (Figure 146) and **157** were synthesized and their absorption and emission properties showed the literature known behaviour of BTDs. Since emission properties of BTDs are rare in the literature, the recorded data gave us design rules for the final BTD-DTE(OMe) **23** conjugate.

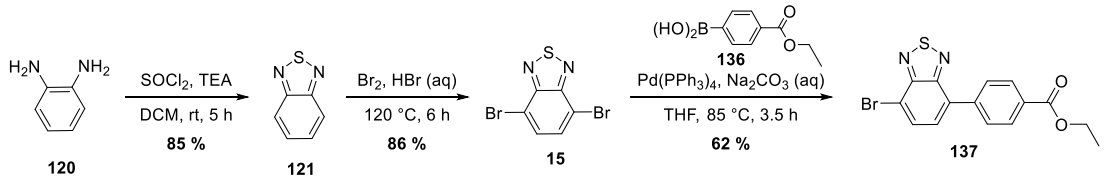

*Figure 146: three-step synthesis to BTD-benzoate **137**.*

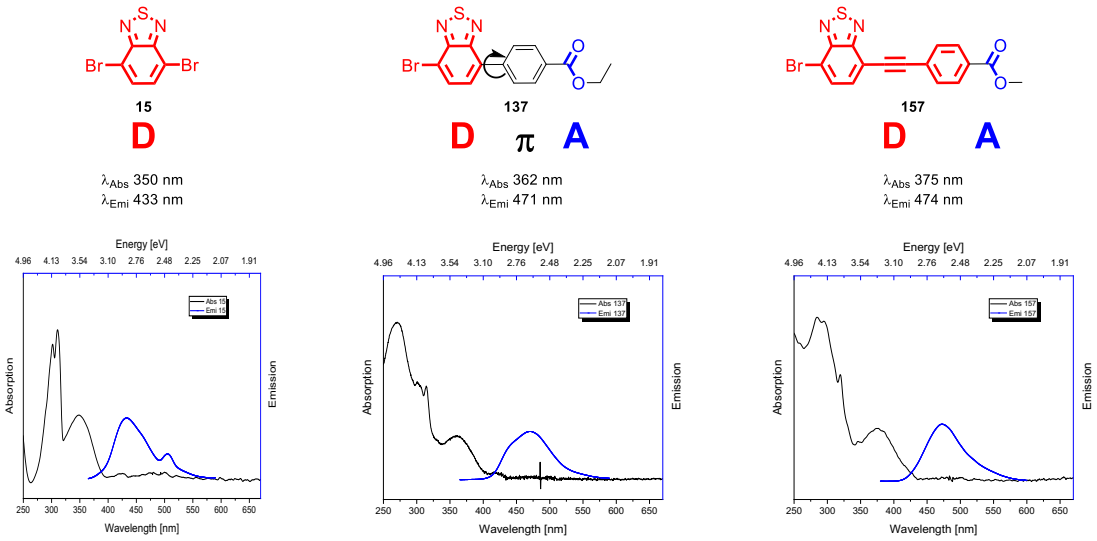

*Figure 147: top: structures of synthesized BTDs **15**, **137** and **157** with absorption (black) and emission (blue) spectra of down: left: **15**, middle: **137**, right: **157**.*

3.3 DTE(OMe)s

The literature known symmetrical DTE(OMe)s **3** and **29** (Figure 148 and Figure 149) were synthesized and a synthetic access with late state introduction of substituents for asymmetrical DTE(OMe)s (**145**, **155**, **147-149**) developed (Figure 152 and Figure 153).

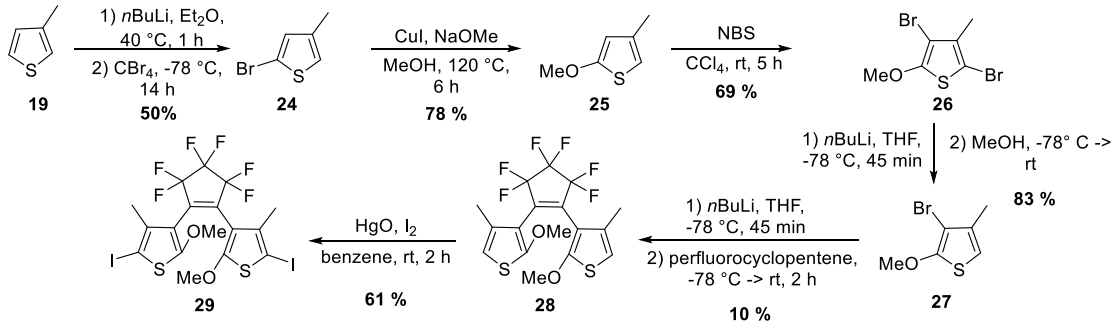

*Figure 148: literature known six-step synthesis of diiodo-DTE(OMe) **29**.*

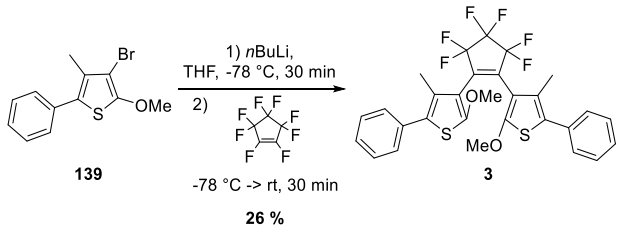

*Figure 149: synthesis of the symmetrical DTE(OMe) **3**.*

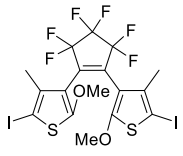

29 λ_{Abs}: OF: 259 nm; CF: **270**, 389, 594 nm

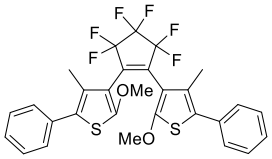

3 λ_{Abs}: OF: 286 nm; CF: **292**, 405, 624 nm

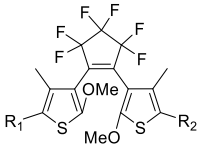

145 R_1 = Cl, R_2 = Ph-Ethyne-TMS
155 R_1 = HOOC-Ph, R_2 = Ph-Ethyne-H
147 R_1 = Cl-Ph, R_2 = Ph-Ethyne-TMS
148 R_1 = MeO-Ph, R_2 = Ph-Ethyne-TMS
149 R_1 = Ph, R_2 = Ph-Ethyne-H

145 λ_{Abs}: OF: 317 nm; CF: **326**, 391, 600 nm
155 λ_{Abs}: OF: 317 nm; CF: **315**, 411, 629 nm
147 λ_{Abs}: OF: 310 nm; CF: **329**, 403, 630 nm
148 λ_{Abs}: OF: 308 nm ; CF: **336**, 409, 636 nm
149 λ_{Abs}: OF: 304 nm; CF: **323**, 405, 629 nm

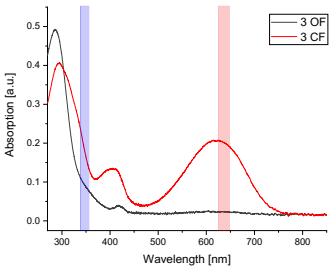

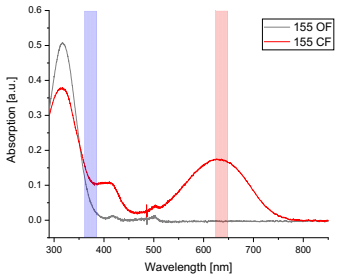

*Figure 150: top: structures of synthesized symmetrical DTE(OMe)s **3** and **29**; down: left: structures of synthesized unsymmetrically substituted DTE(OMe)s **145, 155, 147-149**; middle: absorption spectra of **3** OF (black) and CF (red); right: absorption spectra of **155** OF (black) and CF (red).*

Furthermore, the spectroscopical properties of the photoswitches were investigated and the literature values for **3** confirmed with our analytical techniques. DTE(OMe)s in general show quantitatively switching behaviour under 345 nm irradiation with moderate quantum yields for the cyclization reaction and highly decreased cycloreversion quantum yields under 632 nm irradiation in MeCN. The absorption spectra of DTE(OMe) OFs and CFs are well separated and show fatique resistance over five switching cycles. Diiodo-DTE(OMe) **29** shows the expected photodecomposition in the switching cycles under 345 nm irradiation and should have served as a synthetic access for transition metal mediated couplings. This strategy was cancelled by another synthetic way toward unsymmetrically substituted DTE(OMe)s. However, compound **29** showed well separated IR signatures of **29** OF to **29** CF, which can be used for future applications.

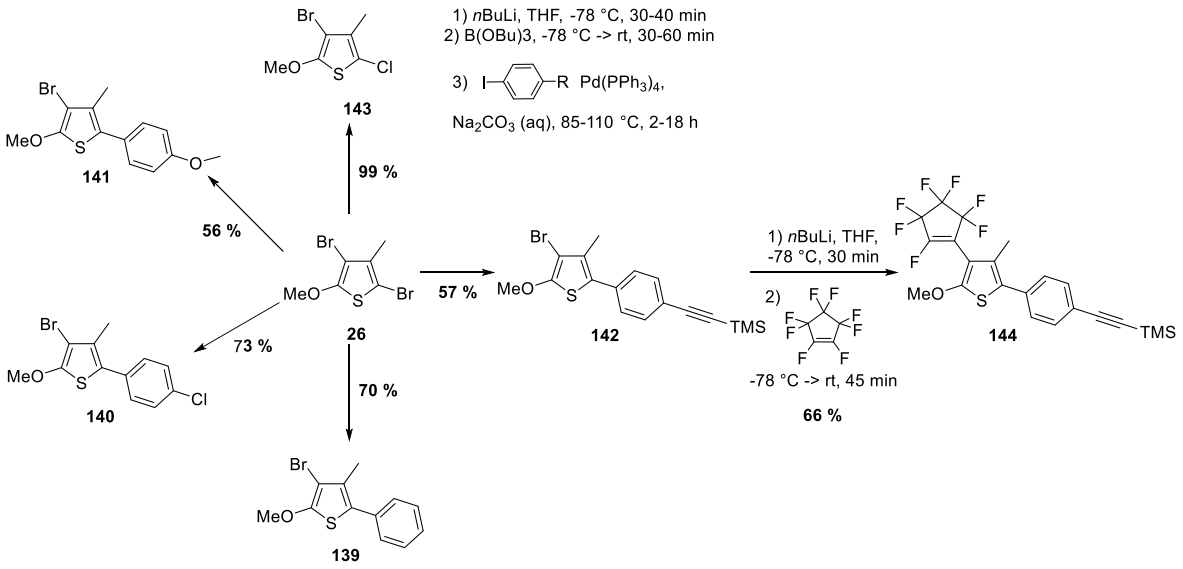

*Figure 151: synthesis of thiophene-phenyls **139-144**.*

With the unsymmetrically substituted DTE(OMe)s **145**, **155**, **147-149** (Figure 152 and Figure 153) the design-rules for the switches were investigated, which showed the expected red-shifts with enlargment of the π-system and an unexpected blue-shift for the phenyl- and thiophene-region for the electron deficient DTE(OMe) **155** upon photocyclisation. All synthesized unsymmetrically substituted DTE(OMe) switches showed quantitative cyclization and ringopening with small quantum yields for the ringclosure, and highly decreased quantum yields for the cycloreversion reaction.

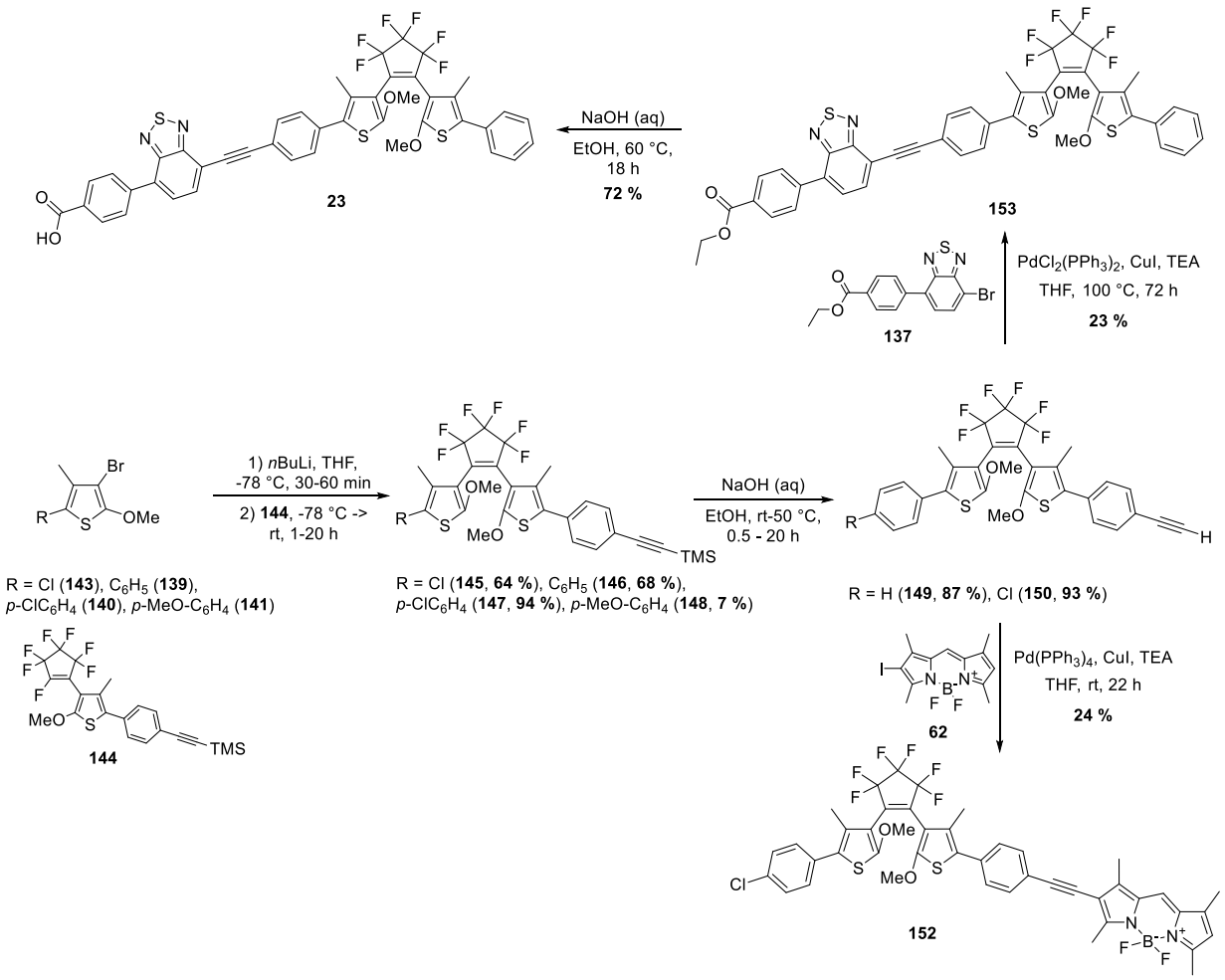

*Figure 152: synthesis of DTE(OMe)-fluorophores **152** and **23**.*

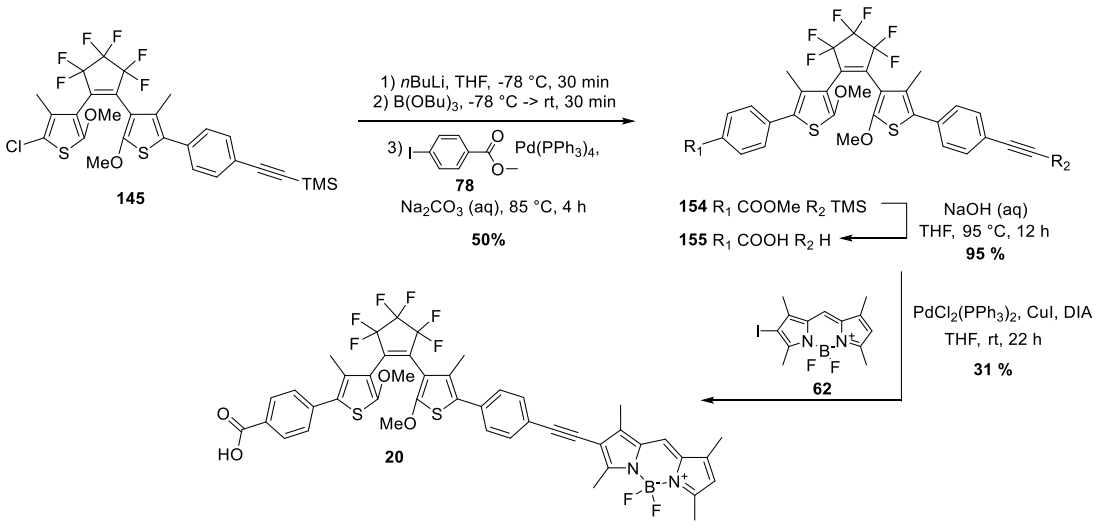

*Figure 153: synthesis of DTE(OMe)-BODIPY **20**.*

3.4 DTE(OMe)-Fluorophores

The attachment of the BODIPY- and BTD-fluorphore moieties to the DTE(OMe) photoswitch in Sonogashira-cross couplings gave the DTE(OMe)-BODIPYs **20** and **152** and the BTD-DTE(OMe) **23**. Chlorophenyl-subsituted DTE(OMe)-BODIPY **152** showed photodecomposition under 345 and 365 nm irradiation in MeCN and DCM. Since the conjugate does not carry an anchor group, further investigations of this conjugate were cancelled. DTE(OMe)-BODIPY **20**, shows fatique resistance over three switching cycles with 345 and 632 nm irradiation in MeCN (Figure 154). With decreased quantum yields for both cyclization and cycloreversion reaction, and quantitative ratio in the pss of DTE(OMe)-BODIPY **20** (CF:OF). The emission was decreased upon photoisomerization, which indicates an energy transfer process in DTE(OMe)-BODIPY **20** CF (FRET). The absorption of the BODIPY-moiety around 530 nm partly overlaps with the broad π-π* DTE(OMe) CF absorption band, which leads to a non-ideal fluorescence excitation of the conjugate.

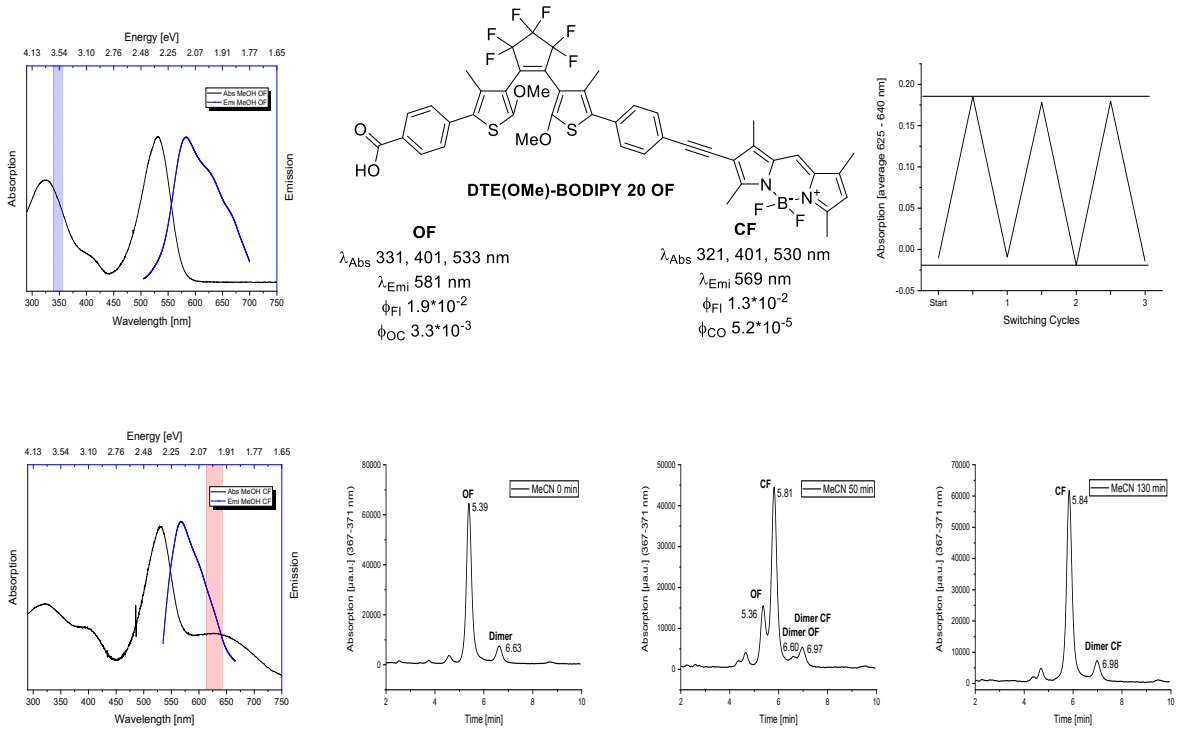

*Figure 154: top: middle: structure of DTE(OMe)-BODIPY **20**; right: switching cycles under 345 and 632 nm irradiation; left: OF absorption (black) and emission (blue); bottom: left: CF absorption (black) and emission (blue); middle and right: LCMS chromatogram of 0 min, 50 min and 130 min, 345 nm irradiation.*

The conjugate BTD-DTE(OMe) **23** shows fatique resistance over three switching cycles with 345 and 632 nm irradiation in MeCN with decreased quantum yields for both reactions, similar to

DTE(OMe)-BODIPY **20**. The ratio in the pss of BTD-DTE(OMe) **23** (CF:OF) is slightly decreased to 98:2 in MeCN and 94:6 in MeOH and the emission after excitation into the well separated BTD band around 400 nm was unexpectly decreased in BTD-DTE(OMe) **23** (OF compared to CF in MeCN) (Figure 155).

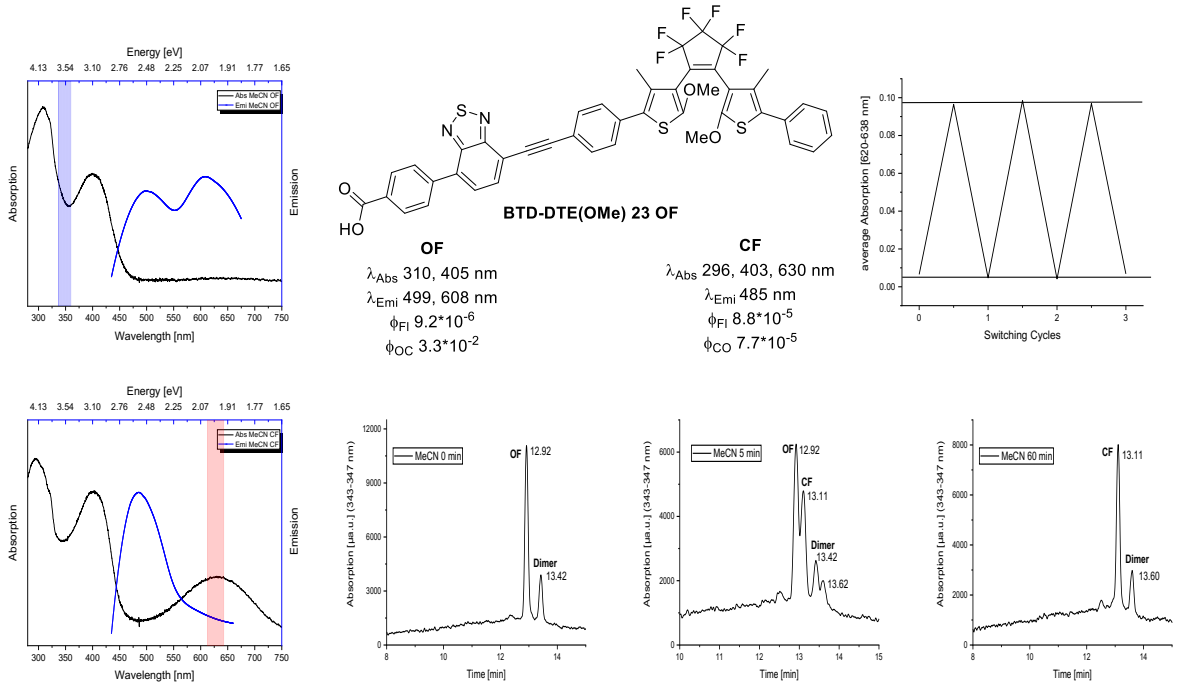

Figure 155: top: middle: structure of BTD-DTE(OMe) ***23****; right: switching cycles under 345 and 632 nm irradiation; left: OF absorption (black) and emission (blue); bottom: left: CF absorption (black) and emission (blue); middle and right: LCMS chromatogram of 0 min, 5 min and 40 min, 345 nm irradiation.*

3.5 SOLVATOCHROMISM

Caused by the unexpected emission behaviour of the differently arranged D-A conjugates with a D-D-π-A kind of arrangement in DTE(OMe)-BODIPY **20** (with a photoswitchable central D, Figure 156) and a D-A-π-A kind of arrangement in BTD-DTE(OMe) **23** (with a photoswitchable external D, Figure 157), the solvatochromic behaviour of both conjugates were investigated. The absorption spectra of DTE(OMe)-BODIPY **20** and BTD-DTE(OMe) **23** OFs and CFs showed minor solvent influence with negative solvatochromism for DTE(OMe)-BODIPY **20** CF, and positive solvatochromism for BTD-DTE(OMe) **23** CF, which was indicated by LIPPERT-MATAGA plots. A different geometrical arrangement between the two states of the conjugates (OF and CF) can be assumed in the ground state of both molecules.

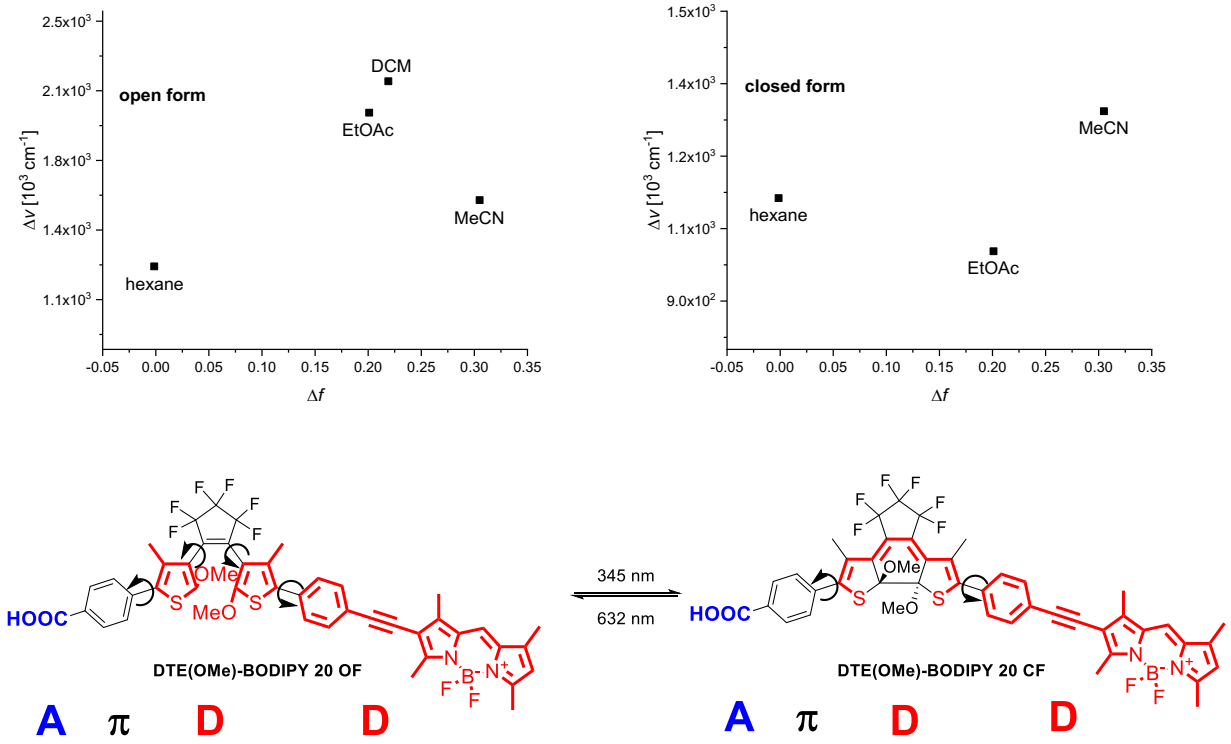

*Figure 156: top: LIPPERT-MATAGA plots of DTE(OMe)-BODIPY **20** left: OF, right: CF; bottom: structures of DTE(OMe)-BODIPY **20** OF and CF.*

With the excitation of the fluorophore-moiety in the conjugates, DTE(OMe)-BODIPY **20** OF showed small solvent dependency with moderate Stokes shifts (38-70 nm), positive solvatochromism (Figure 156) and decreasing fluorescence quantum yields for increasing *Δf*, while BTD-DTE(OMe) **20** OF showed high solvent dependency, high Stokes shifts (76-224 nm), clearly positive solvatochromism (Figure 157), and increasing fluorescence quantum yields for increasing *Δf*. DTE(OMe)-BODIPY **20** CF (Stokes shifts 30-39 nm) and BTD-DTE(OMe) **23** CF (Stokes shifts 70-115 nm) showed decreased solvent influences with expected small fluorescence quantum yields changes. The different OF behaviour of both conjugates to their CFs can be explained by the molecules flexibility with different conformers in the OFs, and highly rigidified structure in the CFs. Furthermore, the strong solvent dependency of BTD-DTE(OMe) **23** OF indicates an ICT character in acetonitrile.

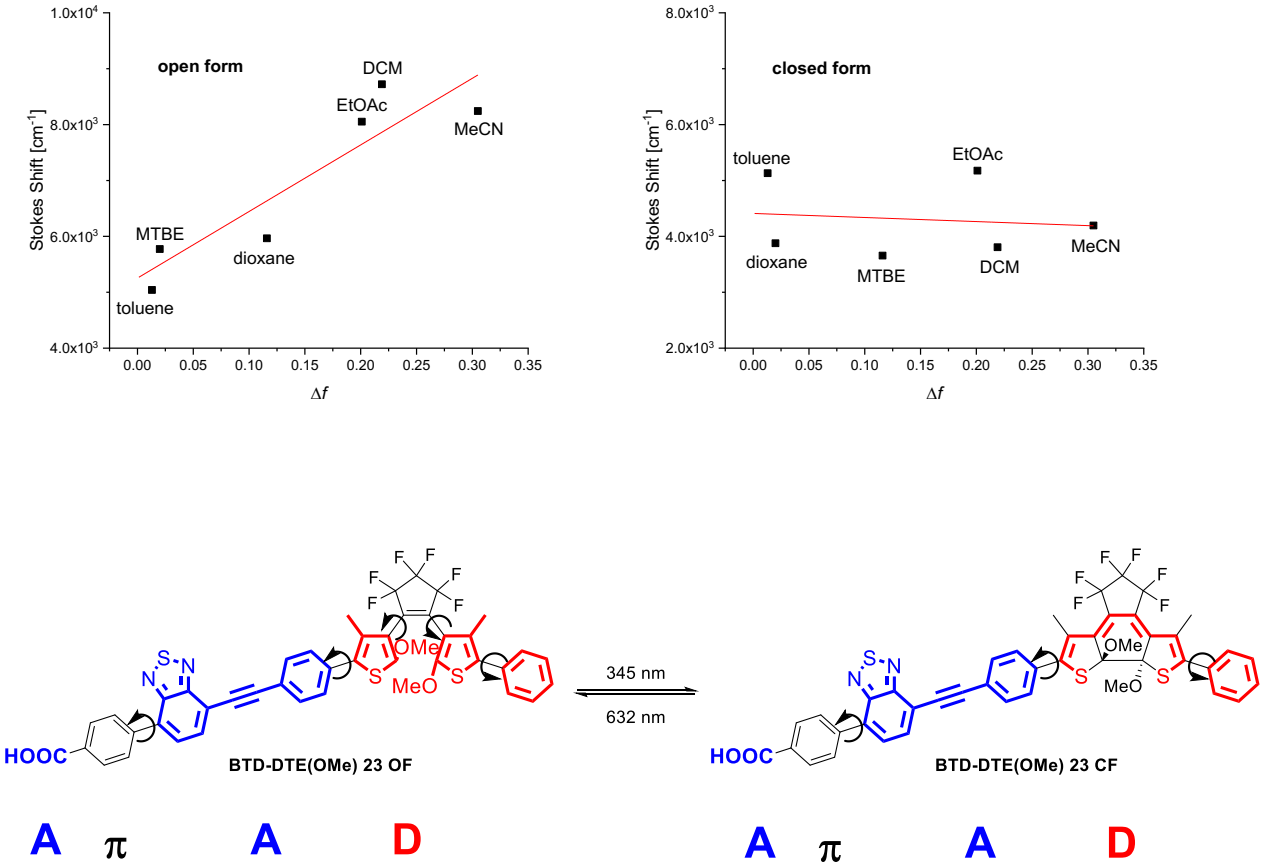

*Figure 157: top: LIPPERT-MATAGA plots of BTD-DTE(OMe) **23** left: OF, right: CF; bottom: structures of DTE(OMe)-BODIPY **23** OF and CF.*

Caused by the different spectroscopical behaviour of DTE(OMe)-BODIPY **20** OF to the photoisomer CF, and highly different behaviour BTD-DTE(OMe) **23** OF to the switched CF, the fluorescence emission can be used as a read-out signal for the two states of the DTE(OMe) photoswitches. Since BODIPYs show a rather small Stokes shift, the emission bands of DTE(OMe)-BODIPY **20** OF and CF overlap. For the emission bands of the two BTD-DTE(OMe) **23** photoisomers, a difference up to 151 nm in DCM between OF and CF can be reached, and the two isomers can be clearly distinguished by their emission spectra. The time resolved investigation of both conjugates DTE(OMe)-BODIPY **20** and BTD-DTE(OMe) **23**, as well as the BODIPY-stick **22** attached on semiconductor surfaces and in solution will reveal further details about the nature of the ground and excited states, and the energy- and electron-transfer-properties of the molecules.

For a further increased difference between the two states of a DTE(OMe)-fluorophore conjugate several improvements are possible. For the DTE(OMe)-BODIPY system **20**, a BODIPY dye with a better emission overlap with the absorption of DTE(OMe) CF, and higher Stokes shifts, will improve the adressability, the on-off modulation, and the fluorescence read-out property. The BTD-DTE(OMe) conjugate **23** could be improved by an either stronger acceptor moiety (withdrawing groups attached to the BTD-ethyne-phenyl unit) or stronger donor group (electron rich residues at the external DTE(OMe) phenyl unit).

4 Experimental Part

4.1 SYNTHESIS

4.1.1 General

Commercially available reagents for synthesis were used without further purification if not mentioned differently. Solvents were used in p.a. quality and were dried by standard procedures prior to use: ethyl acetate over potassium carbonate, DCM, pentane, and cyclohexane over phosphorus pentoxide. Toluene and THF were dried over sodium and potassium/benzophenone. DCM and Et_2O were dried over calcium hydride. Triethylamine (over KOH), Tributylborat and Trimethoxymethane were distilled fractionally and stored over molecular sieve (4 Å). All reactions were monitored by analytical thin-layer chromatography (TLC, silica gel, Merck 60 F254 plates). Final coumpounds DTE(OMe)-BODIPY **20**, chloro-phenyl-DTE(OMe)-BODIPY **152**, BTD-DTE(OME) **23** and DTE(OMe) **3** were purified by column chromatography several times.

4.1.1.1 NMR-spectra

NMR-spectra were recorded with a Bruker Avance 400 MHz or a Bruker AvanceIII 500 MHz. Spectrometer and used deuterated solvents are assigned in the analytical part for each compound. For ^{1}H-NMR and ^{13}C-NMR spectra, the residual solvent peaks were used as internal standards, the chemical shifts are given in ppm relative to tetramethylsilane (TMS), and coupling constants are given in Hz. The numbering (a-z, extension: a*-z*) of the atoms are arbitrary and do not follow the IUPAC nomenclature rules. Some carbon atoms in ^{13}C-NMR spectra were identified by standard techniques, based on heteronuclear decoupling NMR spectroscopy. The resonances of the carbon atoms of the fluorinated cyclopentene moiety of the compounds could not be observed because of the low intensity. For NMR measurements of all DTE switches, amberized NMR tubes from Norell (508-Up) were used (absorption spectra, Figure 158). In small substrate concentrations in NMR, *n*-pentane is visible in all spectra (^{1}H-NMR ($CDCl_3$): δ 0.88 (t, J = 7.0 Hz, 6H), 1.27 (m, 6H); 13C-NMR ($CDCl_3$): δ 14.1, 22.4, 34.2.).

4.1.1.2 Mass spectrometry

High-resolution mass spectra (HRMS) were performed on LTQ Orbitrap XL apparatus or on a Finnigan MAT 95 S, with an ionization potential of 70 eV.

4.1.1.3 IR spectroscopy

Infrared spectra were recorded as attenuated total reflectance (ATR) on a Thermo Nicolet Magna-IR 750 FTIR spectrometer and are reported as wavenumbers in cm^{-1}. The peak intensities were abbreviated as follows: s = strong, m = medium, w = weak.

4.1.1.4 Elemental Analysis

Elemental analysis were performed on Thermo FlashEA 1112 Organic Elemental Analyzer.Deviations between calculated and measured values are reasoned by halogene or sulfur containing samples.

4.1.1.5 Melting points

Melting points were measured with a Büchi SMP-20 melting point determination apparatus using open capillary tubes; the values remain uncorrected. Elemental analyses were performed on Thermo FlashEA 1112 Organic Elemental Analyzer. Melting points were not determined for photoswitchable DTE(OMe)s.

4.1.1.6 UV/Vis and Irraditation conditions

The spectra were recorded using a *Shimadzu* or an *Avantes* spectrometer. For the *Shimadzu* (1601 UV) spectrometer, the samples were irradiated on an optical bench. The irradiation in the ultraviolet region was made with a high-pressure mercury lamp (200 W, 200 HBO, *Osram*) and a suitable filter (326 nm, HW = 10 nm, 2.0 mW/cm^2). The infrared irradiation heating was reduced by a watercooled infrared-filter, focused and directed through a cuvette made of quartz-glass equipped with a magnetic stirring bar. The visible irradiation was produced by a xenon lamp (1000 W, 1000 XBO, *Osram*) and an edge filter (>500 nm, 8.3 mW/cm^2).

For the *Avantes* (AvaSpec Dual-channel Fiber Optic Spectrometer, equipped with the AvaLight-DH-S-BAL light source) spectrometer, the samples were irradiated with external LEDs. The detector slid with was set to 25 µm and the integration time to 2.0 ms. All samples for photochemical studies were prepared in concentrations of $1.8 \cdot 10^{-5}$ M, and degassed with a stream of argon for 15 min. The measurements were carried out inside a 10 mm Quartz SUPRASIL cuvette (Hellma Analytics), under constant stirring of the solution, at the temperature of 20.8 °C ± 0.5. Irradiation was carried out with 345 nm LED (Thorlabs, M340L4, λ_{max} 345 nm, HW = 11 nm, 2.0 mW/cm^2, Emission spectra Figure 158) and 632 nm LED (Thorlabs, M625L3, λ_{max} 632 nm, HW = 18 nm, 250 mW/cm^2, Emission spectra Figure 158). For the UV irradiation, the LED beam was focussed through the solutions in the cuvette holder of the spectrometer. For the visible light irradiation, the cuvette was placed in front of the LED to get the maximum intensity output of the light source. The irradiation was stopped for the UV/Vis measurements to avoid scattered light in the spectra. Quantum yields were determined by using the initial slope method.[83]

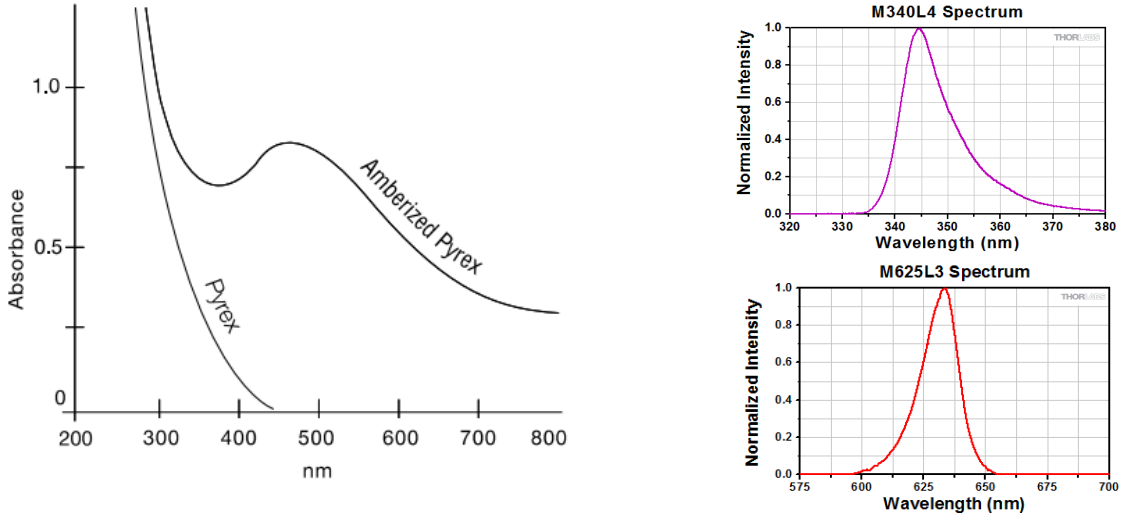

Figure 158: left: Absorption spectra of amberized NMR-Tubes. Spectra provided by Deutero, right: up: emission spectra of ML340L4, down: emission spectra of M625L3. Spectra provided by Thorlabs.

4.1.1.7 Fluorescence

Emission spectra were recorded at 22.0 °C with a F-4500 FL spectrometer (Hitachi). Fluorescence spectra were baseline corrected and the value of absorption at the excitation wavelength and the wavelength-dependent instrument sensitivity <700 nm were taken into account. Quantitative fluorescence was determined using the comparative method with tetramethyl-BODIPY **4** (≈500 nm) in MeCN and rhodamine 101 inner salt (≈600 nm) in MeOH as fluorescence standards.[85] [96] The used method for the determination of ϕFl is not precise for broad emission characteristics.

Samples of non-switchable molecules for fluorescence measurements were prepared as followed. A diluted solution (1.5-2.1·10^{-5} M) was degassed by a slow argon stream and the absorption spectra was determined. The solution was transferred via a styringe to the fluorescence measurements.

Samples of BTD-DTE(OMe) **23** CF/ DTE(OMe)-BODIPY **20** CF for fluorescence measurements were prepared as followed. A solution of pure BTD-DTE(OMe) **23** OF/ DTE(OMe)-BODIPY **20** OF (degassed, 1.8·10^{-5} M) was irradiated with UV-irradiation (345 nm) until the pss was reached (determination via UV/Vis spectra). The BTD-DTE(OMe) **23** CF/ DTE(OMe)-BODIPY **20** CF sample (pss (345 nm)) was diluted (9.0·10^{-6} and 3.6·10^{-6} M), the UV/Vis spectra recorded and the sample transferred to the fluorescence measurements. Samples of BTD-DTE(OMe) **23** OF/ DTE(OMe)-BODIPY **20** OF for fluorescence measurements were prepared as followed. A solution of pure BTD-DTE(OMe) **23** OF/ DTE(OMe)-BODIPY **20** OF (degassed, 1.8·10^{-5} M) was diluted (9.0·10^{-6} and 3.6·10^{-6} M), the UV/Vis spectra were recorded and the sample transferred to the fluorescence measurements. The samples were covered to protect the solutions against daylight.

4.1.2 Procedures

4.1.2.1 1,3,5,7-Tetramethyl-4,4-4,4-difluoro-4-bora-3a,4a-diaza-s-indacene (4)

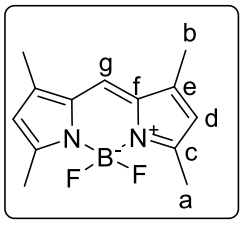

2,4-Dimethylpyrrole (**60**, 2.0 mL, 20.0 mmol) was dissolved in abs DCM (50 mL) and stirred at room temperature. Trimethoxymethane (1.6 mL, 10.0 mmol) and TFA (1.1 mL, 14.3 mmol) were added into the mixture, and stirring was continued for 2 h. The combined organic layer was washed with water and brine, dried (Na_2SO_4) and evaporated. The resulting residue (5.66 g, 28.3 mmol) and triethylamine (4.0 mL) were dissolved in toluene (80 mL) and stirred at room temperature. Borontrifluoride-ethyl ether complex (6.24 mL, 48.0 mmol) was added dropwise to the mixture, and stirring continued for 0.5 h. The reaction mixture was poured into saturated aqueous $NaHCO_3$ solution. The combined organic layer was washed with water and brine, dried (Na_2SO_4) and evaporated. The resulting residue was purified by flashchromatography (silica gel; cyclohexane/toluene: 1/2) to obtain **4** (0.87 g, 3.10 mmol, 85 %) as a red solid.

Rf (cyclohexane/toluene: 1/3): 0.3; **MP**: 214 °C[69]; **^{1}H-NMR** (500 MHz, $CDCl_3$): δ 2.24 (s, 6H, b), 2.53 (s, 6H, a), 6.04 (s, 2H, d), 7.03 (s, 1H, g); **^{13}C-NMR** (125 MHz, $CDCl_3$): δ 11.4 (a), 14.8 (b), 119.1 (d), 120.2 (g), 133.6 (e), 141.3 (f), 156.9 (c); **IR** (ATR): $\tilde{\nu}$: 3115.9(w), 2926.0(w), 1775.6(w), 1669.6(w),1603.5(s) 1574.1(m), 1532.2(m), 1506.1(m), 1468.0(m), 1406.8(m), 1368.7(m), 1226.5(s), 1194.7(m), 1169.6(s), 1154.2(s), 1082.4(m), 1067.4(m), 1040.9(s), 966.6(s), 915.5(m), 888.5(s), 822.0(s), 797.4(s), 718.4(m), 675.0(s), 641.7(m), 634.5(m), 579.0(m), 509.1(m), 496.6(m), 478.7(s), 472.0(s) cm^{-1}; **Elemental Analysis**: calcd. $C_{13}H_{15}BF_2N_2$: C: 62.94, H: 6.09, N: 11.29%; Found C: 59.35, H: 6.11, N: 10.57%; **HRMS** (ESI pos): $[M+H]^+$ *m/z* Calcd for $C_{13}H_{15}BF_2N_2$ 249.1369; Found 249.1368.

4.1.2.2 2-Iodo-1,3,5,7-tetramethyl-4,4-4,4-difluoro-4-bora-3a,4a-diaza-s-indacene (62)

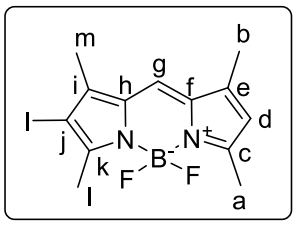

In a solution of abs DCM (400 mL) and **4** (802 mg, 3.23 mmol) at 0 °C, *N*-iodosuccinimide (727 mg, 3.23 mmol) dissolved in abs DCM (100 mL) was added dropwise over 3 h while the solution was vigorously stirred. The reaction was warmed up to room temperature and stirring was continued for 14 h. The solvent was removed *in vacuo* and the resulting residue was purified by

flashchromatography (silica gel; cyclohexane/toluene: 1/1) to yield **62** (890 mg, 2.38 mmol, 74 %) as a red solid.

Rf (cyclohexane/toluene: 1/1): 0.4; **MP**: 216 °C[113]; **^{1}H-NMR** (400 MHz, $CDCl_3$): δ 2.18 (s, 3H, m), 2.23 (s, 3H, b), 2.53 (s, 3H, a), 2.57 (s, 3H, l), 6.09 (s, 1H, d), 7.04 (s, 1H, g); **^{13}C-NMR** (125 MHz, $CDCl_3$): δ 11.5 (b), 13.7 (m), 15.0 (a), 15.6 (l), 80.7 (j), 120.3 (g, d), 132.3 (i), 134.2 (e), 142.4 (h), 143.4 (f), 155.4 (k), 159.3 (c); **IR** (ATR): $\tilde{\nu}$: 2921.6 (w), 1591.9 (m), 1529.3 (m), 1449.7 (m), 1403.4 (m), 1383.7 (m), 1235.7 (m), 1192.3 (m), 1164.3 (m), 1059.2 (s), 968.6 (m), 920.8 (m), 891.4 (m), 840.8 (m), 802.7 (m), 677.4 (m), 644.1 (m), 618.1 (m), 587.7 (m), 580.5 (m), 557.8 (m), 524.5 (m), 499.5 (m), 485.5 (m), 480.2 (m), 474.4 (m), 468.1 (m), 457.0 (m), 448.4 (m), 445.0 (m) cm^{-1}; **Elemental Analysis**: calcd. $C_{13}H_{14}BF_2IN_2$: C: 41.75, H: 3.77, N: 7.49%; Found C: 40.49, H: 3.87, N: 7.29%; **HRMS** (ESI neg): $[M-H]^-$ *m/z* Calcd for $C_{13}H_{14}BF_2IN_2$ 373.0190; Found 373.0183.

4.1.2.3 1-(4-(Dimethylamino)phenyl)ethan-1-one (93)

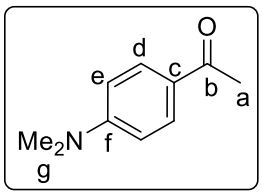

Abs. 1,2-dichloroethane (160 mL) and $AlCl_3$ (253.0 mmol, 34.1 g) was cooled to 0 °C and acetyl chloride (**94**, 205.4 mmol, 14.7 mL) was added. *N,N*-Dimethylanilin (**91**, 158.0 mmol, 20.0 mL, 1.0 Äquiv.) was added dropwise and the mixture stirred for 1 h before the mixture was warmed up to room temperature and stirred for 15 h. The reaction was poured in ice water and neutralized with $NaHCO_3$. The water layer was washed with DCM (4 x 10 mL). The combined organic layer were washed with water (2x5 mL), dried over Na_2SO_4 and the solvent was removed in *vacuo*. Purification with flash chromatography (pentane/DCM: 4/1 -> 1/2) yielded **93** (44, 4.65 g, 28.5 mmol, 18 %) as a yellow solid.

Rf (DCM/pentane, 2/1): 0.3; MP: 106 °C[114]; **^{1}H-NMR** (500 MHz, $CDCl_3$): δ 2.50 (s, 3H,a), 3.05 (s, 6H, g), 6.64 (d, *J* = 9.1 Hz, 2 H, e) 7.86 (d, *J* = 9.1 Hz, 2H, d); **^{13}C-NMR** (500 MHz, $CDCl_3$): δ 26.1 (a), 40.1 (g), 110.7 (e), 125.5 (c), 130.6 (d), 153.5 (f), 196.5 (b); **IR** (ATR): ṽ: 3290 (w), 2905 (w), 2817 (w), 2653 (w), 1648 (w), 1586 (w), 1548 (w), 1525 (w), 141 (w), 1356 (m), 1313 (w), 1284 (w), 1229, (w), 1188 (m), 1068 (m), 943 (m), 811 (s), 656 (m), 593 (s), 562 (s), 298 (s); **Elemental Analysis**: calcd. $C_{10}H_{13}NO$: C: 73.59, H: 8.03, N: 8.58%; Found: C: 74.21, H: 7.97, N: 8.42%; **HRMS** (ESI pos): $[M+H]^+$ *m/z* Calcd for $C_{10}H_{13}NO$ 164.1031; Found 164.1066.

4.1.2.4 (E)-1-(4-(Dimethylamino)phenyl)-3-phenylprop-2-en-1-one (100)

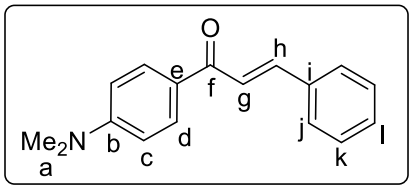

1-(4-Dimethylamino)phenyl)-3-phenylprop-2-en-1-one (**93**, 27.7 mmol, 4.70 g) was dissolved in ethanol (72 mL) and NaOH (2 N, 325 mmol, 108 mL) was added, and the solution stirred vigorously at 0 °C. Benzaldehyd (**99**, 30.0 mmol, 3.00 mL) was added slowly and the reaction stirred for 3 h at 0 °C before the mixture was warmed up to room temperature and stirred for 72 h. The precipitate was filtered and washed with cold water until neutralization. Purification with flash chromatography (pentane/DCM: 3/1 -> 3/2) gave **100** (5.37 g, 21.4 mmol, 77%) as a colorless solid.

Rf (DCM/pentane: 2/1): 0.35: **MP:** 171°C[77]; **^{1}H-NMR** (500 MHz, $CDCl_3$): δ 3.06 (s, 6 H, a), 6.69 (d, *J* = 9.1 Hz, 2H, c), 7.38 (m, 3H, k, l), 7.58 (d, *J* = 15.3 Hz, 1H, g), 7.63 (d, *J* = 7.5 Hz, 2H, j), 7.78 (d, *J* = 15.3 Hz, 1H, h), 8.00 (d, J = 9.1 Hz, 2H, d); **^{13}C-NMR** (500 MHz, $CDCl_3$): δ 40.1 (a), 110.9 (c), 122.3 (g), 126.1 (e), 128.3 (j), 128.9 (k), 130.0 (l), 130.9 (d), 135.6 (i), 142.6 (h), 153.5 (b), 187.8 (f); **IR** (ATR): ṽ: 2902 (w), 2804 (w), 1644 (w), 1582 (w), 1568 (w), 1540 (w), 1495 (w), 1446 (w), 1376 (w), 1342 (w), 1328 (w), 1308 (w), 1289 (w), 1235 (w), 1178 (w), 1127 (w), 1066 (w), 989 (m), 944 (w), 868 (w), 822 (s), 767 (s), 736 (m), 701 (m), 675 (m), 604 (w), 560 (m), 506 (w);); **Elemental Analysis**: calcd.C17H17NO: C: 81.24; H: 6.82; N: 5.57%; Found: C: 81.13; H: 6.71; N: 5.50%; **HRMS** (ESI pos): $[M+H]^+$ *m/z* Calcd for C17H17NO: 252.1344; Found 252.1377.

4.1.2.5 1-(4-(Dimethylamino)phenyl)-4-nitro-3-phenylbutan-1-one (105)

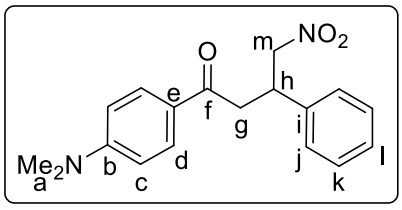

(*E*)-1-(4-(Dimethylamino)phenyl)-3-phenyl-prop-2-en-1-one (**100**, 3.70 g, 13.9 mmol), diethylamine (7.16 mL, 19.9 mmol), and nitromethane (10.1 mL, 209 mmol) were dissolved in abs. methanol (140 mL), and the mixture heated for 24 h under reflux. The solvent was removed in *vacuo* and the residue was purifed by column chromatography (cyclohexane/EtOAc: 7/2 -> 3/1).The product (**105**, 4.00 g, 12.8 mmol, 92%) was obtained as a brown solid.

Rf (Cyclohexane/EtOAc: 7/2): 0.4; **MP**: 86.6 °C[38]; **^{1}H-NMR** (500 MHz, $CDCl_3$): δ 3.06 (s, 6H, a), 3.25 (dd, *J* = 17.0 Hz, *J* = 8.1 Hz, 1H, g), 3.33 (dd, *J* = 17.0 Hz, *J* = 8.1 Hz, 1H, g) , 4.21 (dd, *J* = 6.1 Hz, *J* = 8.2 Hz, 1H, h), 4.68 (dd, *J* = 12.5 Hz, *J* = 8.7 Hz, 1H, m), 4.87 (dd, *J* = 12.5 Hz, *J* = 8.7 Hz, 1H, m), 6.64 (d, *J* = 9.1 Hz, 2H, c), 7.29 (m, 5H, j, k, l), 7.84 (d, *J* = 9.1 Hz, 2H, d); **^{13}C-NMR** (500 MHz, $CDCl_3$): δ 39.8 (h), 40.1 (a), 40.9 (g), 79.8 (m), 110.8 (c), 124.4 (e), 127.6 (j), 127.8 (l), 129.1 (k), 130.4 (d), 139.8 (i), 153.7 (b), 194.7 (f); **IR** (ATR) ṽ:

2914 (w), 1646 (w), 1594 (w), 1545 (w), 1495 (w), 143 (w), 1407 (w), 1375 (w), 1273 (w), 1242 (w), 1170 (w), 1094 (w), 1066 (w), 982 (w), 946 (w), 901 (w), 810 (w), 769 (w), 701 (w), 605 (w), 569 (w), 497 (w); **Elemental Analysis**: calcd. $C_{18}H_{20}N_2O_3$: C: 69.21; H: 6.45; N: 8.97%; Found C: 70.14; H: 6.54; N: 8.85%; **HRMS** (ESI pos): $[M+H]^+$ *m/z* Calcd for $C_{18}H_{20}N_2O_3$: 313.1507; Found 313.1541.

4.1.2.6 (Z)-4-(2-((5-(4-(Dimethylamino)phenyl)-3-phenyl-1H-pyrrol-2-yl)imino)-3-phenyl-2H-pyrrol-5-yl)-N,N-dimethylaniline (110)

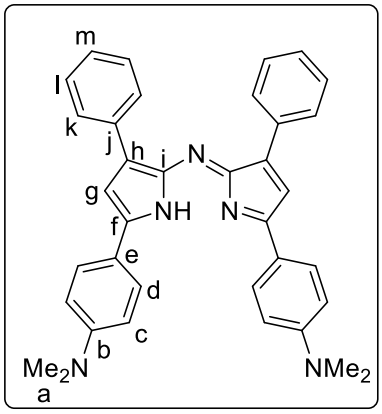

1-(4-(Dimethylamino)phenyl)-4-nitro-3-phenylbutan-1-one (**105**, 3.50 g, 11.2 mmol) and ammonium acetate (32.0 g, 415 mmol) were dissolved in ethanol (112 mL) and heated under reflux for 24 h. The mixture was cooled to rt and the precipitate filtered. Washing with ethanol yielded the product (**110**, 685 mg, 1.30 mmol, 24%) as a green solid.

Rf (cyclohexane/EtOAc: 3/1): 0.4; **MP:** 233.3 °C[38], **^{1}H-NMR** (500 MHz, $CDCl_3$): δ 3.09 (s, 12H, a), 6.82 (d, *J* = 8.9 Hz, 4H, c), 7.12 (s, 2H, g), 7.32 (t, *J* = 7.3 Hz, 2H, m), 7.41 (t, *J* = 7.3 Hz, *J* = 7.8 Hz, 4H, l), 7.86 (d, *J* = 8.9 Hz, 4H, d), 8.09 (d, *J* = 7.8 Hz , 4H, k); **^{13}C-NMR** (500 MHz, $CDCl_3$): δ 40.4 (a), 112.4 (c), 113.9 (g), 120.4 (e), 127.5 (m), 128.1 (l), 128.2 (d), 129.1 (k), 134.5 (j), 141.2 (h), 149.5 (i), 151.5 (b), 154.0 (f); **IR** (ATR): $\tilde{\nu}$: 2850 (w), 2797 (w), 2110 (w), 1699 (w), 1595 (s), 1513 (m), 1463 (m), 1426 (s), 1405 (s), 1349 (s), 1314 (w), 1251 (s), 1187 (s), 1164 (s), 1122 (s), 1072 (m), 1042 (m), 1011 (w), 966 (s), 944 (s), 902 (s), 809 (s), 789 (s), 759 (s), 688 (s), 670 (s), 653 (s), 595 (w), 564 (s), 510 (m), 457 (w); **Elemental Analysis** calcd $C_{36}H_{33}N_5$: C: 80.72; H: 6.21; N: 13.07%; Found C: 75.39; H: 5.89; N: 11.07%; **HRMS** (ESI pos): $[M+H]^+$ *m/z* Calcd for $C_{36}H_{33}N_5$: 536.2770; Found 536.2785.

4.1.2.7 4,4'-(5,5-difluoro-1,9-diphenyl-5H-4λ⁴,5λ⁴-dipyrrolo[1,2-c:2',1'-f][1,3,5,2]triazaborinine-3,7-diyl)bis(N,N-dimethylaniline) (21)

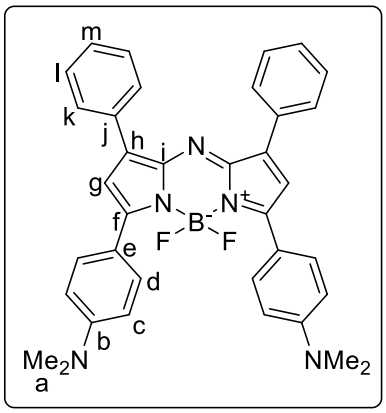

[5-(4-Dimethylaminophenyl)-3-phenyl-1H-pyrrolo-2-yl]-[5-(4-dimethyl-amino-phenyl)-3-phenylpyrrolo-2-yliden]amine (**110**, 600 mg, 1.20 mmol) was dissolved in DCM (110 mL) and diisopropylethylamine (2.00 mL, 11.7 mmol) was added. The mixture was cooled to 0 °C, BF_3-etherate (2.10 mL, 16.5 mmol) was added slowly under vigerously stirring and the reaction was stirred for 24 h at RT. The reaction was quenched with dest. H_2O (30 mL), washed with DCM (3 x 10 mL) and dried over Na_2SO_4. The solvent was removed in *vacuo*. Purification via flash chromatography (cyclohexane/EtOAc: 7/2 -> 1/1) yielded the product (**21**, 574 mg, 0.98 mmol, 84 %) as a violet solid.

Rf (cyclohexane/EtOAc: 3/1): 0.32; **MP:** 257.7 °C[38]; **^{1}H-NMR** (500 MHz, $CDCl_3$): δ 09 (s, 12H, a), 6.8 (d, *J* = 8.9 Hz, 4H, c), 7.1 (s, 2H, g), 7.39 (t, *J* = 7.4 Hz, 2H, m), 7.46 (t, *J* = 7.4 Hz, *J* = 7.8 Hz, 4H, l), 8.1 (d, *J* = 7.8 Hz , 4H, k), 8.2 (d, *J* 8.9 Hz, 4H, d); **^{13}C-NMR** (500 MHz, $CDCl_3$): δ 40.2 (a), 112.0 (c), 118.1 (g), 119.3 (e), 128.5 (l), 128.7 (m), 129.3 (k), 131.8 (d), 133.2 (j), 141.0 (h), 145.3 (i),151.9 (b), 156.5 (f); **IR** (ATR): ṽ: 2919 (w), 2848 (w), 1705 (w), 1594 (w), 1534 (w), 1482 (w), 1457 (w), 1404 (w), 1362 (w), 1317 (w), 1281 (w), 1204 (w), 1160 (w), 1135 (w), 1087 (w), 1029 (w), 1006 (w), 862 (w), 816 (w), 765 (w), 741 (w), 683 (w), 608 (w), 547 (w), 472 (w); **Elemental Analysis**: calcd. $C_{36}H_{32}BF_2N_5$: C: 74.1; H: 5.71; N: 9.62%; Found C: 68.83; H: 6.96; N: 9.21%; **HRMS** (EI, 70 eV, RT): $[M]^+$ *m/z* Calcd for $C_{36}H_{32}BF_2N_5$, 583,2719; found 583.2706.

4.1.2.8 ((4-Iodophenyl)ethynyl)trimethylsilane (41)

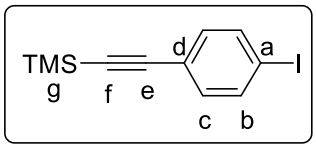

1,4-Diiodobenzene (7.62 g, 23.1 mmol), bis-(triphenylphosphine)palladium(II)-dichloride (220 mg, 7 mol%) and copper(I)-iodide (122 mg, 14 mol%) were dissolved in abs THF (40 mL) and triethylamine (3 mL, 2.19 mmol). The solution was heated to 40 °C and ethinyltrimethylsilane (1.4 g, 14.3 mmol) was added dropwise within 1 h. After 5 h at 40 °C, the reaction mixture was cooled to room temperature diluted with diethylether and extracted with HCl (1 N). The combined organic layers were

dried (Na_2SO_4) and concentrated *in vacuo*. Purification by flashchromatography (silica gel; pentane) gave **41** (2.71 g, 9.02 mmol, 63 %) as a colorless solid.

Rf (pentane): 0.6; **MP**: 69-70 °C; **^{1}H-NMR** (500 MHz, $CDCl_3$): δ 0.24 (s, 9 H, g), 7.16-7.19 (m, *J* = 8.6 Hz, 2H, c), 7.62-7.65 (m, *J* = 8.6 Hz, 2H, b)[8]; **^{13}C-NMR** (125 MHz, $CDCl_3$): δ 0.0 (g), 94.6 (f), 96.0 (a), 104.1 (e), 122.8 (d), 133.6 (c), 137.5 (b); **IR** (ATR): $\tilde{\nu}$:3263.4 (s), 2956.8 (m, 2898.5 (s), 2156.0 (w), 1904.4 (s), 1647.4 (s), 1577.5 (s), 1481.1 (w), 1471.9 (w), 1414.5 (s), 1388.5 (m), 1296.9 (s), 1244.3 (w), 1214.0 (w), 1093.0 (s), 1055.4 (m), 1005.2 (w), 838.9 (w), 818.2 (w), 813.8 (w), 756.4 (w), 699.6 (w), 656.6 (w), 529.8 (w) cm^{-1}; **Elemental Analysis** calcd for $C_{11}H_{13}ISi$: C: 44.01, H: 4.36%; Found: C: 44.70, H: 4.50%; **HRMS** (EI, 70 eV, RT): $[M+H]^+$ *m/z* Calcd for $C_{11}H_{12}ISi$ 299.9813; Found 299.9826.

4.1.2.9 Methyl 4-((trimethylsilyl)ethynyl)benzoate (79)

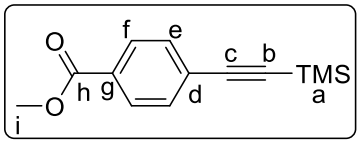

p-Iodo-methyl-benzoate (**78**, 357 mg, 1.36 mmol), $PdCl_2(PPh_3)_2$ (38 mg, 54 µmol) and copper(I)-iodide (21 mg, 109 µmol) were dissolved in abs. THF (12 mL) and abs. TEA (3 mL). Ethinyltrimethylsilane (213 µL, 1.50 mmol) was added and the reaction mixture afterwards heated at 80 °C for 5 h. After cooling to rt, water was added to the mixture and extracted with Et_2O (3 x 20 mL). The combined organic layer were washed with brine and sat. NH_4Cl-solution and dried over Na_2SO_4. Purification with flash column chromatography (silica gel, pentane/EtOAc: 2/1) yielded **79** (300 mg, 1.29 mmol, 95 %) as a colourless solid.

Rf (Pentane): 0.15; **MP**: 55 °C; **^{1}H-NMR** (500 MHz, $CDCl_3$): δ 0.26 (s, 9H, a), 3,91 (s, 3H, i), 7.51 (m, *J* = 8.6 Hz, 2H, e), 7.96 (m, *J* = 8.6 Hz, 2H, f)[71]; **^{13}C-NMR** (125 MHz, $CDCl_3$): δ 0.0 (a), 52.3 (i), 97.8 (b), 104.2 (c), 127.9 (d), 129.5 (f), 129.9 (g), 132.0 (e), 166.6 (h); **IR** (ATR): $\tilde{\nu}$: 2953.0 (m), 2901.4 (m), 2849.8 (w), 2160.8 (m), 1716.3 (s), 1603.0 (m), 1560.1 (m), 1497.0 (w), 1443.0 (m), 1405.9 (m), 1373.6 (w) 1307.0 (m), 1275.7 (s), 1243.4 (s), 1217.3 (s), 1170.6 (s), 1109.8 (s), 1098.7 (s), 1017.3 (m), 962.3 (m), 835.5 (s), 770.4 (s), 757.9 (s), 695.7 (s), 666.3 (s) 540.5 (m); **Elemental Analysis** calcd for $C_{13}H_{16}O_2Si$: C: 67.20, H: 6.94%; Found C: 67.37, H: 6.99%; HRMS (APCI pos): $[M+H]^+$ *m/z* Calcd for $C_{13}H_{16}O_2Si$: 233.0992; Found 233.0993.

4.1.2.10 4-Ethynylbenzoic acid (80)

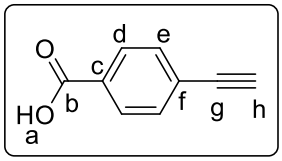

TMS-acetylene **79** (290 mg, 1.25 mmol) was dissolved in ethanol (4 mL) and the reaction mixture cooled to 0 °C. 1 N aq. NaOH-solution (1 mL) was added dropwise and the resulting suspension warmed up in 15 h to rt. Afterwards, the mixture was acidified by HCl (2 N to pH 1) and washed with Et_2O (5 x 20 mL). The combined organic layers were dried over Na_2SO_4 and the solvent removed under *vacuo*. Filtration through a small layer of silica yielded **80** (180 mg, 1.23 mmol, 99 %) as a colourless solid.

Rf (EtOAc/pentane: 2/1 + 1 % acetic acid): 0.41; **MP:** 210 C (decomposition); **^{1}H-NMR** (500 MHz, d_6-DMSO): δ 4.43 (s, 1H, h) 7.59 (m, *J* = 8.4 Hz, 2H, e), 7.93 (m, *J* = 8.4 Hz, 2H, d), 13.14 (s, 1H, a)[71]; **^{13}C-NMR** (125 MHz, d_6-DMSO): δ 83.2 (h), 84.0 (g), 126.5 (f), 130.0 (d), 131.4 (c), 132.4 (e), 167.1 (b); **IR** (ATR): $\tilde{\nu}$: 3299.6 (w), 3264.4 (m), 3099.5 (w), 3074.9 (m), 2922.6 (m), 2849.3 (m), 2658.9 (m), 2551.8 (m), 1903.9 (w), 1818.1 (w), 1674.4 (s), 1606.9 (m), 1562.1 (m), 1507.1 (m), 1426.1 (m), 1404.4 (m), 1321.0 (s), 1283.9 (m), 1178.3 (m), 1126.7 (m), 1114.2 (m), 1018.2 (m), 979.2 (m), 927.1 (m), 859.6 (s), 830.2 (m), 768.5 (s), 746.3 (m), 694.7 (s), 672.6 (s), 635.9 (s), 572.3 (s), 551.1 (s), 524.1 (s), 504.3 (s); **Elemental Analysis** calcd for $C_9H_5O_2$: 73.97, H: 4.14%; Found C: 74.10, H: 4.75%; **HRMS** (Esi neg): $[M\text{-}H^+]^-$ *m/z* Calcd for $C_9H_5O_2$: 145.0295; Found 145.0290.

4.1.2.11 4-((4-boronophenyl)ethynyl)benzoic acid (81)

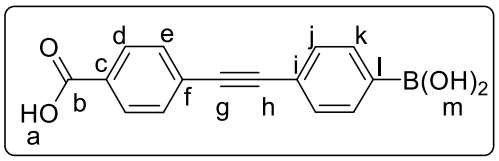

4-Ethinylbenzoic acid (**80**, 67 mg, 458 µmol), 4-iodophenylboronic acid (113 mg, 458 µmol), $Pd(PPh_3)_4$ (33 mg, 28.6 µmol) and copper(I) iodide (5 mg, 26.3 µmol) were dissolved in abs. THF (15 mL) and abs. diisopropyl amine (8 mL). The reaction mixture was stirred at room temperature for 20 h. The suspension was taken into 1 N HCl (10 mL) and extracted with DCM (4x20 mL). After drying of the combined organic layers over Na_2SO_4, and removing of the solvent in *vacuo*, flash column chromatography (EtOAc + 1 % acetic acid) yielded **81** (40.0 mg, 151 µmol, 33 %) as a brown solid.

Rf (DCM/MeOH: 9/1 + 1 % acetic acid): 0.7; **MP:** 208-209 °C; **^{1}H-NMR** (500 MHz, d_6-DMSO): δ 3.17 (s, m), 7.54 (d, *J* = 7.9 Hz, 2H, e), 7.66 (d, *J* = 8.1 Hz, 2H, j), 7.84 (d, *J* = 7.9 Hz, 2H, d), 7.97 (d, *J* = 8.1 Hz, 2H, k), 8.28 (bs, 1 H, a); A second signal set in ^{1}H- und ^{13}C-NMR could be a hint for di- and trimers; **^{13}C-NMR** (125 MHz, d_6-DMSO): δ 89.4 (5), 92.2 (7), 123.2 (8), 126.5 (1), 129.6 (3), 130.5 (9), 131.2 (4), 131.6 (2), 134.4 (10),

135.4 (11), 166.9 (6); **IR** (ATR): $\tilde{\nu}$: 2918.25 (w), 2535.45 (w), 1678.73 (m), 1605.93 (m), 1558.68 (w), 1544.22 (w), 1473.83 (w), 1422.24 (m), 1400.55 (m), 1347.03 (m), 1314.25 (m), 1297.38 (m), 1280.50 (m), 1174.44 (m), 1105.49 (m), 1088.62 (m), 1011.00 (m), 937.72 (m), 859.61 (m), 833.58 (m), 770.42 (m), 737.64 (m), 693.77 (m), 660.02 (m), 637.84 (m), 555.40 (m), 528.88 (m), 514.90 (m), 504.29 (m); **Elemental Analysis** calcd for $C_{15}H_{11}BO_4$: C: 67.72, H: 4.17%; Found: C: 66.28, H: 4.62%; **HRMS** (Esi neg): $[M\text{-}H^+]^-$ *m/z* Calcd for $C_{15}H_{11}BO_4$: 265.0678; Found 265.0678.

4.1.2.12 4-((4-(5,5-Difluoro-1,3,7,9-tetramethyl-5H-5λ^4,6λ^4-dipyrrolo[1,2-c:2',1'-f][1,3,2]diazaborinin-2-yl)phenyl)ethynyl)benzoic acid (22)

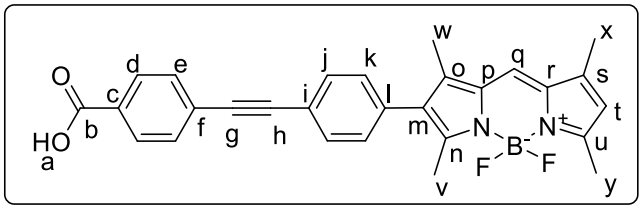

The boronic acid **81** (180 mg, 676 µmol) and iodo-BODIPY **62** (253 mg, 676 µmol) were dissolved in abs. THF (26 mL) and degassed. Then 20% aq. Na_2CO_3 solution (7 mL), and $Pd(PPh_3)_4$ (40 mg, 43.3 µmol) were added and the reaction heated to 95 °C for 6 h. The cooled down mixture was acidified with aq. HCl (1 N) and extracted with DCM (3 x 50 mL). The combined organic layer was dried over Na_2SO_4 and the solvent removed in *vacuo*. Purification by column chromatography (silica gel, DCM/MeOH: 95/5 + 0.5 % acetic acid) yielded **22** (36 mg, 76.9 µmol, 12 %) as a red solid.

Rf (DCM/MeOH: 9/1 + 1 % acetic acid): 0.8; **MP:** 224 °C (Decomposition), **^{1}H-NMR** (500 MHz, d_6-DMSO): δ 2.29 (s, 3H, w), 2.31 (s, 3H, x), 2.46 (s, 3 H, v), 2.47 (s, 3H, y), 6.27 (s, 1H, t), 7.44 (m, *J* = 8.4 Hz, 2H, k), 7.66 (m, *J* = 8.4 Hz, 2H, j), 7.68 (m, *J* = 8.5 Hz, 2H, e), 7.80 (s, 1H, q) 7.98 (dm, *J* = 8.5 Hz, 2 H, d), 13.00 (bs, 1H, a); **^{13}C-NMR** (125 MHz, d_6-DMSO): δ 10.1 (w), 11.0 (x), 13.2 (v), 14.4 (y), 89.0 (g), 91.9 (h), 119.6 (t), 120.3 (i), 122.6 (q), 126.6 (f), 126.7 (c), 129.6 (e), 129.8 (j), 129.9 (m), 131.5 (k), 131.6 (d), 132.1 (o), 133.6 (s), 134.0 (l), 137.5 (p), 142.9 (r), 152.8 (n), 157.2 (u), 166.8 (b); **IR** (ATR): $\tilde{\nu}$: 2917.29 (w), 2848.83 (w), 2663.21 (w), 2539.79 (w), 1737.55 (w), 1686.93 (m), 1610.75 (m), 1599.66 (m), 1525.42 (w), 1462.26 (w), 1411.64 (m), 1393.32 (w), 1366.32 (m), 1309.91 (w), 1290.14 (w), 1232.77 (m), 1194.69 (m), 1162.38 (m), 1141.17 (m), 1120.44 (m), 1094.4 (m), 1047.64 (m), 995.57 (m), 972.91 (m), 929.52 (w), 895.29 (m), 857.204 (m), 823.46 (m), 797.90 (w), 785.85 (w), 768.98 (m), 737.16 (w), 719.80 (w), 687.50 (w), 677.37 (m), 637.36 (w), 625.79 (w), 605.54 (w), 579.02 (w), 555.40 (m), 527.92 (m), 516.35 (m), 502.85 (w); **Elemental Analysis** calcd for $C_{28}H_{23}BF_2N_2O_2$: C: 71.81, H: 4.95, N: 5.98%; Found: C: 68.46, H: 5.30, N: 5.67%; **HRMS** (Esi neg): $[M\text{-}H^+]^-$ *m/z* Calcd for $C_{28}H_{23}BF_2N_2O_2$: 467.1748; Found 467.1742.

4.1.2.13 Benzo[c][1,2,5]thiadiazole (121)

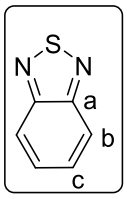

To a solution of 1,2-phenylenediamine (1**20**, 10.0 g, 92.5 mmol) in abs DCM (300 mL) and abs triethylamine (51 mL), thionylchloride (13.5 mL, 187 mmol) was added dropwise and the reaction stirred for 5 h at room temperature. After removing the solvent *in vacuo*, the resulting residue was dissolved in DCM and extracted with water and brine. The combined organic layers were dried (Na_2SO_4) and evaporated *in vacuo* to give pure 1**21** (10.7 g, 78.3 mmol, 85 %) as a red solid.

Rf (EtOAc/cyclohexane: 1/5): 0.5; **MP:** 42-44 °C[115]; **^{1}H-NMR** (500 MHz, $CDCl_3$): δ 7.59 (m, 2H, c), 8.01 (m, 2H, b); **^{13}C-NMR** (125 MHz, $CDCl_3$): δ 121.7 (b), 129.4 (c), 154.9 (a); **IR** (ATR): $\tilde{\nu}$: 3968.3 (w), 3909.0 (w), 3089.9 (m), 3052.3 (m, Ar-H), 2716.7 (w), 2126,6 (w), 1965.6 (w), 1942.0 (w), 1915.4 (w), 1836.9 (w), 1811.3 (w), 1713.4 (w), 1607.4 (m, C=N), 1527.3 (m), 1520.1 (m), 1478.7 (m), 1434.8 (m), 1362.5 (m), 1331.6 (m), 1273.3 (m), 1230.4 (m), 1138.8 (m,), 1131.5 (m), 1099.7 (m), 989.3 (w), 980.1 (m), 950.3 (m), 918.0 (m), 848.0 (s), 812.8 (s,), 761.3 (m), 742.0 (s), 652.8 (m), 623.4 (m), 588.2 (m), 548.2 (m), 540.0 (w), 532.7 (m), 527.9 (s,), 501.9 (m); **Elemental Analysis** calcd for $C_6H_4N_2S$: C: 52.92, H: 2.96, N: 20.57, S: 23.54%; Found: C: 52.79, H: 2.84, N: 20.41, S: 23.81%; **HRMS** (APCI): $[M+H]^+$ *m/z* Calcd for $C_6H_4N_2OS$ 137.0168; Found 137.0168.

4.1.2.14 4,7-Dibromobenzo[c][1,2,5]thiadiazole (15)

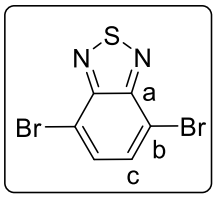

In a solution of aq HBr (55 mL) compound **121** (2.0 g, 14.7 mmol) was dissolved and bromine (2.2 mL, 8.82 mmol) added dropwise. Afterwards the reaction mixture was heated at 125 °C for 6 h. After cooling to room temperature, the mixture was washed with sat. $NaHSO_3$ and extracted with DCM. The combined organic layers were dried (Na_2SO_4) and the solvents removed *in vacuo* to yield **15** (3.7 g, 12.6 mmol, 86 %) as an orange solid.

Rf (DCM): 0.8; **MP:** 179-182 °C[115]; **^{1}H-NMR** (500 MHz, $CDCl_3$): δ 7.72 (s, 2H, c); **^{13}C-NMR** (125 MHz, $CDCl_3$): δ 114.1 (b), 132.5 (c), 153.1 (a); **IR** (ATR): $\tilde{\nu}$: 3078.8 (w, Ar-H), 3046.5 (m), 2988.6 (w), 2955.9 (w), 2924.5 (w), 2849.3 (w), 1858.6 (w), 1713.4 (w,), 1652.2 (w, C=N), 1587.1 (m), 1497.9 (m), 1475.8 (m), 1378.4 (m), 1328.7 (w), 1315.7 (m,), 1309.4 (m), 1272.3 (m), 1183.1 (s), 1142.6 (m), 1081.4 (m), 1019.2 (m), 969.1 (w), 934.8 (s), 873.1 (s), 841.8 (s), 830.2 (s), 823.9 (s), 806.6 (s), 745.8 (m), 727.0 (m), 688.5 (m), 664.4 (m), 618.1 (m), 585.3 (s, 2 × C-Br), 562.1 (m), 526.0 (m), 518.8 (m), 499.0 (m), 487.4 (s), 482.6 (s); **Elemental**

Analysis calcd for $C_6H_2Br_2N_2S$: C: 24.52, H: 0.69, N: 9.53, S: 10.91%; Found: C: 24.65, H: 0.80, N: 8.27, S: 11.71%; **HRMS** (EI, 70 eV, RT): $[M+H]^+$ *m/z* Calcd for $C_6H_2Br_2N_2S$ 291.8300; Found 291.8314.

4.1.2.15 Ethyl 4-(7-bromobenzo[c][1,2,5]thiadiazol-4-yl)benzoate (137)

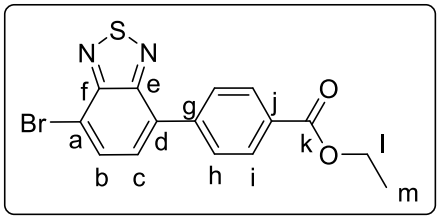

In a solution of abs THF (40 mL) and aq 20 % Na_2CO_3 (25 mL), (4-(ethoxycarbonyl)phenyl)boronic acid (350 mg, 1.80 mmol), **15** (796 mg, 2.71 mmol) and $Pd(PPh_3)_4$ (100 mg, 86.5 µmol) were dissolved and the mixture heated to 85 °C for 3.5 h. The mixture was poured into EtOAc and extracted with H_2O. The combined organic layers were dried (Na_2SO_4) and the solvent removed *in vacuo*. Purification by flashchromatography (silica gel; pentane/ETOAC: 9/1) gave **137** (339 mg, 1.10 mmol, 62 %) as a yellow solid.

Rf (pentane/EtOAc: 6/1): 0.9; **MP**: 187-191 °C; **^{1}H-NMR** (500 MHz, $CDCl_3$): δ 1.42 (t, *J* = 7.1 Hz, 3H, m), 4.42 (q, *J* = 7.1 Hz, 2H, l), 7.61 (d, *J* = 7.5 Hz, 1H , c), 7.93 (d, *J* = 7.5 Hz, 1H, b), 7.94-7.99 (m, *J* = 8.2 Hz,2H, h), 8.18-8.21 (m, *J* = 8.2 Hz, 2H, i)[80]; **^{13}C-NMR** (125 MHz, $CDCl_3$): δ 14.5 (m), 61.3 (l), 114.3 (a), 128.8 (c), 129.2 (h), 130.0 (i), 130.6 (j), 132.3 (b), 133.0 (d), 140.9 (g), 153.0 (e), 154.0 (f), 166.4 (k); **IR** (ATR): $\tilde{\nu}$: 1709 (m), 1607 (w), 1505 (w), 1478 (w), 1446 (w), 1412 (w), 1394 (w), 1367 (w), 1332 (w), 1317 (w), 1269 (s), 1185 (m), 1150 (w), 1126 (m), 1111 (m), 1097 (m), 1029 (w), 1021 (w), 945 (w), 935 (w), 883 (m), 867 (w), 849 (w), 841 (w), 835 (w), 830 (w), 790 (w), 765 (s), 701 (m), 620 (w), 587 (w), 558 (w), 516 (w), 497 (w), 484 (w), 463 (w), 447 (w); **Elemental Analysis** calcd for $C_{15}H_{11}BrN_2OS$: C: 49.60; H: 3.05; N: 7.71; S: 8.83%; Found: C: 48.60; H: 3.05; N: 7.51; S: 8.49%; **HRMS** (APCI): $[M+H]^+$ *m/z* Calcd for $C_{15}H_{11}BrN_2OS$ 362.9797; Found 362.9789.

4.1.2.16 2-Bromo-4-methylthiophene (24)

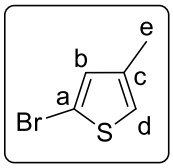

To a solution of 3-methylthiophene (**19**, 10 mL) in abs. Et_2O (100 00mL), abs. TMEDA (17.2 mL, 114 mol) and *n*-Butyllithium (2.5 M in hexane, 45.3 mL, 114 mmol) were dropwise added subsequently under vigerously stirring. The reaction mixture was heated under reflux for 30 min, before cooling down to -70 °C. Tetrabromomethane (22.6 g, 68.3 mmol) in portions was added. The reaction was stirred for 17 h and warmed up to room temperature before poured into water (0 °C). The organic layer was removed and the water layer extracted with Et_2O (3 x 500 mL). The combined organic layer were washed with 6 N HCl (100 mL), sat. $NaHCO_3$-solution (100 ml) and brine (100 ml) and dried over Na_2SO_4. The solvent was removed *in vacuo* and purification of

the residue with column chromatograph (silica gel, pentane) yielded **24** (12.3 g, 69.4 mmol, 68 %) as a light yellow oil.

Rf (pentane): 0.9; **^{1}H-NMR** (400 MHz, $CDCl_3$): δ 2.23 (d, *J* = 1.2 Hz, 3H, e), 6.80 (m, 1H, d), 6.86 (d, *J* = 1.6 Hz, 1H, b)[60]; **^{13}C-NMR** (100.6 MHz, $CDCl_3$): δ 16.0 (e), 111.8 (a), 122.1 (d), 132.0 (b), 138.5 (c); **IR** (ATR): $\tilde{\nu}$: 3091.3(w), 2921.1(m), 1646.4(w), 1543.7(w), 1450.7(w), 1408.7(m), 1379.8(w), 1355.7(w), 1232.3(w), 1192.8(m), 1143.6(w), 1032.7(w), 995.1(m), 978.7(m), 918.4(m), 848.5(m), 826.8(m), 762.2(w), 728.5(m), 703.4(w), 24 683.2(m), 656.2(m), 594.0(w), 584.8(m), 558.8(m), 546.7(m), 539.5(w), 523.1(w), 515.4(w), 507.7(w), 498.5(w), 491.3(w), 484.5(w),477.8(w), 474.4(w), 470.5(m), 465.2(m), 457.5(m), 446.9(m), 441.1(m), 436.8(w), 432.0(m), 426.7(w), 417.5(m), 409.8(m), 404.0(m) cm^{-1},**HRMS** (APCI): $[M]^-$ *m/z* Calcd for C_5H_5BrS: 175.9301; found: 175.9288.

4.1.2.17 2-Methoxy-4-methylthiophene (25)

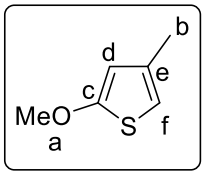

To a solution of anhydrous sodium methoxide (5.4 M in methanol, 28.0 mL, 130 mmol) was added 2-bromo-4-methylthiophene (**24**, 14.3 g, 81 mmol) and copper(*I*) bromide (1.17 g, 8.20 mmol), and the mixture was heated at 120 °C for 8 h. The reaction mixture was cooled to room temperature, and sodium cyanide (5 g in 30 mL water) was added under vigorous stirring. The aqueous layer was extracted with Et_2O (5 x 30 mL). The combined organic layers were dried over Na_2SO_4, and after evaporation of the solvent in *vacuo*, the residue was purified with column chromatography (pentane) to yield product **25** (8.00 g, 62.4 mmol, 78%) as a colorless oil.

Rf (Pentan): 0.28; **SP:** 85 °C (10 mbar); **^{1}H-NMR** (500 MHz, $CDCl_3$): δ 2.20 (d, *J* = 1.1 Hz, 3 H, b), 3.90 (s, 3 H, a), 6.07-6.09 (m, 1 H, f), 6.16-6.18 (m, 1 H, d)[116]; **^{13}C-NMR** (125 MHz, $CDCl_3$): δ 16.9 (b), 60.83 (a), 106.2 (d), 106.6 (f), 135.4 (e), 166.1 (c); **HRMS**: (EI, 70 eV, RT): $[M]^+$ *m/z* Calcd for C_6H_8OS: 128.0290; found: 128.0288.

4.1.2.18 2,4-Dibromo-5-methoxy-3-methylthiophene (26)

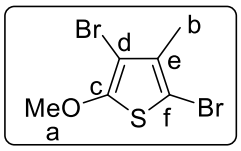

A tetrachloromethane solution (20 mL) containing **25** (2.5 g, 19.5 mmol) was stirred at 0 °C. *N*-Bromosuccinimde (6.9 g, 39.0 mmol) in CCl_4 (15 mL) was added in portions within 2 h and then the reaction mixture was stirred for 3 h at room temperature. After cooling (0 °C), the suspension was filtered and the solvents were evaporated *in vacuo*.

The residue was purified by flashchromatography (silica gel; pentane) to give **26** (3.8 g, 13.2 mmol, 69 %) as a yellow oil.

Rf (pentane): 0.6; **BP:** 140 °C (0.6 mbar); **^{1}H-NMR** (400 MHz, $CDCl_3$): δ 2.14 (s, 3H, b), 3.92 (s, 3H, a)[29]; **^{13}C-NMR** (100 MHz, $CDCl_3$): δ 16.0 (b), 62.1 (a), 94.0 (d), 94.7 (f), 134.5 (e), 157.5 (c); **IR** (ATR): $\tilde{\nu}$: 2918.3 (w), 2827.1 (w), 1617.0 (w), 1561.1 (s), 1502.3 (m), 1449.7 (m), 1429.5 (m), 1379.3 (m), 1337.4 (m), 1236.6 (s), 1152.3 (s), 1059.7 (m), 991.2 (s), 938.7 (s), 810.0 (s), 754.5 (m), 689.9 (m), 655.7 (m), 631.6 (m), 614.2 (m), 559.7 (m), 550.1 (m), 533.2 (m) cm^{-1}; **Elemental Analysis** calcd for $C_6H_6Br_2OS$: C: 25.20; H: 2.11; S: 11.21%; Found: C: 25.44, H: 2.14, S: 11.58%; **HRMS** (APCI): $[M+H]^+$ *m/z* Calcd for $C_6H_6Br_2OS$ 286.8558; Found 286.8549.

4.1.2.19 3-Bromo-5-chloro-2-methoxy-4-methylthiophene (4)

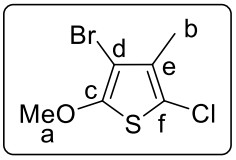

To a stirred solution of **17** (400 mg, 1.39 mmol) in abs THF (10 mL) at -78 °C *n*-BuLi (2.5 M in hexane, 0.59 mL, 1.47 mmol) was added dropwise and the solution left for 30 min while stirring. *N*-Chlorosuccinimide (280 mg, 2.09 mmol) dissolved in abs THF (5 mL) was added and the solution was warmed up to room temperature within 30 min. After removing the solvents *in vacuo*, the residue was subjected to column chromatography (silica gel; pentane) to yield **4** (334 mg, 1.38 mmol, 99 %) as colorless oil.

Rf (pentane): 0.5; **^{1}H-NMR** (400 MHz, $CDCl_3$): δ 2.13 (s, 3H), 3.91 (s, 3H); **^{13}C-NMR** (125 MHz, $CDCl_3$): δ 14.2, 62.3, 94.1, 111.6, 132.0, 154.9; **IR** (ATR): $\tilde{\nu}$: 2919.7 (w), 2827.61 (w), 2738.91 (w), 2466.99 (w), 1702.35 (w), 1563.99 (s), 1506.13 (m), 1451.17 (m), 1429.48 (m), 1379.82 (m), 1341.25 (w), 1293.52 (w), 1237.59 (s), 1152.74 (s), 1109.83 (w), 1072.23 (w), 1003.77 (s), 969.537 (m) 947.359 (m), 901.076 (w), 811.885 (s), 796.939 (m), 714.497 (w), 660.982 (m), 633.984 (w), 610.36 (w), 556.363 (w); **Elemental Analysis** calcd for $C_6H_6BrClOS$: C: 29.84; H: 2.50; S: 13.27%; Found: C: 30.24, H: 2.37, S: 13.10%, **HRMS** (APCI): $[M+H]^+$ *m/z* Calcd for $C_6H_6ClBrOS$ 240.9084; Found 240.9086.

4.1.2.20 3-Bromo-2-methoxy-4-methylthiophene (27)

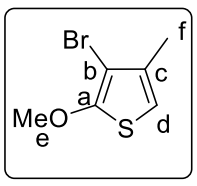

Compound **26** (1.48 g, 5.18 mmol) was dissolved in abs. Et_2O (8 mL) and cooled down to -78 °C. *n*-Butyllithium (2.5 M in hexane, 5.18 mmol) was added dropwise under vigerously stirring and the solution kept for 30 min at -78 °C. Afterwards, MeOH (5 mL) was added and the solution allowed to warm up to rt. The reaction mixture was poured

into water (0 °C) and the water layer extracted with Et_2O (3 x 30 mL). The combined organic layers were washed with NH_4Cl (15 mL), dried over Na_2SO_4 and the solvent removed in vacuo. Purification via column chromatography (silica gel, pentan) yielded 27 (880 mg, 4.24 mmol, 83 %) as a colourless oil.

Rf (Pentan): 0.44; **^{1}H-NMR** (400 MHz, $CDCl_3$): δ 2.11 (p, *J* = 1.0 Hz, 3H, f), 3.94 (s, 3H, e), 6.34 (q, *J* = 1.2 Hz, 1H,d)[29]; **^{13}C-NMR** (100.6 MHz, $CDCl_3$): δ 15.9 (f), 61.6 (e), 103.0 (b), 107.7 (d), 134.8 (c), 166.9 (a); **IR** (ATR): $\tilde{\nu}$: 2949.6(w), 2919.2(w), 1778.5(w), 1678.2(s), 1626.2(m), 1544.2(m), 1504.7(m), 1476.7(m), 1431.4(m), 1399.6(m), 1374.0(m), 1236.1(m), 1209.6(m), 1150.3(m), 1099.7(m), 1040.9(m), 997.0(m), 960.4(m), 907.8(m), 784.9(s), 758.4(s), 719.3(m), 693.8(m), 669.2(m), 621.0(m), 609.4(m), 592.5(m), 578.5(m), 558.8(m), 534.2(m), 527.0(m), 519.7(m); **Elemental Analysis** calcd for C_6H_7BrOS: C: 34.80; H: 3.41; S: 15.48%; Found C: 34.32 H: 3.07 S: 15.94%; **HRMS** ((EI, 70 eV, RT): $[M]^+$ *m/z* Calcd for C_6H_7BrOS: 206.9474; found 206.9470.

4.1.2.21 ((4-(4-Bromo-5-methoxy-3-methylthiophen-2-yl)phenyl)ethynyl)trimethylsilane (19)

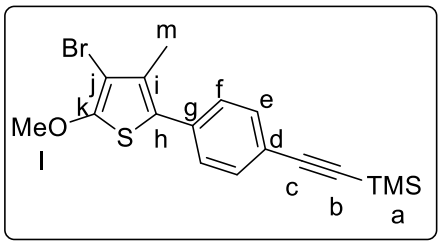

In a solution of abs THF (20 mL) compound **17** (815 mg, 2.85 mmol) was dissolved and the reaction mixture cooled to -78 °C. *n*-BuLi (2.5 M in hexane, 1.16 mL, 2.91 mmol) was added dropwise and the solution left for 30 min while stirring. Then $B(OBu)_3$ (930 µL, 3.42 mmol) was added and the solution warmed up to room temperature within 30 min. A degassed aq solution of 20 % Na_2CO_3 (8 mL), $Pd(PPh_3)_4$ (66 mg, 0.06 mmol) and compound **18** (neat, 843 mg, 2.81 mmol) were added, and the mixture was heated for 2 h at 85 °C. The resulting suspension was diluted with Et_2O and extracted with water. The combined organic layer was dried (Na_2SO_4) and concentrated *in vacuo*. The crude product was purified by flashchromatography (silica gel; pentane) to obtain **19** (611 mg, 1.61 mmol, 57 %) as a yellow solid.

Rf (pentane): 0.3; **MP:** 68 °C; **^{1}H-NMR** (500 MHz, $CDCl_3$): δ 0.26 (s, 9H, a), 2.24 (s, 3H, m), 3.99 (s, 3H, l), 7.31-7.34 (m, *J* = 8.4 Hz, 2H, f), 7.47-7.49 (m, *J* = 8.4 Hz, 2H, e); **^{13}C-NMR** (125 MHz, $CDCl_3$): δ 0.1 (a), 15.4 (m), 61.8 (l), 95.4 (b), 96.3 (j), 104.8 (c), 122.0 (d), 123.4 (h), 128.7 (f), 131.2 (i), 132.3 (e), 134.6 (g), 158.0 (k); **IR** (ATR): $\tilde{\nu}$: 2957.3 (w), 2147.8 (m), 1599.2 (w), 1557.2 (m), 1543.7 (m), 1508.1 (s), 1484.0 (m), 1445.4 (m), 1428.5 (m), 1403.4 (m), 1374.5 (m), 1356.2 (m), 1273.8 (m), 1245.8 (s), 1227.0 (m), 1155.6 (m), 1114.7 (m), 1051.0 (m), 1014.4 (m), 976.8 (m), 946.4 (w), 934.3 (w), 836.0 (s), 762.2 (s), 699.1 (m), 647.5 (m),

631.1 (m), 582.4 (m), 568.9 (m), 559.7 (s), 533.7 (m), 524.1 (m), 515.4 (m), 505.7 (m), 493.7 (m); **Elemental Analysis** calcd for $C_{17}H_{19}BrOSSi$: C: 53.82, H: 5.05, S: 8.45%; Found: C: 55.02%, H: 4.96, S: 7.28%; **HRMS** (EI, 70 eV, RT)): $[M+H]^+$ *m/z* Calcd for $C_{17}H_{18}BrOSSi$ 378.0107; Found 378.0138.

4.1.2.22 3-Bromo-2-methoxy-4-methyl-5-phenylthiophene (139)

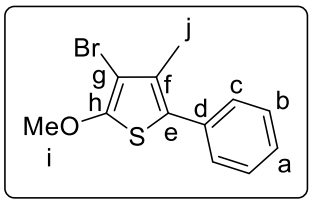

A solution of **26** (500 mg, 1.7 mmol) in abs THF (10 mL) was cooled to -78 °C and *n*-BuLi (2.5 M in hexane, 0.73 mL, 1.8 mmol) was added dropwise. The mixture was stirred for 30 min at -78 °C before tributylborate (neat, 0.57 mL, 2.1 mmol) was added, and the mixture warmed up to room temperature in 60 min. A degassed aq solution of 20 % Na_2CO_3, iodo-benzene (195 µL, 1.7 mmol) via syringe and $Pd(PPh_3)_4$ (101 mg, 90 µmol) were added, and the reaction mixture stirred for 3.5 h at 95 °C. After cooling to room temperature, the mixture was poured into water and extracted with Et_2O. The combined organic layer was dried (Na_2SO_4) and the solvents removed *in vacuo*. The residue was purified by flashchromatography (silica gel; pentane) to yield **139** (340 mg, 1.2 mmol, 70 %) as a colorless solid.

Rf (pentane): 0.3; **MP**: 55-56 °C[31]; **^{1}H-NMR** (500 MHz, $CDCl_3$): δ 2.25 (s, 3H, j), 3.99 (s, 3H, i), 7.29-7.34 (m, 1H, a). 7.38-7.41 (m, 4H, b, c); **^{13}C-NMR** (125 MHz, $CDCl_3$): δ 15.3 (j), 61.8 (i), 96.1 (g), 124.1 (e), 127.4 (a), 128.7 (b), 129.2 (c), 130.5 (f), 134.5 (d), 157.6 (h); **IR** (ATR): $\tilde{\nu}$: 3003.6 (w), 2912.9 (m), 2851.7 (w), 1983.4 (w), 1911.6 (w), 1889.4 (w), 1816.1 (w), 1761.7 (w), 1687.9 (w), 1598.2 (w), 1559.2 (s), 1508.1 (s), 1483.0 (s), 1426.6 (s), 1388.5 (m), 1377.4 (m), 1313.3 (w),1281.9 (m), 1265.1 (m), 1221.2 (s), 1182.6 (m), 1146.5 (s), 1082.4 (m),1048.6 (s), 1013.9 (s), 999.4 (m),971.5 (s), 937.2 (m), 917.0 (m), 820.6 (s), 766.1 (s), 711.6 (s), 699.1 (s), 632.5 (m), 591.1 (s), 555.4 (m), 518.8 (m), 474.4 (m); **Elemental Analysis** calcd for $C_{12}H_{12}BrOS$: C: 50.90, H: 3.92, S: 11.32%; Found: C: 50.84, H: 4.01, S: 11.15%; **HRMS** (EI, 70 eV, RT): $[M]^-$ *m/z* Calcd for $C_{12}H_{12}BrOS$ 281.9709; Found 281.9712.

4.1.2.23 3-Bromo-2-methoxy-5-(4-methoxyphenyl)-4-methylthiophene (141)

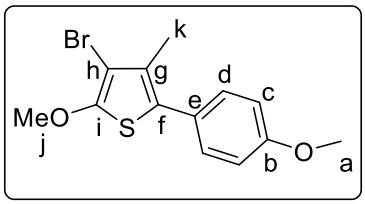

Dibromothiophene **26** (1.47 g, 5.15 mmol) was dissolved in abs. THF (50 mL) and the solution cooled down to -78 °C. Then, *n*-butyllithium (2.5 M in hexane, 2.16 mL, 5.41 mmol) was added dropwise and the reaction mixture stirred for 40 min at -78 °C. Then tributylborate (1.67 mL, 6.18 mmol) was added and the reaction mixture warmed up to rt in 1 h. In a second flask, 20% aq. Na_2CO_3-solution (35 mL) was degassed with N_2-flow. The boronic acid, iodoanisol (1.8 g, 7.73 mmol)

and $Pd(PPh_3)_4$ (119 mg, 0.10 mmol) were added to the aq. solution and the mixture heated at 110 °C for 18 h. After the reaction was cooled down to rt, water was added and the mixture extracted with Et_2O (3 x 100 mL). The combined organic layers were dried over Na_2SO_4 and the solvent removed *in vacuo*. Purification with column chromatography (silica gel, pentane) yielded **141** (0.90 g, 2.87 mmol, 56 %) as a colourless solid.

Rf (Pentan): 0.48; **MP** 94-95 °C; **^{1}H-NMR** (400 MHz, $CDCl_3$): δ 2.21 (s, 3 H, k), 3.84 (s, 3 H, a), 3.97 (s, 3 H, j), 6.93 (s, 3 H, c), 7.31 (s, 3 H, d); **^{13}C-NMR** (100.6 MHz, $CDCl_3$): δ 15.1 (k), 55.5 (a) 61.9 (j), 95.8 (h), 114.2 (c), 124.0 (f), 126.9 (e), 129.8 (g), 130.5 (d), 157.0 (i), 159.1 (b); **IR** (ATR): $\tilde{\nu}$: 2954.4 (m), 2928.4 (w), 2831.5 (w), 1887.5 (w), 1727.4 (w), 1605.0 (m), 1558.7 (m), 1520.6 (s), 1491.7 (s), 1438.6 (s), 1424.2 (s), 1408.7 (m), 1379.8 (m), 1308.9 (m), 1294.0 (s), 1267.5 (m), 1249.2 (s), 1226.5 (s), 1180.2 (s), 1153.2 (s), 1116.1 (m), 1050.1 (s), 1035.6 (s), 1008.1 (s), 976.8 (s), 962.8 (s), 933.4 (m), 838.9 (s), 830.7 (s), 822.0 (s), 795.0 (s), 669.2 (m), 638.8 (m), 558.3 (s), 540.5 (m), 526.5 (s), 512.0 (m), 505.3 (m), 491.8 (m), 445.5 (m); **Elemental Analysis** calcd for $C_{13}H_{13}BrO_2S$: C: 49.85, H: 4.18, S: 10.24%; Found C: 50.62, H: 4.20, S: 10.22%; **HRMS** (EI, 70 eV, RT): $[M]^-$ *m/z* Calcd for 311.98196; Found 311.98292.

4.1.2.24 3-Bromo-5-(4-chlorophenyl)-2-methoxy-4-methylthiophene (140)

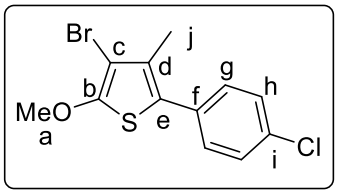

Dibromothiophene **26** (1.00 g, 3.50 mmol) was dissolved in abs. THF (20 mL) and cooled to -78 °C. Under vigorously stirring *n*-butyllithium (2.5 M in hexane, 965 µL, 3.57 mmol) was added dropwise and the solution kept at -78 °C for 30 min. Tributylborate (1.31 mL, 5.25 mmol) was added via syringe and the mixture was allowed to warm up to room temperature in 45 min. In a second flask 20% aq. Na_2CO_3-solution (20 ml) and THF (10 mL) were degassed under nitrogen, and 4-iodo-trimethylsilylethinylphenyl (1.00 g, 4.20 mmol), $Pd(PPh_3)_4$ (210 mg, 180 µmol) and the *in situ* prepared boronic acid were added via cannula. The mixture was heated at 70 °C for 5 h and cooled down to room temperature. The aq. layer was extracted with diethylether (3 x 50 ml), the combined organic layer dried over Na_2SO_4 and the solvent removed in *vacuo*. Purification by flash column chromatography (pentane) yielded **140** (808 mg, 2.55 mmol, 73 %) as a yellow solid.

Rf (pentane/DCM: 2/1): 0.26; **MP:** 92.2-92.6 °C; **^{1}H-NMR** (500 MHz, $CDCl_3$): δ: 2.23 (s, 3H, j), 3.98 (s, 3H, a), 7.31 (m, *J* = 8.7 Hz, h), 7.36 (m, *J* = 8.7 Hz, g); **^{13}C-NMR** (125 MHz, $CDCl_3$): δ: 15.3 (j), 61.9 (a), 96.2 (c), 122.7 (e), 128.9 (g), 130.4 (h), 131.1 (d), 133.0 (f), 133.4 (i), 157.9 (b); **IR** (ATR): $\tilde{\nu}$: 2957.8 (s), 2919.7 (s), 2828.6

(s), 1902.4 (s), 1589.1 (s), 1553.4 (m), 1508.1 (m), 1478.2 (m), 1447.3 (m), 1423.2 (m), 1397.7 (m), 1378.9 (m), 1353.3 (s), 1264.1 (m), 1227.5 (w), 1155.2 (w), 1094.4 (m), 1051.0 (m), 1031.2 (s), 1016.3 (s), 1008.1 (m), 977.7 (w), 931.4 (m), 828.3 (w), 817.7 (w), 741.5 (w), 710.6 (s), 629.2 (s), 567.5 (w), 561.7 (w), 516.3 (w), 491.8 (w), 459.9 (w), 453.7 (m); **Elemental Analysis** calcd for $C_{12}H_{10}BrClOS$: C: 45.38, H: 3.17, S: 10.09%; Found: C: 47.07, H: 3.24, S: 10.26%; **HRMS** (EI, 70 eV, RT): $[M]^-$ *m/z* Calcd for $C_{12}H_{10}BrClOS$: 315.9330; found: 315.9324.

4.1.2.25 ((4-(5-Methoxy-3-methyl-4-(perfluorocyclopent-1-en-1-yl)thiophen-2-yl)phenyl)ethynyl)trimethylsilane (144)

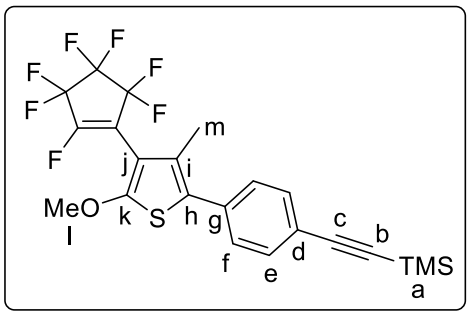

Compound **143** (985 mg, 2.60 mmol) was dissolved in abs THF (10 mL) and the solution cooled to -78 °C. *n*-Butyllithium (2.5 M in hexane, 1.06 mL, 2.66 mmol) was added dropwise and the solution stirred at -78 °C for 30 min, before to the mixture perfluorocyclopentene (662 mg, 3.12 mmol) was added via syringe, and the reaction mixture warmed up to room temperature in 45 min. After addition of H_2O the mixture was extracted with Et_2O. The combined organic layers were dried (Na_2SO_4) and the solvents removed *in vacuo*. Purification by flashchromatography (silica gel; pentane) gave **144** (838 mg, 1.70 mmol, 66%) as a colorless solid.

Rf (pentane/DCM: 4/1): 0.6; **MP:** 93-96 °C; **^{1}H-NMR** (400 MHz, $CDCl_3$): δ 0.27 (s, 9H, a), 2.11 (s, 3H, m), 3.97 (s, 3H, l), 7.32-7.35 (m, *J* = 8.6 Hz, 2H, f), 7.48-7.52 (m, *J* = 8.6 Hz, 2H, e); **^{13}C-NMR** (125 MHz, $CDCl_3$): δ 0.1 (a), 14.2 (m), 61.8 (l), 95.6 (b), 104.3 (c), 104.8 (i), 122.3 (d), 124.6 (h), 129.0 (e), 130.6 (j), 132.3 (f), 134.0 (g), 165.6 (k); **IR** (ATR): $\tilde{\nu}$ 2963.1(w), 2156.5(w), 1711.0(w), 1602.1(w), 1564.0(w), 1515.3(m), 1487.8(2), 1451.7(w), 1400.1(m), 1330.2(m), 1313.3(m), 1275.7(m), 1248.2(m), 1228.4(m), 1198.1(m), 1141.7(m), 1112.7(s), 1094.4(m), 1043.8(m), 1004.2(m), 971.0(s), 939.6(w), 914.6(m), 837.9(s), 759.3(s), 730.9(m), 702.0(m), 685.6(m), 643.6(m), 633.0(m), 625.8(m), 608.9(m), 577.1(m), 553.5(s), 541.9(m), 508.2(w),

500.4(w), 491.8(m); **Elemental Analysis** calcd for $C_{17}H_{18}BrOSSi$: C: 53.65, H: 3.89, S: 6.51%; Found C: 51.31, H: 3.89, S: 5.75%: **HRMS** (EI, 70 eV, RT): $[M]^+$ *m/z* Calcd for $C_{17}H_{18}BrOSSi$ 492.0814; Found 492.0823.

4.1.2.26 3,3'-(Perfluorocyclopent-1-ene-1,2-diyl)bis(2-methoxy-4-methylthiophene) (28)

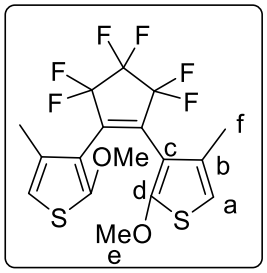

To a solution of bromothiophene **27** (740 mg, 3.57 mmol) in abs. Et_2O (12 mL) cooled to -78 °C, *n*-butyllithium (2.5 M in hexane, 1.43 ml, 3.60 mmol) was added dropwise and the mixture stirred for 2 h at -78 °C. Perfluorocyclopentene (373 mg, 1.76 mmol) was added in one portion via syringe and the resulting mixture stirred for 5 h at -30 °C before warming up to rt in 2 h. Then, Et_2O (30 mL) was added and the organic layer washed with aq. 1 N HCl (10 mL), sat. aq. $NaHCO_3$ (20 mL) and water (20 mL). The combined organic layer were dried over Na_2SO_4 and the solvent removed in vauo. Purification with column chromatography (silica gel, pentane) gave **28** (317 mg, 0.74 mmol, 21%) as a yellowish solid.

Rf (pentane): 0.13; **MP:** n. d.; **^{1}H-NMR** (400 MHz, $CDCl_3$): δ 2.02 (brs, 6H, f), 3.75 (s, 6H, e), 6.21 (q, *J* = 1.1 Hz, 2H, a); **^{13}C-NMR** (100.6 MHz, $CDCl_3$): δ 15.7 (f), 61.4 (e), 107.2 (a), 109.2 (c), 135.3 (b), 165.0 (d); **HRMS** (EI, 70 eV, RT): $[M]^+$ *m/z* Calcd for $C_{18}H_{23}F_6O_2S_2$: 428.0334, found 428.0342.

4.1.2.27 4,4'-(Perfluorocyclopent-1-ene-1,2-diyl)bis(2-iodo-5-methoxy-3-methylthiophene) (29)

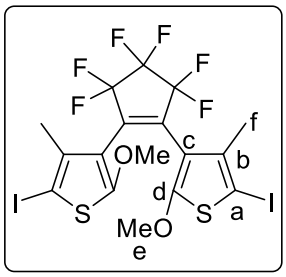

DTE(OMe) **28** (31 mg, 72.0 µmol) in benzene (1.5 mL) was stirred at rt. Iodine (56 mg, 221 µmol) and HgO (48 mg, 221 µmol) were added in portions, and the mixture was stirred for 2 h, then filtered, washed with $Na_2S_2O_3$ (5 mL) and water (5 mL). The combined organic layers were dried over Na_2SO_4 and the solvent removed *in vacuo*. Purification with column chromatography (silica gel, pentane) yielded **29** (30 mg, 44.1 µmol, 61%) as yellowish solid.

Rf (pentane): 0.15; **MP:** n. d.; **^{1}H-NMR** (500 MHz, $CDCl_3$): δ 1.96 (s, 3H, f), 3.77 (s, 3H, e); **^{13}C-NMR** (125 MHz, $CDCl_3$): δ 18.0 (f), 59.5 (a), 61.5 (e), 108.4 (c), 139.5 (b), 162.6 (d); **HRMS** (EI, 70 eV, RT): $[M]^+$ *m/z* Calcd for: $C_{17}H_{12}F_6I2O_2S_2$: 679.8272; 679.8261.

4.1.2.28 4,4'-(Perfluorocyclopent-1-ene-1,2-diyl)bis(5-methoxy-3-methyl-2-phenylthiophene) (3)

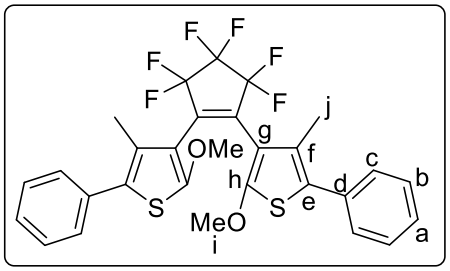

To a stirred solution of **139** (288 mg, 1.01 mmol) in abs THF (12 mL) at -78 °C, *n*-BuLi (2.5 M in hexane, 0.43 mL, 1.06 mmol) was added dropwise and the mixture stirred for 30 min. Perfluorocyclopentene (107 mg, 0.5 mmol) was added quickly and the reaction mixture warmed up to room temperature in 30 min. The reaction mixture was poured into water and extracted with Et_2O. The combined organic layers were dried (Na_2SO_4), the solvents removed *in vacuo* and the residue purified by flashchromatography (silica gel; pentane/ETOAC: 9/1) to give **3** (75 mg, 1.29 mmol, 26 %) as a colourless solid.

Rf (pentane): 0.1; **MP:** n. d.; **^{1}H-NMR** (500 MHz, $CDCl_3$): δ 2.12 (s, 3H, j), 3.80 (s, 3H, i), 7.28-7.32 (m, 1H, a), 7.37-7.41 (m, 4H, c, b)[11]; **^{13}C-NMR** (125 MHz, $CDCl_3$): 14.2 (j), 61.4 (i), 110.4 (g), 124.6 (e), 127.2 (a), 128.7 (c), 129.3 (b), 130.7 (f), 134.3 (d), 163.5 (h); **HRMS** (APCI): $[M+H]^+$ *m/z* Calcd for $C_{29}H_{22}F_6O_2S_2$: 581.1038; Found 581.1022.

4.1.2.29 ((4-(4-(3,3,4,4,5,5-Hexafluoro-2-(2-methoxy-5-(4-methoxyphenyl)-4-methylthiophen-3-yl)cyclopent-1-en-1-yl)-5-methoxy-3-methylthiophen-2-yl)phenyl)ethynyl)trimethylsilane (148)

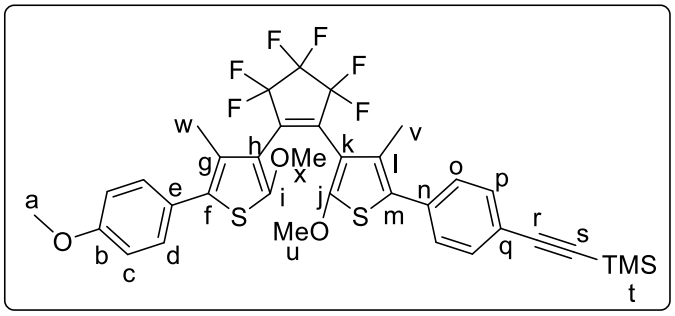

3-Bromo-2-methoxy-5-(4-methoxyphenyl)-4-methylthiophene (**141**, 190 mg, 0.61 mmol) was dissolved in abs. THF (5 mL) and the reaction mixture cooled to -78 °C. Under vigorously stirring *n*-butyllithium (2.5 M in hexane, 0.26 mL, 0.64 mmol) was added dropwise and the solution stirred for 45 min. Afterwards, the perfluorocompound **144** (230 mg, 0.467 mmol) dissolved in 10 mL abs. THF was added and the solution was allowed to warm up in 20 h. After removing of the solvent under *vacuo*, the residue was purified by flash column chromatography several times (Pentan/EtOAc = 8/1 -> 10/1) to yield **148** (44.0 mg, 62.0 µmol, 7%) as a yellow solid.

Rf (pentane/EtOAc: 10/1): 0.26; **MP:** n.d.; (**^{1}H-NMR** (700 MHz, $CDCl_3$): δ: 0.26 (s, 9H, t), 2.05 (s, 3H, w), 2.09 (s, 3H, v), 3.77 (s, 3H, x), 3.78 (s, 3H, u), 3.83 (s, 3H, a), 6.91 (m, *J* = 8.7 Hz, c), 7.28 (m, *J* = 8.7 Hz, d), 7.30 (m, *J* = 8.3 Hz, o), 7.46 (m, *J* = 8.7 Hz, p); **^{13}C-NMR** (175 MHz, $CDCl_3$): δ: 0.11 (t), 14.1 (w), 14.4 (v), 55.5 (a),

61.5 (u, x), 95.3 (s), 104.9 (r), 110.2 (h), 110.7 (k), 114.1 (c), 121.8, (q), 123.9 (m), 124.5 (f), 126.6 (e), 128.8 (o), 129.9 (g), 130.6 (d), 131.5 (l), 132.3 (p), 134.5 (n), 159.0 (b), 162.9 (i), 163.9 (j); **HRMS** (APCI): $[M+H]^+$ *m/z* Calcd for $C_{35}H_{32}F_6O_3S2Si$: 707.1539, Found 707.1522.

4.1.2.30 ((4-(4-(2-(5-(4-Chlorophenyl)-2-methoxy-4-methylthiophen-3-yl)-3,3,4,4,5,5-hexafluorocyclopent-1-en-1-yl)-5-methoxy-3-methylthiophen-2-yl)phenyl)ethynyl)trimethylsilane (147)

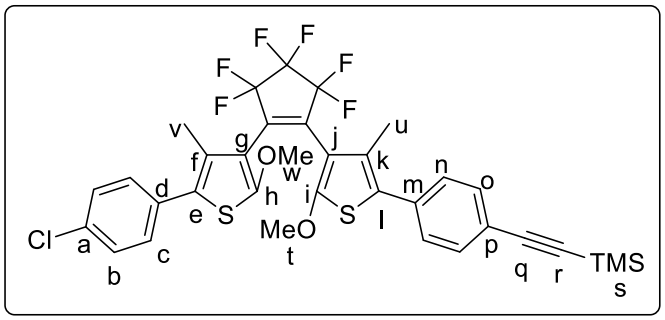

Compound **140** (715 mg, 2.44 mmol) was dissolved in abs. THF (60 mL) and the solution cooled to -78 °C. Then *n*-butyllithium (2.5 M in hexane, 981 µL, 2.45 mmol) was added dropwise, and the solution kept for 1 h at -78 °C, before **144** (598 mg, 1.21 mmol) was added neat. The reaction mixture was allowed to warm up to room temperature in 1 h, and the solvents were removed under *vacuo*. The residue was taken into water and extracted with diethylether (3 x 40 mL). The combined organic layer were dried over Na_2SO_4, the solvent removed under vacuo and the residue purified by flash column chromatography (pentane/DCM: 5/1). The product **147** (802 mg, 1.13 mmol, 94 %) was obtained as colorless solid.

Rf (pentane/DCM: 5/1): 0.2; **MP:** n. d.; **^{1}H-NMR** (500 MHz, $CDCl_3$): δ: 0.25 (s, 9H, s), 2.07 (s, 3 H, v), 2.09 (s, 3H, u), 3.79 (s, 3H, t), 3.80 (s, 3H, w), 7.28 (m, *J* = 8.5 Hz, 2H, c), 7.29 (m, *J* = 8.1 Hz, 2H, n), 7.34 (*m*, *J* = 8.5 Hz, 2H, b), 7.46 (m, *J* = 8.2 Hz, 2H, o); **^{13}C-NMR** (125 MHz, $CDCl_3$): δ: 0.1 (s), 14.2 (v), 14.4 (u), 61.5 (w, t), 95.4 (r), 104.9 (q), 110.4 (g), 110.6 (j), 121.9 (p), 123.3 (e), 124.0 (l), 128.8 (n), 128.9 (c), 130.4 (b), 131.2 (f), 131.4 (k), 132.3 (o), 132.7 (d), 133.2 (a), 134.4 (m), 163.7 (h), 163.9 (i); **HRMS** (APCI): $[M+H]^+$ *m/z* Calcd for $C_{34}H_{29}ClF_6O_2S_2Si$: 711.1044; found 711.1036.

4.1.2.31 2-(4-Chlorophenyl)-4-(2-(5-(4-ethynylphenyl)-2-methoxy-4-methylthiophen-3-yl)-3,3,4,4,5,5-hexafluorocyclopent-1-en-1-yl)-5-methoxy-3-methylthiophene (150)

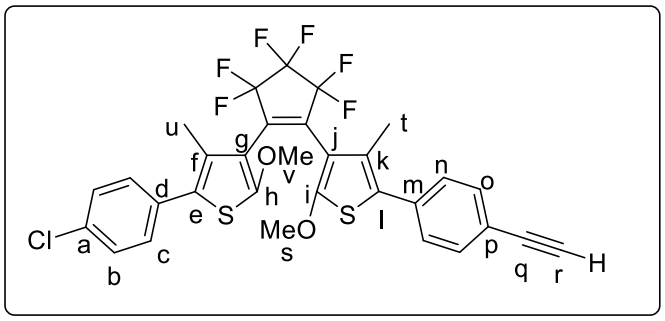

Compound **147** (242 mg, 340 µmol) was dissolved in ethanol (10 mL) and THF (6 mL) before aq. NaOH (2 N, 180 µL,, 357 µmol) was added dropwise at room temperature, and then the solution was stirred for 30 min. The solvent was removed *in vacuo* and the residue was purified by flash column chromatography (pentane/DCM: 5/1) to obtain **150** (201 mg, 315 µmol, 93 %) as a colourless solid.

Rf (pentane/DCM: 4/1): 0.4; **MP:** n. d.; **^{1}H-NMR** (500 MHz, $CDCl_3$): δ: 2.08 (s, 3H, u), 2.11 (s, 3H, t), 3.12 (s, 1H, r), 3.79 (s, 3H, s), 3.80 (s, 3 H, v), 7.29 (m, *J* = 8.57 Hz, 2H, b), 7.33 (m, *J* = 8.38 Hz, 2H, n), 7.35 (m, *J* = 8.55 Hz, 2H, c), 7.50 (m, *J* = 8.29 Hz, 2H, o); **^{13}C-NMR** (125 MHz, $CDCl_3$): δ: 14.2 (u), 14.4 (t), 61.5 (s, v), 78.2 (r), 83.5 (q), 110.4 (f), 110.6 (k), 120.8 (p), 123.3 (e), 123.9 (l), 128.9 (b, n), 130.4 (c), 131.2 (g), 131.4 (j), 132.4 (o), 132.7 (d), 133.2 (a), 134.8 (m), 163.7 (h), 164.0 (i); **HRMS** (APCI): $[M+H]^+$ *m/z* Calcd for $C_{31}H_{21}ClF_{62}S_2$: 639.0648; Found 639.0691.

4.1.2.32 2-((4-(4-(2-(5-(4-Chlorophenyl)-2-methoxy-4-methylthiophen-3-yl)-3,3,4,4,5,5-hexafluorocyclopent-1-en-1-yl)-5-methoxy-3-methylthiophen-2-yl)phenyl)ethynyl)-5,5-difluoro-1,3,7,9-tetramethyl-5H-5λ^4,6λ^4-dipyrrolo[1,2-c:2',1'-f][1,3,2]diazaborinine (152)

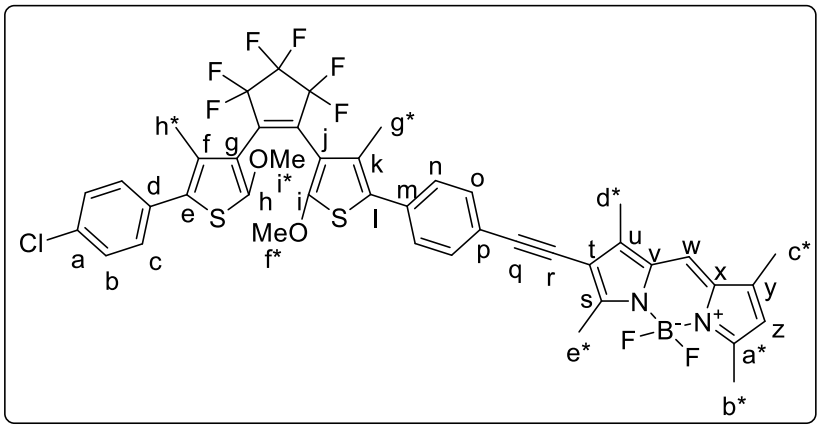

Compounds **150** (110 mg, 172 µmol), **62** (61 mg, 164 µmol), $Pd(PPh_3)_4$ (20 mg, 17.0 µmol) and copper(I)-iodide (3.2 mg, 17.2 µmol) were dissolved in a mixture of abs. THF (10 mL) and abs. TEA (9 mL) and the reaction solution stirred at room temperature for 22 h. The solvent was removed *in vacuo* and the residue purified by flash column chromatography (pentane/toluene: 3/2) to obtain **152** (35 mg, 40.2 µmol, 24 %) as a yellow solid.

Rf (pentane/toluene: 4/3): 0.4; **MP:** n. d.; **^{1}H-NMR** (500 MHz, $CDCl_3$): 2.08 (s, 3H, h*), 2.12 (s, 3H, g*), 2.27 (s, 3H, c*), 2.36 (s, 3H, d*), 2.56 (s, 3H, b*), 2.67 (s, 3H, e*), 3.80 (2 s, 6H, f*, i*), 6.11 (s, 1H, z), 7.08 (s, 1H, w), 7.29 (m, *J* = 8.5 Hz, 2H, b), 7.32 (m, *J* = 8.7 Hz, 2H, c), 7.33 (m, *J* = 8.5 Hz, 2H, n), 7.50 (m, *J* = 8.5 Hz, 2H, o); **^{13}C-NMR** (125 MHz, $CDCl_3$): 10.8 (d*), 11.5 (c*), 13.7 (e*), 14.2 (h*), 14.4 (g*), 15.0 (b*), 61.5 (f*, i*), 83.0 (r), 95.5 (q), 110.4 (g), 110.6 (j), 113.5 (t), 120.2 (z), 120.6 (w), 122.3 (p), 123.3 (e), 124.1 (l), 128.9 (c, n), 130.4 (b), 131.2 (f, k), 131.6 (o), 131.8 (u), 132.7 (d), 133.2 (m), 134.0 (a), 134.8 (y), 140.9 (v), 143.0 (x), 157.7 (s), 159.4 (a*), 163.7 (h), 163.8 (i); HRMS (APCI pos): [M+H$^+$] m/z Calcd for $C_{44}H_{34}BClF_8N_2O_2S_2$ 885.1788; Found 885.1737.

4.1.2.33 ((4-(4-(2-(5-Chloro-2-methoxy-4-methylthiophen-3-yl)-3,3,4,4,5,5-hexafluorocyclopent-1-en-1-yl)-5-methoxy-3-methylthiophen-2-yl)phenyl)ethynyl)trimethylsilane (145)

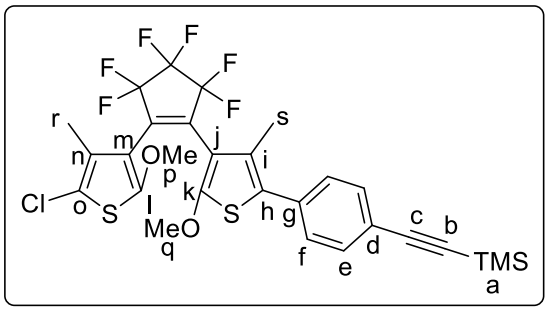

To a solution of **143** (230 mg, 952 µmol) in abs THF (6 mL) at -78 °C, *n*-BuLi (2.5 M in hexane, 390 µL, 991 µmol) was added dropwise and the solution stirred for 30 min. Compound **144** (320 mg, 650 µmol) was added as a solid and the mixture warmed up to room temperature in 60 min. The reaction was quenched with water, extracted with Et_2O (3 x 30 mL), the organic layer dried (Na_2SO_4) and the solvents removed *in vacuo*. Purification by flashchromatography (silica gel; pentane) gave **145** (252 mg, 396 µmol, 64 %) as a yellow solid.

Rf (pentane): 0.3; **MP:** n. d.; **^{1}H-NMR** (500 MHz, $CDCl_3$): δ 0.26 (s, 9H, a), 1.98 (s, 3H, r), 2.06 (s, 3H, s), 3.73 (s, 3H, q), 3.82 (s, 3H, p), 7.28-7.31 (m, *J* = 8.4 Hz, 2H, f), 7.44-7.48 (m, *J* = 8.4 Hz, 2H, e); **^{13}C-NMR** (125 MHz, $CDCl_3$): δ 0.1 (a), 12.8 (r), 14.5 (s), 61.5 (p), 61.9 (q), 95.4 (b), 104.9 (c), 108.8 (o), 110.2 (j), 112.2 (m), 121.9 (d), 124.1 (h), 128.8 (f), 131.1 (n), 132.0 (i), 132.3 (e), 134.3 (g), 160.8 (k), 163.9 (l); **HRMS** (APCI pos): [M+H]$^+$ *m/z* Calcd for $C_{28}H_{25}ClF_6O_2S_2Si$ 635.0731; Found 635.0735.

4.1.2.34 Methyl 4-(4-(3,3,4,4,5,5-hexafluoro-2-(2-methoxy-4-methyl-5-(4-((trimethylsilyl)ethynyl)phenyl)thiophen-3-yl)cyclopent-1-en-1-yl)-5-methoxy-3-methylthiophen-2-yl)benzoate (154)

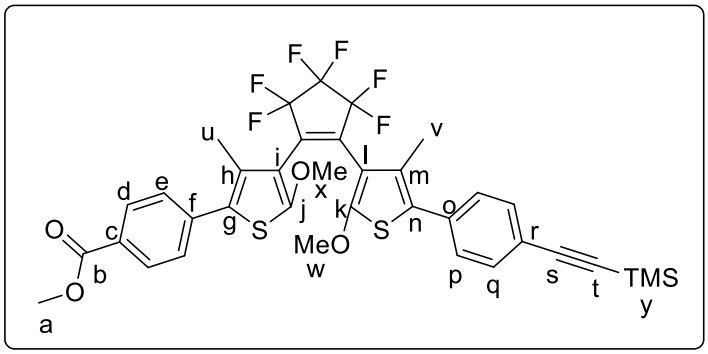

A solution of **145** (155 mg, 246 µmol) in abs THF (5 mL) was cooled to -78 °C and *n*-BuLi (2.5 M in hexane, 103 µL, 257 µmol) was added dropwise, and the solution stirred for 30 min. Then tributylborate was (100 µL, 368 µmol) added and stirring continued for 30 min. Afterwards 20% aqueous Na_2CO_3 solution (5 mL), $Pd(PPh_3)_4$ (28 mg, 25 µmol) and 4-iodo benzoic acid methylester (71 mg, 270 µmol) were added, and the reaction mixture heated to 85 °C for 4 h. The mixture was poured into H_2O, extracted with Et_2O (3 x 30 mL), the organic layer was dried (Na_2SO_4), and the solvents removed *in vacuo*. Purification via flashchromatography (silica gel; pentane/DCM: 5/1 -> 3/2) yielded **154** (90 mg, 122 µmol, 50 %) as a yellow solid.

Rf (pentane/DCM: 4/1): 0.1; **MP:** n. d.; **^{1}H-NMR** (500 MHz, $CDCl_3$): δ 0.26 (s, 9H, y), 2.11 (s, 3H, v), 2.15 (s, 3H, u), 3.80 (s, 3H, x), 3.81 (s, 3H, w), 3.93 (s, 3H, a) 7.28-7.32 (m, *J* = 8.0 Hz, 2H, e), 7.43-7.46 (m, *J* = 8.1 Hz, 2H, p), 7.46-7.49 (m, *J* = 8.0 Hz, 2H), 8.02-8.05 (m, *J* = 8.1 Hz, 2H, d); **^{13}C-NMR** (125 MHz, $CDCl_3$): δ 0.1 (y), 14.3 (v), 14.5 (u), 52.2 (a), 61.5 (w, x), 95.4 (t), 104.8 (s), 110.4 (l), 110.7 (i), 121.9 (r), 123.5 (g), 124.0 (n), 128.5 (c), 128.7 (p, q), 130.0 (e), 131.3 (m), 132.2 (d), 132.4 (h), 134.4 (o), 138.9 (f), 163.9 (k), 164.4 (j), 166.8 (b); **HRMS** (APCI pos): $[M+H]^+$ *m/z* Calcd for $C_{36}H_{32}F_6O_4S_2Si$ 735.1490; Found 735.1490.

4.1.2.35 4-(4-(2-(5-(4-Ethynylphenyl)-2-methoxy-4-methylthiophen-3-yl)-3,3,4,4,5,5-hexafluorocyclopent-1-en-1-yl)-5-methoxy-3-methylthiophen-2-yl)benzoic acid (155)

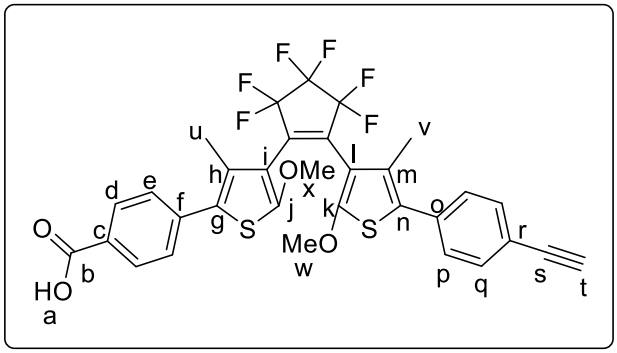

To a solution of **154** (132 mg, 180 µmol) in THF (7 mL), aqueous 2 N NaOH (1.0 mL, 2.0 mmol) was added and the mixture was heated at 95 °C for 12 h. After cooling down to room temperature, the suspension was diluted with aqueous saturated NH_4Cl solution, extracted with Et_2O (5 x 20 mL) and the organic layer dried over Na_2SO_4. Removing the

solvents *in vacuo* gave **155** (mixture of monomer and dimer; 115 mg, 177 µmol, 99 %) as a colorless solid, which was used in the next step without further purification.

Rf (cyclohexane/EtOAc: 1/1 + 0.1 % acetic acid): 0.6; **MP:** n. d.; **^{1}H-NMR** (500 MHz, d_6-DMSO): δ 2.07 (s, 3H, v), 2.10 (s, 3H, u), 3.82 (s, 3H, w), 3.83 (s, 3H, x), 4.24 (s, 1H, t), 7.39-7.42 (m, *J* = 8.3 Hz, 2H, p), 7.50-7.52 (m, *J* = 8.3 Hz, 2H, q), 7.52-7.54 (m, *J* = 7.8 Hz, 2H, e), 7.95-7.98 (m, *J* = 8.2 Hz, 2H, d); **^{13}C-NMR** (125 MHz, d_6-DMSO): δ 14.0 (u), 14.1 (v), 61.7 (x), 61.8 (w), 81.7 (t), 83.1 (s), 108.6 (h), 108.8 (m), 120.5 (r), 122.8 (g), 123.0 (n), 128.4 (e), 128.7 (p), 129.2 (c), 129.9 (d), 131.3 (i), 131.5 (l), 132.2 (q), 133.7 (o), 137.5 (f), 164.6 (j, HMBC), 164.7 (k, HMBC), 166.9 (b); **HRMS** (Esi neg): $[M]^-$ *m/z* Calcd for $C_{32}H_{23}F_6O_4S_2$ 648.0869; Found 648.0855.

4.1.2.36 4-(4-(2-(5-(4-((5,5-Difluoro-1,3,7,9-tetramethyl-5H-5λ^4,6λ^4-dipyrrolo[1,2-c:2',1'-f][1,3,2]diazaborinin-2-yl)ethynyl)phenyl)-2-methoxy-4-methylthiophen-3-yl)-3,3,4,4,5,5-hexafluorocyclopent-1-en-1-yl)-5-methoxy-3-methylthiophen-2-yl)benzoic acid (20)

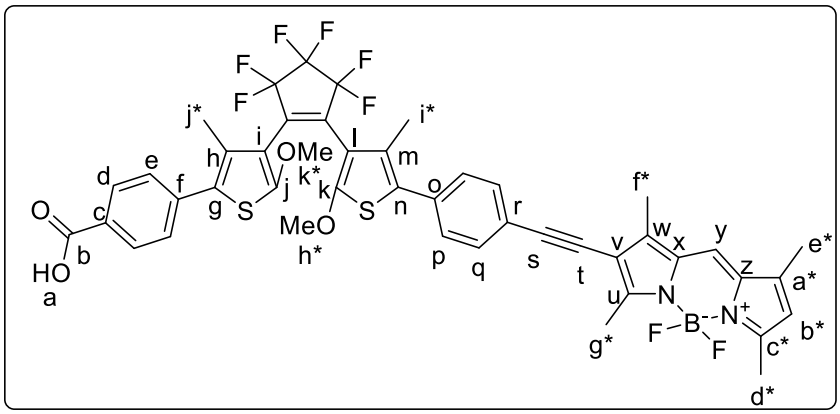

A solution of **155** (57 mg, 151 µmol), **62** (98 mg, 151 µmol), $PdCl_2(PPh_3)_2$ (3 mg, 3 µmol) and CuI (2 mg, 10 µmol) in abs THF (14 mL) and diisopropylamine (40 µL) was stirred at room temperature for 22 h. The resulting mixture was poured into HCl (1 N, 10 mL) and extracted with DCM (4 x 20 mL), the organic layer was dried (Na_2SO_4) and the solvents removed *in vacuo*. Purification by flashchromatography (silica gel; cyclohexane/ETOAC: 1/1 + 0.1 % acetic acid) and lyophilization gave **20** (41 mg, 45.8 µmol, 31 %) as a pink solid.

Rf (cyclohexane/EtOAc: 1/1 + 0.1 % acetic acid): 0.5; **MP:** n. d.; **^{1}H-NMR** (500 MHz, $CDCl_3$): δ 2.13 (s, 3H, i*), 2.16 (s, 3H, j*), 2.27 (s, 3H, e*), 2.35 (s, 3H, f*), 2.56 (s, 3H, d*), 2.66 (s, 3H, g*), 3.81 (s, 3H, h*), 3.82 (s, 3H, k*), 6.10 (s, 1H, b*), 7.08 (s, 1H, y), 7.33-7.36 (m, *J* = 8.2 Hz, 2H, p), 7.44-7.48 (m, *J* = 8.0 Hz, 2H, e), 7.50-7.53 (m, *J* = 8.2 Hz, 2H, q), 8.10-8.13 (m, *J* = 8.0 Hz, 2H, d), **^{13}C-NMR** (125 MHz, $CDCl_3$): δ 10.8 (f*), 11.5 (e*), 13.6 (g*), 14.4 (i*), 14.6 (j*), 15.0 (d*), 61.5 (h*, k*), 83.0 (t), 95.5 (s), 110.4 (m), 110.8 (h), 113.5 (v), 120.2 (b*), 120.6 (y), 122.4 (r), 123.3 (g), 124.1 (n), 128.2 (c), 128.8 (e), 128.9 (p), 130.7 (d), 131.2 (l), 131.6

(q), 131.8 (w), 132.3 (i), 133.9 (o), 134.8 (a*), 139.8 (f), 140.9 (x), 143.0 (z), 157.7 (u), 159.4 (c*), 163.8 (k), 164.6 (j), 171.1 (b); HRMS (Esi neg): $[M]^-$ *m/z* Calcd for $C_{45}H_{35}BF_8N_2O_4S_2$ 898.1931; Found 898.1884.

4.1.2.37 ((4-(4-(3,3,4,4,5,5-Hexafluoro-2-(6-methoxy-2-methyl-3-(phenylthio)phenyl)cyclopent-1-en-1-yl)-5-methoxy-3-methylthiophen-2-yl)phenyl)ethynyl)trimethylsilane (146)

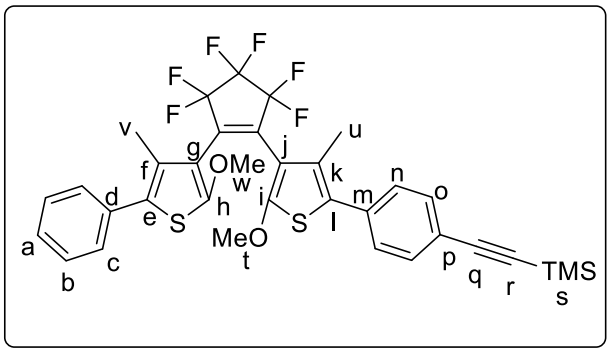

To a solution of **139** (721 mg, 463 µmol) in abs THF (10 mL) at -78 °C, *n*-BuLi (190 µl, 477 µmol) was added dropwise and the solution stirred for 30 min at -78 °C. Compound **144** (228 mg, 463 µmol) was added and the solution was warmed up to room temperature for 60 min. The solution was poured into water, extracted with Et_2O (3 x 30 mL) and the organic layer dried (Na_2SO_4). Removing the solvents *in vacuo* and purification by flashchromatography (silica gel; pentane) yielded **146** (212 mg, 313 µmol, 68 %) as a yellow solid.

Rf (pentane): 0.2*;* **MP:** n. d.; **^{1}H-NMR** (500 MHz, $CDCl_3$): δ 0.27 (s, 9H, s), 2.10 (s, 6H, u, v), 3.79 (2 s, 6H, t, w), 7.28-7.31 (m, 3H, n, a), 7.35-7.39 (m, 4H, b, c), 7.46-7.48 (m, *J* = 8.5 Hz, 2H, o); **^{13}C-NMR** (125 MHz, $CDCl_3$): δ 0.1 (s), 14.2 (u), 14.4 (v), 61.5 (t, w), 95.3 (r), 104.7 (q), 110.4 (k), 110.7 (f), 121.8 (p), 123.9 (l), 124.7 (e), 127.3 (a), 128.7 (c), 128.8 (n), 129.3 (b), 130.6 (j), 131.4 (g), 132.3 (o), 134.3 (d), 134.5 (m), 163.5 (h, i); **HRMS** (APCI pos): $[M+H]^+$ *m/z* Calcd for $C_{34}H_{30}F_6O_4S_2Si$ 677.1433; Found 677.1428.

4.1.2.38 2-(4-Ethynylphenyl)-4-(3,3,4,4,5,5-hexafluoro-2-(2-methoxy-4-methyl-5-phenylthiophen-3-yl)cyclopent-1-en-1-yl)-5-methoxy-3-methylthiophene (149)

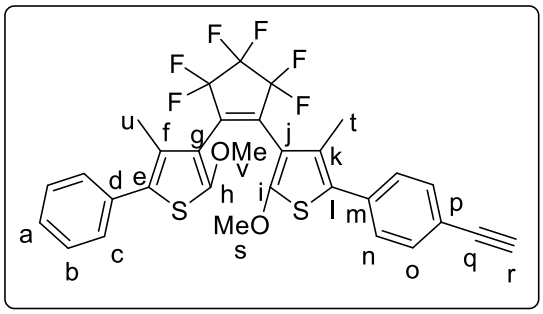

To a solution of **146** (129 mg, 190 µmol) dissolved in MeOH (12 mL) stirred at room temperature aqueous NaOH (2 N, 600 µl) was added, and the mixture heated to 50 °C for 20 h. The resulting mixture was cooled to room temperature, poured into HCl (3 N, 10 mL) and extracted with Et_2O (4 x 20 mL). The organic layer was dried (Na_2SO_4) and the solvents removed *in vacuo* to yield **149** (100 mg, 165 µmol, 87 %) as a white solid.

Rf (pentane): 0.2; **MP:** n. d.; **^{1}H-NMR** (500 MHz, $CDCl_3$): δ 2.11 (2 s, 6H, t, u), 3.12 (s, 1H, r), 3.79 (s, 3H, v), 3.80 (s, 3H, s), 7.28-7.31 (m, 1H, a), 7.32-7.34 (m,2H, *J* = 8.5 Hz, n), 7.35-7.39 (m, 4H, b, c), 7.48-7.51 (m,

J = 8.4 Hz, p); **^{13}C-NMR** (125 MHz, $CDCl_3$): δ 14.2 (t), 14.4 (u), 61.5 (s, v), 78.1 (r), 83.5 (q), 110.3 (f), 110.7 (k), 120.8 (p), 123.8 (l), 124.7 (e), 127.3 (a), 128.7 (c), 128.9 (n), 129.3 (b), 130.6 (g), 131.5 (j), 132.4 (o), 134.3 (d), 134.9 (m), 163.5 (h), 164.0 (i); **HRMS** (EI, 70 eV, RT): $[M]^+$ *m/z* Calcd for $C_{31}H_{22}F_6O_2S_2$ 604.0959; Found 604.0960.

4.1.2.39 Ethyl 4-(7-((4-(4-(3,3,4,4,5,5-hexafluoro-2-(2-methoxy-4-methyl-5-phenylthiophen-3-yl)cyclopent-1-en-1-yl)-5-methoxy-3-methylthiophen-2-yl)phenyl)ethynyl)benzo[c][1,2,5]thiadiazol-4-yl)benzoate (153)

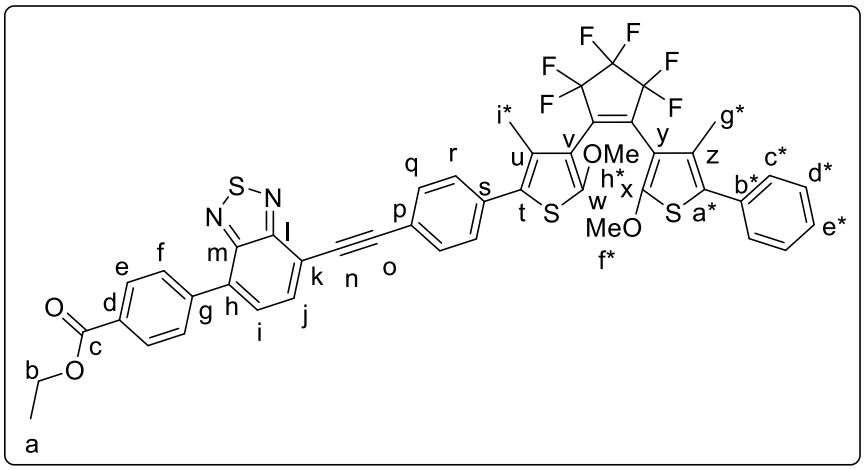

A solution of **149** (47 mg, 83 µmol), **137** (30 mg, 83 µmol), $PdCl_2(PPh_3)_2$ (6 mg, 8.3 µmol) and CuI (2 mg, 8.3 µmol) in abs THF (6 mL) and TEA (6 mL) was heated to 100 °C for 72 h. After cooling to room temperature, the mixture was poured into HCl (1 N) and extracted with Et_2O (3 x 30 mL). The organic layer was dried (Na_2SO_4), the solvents removed *in vacuo* and the crude product purified by flashchromatography (silica gel; cyclohexane/EtOAc: 20/1 + 0.1 % acetic acid). Lyophilization gave **153** (16 mg, 19 µmol, 23 %) as an orange solid.

Rf (pentane/DCM: 9/1): 0.2; **MP:** n. d.; **^{1}H-NMR** (500 MHz, $CDCl_3$): δ 1.43 (q, *J* = 7.0 Hz, 3H, a), 2.11 (s, 3H, g*), 2.15 (s, 3H, i*), 3.80 (s, 3H, r*), 3.81 (s, 3H, h*), 4.43 (t, *J* = 7.0 Hz, 2H, b), 7.27-7.32 (m, 1H, e*), 7.36-7.39 (m, 4H, c*, d*), 7.40-7.42 (m, *J* = 8.4 Hz, 2H, r), 7.68-7.70 (m, *J* = 8.4 Hz, 2H, q), 7.77 (d, *J* = 7.4 Hz, 1H, i), 7.91 (d, *J* = 7.3 Hz, 1H, j), 8.04-8.07 (m, *J* = 8.5 Hz, 2H, f), 8.20-8.22 (m, *J* = 8.5 Hz, 2H, e);**^{13}C-NMR** (125 MHz, $CDCl_3$): δ 14.3 (g*, i*), 14.4 (a), 61.3 (b), 61.5 (f*, h*), 86.4 (o), 96.5 (n), 110.4 (z), 110.8 (u), 116.9 (k), 121.2 (p), 124.7 (a*), 127.3 (e*), 128.3 (i), 128.7 (r), 129.0 (t, c*), 129.3 (f, d*), 130.0 (e), 130.6 (d), 131.0 (v), 131.8 (y), 132.3 (q), 132.9 (j), 133.6 (h), 134.3 (b*), 135.1 (s), 141.3 (g), 153.2 (m), 155.4 (l), 161.7 (w, x), 166.5 (c); **HRMS** (APCI pos): $[M+H]^+$ *m/z* Calcd for $C_{46}H_{36}F_6N_2O_4S_3$ 887.1501; Found 887.1503.

4.1.2.40 4-(7-((4-(4-(3,3,4,4,5,5-Hexafluoro-2-(2-methoxy-4-methyl-5-phenylthiophen-3-yl)cyclopent-1-en-1-yl)-5-methoxy-3-methylthiophen-2-yl)phenyl)ethynyl)benzo[c][1,2,5]thiadiazol-4-yl)benzoic acid (23)

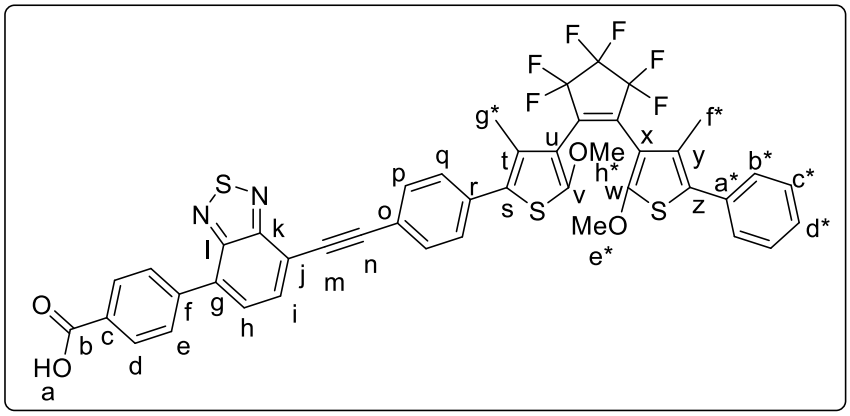

To a solution of **153** (16 mg, 18.0 µmol) in MeOH (12 mL) aqueous NaOH (2 N, 500 µl) was added and the solution was heated at 60 °C for 18 h. The solvents were removed *in vacuo* and the product dissolved into 1 N HCl and extracted with DCM (3 x 50 mL). After drying (Na_2SO_4) and removing of the solvents *in vacuo*, the crude product was purified by flashchromatography (silica gel; EtOAc/cyclohexane: 1/3 + 0.1 % acetic acid) to yield **23** (11 mg, 12.8 µmol, 72 %) as an orange solid.

Rf (pentane/EtOAc: 3/4 + 0.1 % acetic acid): 0.5; **MP:** n. d.; **^{1}H-NMR** (700 MHz, $CDCl_3$): δ 2.11 (s, 3H, f*), 2.15 (s, 3H, g*), 3.81 (2 s, 6H, e*, h*) 7.28-7.31 (m, 1H, d*), 7.36-7.39 (m, 4H, c*, b*), 7.40-7.42 (m, *J* = 8.2 Hz, 2H, q), 7.67-7.70 (m, *J* = 8.1 Hz, 2H, p), 7.79 (d, *J* = 6.7 Hz, 1H, h), 7.92 (d, *J* = 6.7 Hz, 1H, i), 8.07-8.10 (m, *J* = 6.7 Hz, 2H, e), 8.28 (brd, 2H, d); **^{13}C-NMR** (125 MHz, $CDCl_3$): δ 14.3 (f*), 14.5 (g*), 61.5 (e*, h*), 86.3 (m), 96.7 (n), 110.4 (y), 110.8 (t), 117.2 (j), 121.2 (o), 123.9 (s), 124.7 (z), 127.3 (d*), 128.4 (b*), 128.7 (d, h), 129.0 (q), 129.3 (e), 129.5 (c*), 130.7 (c), 131.0 (d), 131.6 (x), 131.8 (u), 132.3 (p), 132.9 (i), 133.4 (g), 134.3 (a*), 135.1 (r), 142.1 (f), 153.1 (l), 155.4 (k), 162.7 (w, HMBC), 163.6 (v, HMBC); **HRMS** (Esi pos): $[M+H]^+$ *m/z* Calcd for $C_{44}H_{28}F_6N_2O_4S_3$ 859.1188; Found 859.1144.

5 Appendix

5.1 NMR-Spectra

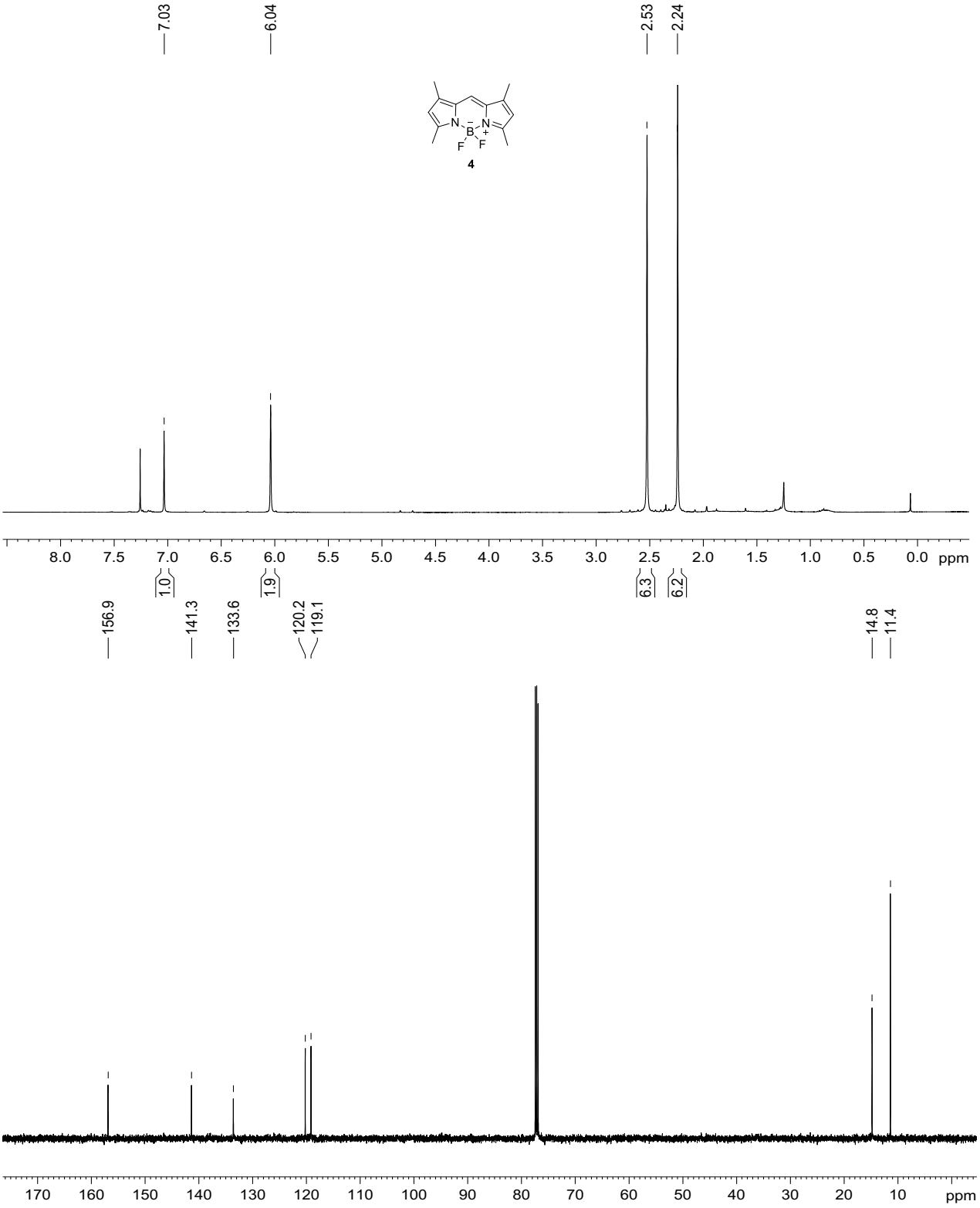

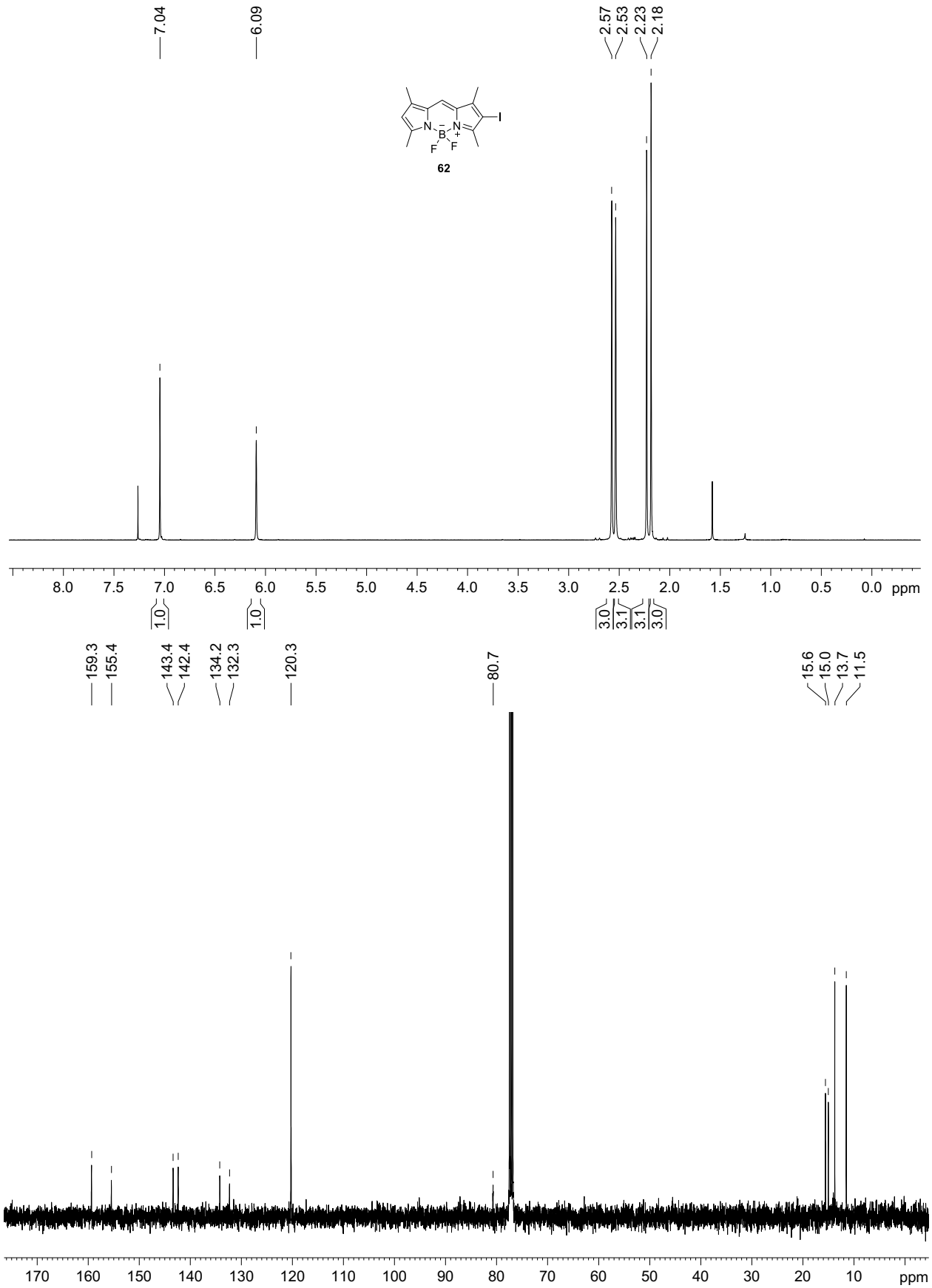
7.04
6.09
2.57
2.53
2.23
2.18
62
8.0 7.5 7.0 6.5 6.0 5.5 5.0 4.5 4.0 3.5 3.0 2.5 2.0 1.5 1.0 0.5 0.0 ppm
1.0
1.0
3.0
3.1
3.1
3.0
159.3
155.4
143.4
142.4
134.2
132.3
120.3
80.7
15.6
15.0
13.7
11.5
170 160 150 140 130 120 110 100 90 80 70 60 50 40 30 20 10 ppm

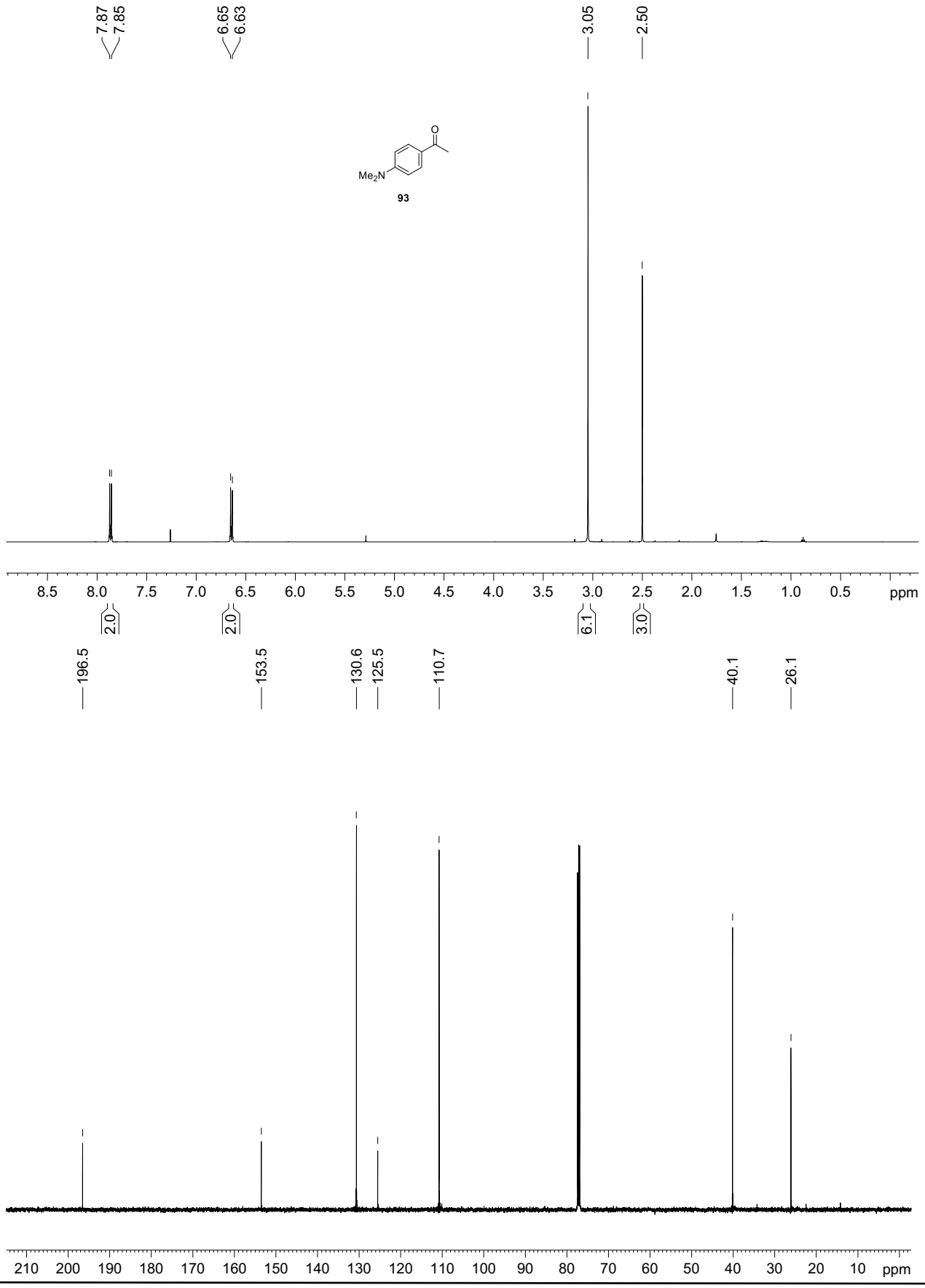
7.87
7.85
6.65
6.63
3.05
2.50
O
Me2N
93
8.5 8.0 7.5 7.0 6.5 6.0 5.5 5.0 4.5 4.0 3.5 3.0 2.5 2.0 1.5 1.0 0.5 ppm
2.0
2.0
6.1
3.0
196.5
153.5
130.6
125.5
110.7
40.1
26.1
210 200 190 180 170 160 150 140 130 120 110 100 90 80 70 60 50 40 30 20 10 ppm

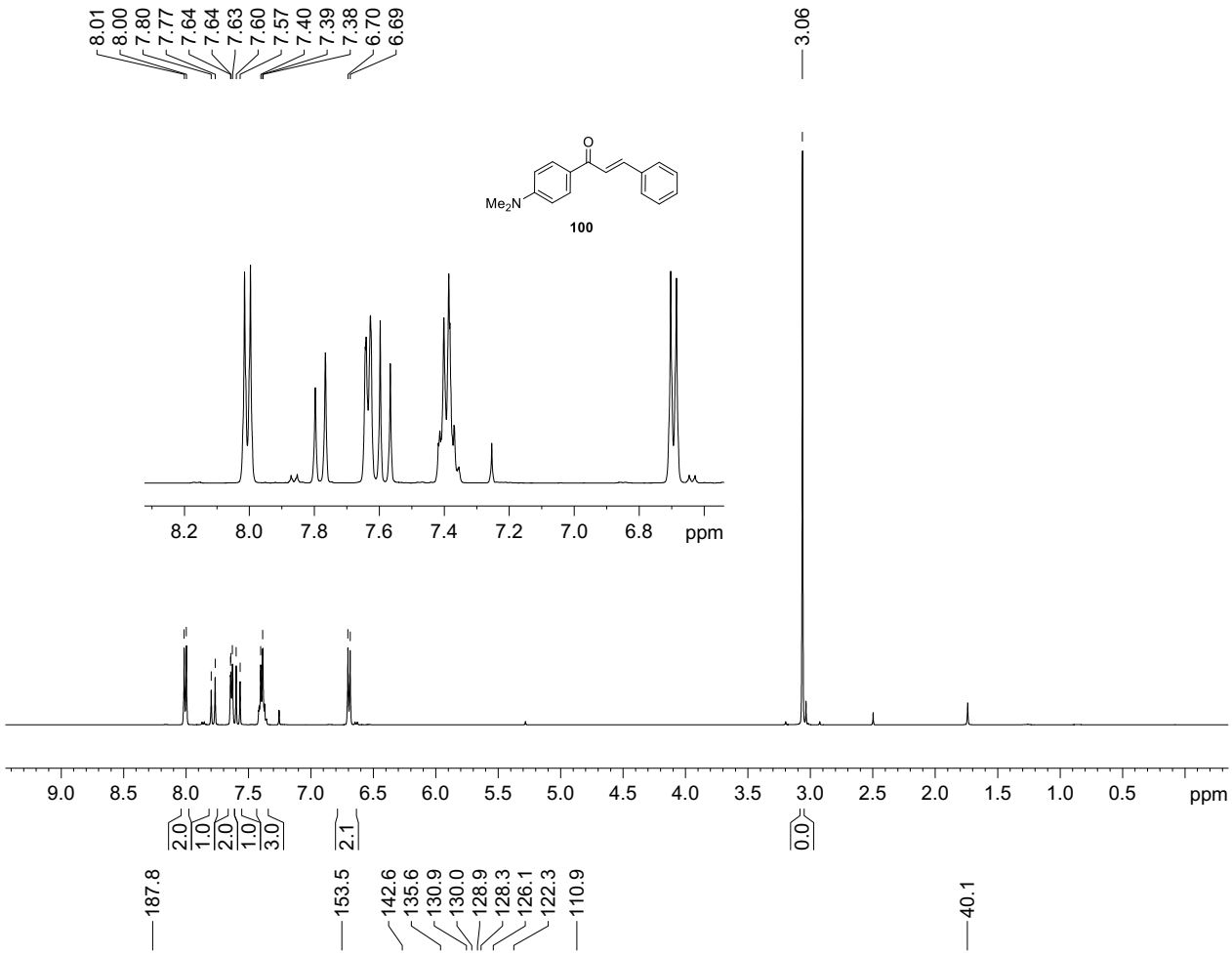
8.01
8.00
7.80
7.77
7.64
7.64
7.63
7.60
7.57
7.40
7.39
7.38
6.70
6.69
3.06
Me2N
100
8.2
8.0
7.8
7.6
7.4
7.2
7.0
6.8
ppm
9.0
8.5
8.0
7.5
7.0
6.5
6.0
5.5
5.0
4.5
4.0
3.5
3.0
2.5
2.0
1.5
1.0
0.5
ppm
2.0
1.0
2.0
1.0
3.0
2.1
0.0

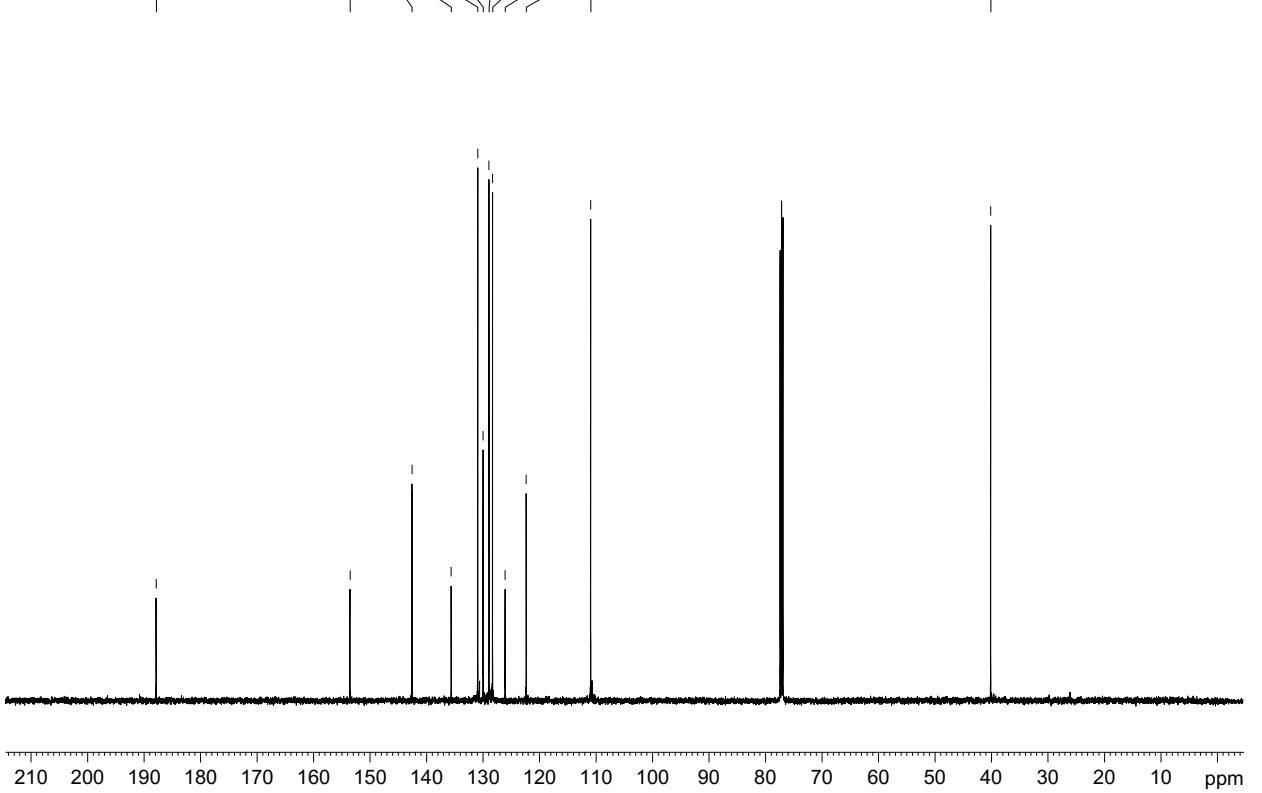
187.8
153.5
142.6
135.6
130.9
130.0
128.9
128.3
126.1
122.3
110.9
40.1
210
200
190
180
170
160
150
140
130
120
110
100
90
80
70
60
50
40
30
20
10
ppm

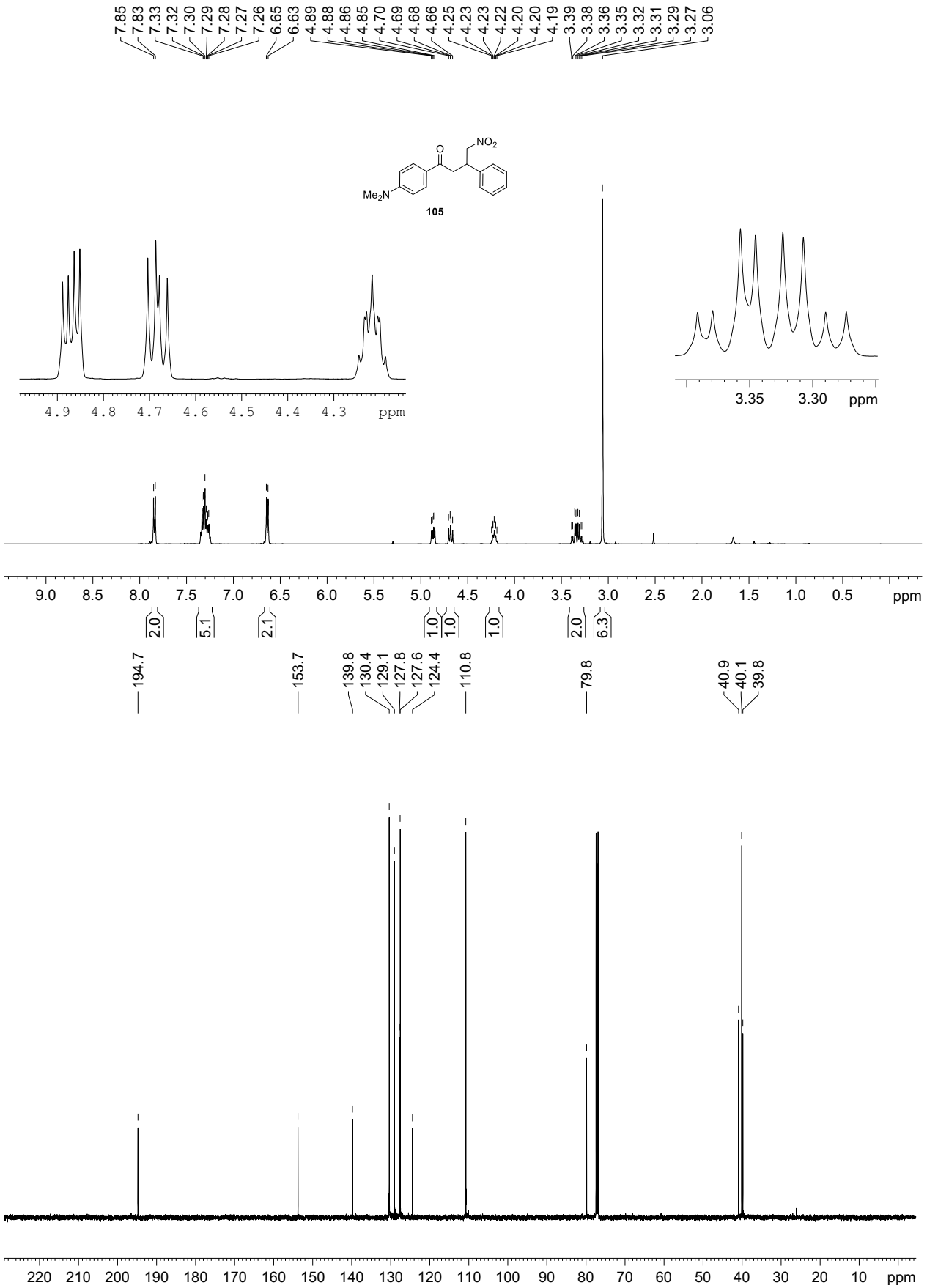
7.85
7.83
7.33
7.32
7.30
7.29
7.28
7.27
7.26
6.65
6.63
4.89
4.88
4.86
4.85
4.70
4.69
4.68
4.66
4.25
4.23
4.22
4.20
4.20
4.19
3.39
3.38
3.36
3.35
3.32
3.31
3.29
3.27
3.06
NO2
O
Me2N
105
4.9 4.8 4.7 4.6 4.5 4.4 4.3 ppm
3.35 3.30 ppm
9.0 8.5 8.0 7.5 7.0 6.5 6.0 5.5 5.0 4.5 4.0 3.5 3.0 2.5 2.0 1.5 1.0 0.5 ppm
2.0
5.1
2.1
1.0
1.0
1.0
2.0
6.3
194.7
153.7
139.8
130.4
129.1
127.8
127.6
124.4
110.8
79.8
40.9
40.1
39.8
220 210 200 190 180 170 160 150 140 130 120 110 100 90 80 70 60 50 40 30 20 10 ppm

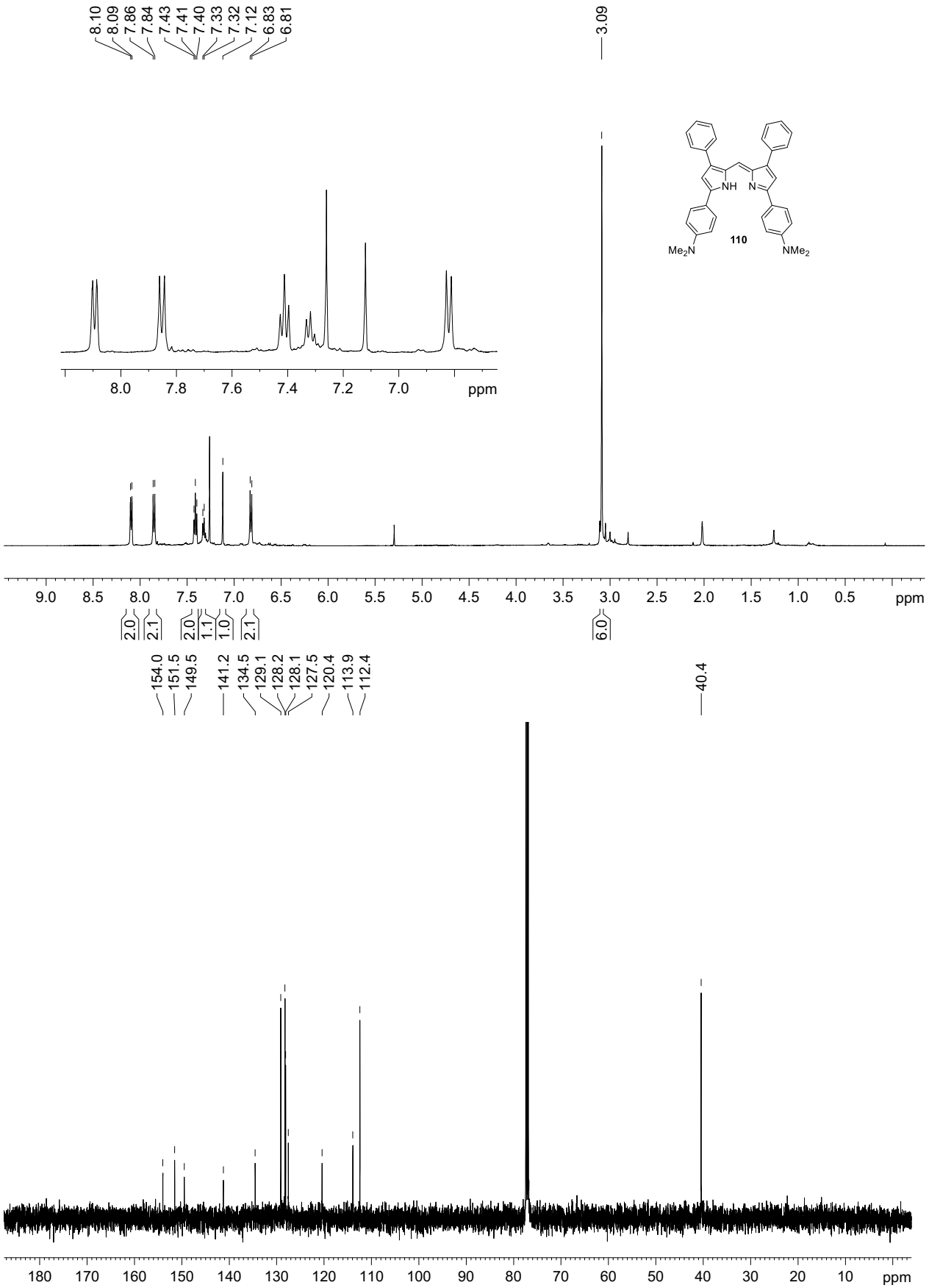
8.10
8.09
7.86
7.84
7.43
7.41
7.40
7.33
7.32
7.12
6.83
6.81
3.09
NH
N
Me2N
NMe2
110
8.0
7.8
7.6
7.4
7.2
7.0
ppm
9.0
8.5
8.0
7.5
7.0
6.5
6.0
5.5
5.0
4.5
4.0
3.5
3.0
2.5
2.0
1.5
1.0
0.5
ppm
2.0
2.1
2.0
1.1
1.0
2.1
6.0
154.0
151.5
149.5
141.2
134.5
129.1
128.2
128.1
127.5
120.4
113.9
112.4
40.4
180
170
160
150
140
130
120
110
100
90
80
70
60
50
40
30
20
10
ppm

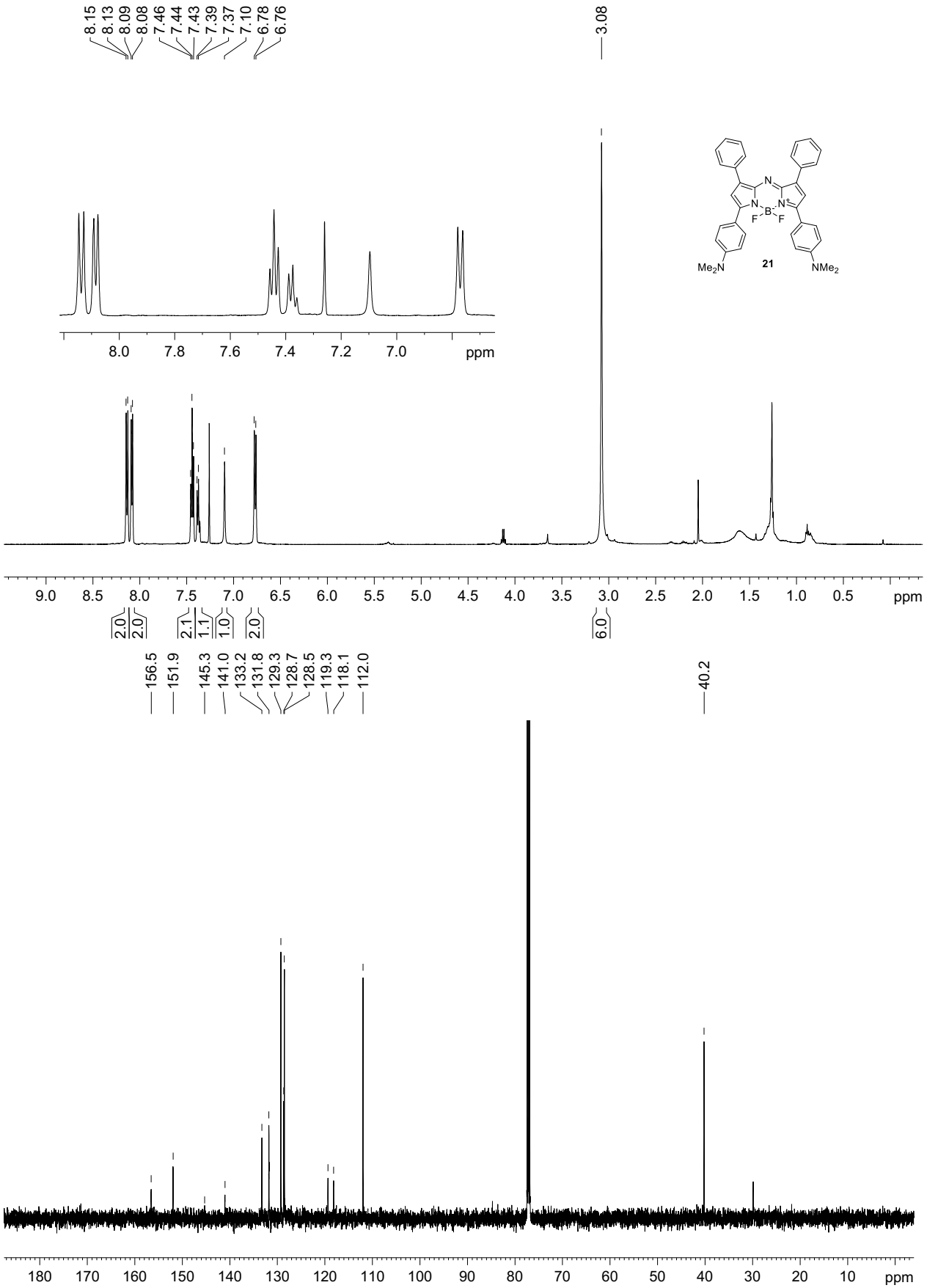
8.15
8.13
8.09
8.08
7.46
7.44
7.43
7.39
7.37
7.10
6.78
6.76
3.08
Me2N
21
NMe2
ppm
2.0
2.0
2.1
1.1
1.0
2.0
6.0
156.5
151.9
145.3
141.0
133.2
131.8
129.3
128.7
128.5
119.3
118.1
112.0
40.2

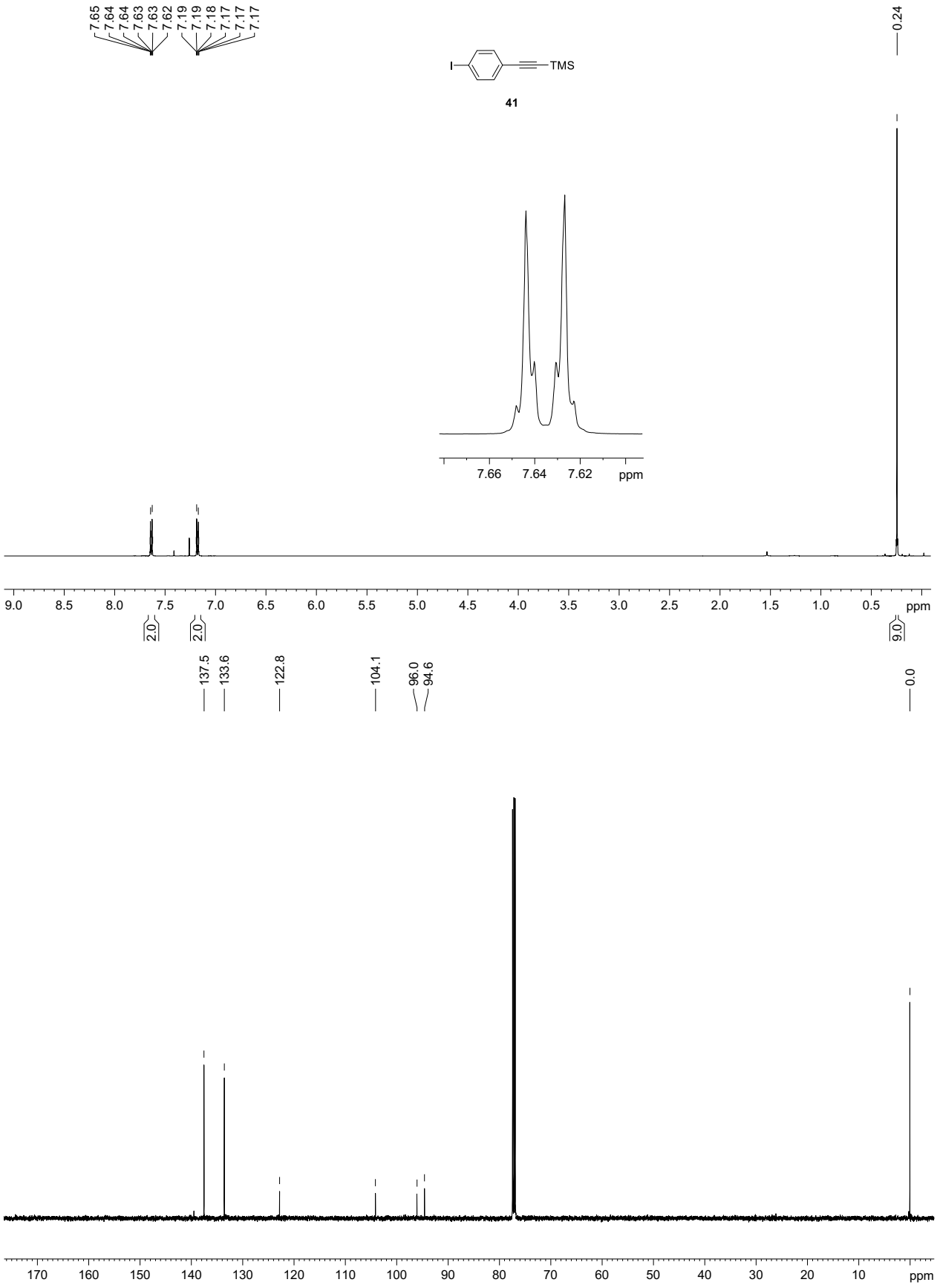
7.65
7.64
7.64
7.63
7.63
7.62
7.19
7.19
7.18
7.17
7.17
7.17
TMS
41
0.24
7.66
7.64
7.62
ppm
9.0
8.5
8.0
7.5
7.0
6.5
6.0
5.5
5.0
4.5
4.0
3.5
3.0
2.5
2.0
1.5
1.0
0.5
ppm
2.0
2.0
9.0
137.5
133.6
122.8
104.1
96.0
94.6
0.0
170
160
150
140
130
120
110
100
90
80
70
60
50
40
30
20
10
ppm

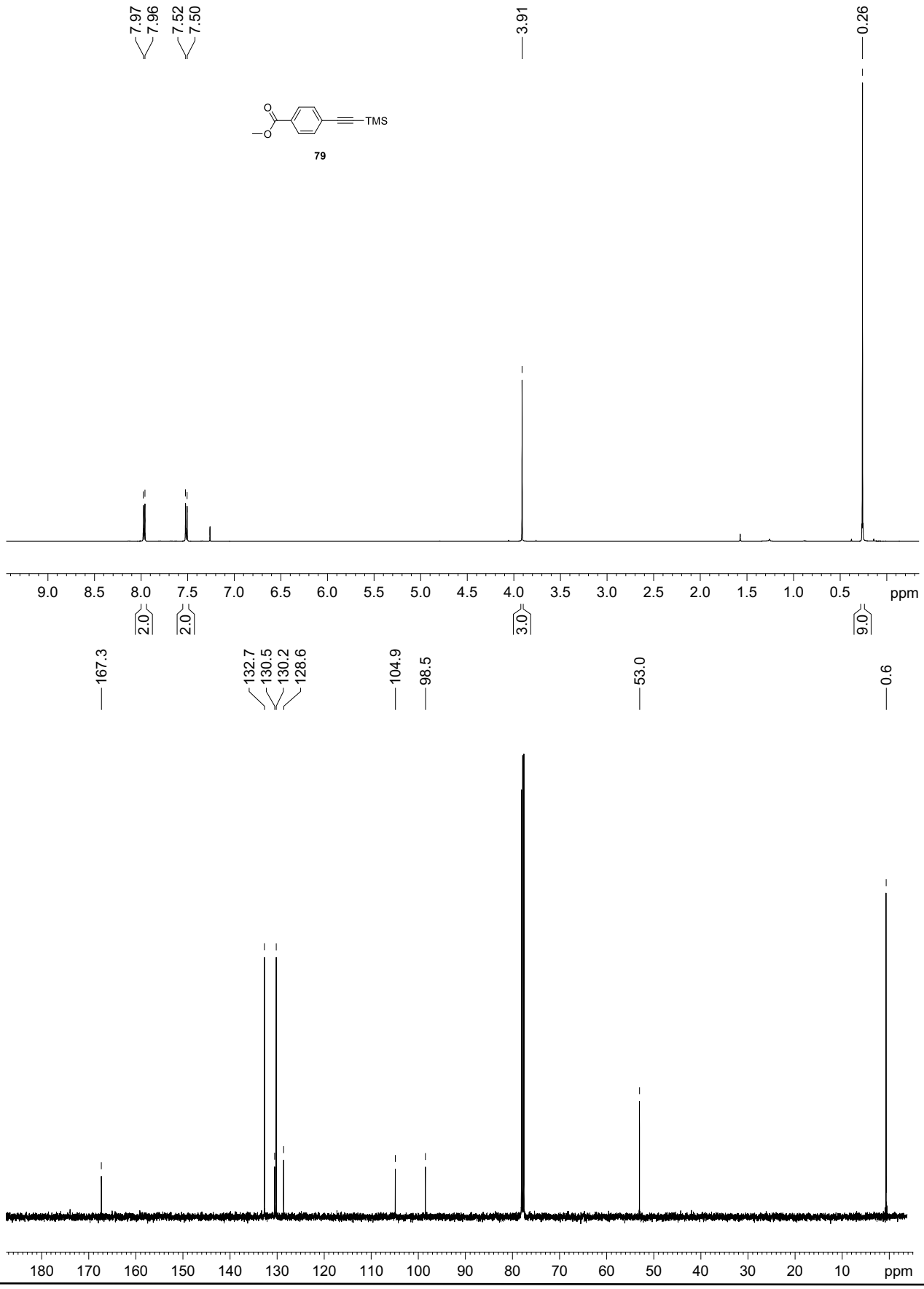
7.97
7.96
7.52
7.50
3.91
0.26
TMS
79
9.0 8.5 8.0 7.5 7.0 6.5 6.0 5.5 5.0 4.5 4.0 3.5 3.0 2.5 2.0 1.5 1.0 0.5 ppm
2.0
2.0
3.0
9.0
167.3
132.7
130.5
130.2
128.6
104.9
98.5
53.0
0.6
180 170 160 150 140 130 120 110 100 90 80 70 60 50 40 30 20 10 ppm

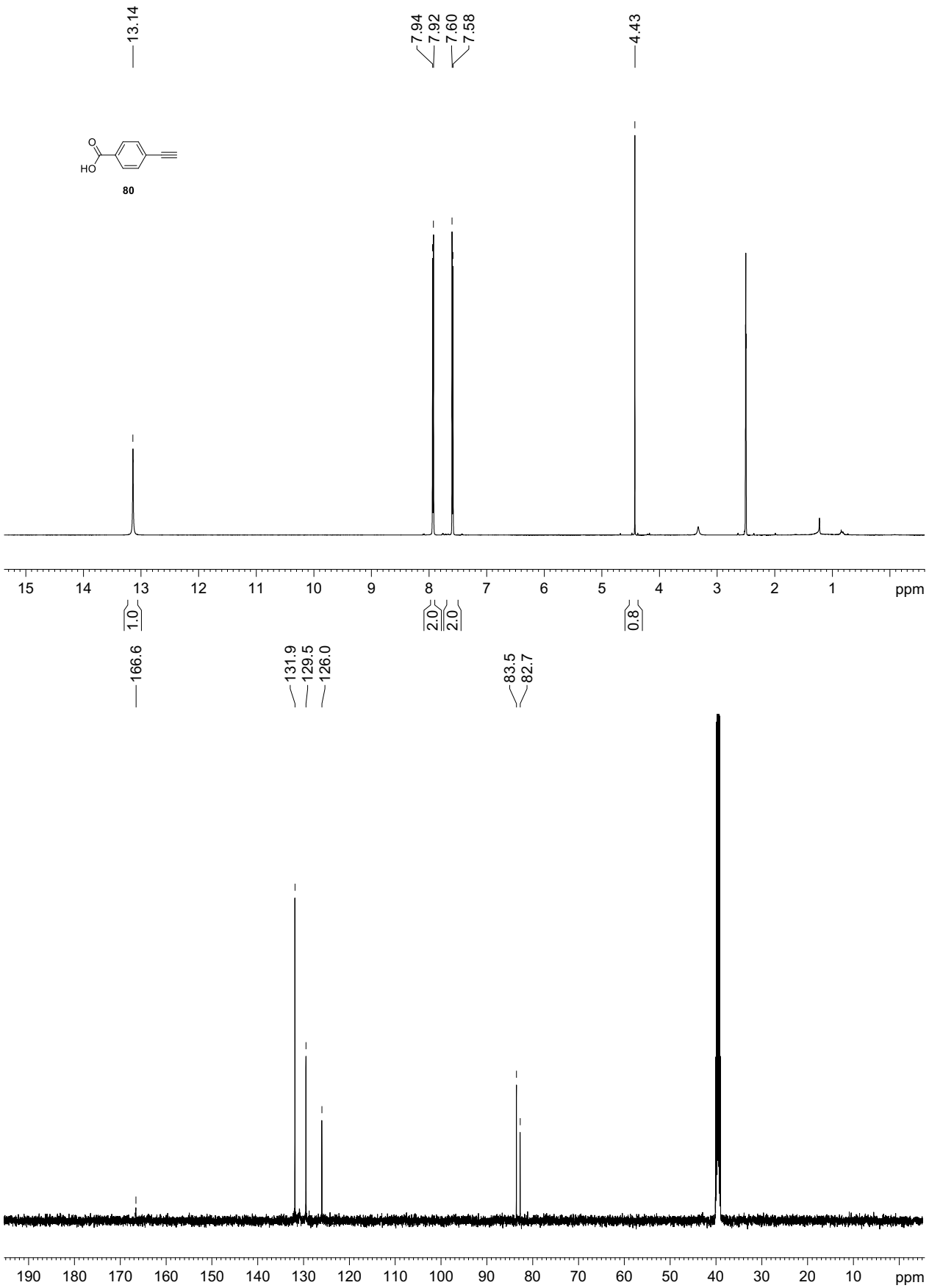
13.14
7.94
7.92
7.60
7.58
4.43
HO
O
80
15 14 13 12 11 10 9 8 7 6 5 4 3 2 1 ppm
1.0
2.0
2.0
0.8
166.6
131.9
129.5
126.0
83.5
82.7
190 180 170 160 150 140 130 120 110 100 90 80 70 60 50 40 30 20 10 ppm

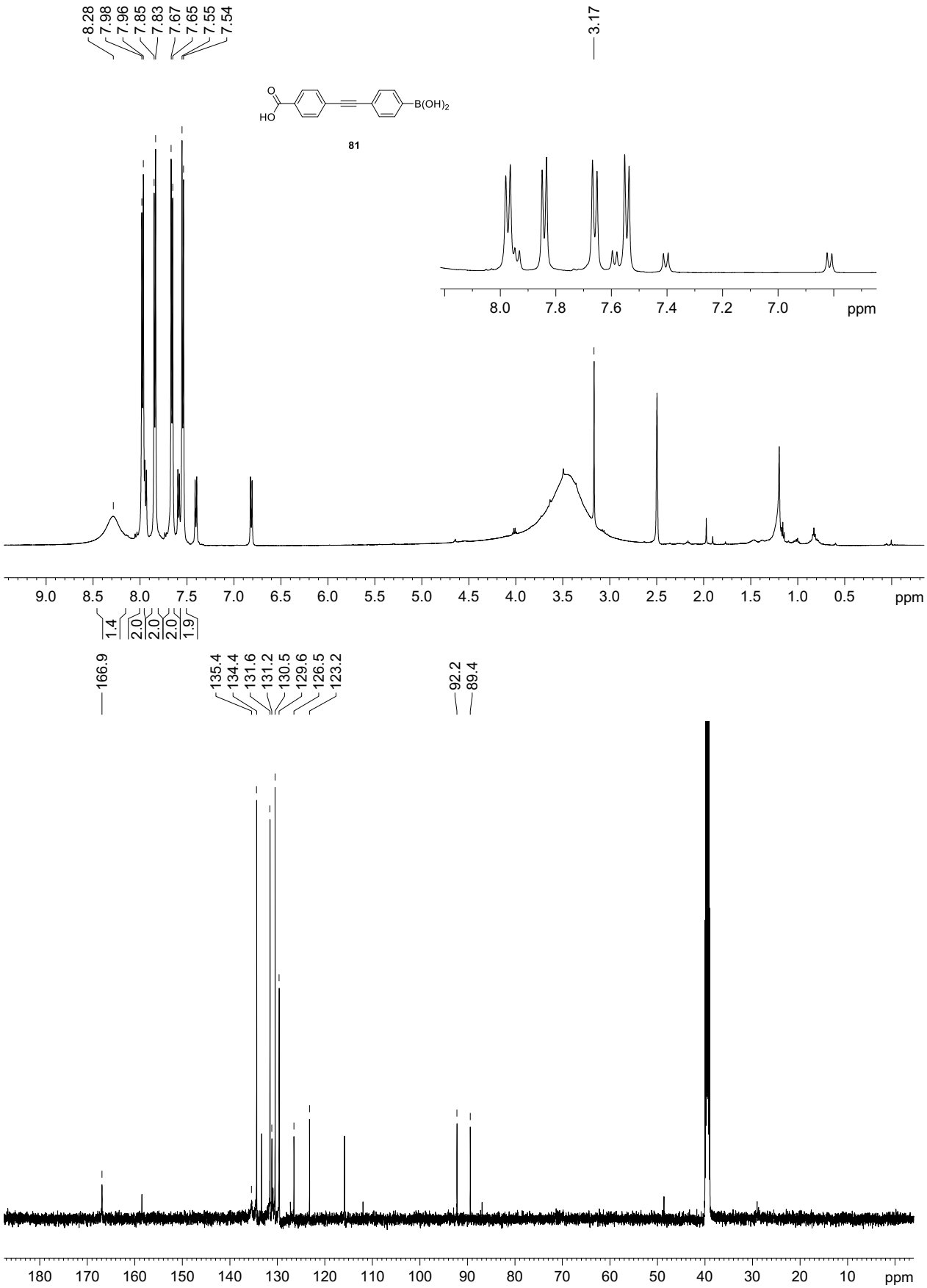
8.28
7.98
7.96
7.85
7.83
7.67
7.65
7.55
7.54
3.17
HO
O
B(OH)2
81
8.0
7.8
7.6
7.4
7.2
7.0
ppm
9.0
8.5
8.0
7.5
7.0
6.5
6.0
5.5
5.0
4.5
4.0
3.5
3.0
2.5
2.0
1.5
1.0
0.5
ppm
1.4
2.0
2.0
2.0
1.9
166.9
135.4
134.4
131.6
131.2
130.5
129.6
126.5
123.2
92.2
89.4
180
170
160
150
140
130
120
110
100
90
80
70
60
50
40
30
20
10
ppm

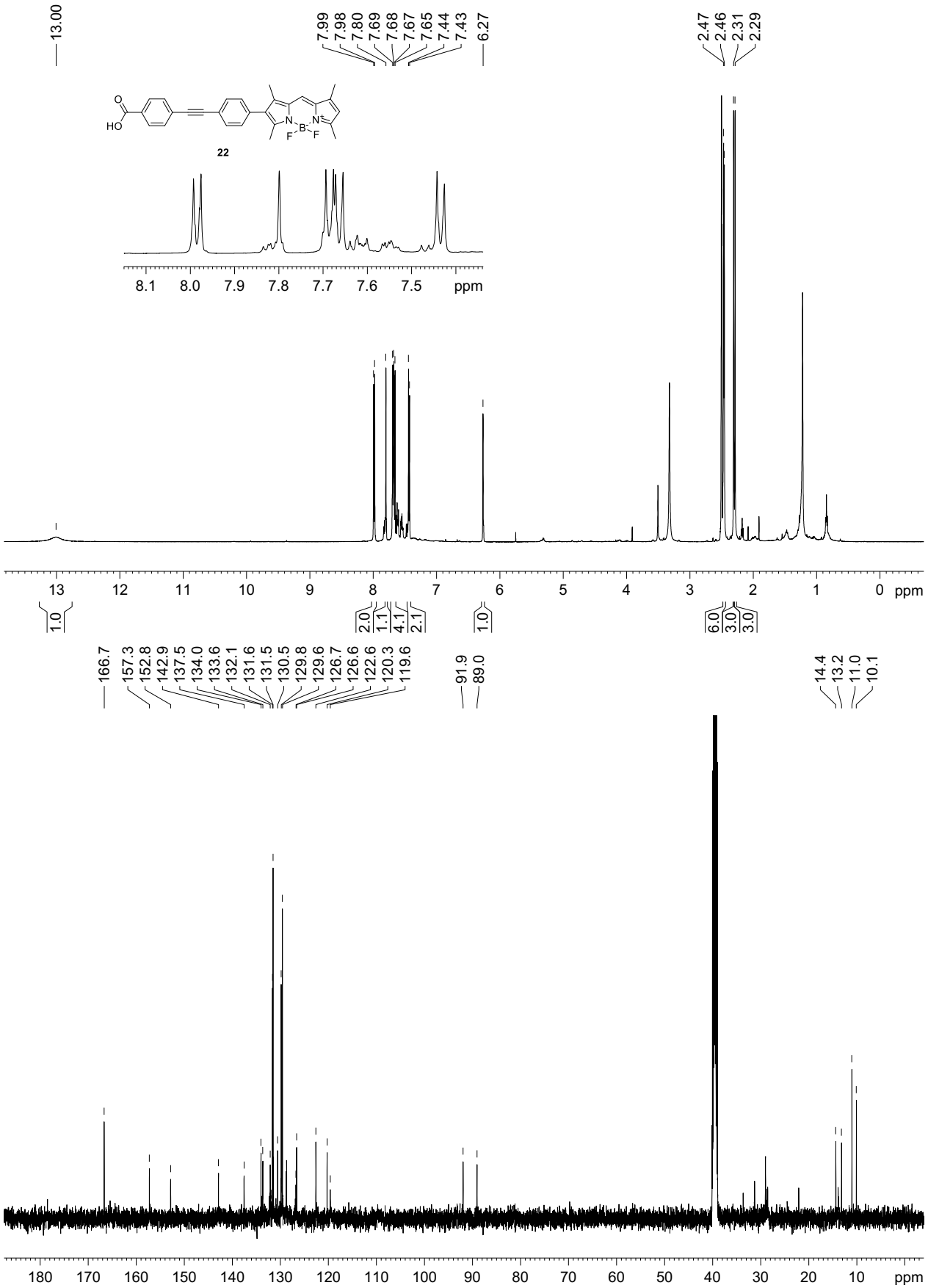
13.00
7.99
7.98
7.80
7.69
7.68
7.67
7.65
7.44
7.43
6.27
2.47
2.46
2.31
2.29
HO
O
N
B
F
F
N+
22
8.1
8.0
7.9
7.8
7.7
7.6
7.5
ppm
13
12
11
10
9
8
7
6
5
4
3
2
1
0
ppm
1.0
2.0
1.1
4.1
2.1
1.0
6.0
3.0
3.0
166.7
157.3
152.8
142.9
137.5
134.0
133.6
132.1
131.6
131.5
130.5
129.8
129.6
126.7
126.6
122.6
120.3
119.6
91.9
89.0
14.4
13.2
11.0
10.1
180
170
160
150
140
130
120
110
100
90
80
70
60
50
40
30
20
10
ppm

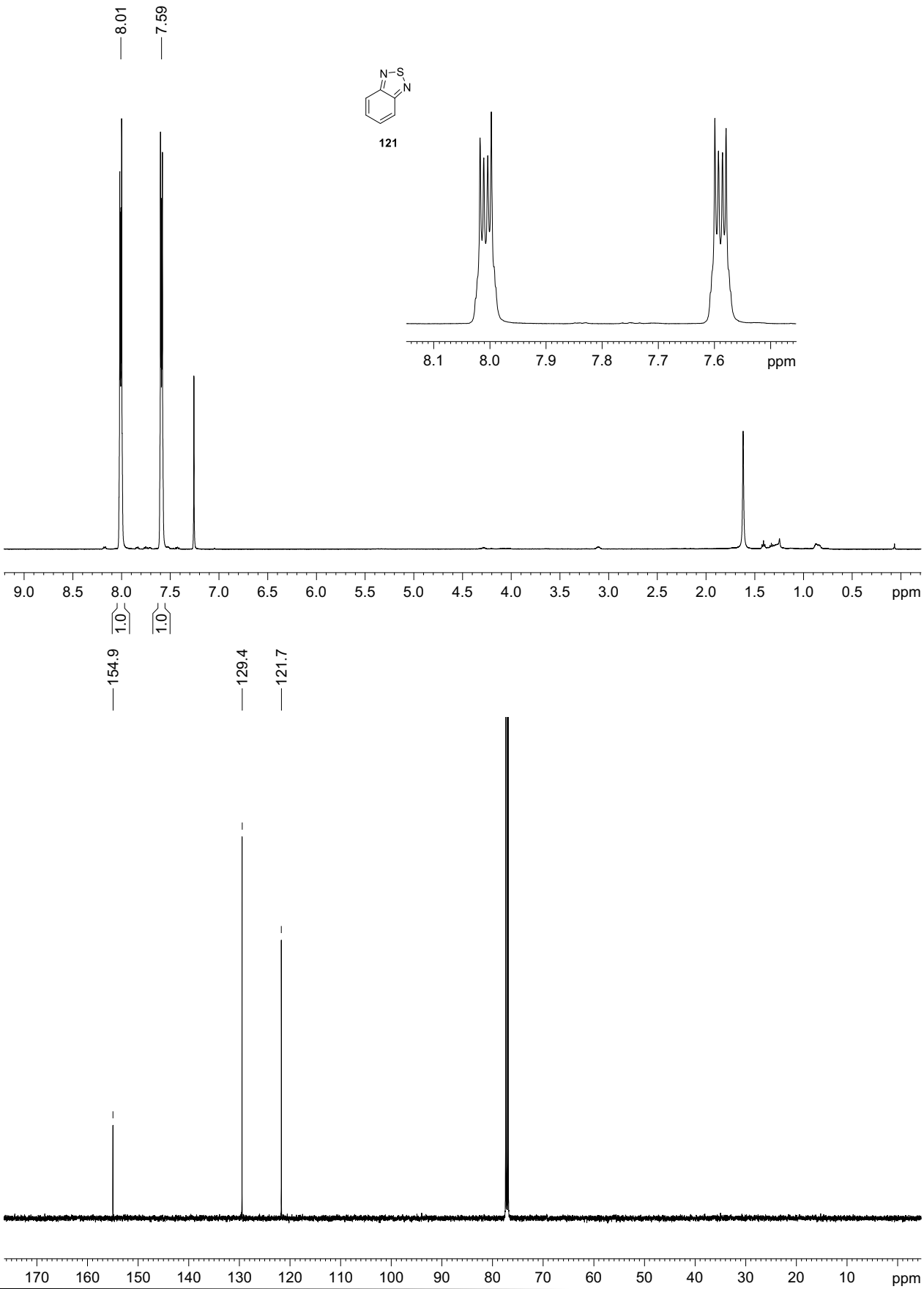
8.01
7.59
121
8.1
8.0
7.9
7.8
7.7
7.6
ppm
9.0
8.5
8.0
7.5
7.0
6.5
6.0
5.5
5.0
4.5
4.0
3.5
3.0
2.5
2.0
1.5
1.0
0.5
ppm
1.0
1.0
154.9
129.4
121.7
170
160
150
140
130
120
110
100
90
80
70
60
50
40
30
20
10
ppm

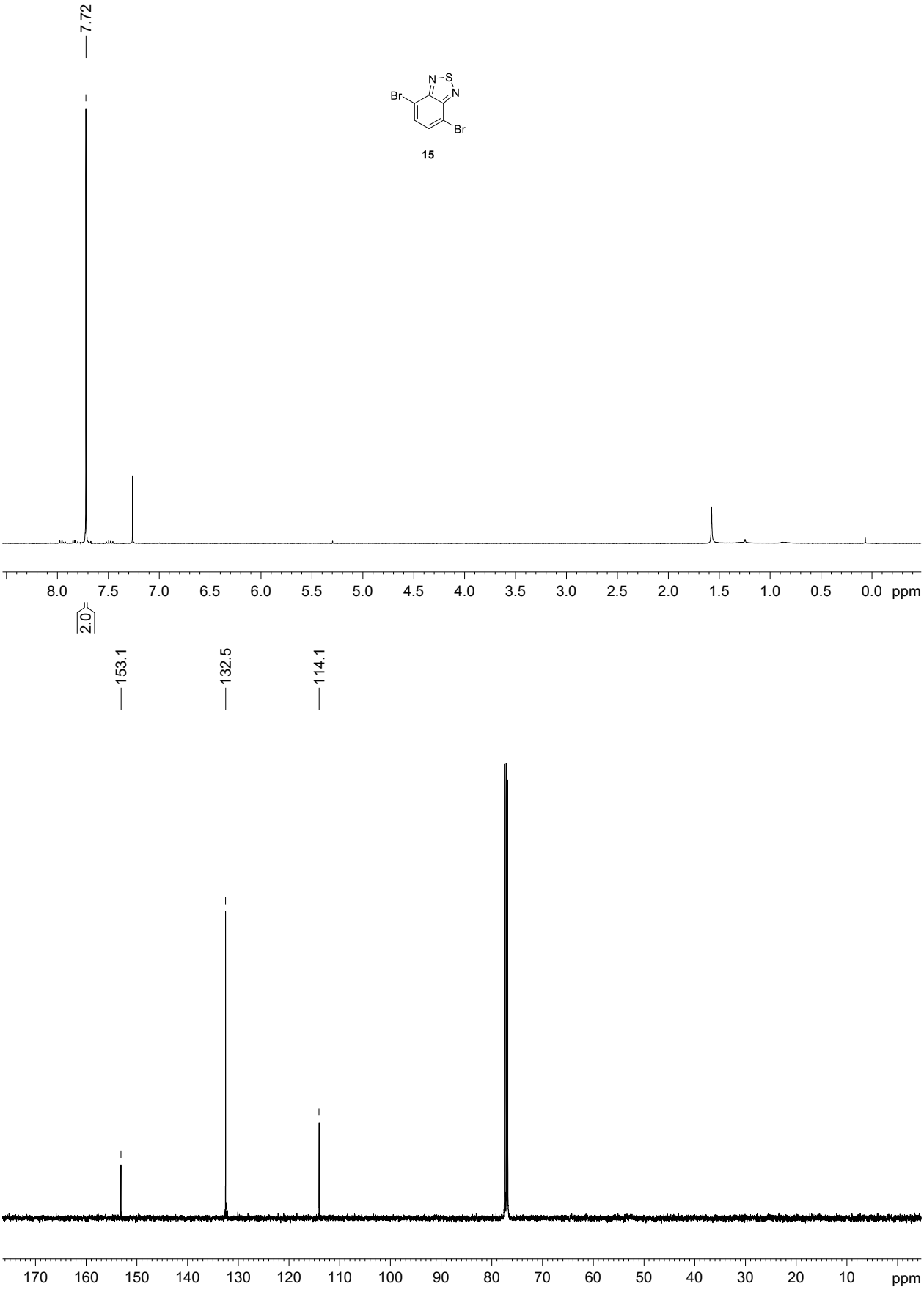
7.72
Br
N
S
N
Br
15
8.0
7.5
7.0
6.5
6.0
5.5
5.0
4.5
4.0
3.5
3.0
2.5
2.0
1.5
1.0
0.5
0.0
ppm
2.0
153.1
132.5
114.1
170
160
150
140
130
120
110
100
90
80
70
60
50
40
30
20
10
ppm

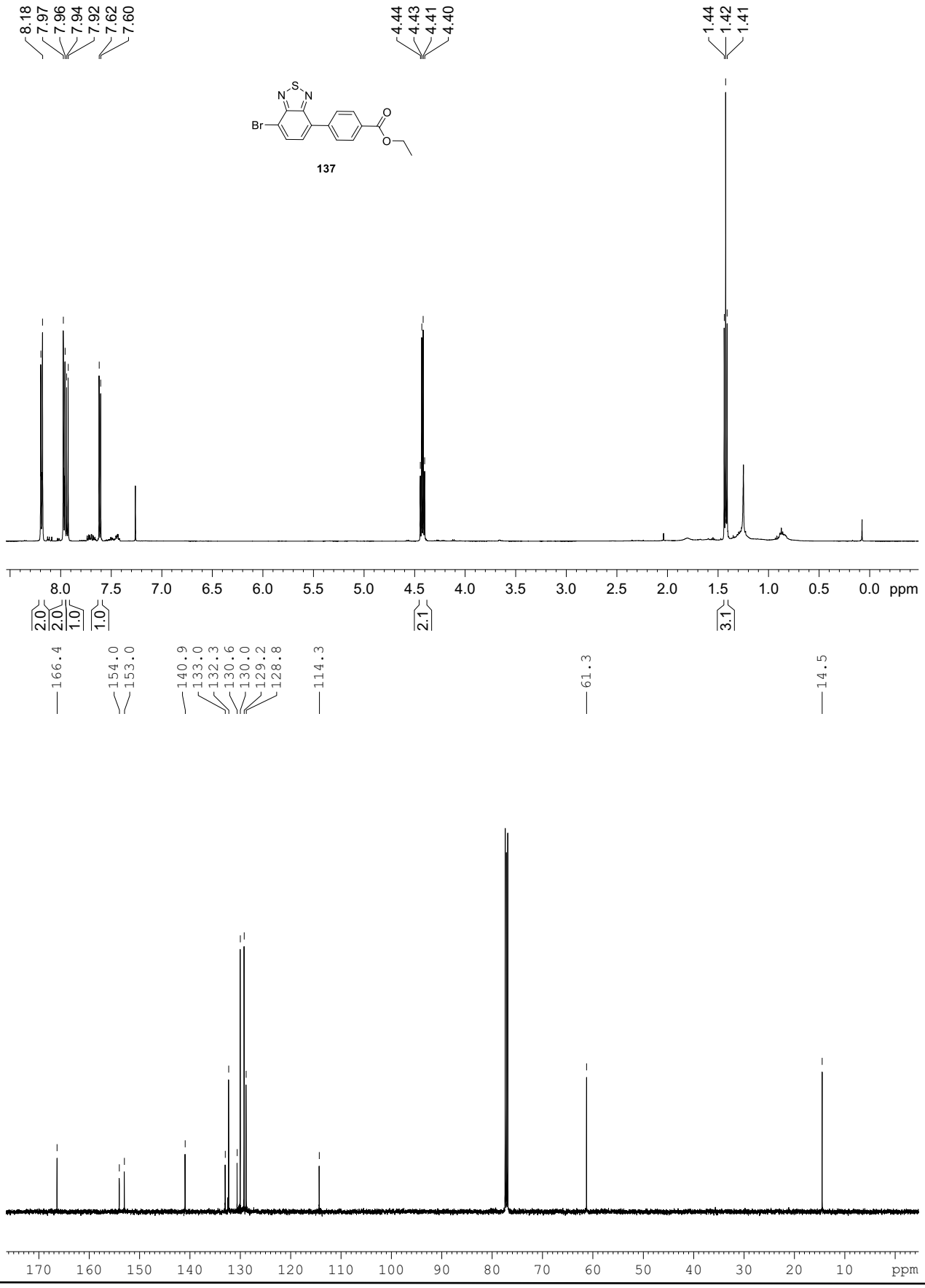
8.18
7.97
7.96
7.94
7.92
7.62
7.60
4.44
4.43
4.41
4.40
1.44
1.42
1.41
Br
O
O
137
8.0 7.5 7.0 6.5 6.0 5.5 5.0 4.5 4.0 3.5 3.0 2.5 2.0 1.5 1.0 0.5 0.0 ppm
2.0
2.0
1.0
1.0
2.1
3.1
166.4
154.0
153.0
140.9
133.0
132.3
130.6
130.0
129.2
128.8
114.3
61.3
14.5
170 160 150 140 130 120 110 100 90 80 70 60 50 40 30 20 10 ppm

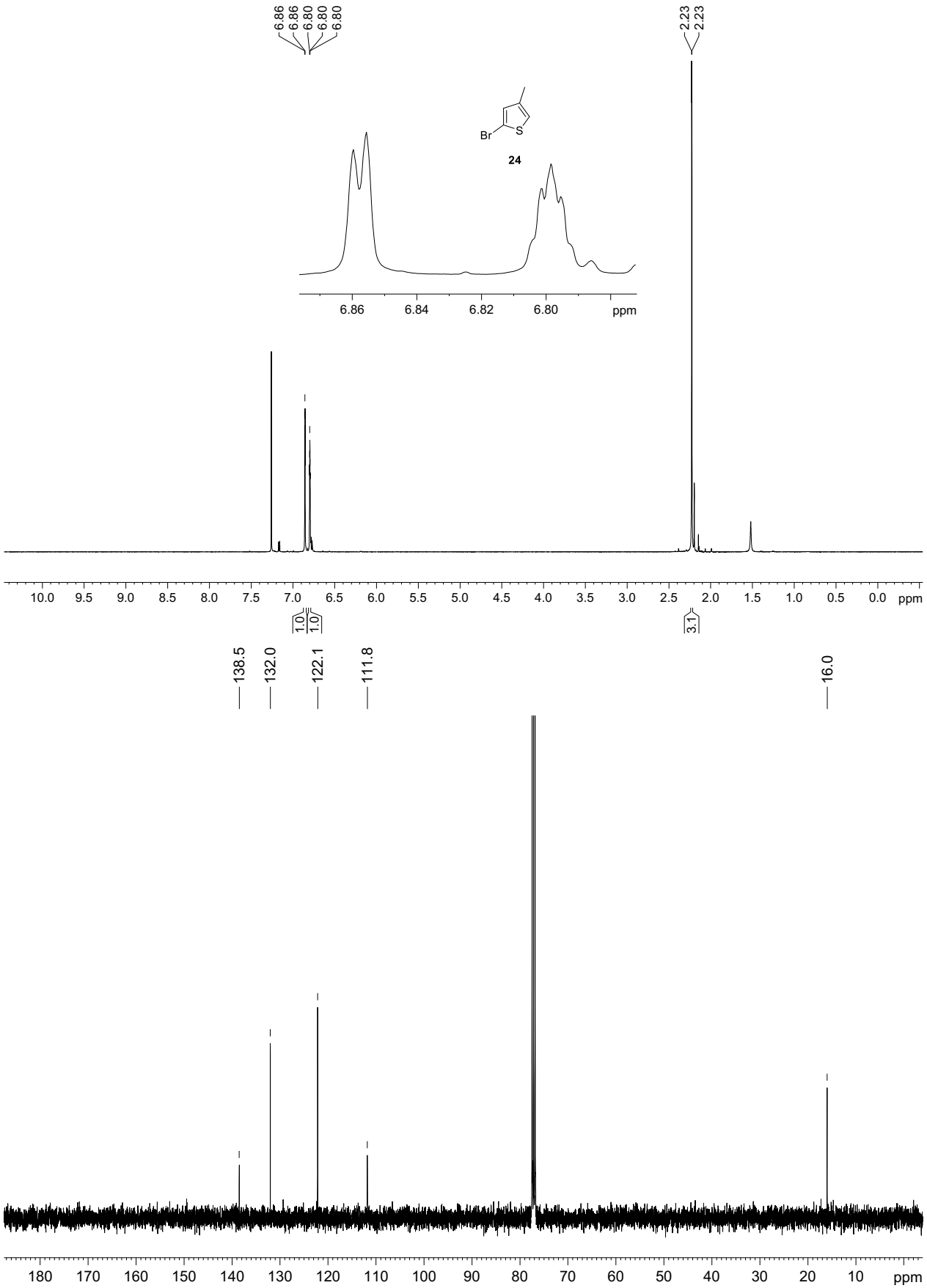
6.86
6.86
6.80
6.80
6.80
2.23
2.23
Br
S
24
6.86
6.84
6.82
6.80
ppm
10.0
9.5
9.0
8.5
8.0
7.5
7.0
6.5
6.0
5.5
5.0
4.5
4.0
3.5
3.0
2.5
2.0
1.5
1.0
0.5
0.0
ppm
1.0
1.0
3.1
138.5
132.0
122.1
111.8
16.0
180
170
160
150
140
130
120
110
100
90
80
70
60
50
40
30
20
10
ppm

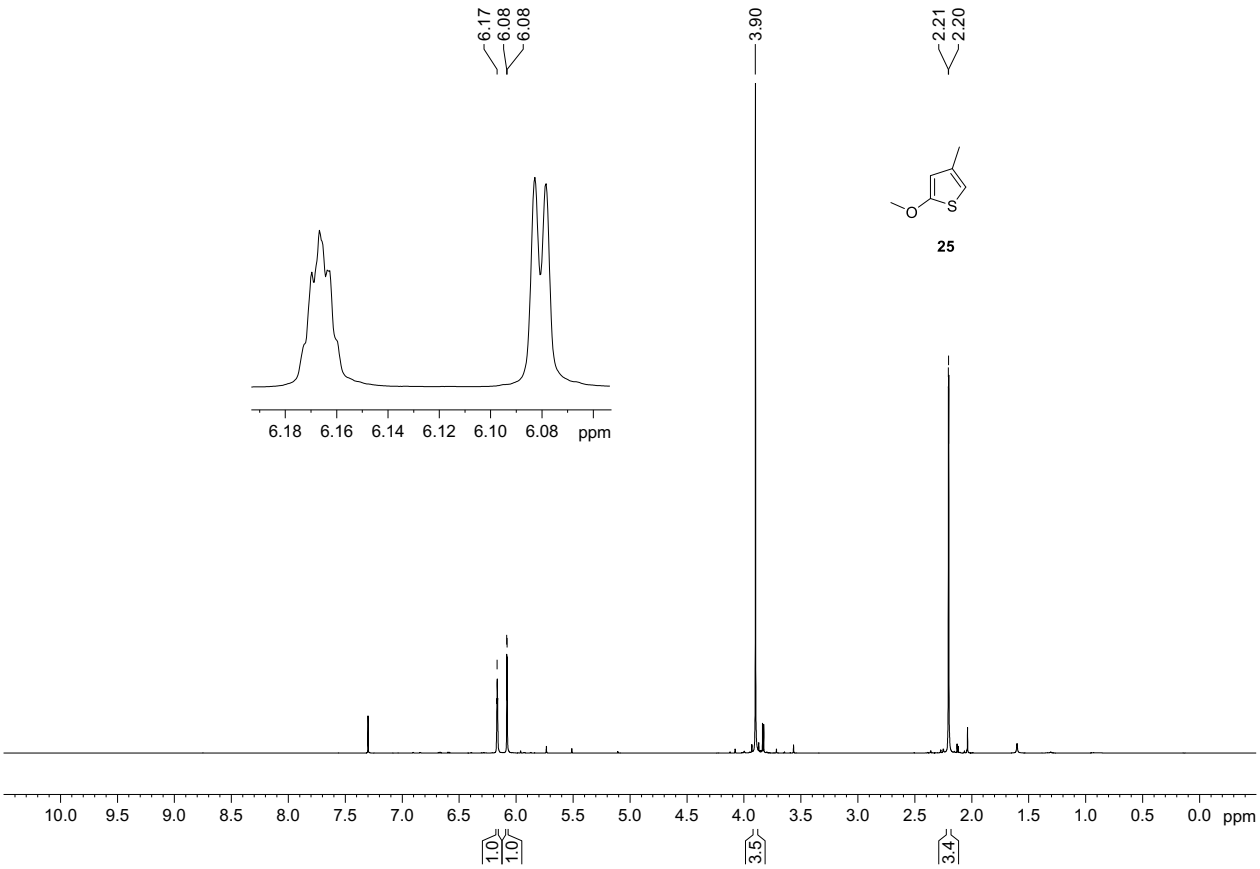
6.17
6.08
6.08
3.90
2.21
2.20
6.18 6.16 6.14 6.12 6.10 6.08 ppm
O
S
25
10.0 9.5 9.0 8.5 8.0 7.5 7.0 6.5 6.0 5.5 5.0 4.5 4.0 3.5 3.0 2.5 2.0 1.5 1.0 0.5 0.0 ppm
1.0
1.0
3.5
3.4

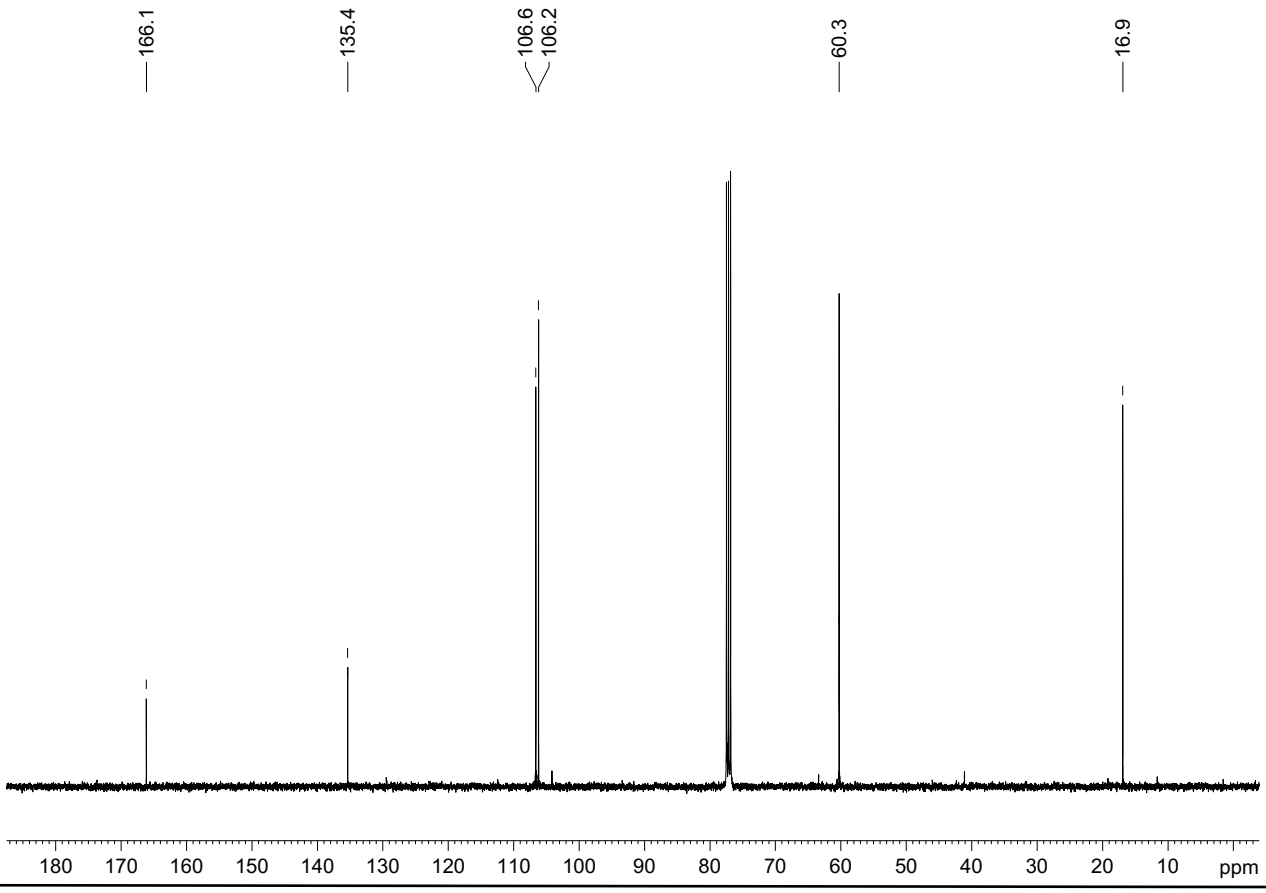
166.1
135.4
106.6
106.2
60.3
16.9
180 170 160 150 140 130 120 110 100 90 80 70 60 50 40 30 20 10 ppm

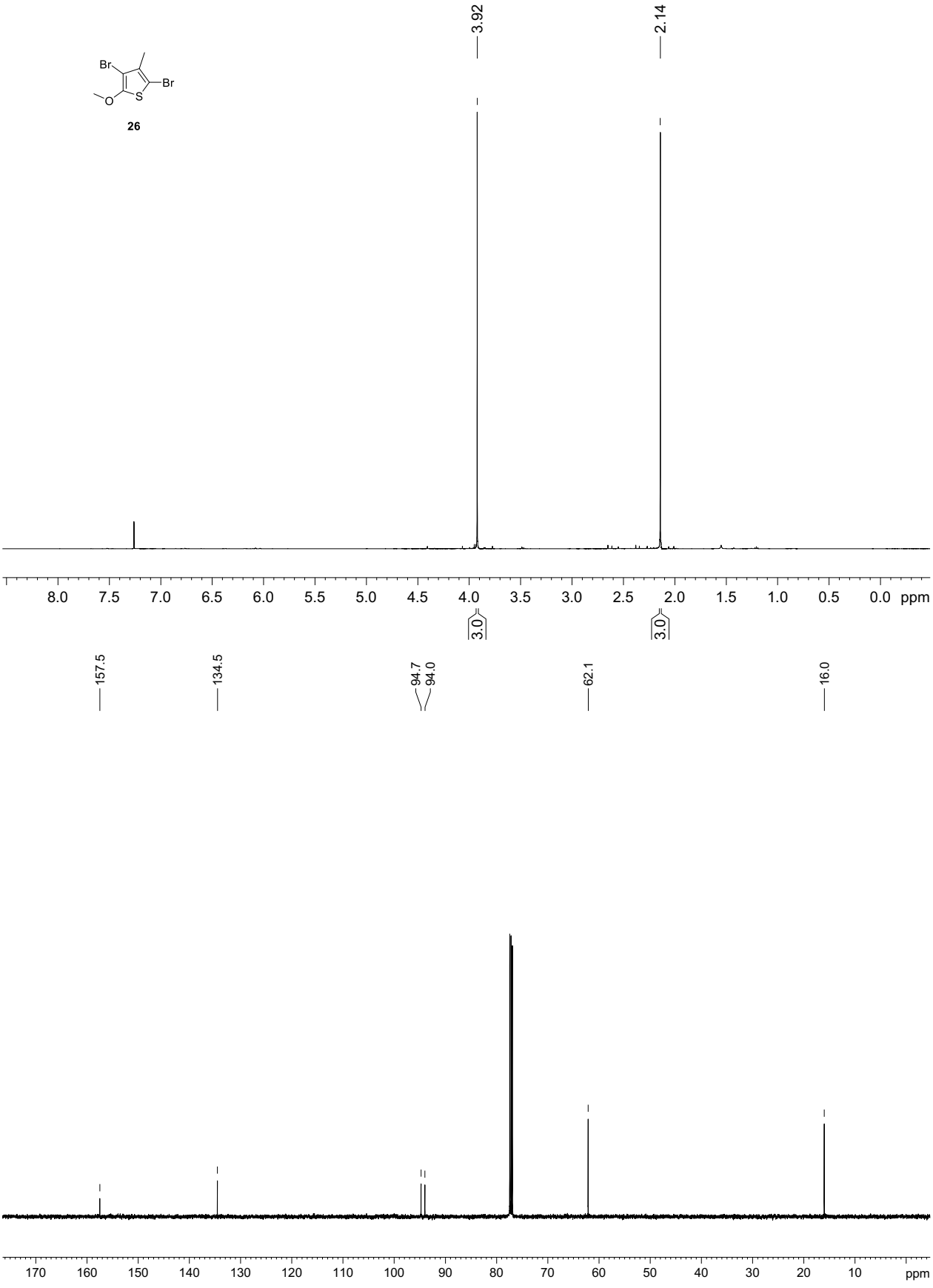
Br
Br
O
S
26
3.92
2.14
8.0 7.5 7.0 6.5 6.0 5.5 5.0 4.5 4.0 3.5 3.0 2.5 2.0 1.5 1.0 0.5 0.0 ppm
3.0
3.0
157.5
134.5
94.7
94.0
62.1
16.0
170 160 150 140 130 120 110 100 90 80 70 60 50 40 30 20 10 ppm

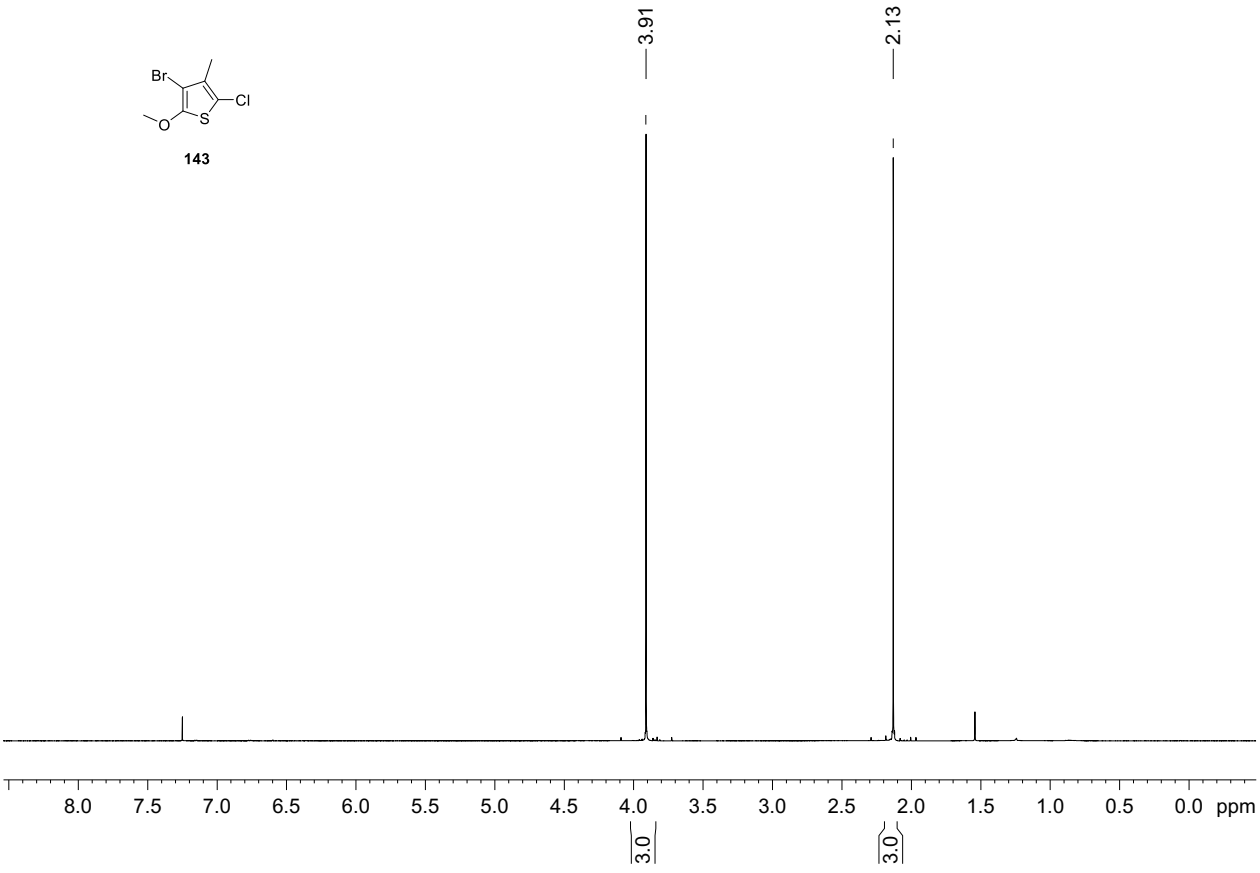
Br
Cl
O
S
143
3.91
2.13
8.0 7.5 7.0 6.5 6.0 5.5 5.0 4.5 4.0 3.5 3.0 2.5 2.0 1.5 1.0 0.5 0.0 ppm
3.0
3.0

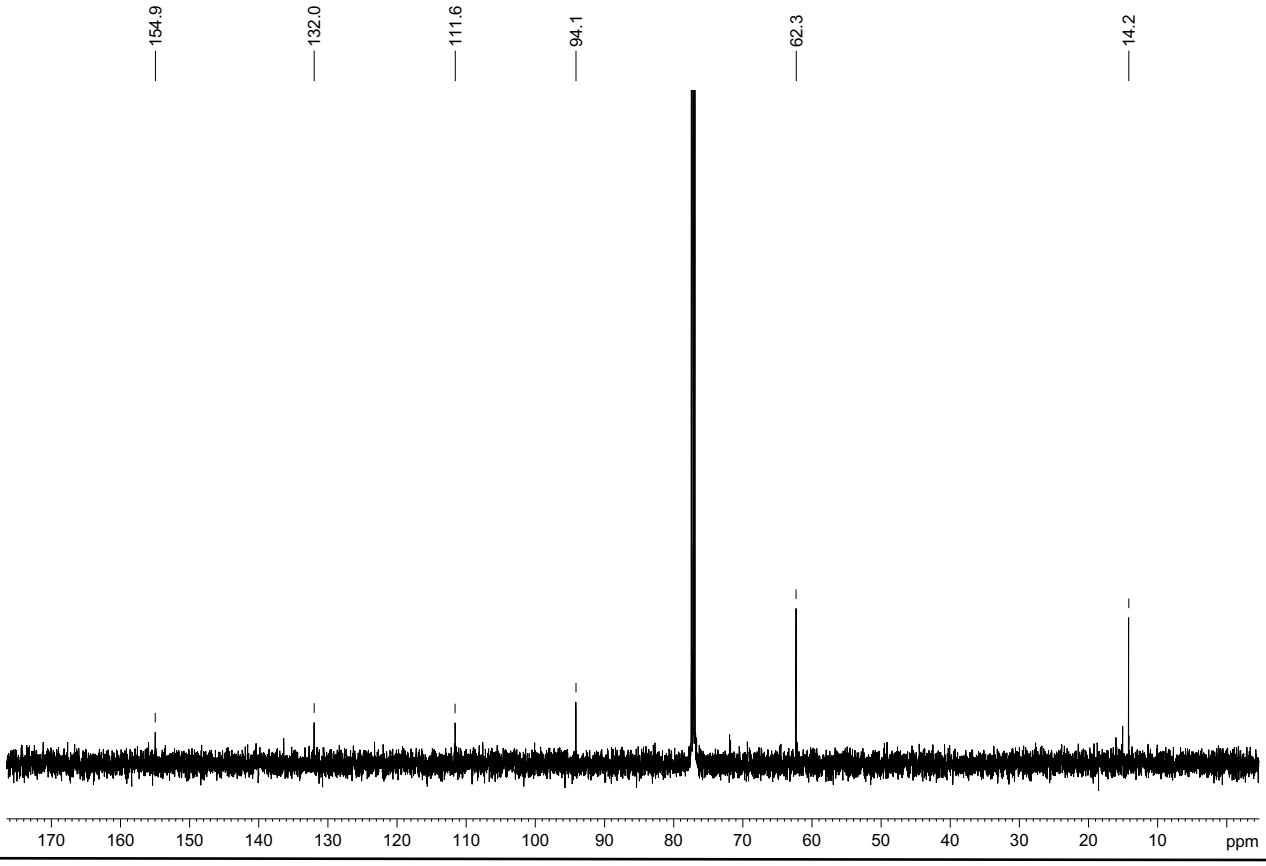
154.9
132.0
111.6
94.1
62.3
14.2
170 160 150 140 130 120 110 100 90 80 70 60 50 40 30 20 10 ppm

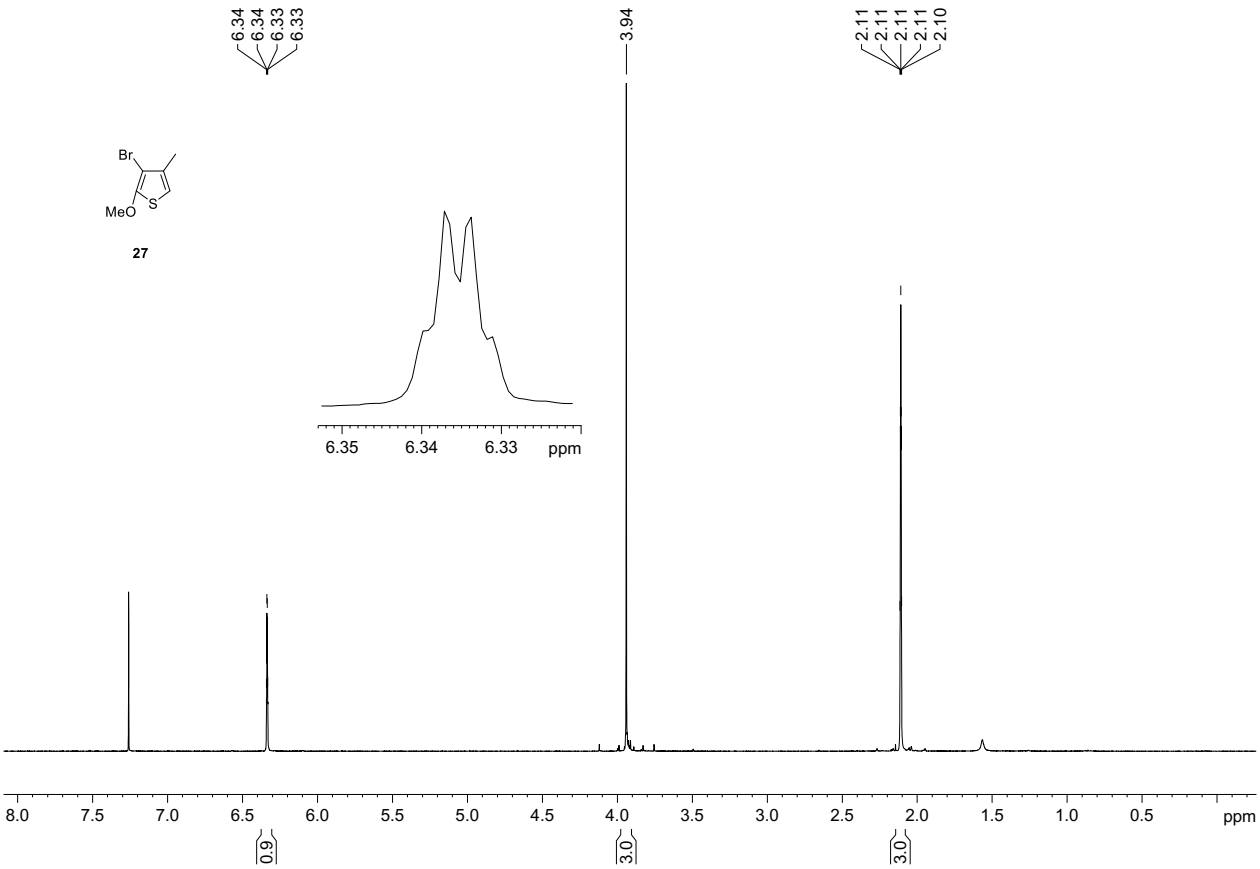
6.34
6.34
6.33
6.33
3.94
2.11
2.11
2.11
2.11
2.10
Br
MeO
S
27
6.35
6.34
6.33
ppm
8.0
7.5
7.0
6.5
6.0
5.5
5.0
4.5
4.0
3.5
3.0
2.5
2.0
1.5
1.0
0.5
ppm
0.9
3.0
3.0

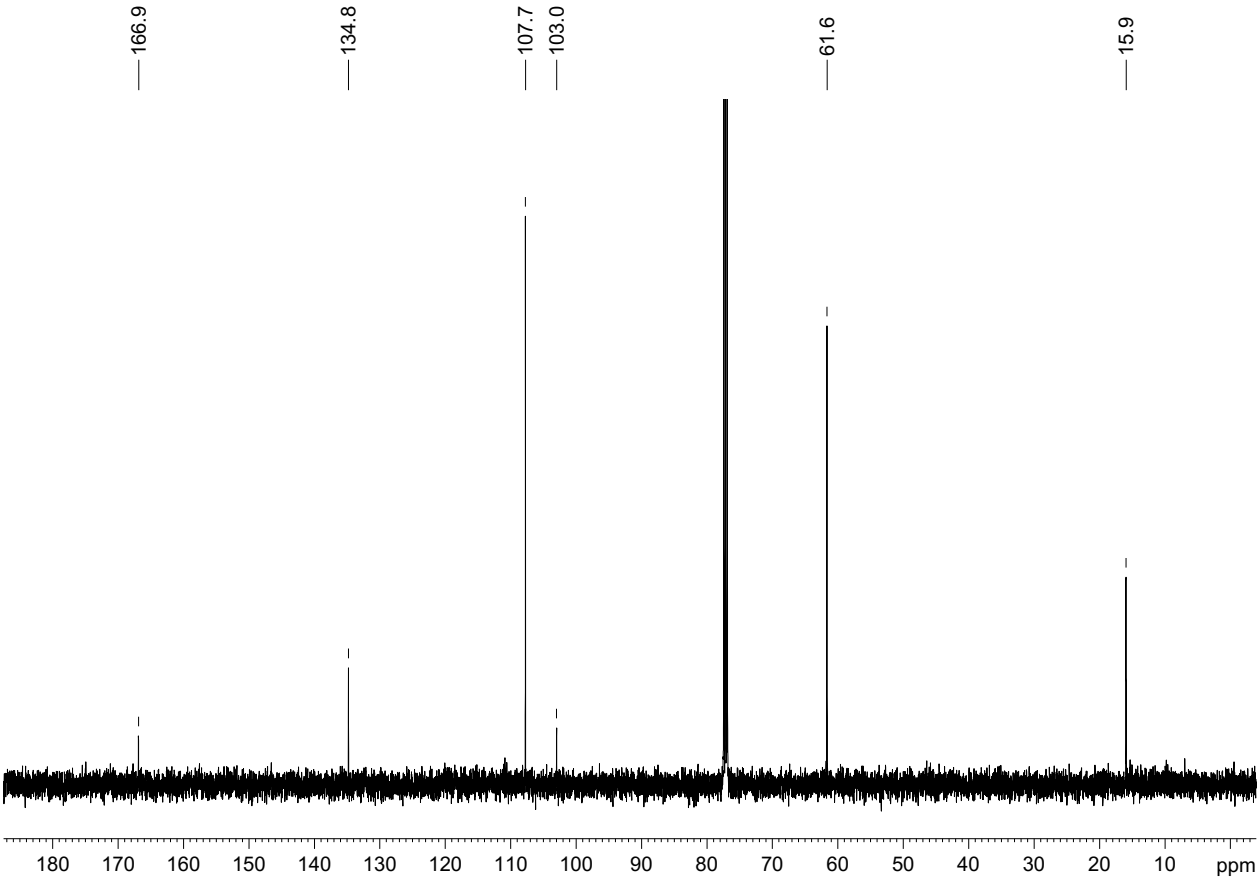
166.9
134.8
107.7
103.0
61.6
15.9
180
170
160
150
140
130
120
110
100
90
80
70
60
50
40
30
20
10
ppm

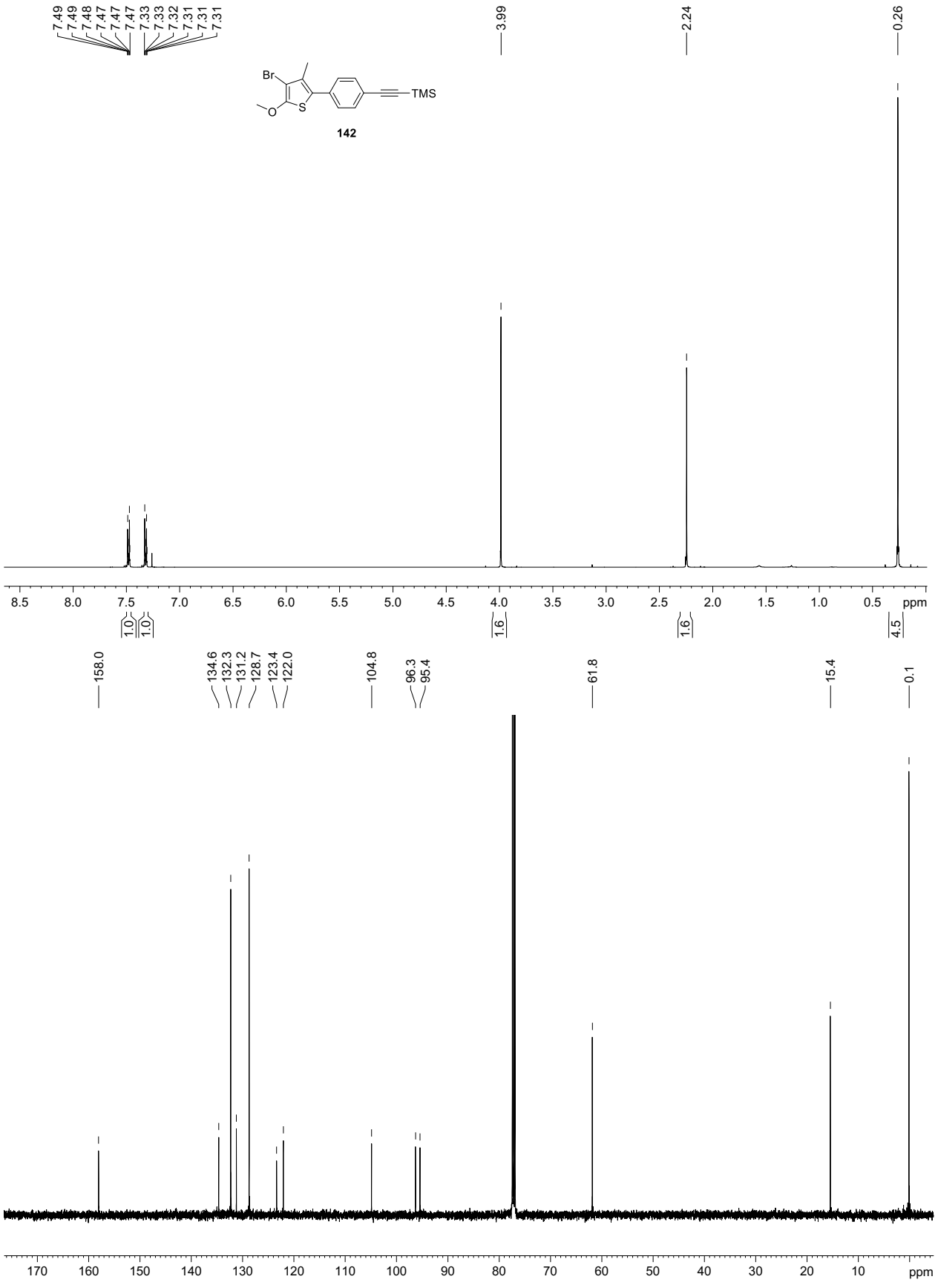
7.49
7.49
7.48
7.47
7.47
7.47
7.33
7.33
7.32
7.31
7.31
7.31
3.99
2.24
0.26
Br
TMS
O
S
142
8.5
8.0
7.5
7.0
6.5
6.0
5.5
5.0
4.5
4.0
3.5
3.0
2.5
2.0
1.5
1.0
0.5
ppm
1.0
1.0
1.6
1.6
4.5
158.0
134.6
132.3
131.2
128.7
123.4
122.0
104.8
96.3
95.4
61.8
15.4
0.1
170
160
150
140
130
120
110
100
90
80
70
60
50
40
30
20
10
ppm

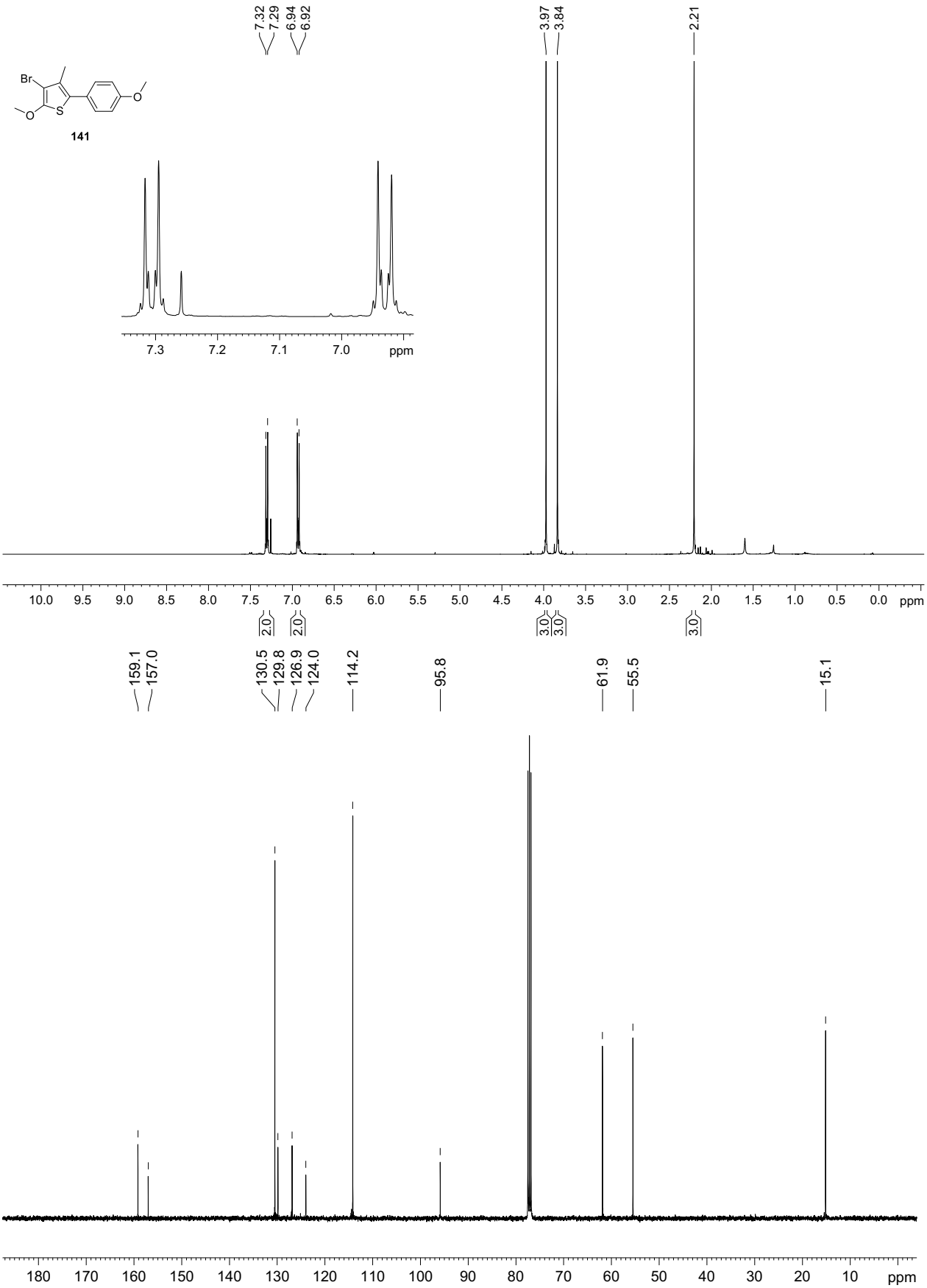
7.32
7.29
6.94
6.92
3.97
3.84
2.21
Br
O
S
O
141
7.3
7.2
7.1
7.0
ppm
10.0 9.5 9.0 8.5 8.0 7.5 7.0 6.5 6.0 5.5 5.0 4.5 4.0 3.5 3.0 2.5 2.0 1.5 1.0 0.5 0.0 ppm
2.0
2.0
3.0
3.0
3.0
159.1
157.0
130.5
129.8
126.9
124.0
114.2
95.8
61.9
55.5
15.1
180 170 160 150 140 130 120 110 100 90 80 70 60 50 40 30 20 10 ppm

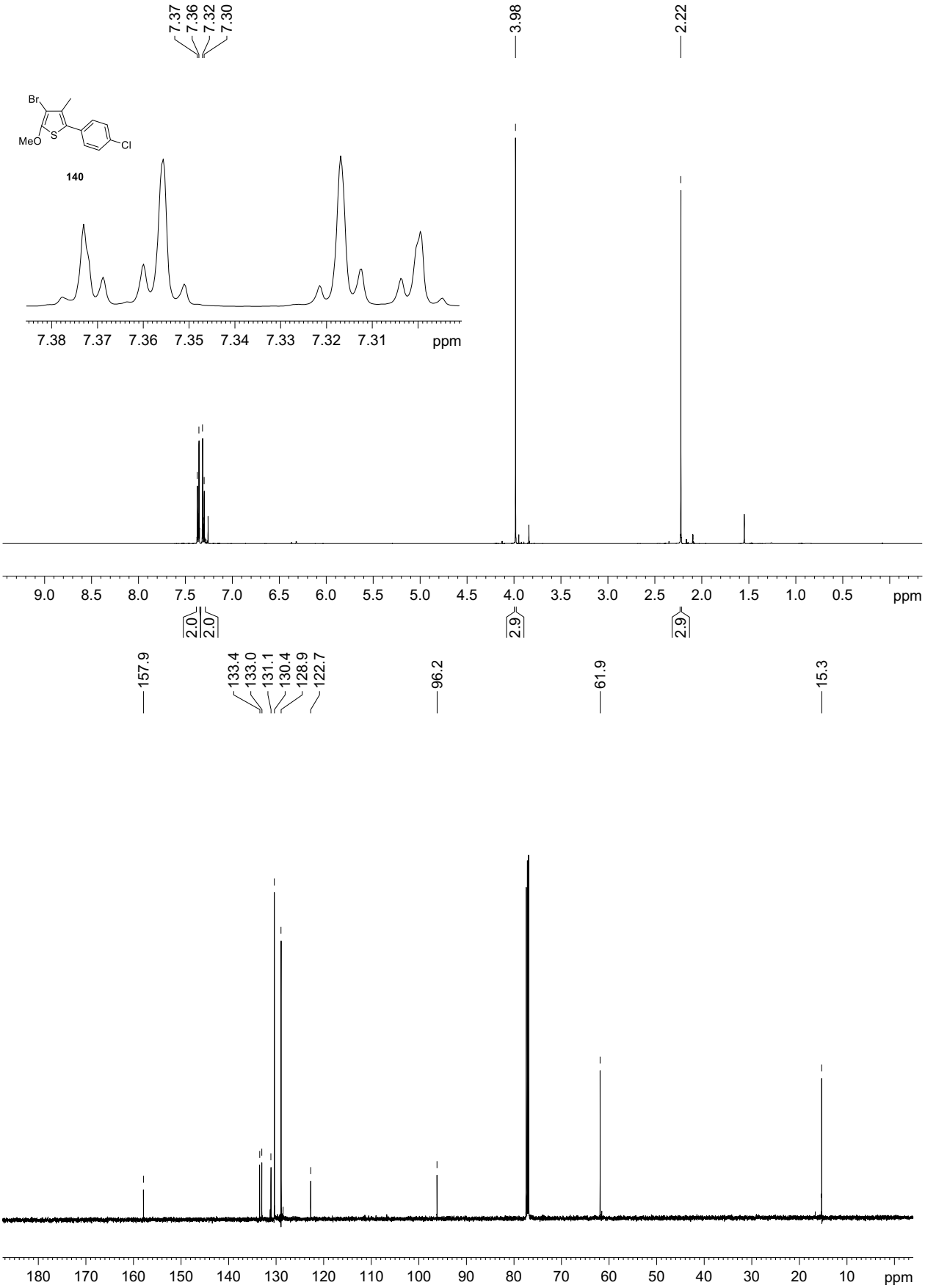
7.37
7.36
7.32
7.30
3.98
2.22
Br
MeO
S
Cl
140
7.38 7.37 7.36 7.35 7.34 7.33 7.32 7.31 ppm
9.0 8.5 8.0 7.5 7.0 6.5 6.0 5.5 5.0 4.5 4.0 3.5 3.0 2.5 2.0 1.5 1.0 0.5 ppm
2.0
2.0
2.9
2.9
157.9
133.4
133.0
131.1
130.4
128.9
122.7
96.2
61.9
15.3
180 170 160 150 140 130 120 110 100 90 80 70 60 50 40 30 20 10 ppm

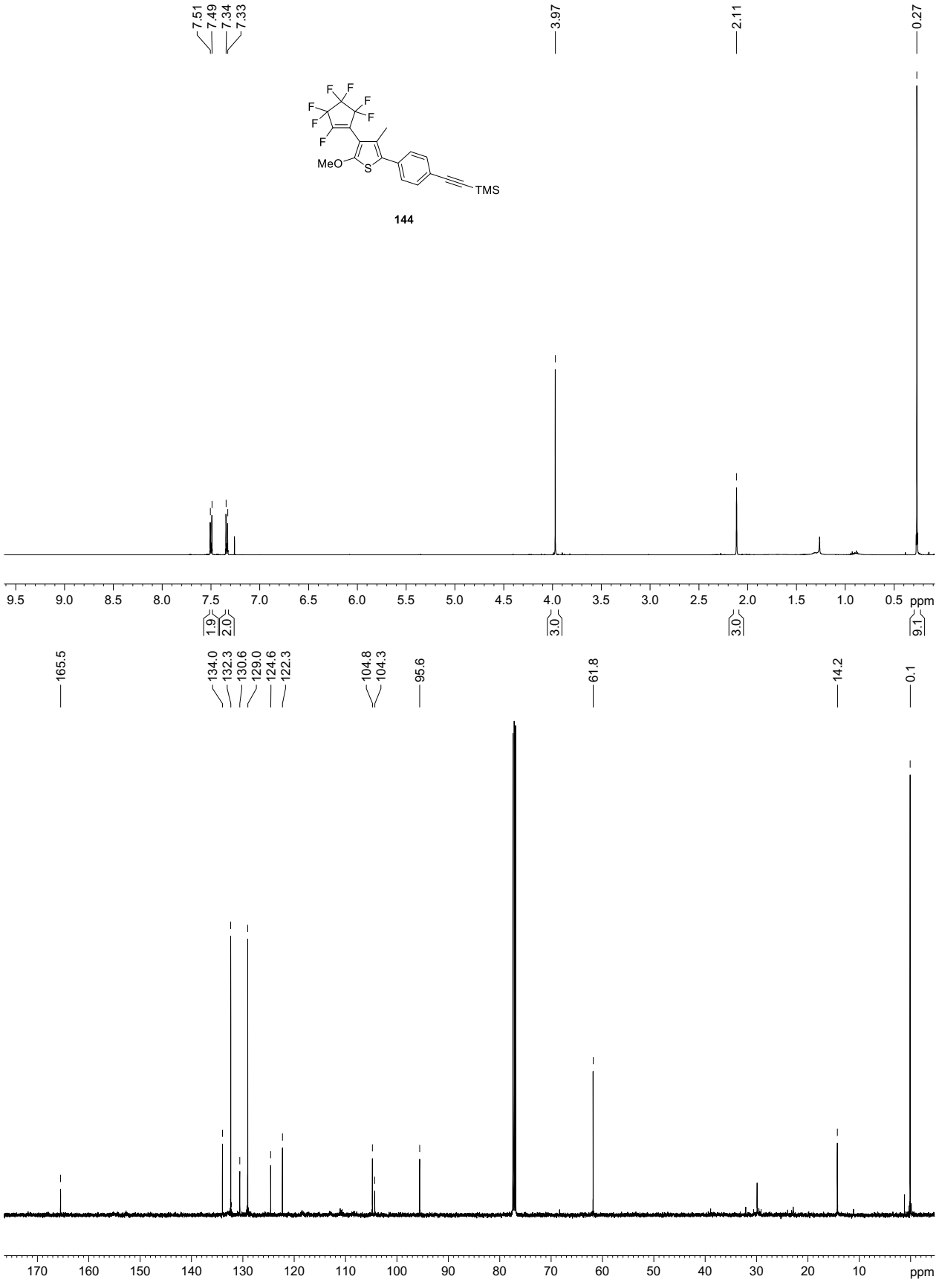
7.51
7.49
7.34
7.33
3.97
2.11
0.27
F
F
F
F
F
F
MeO
S
TMS
144
9.5
9.0
8.5
8.0
7.5
7.0
6.5
6.0
5.5
5.0
4.5
4.0
3.5
3.0
2.5
2.0
1.5
1.0
0.5
ppm
1.9
2.0
3.0
3.0
9.1
165.5
134.0
132.3
130.6
129.0
124.6
122.3
104.8
104.3
95.6
61.8
14.2
0.1
170
160
150
140
130
120
110
100
90
80
70
60
50
40
30
20
10
ppm

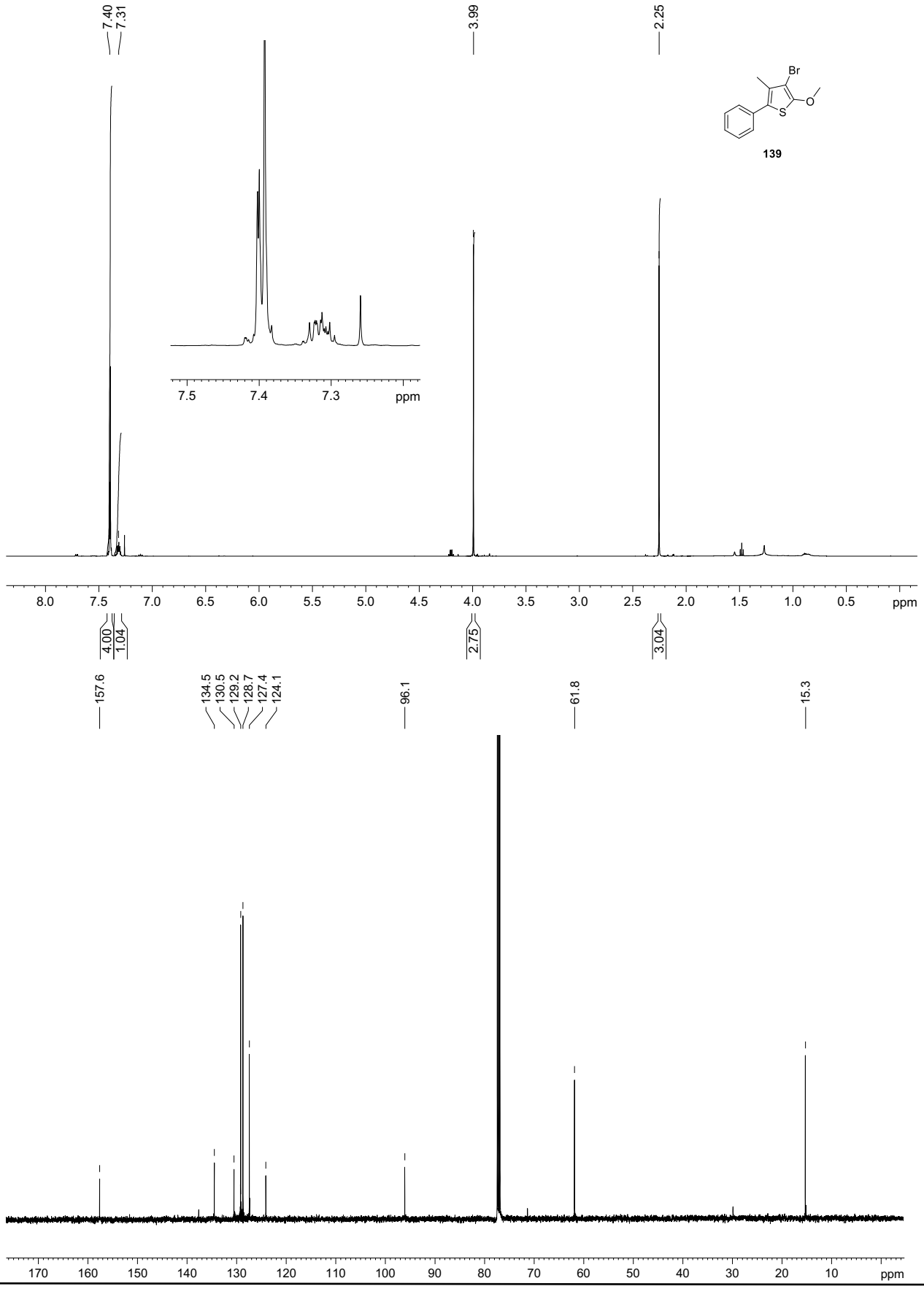
7.40
7.31
3.99
2.25
Br
O
S
139
7.5
7.4
7.3
ppm
8.0
7.5
7.0
6.5
6.0
5.5
5.0
4.5
4.0
3.5
3.0
2.5
2.0
1.5
1.0
0.5
ppm
4.00
1.04
2.75
3.04
157.6
134.5
130.5
129.2
128.7
127.4
124.1
96.1
61.8
15.3
170
160
150
140
130
120
110
100
90
80
70
60
50
40
30
20
10
ppm

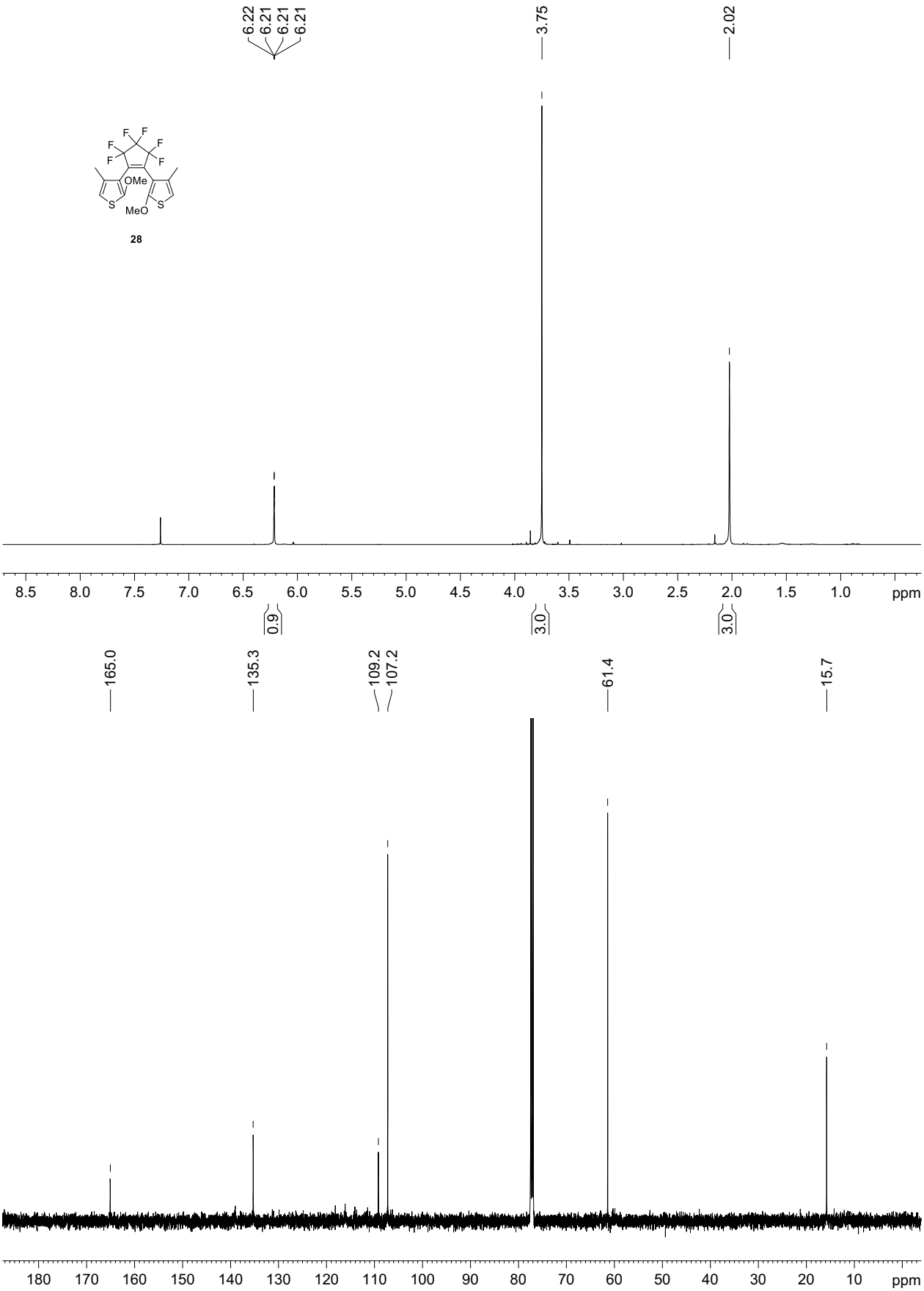
6.22
6.21
6.21
6.21
3.75
2.02
F
F
F
F
F
F
OMe
MeO
S
S
28
8.5
8.0
7.5
7.0
6.5
6.0
5.5
5.0
4.5
4.0
3.5
3.0
2.5
2.0
1.5
1.0
ppm
0.9
3.0
3.0
165.0
135.3
109.2
107.2
61.4
15.7
180
170
160
150
140
130
120
110
100
90
80
70
60
50
40
30
20
10
ppm

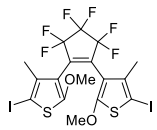
F
F
F
F
F
F
OMe
MeO
S
S
I
I

29

3.77
1.96
8.0
7.5
7.0
6.5
6.0
5.5
5.0
4.5
4.0
3.5
3.0
2.5
2.0
1.5
1.0
0.5
ppm
3.0
3.0

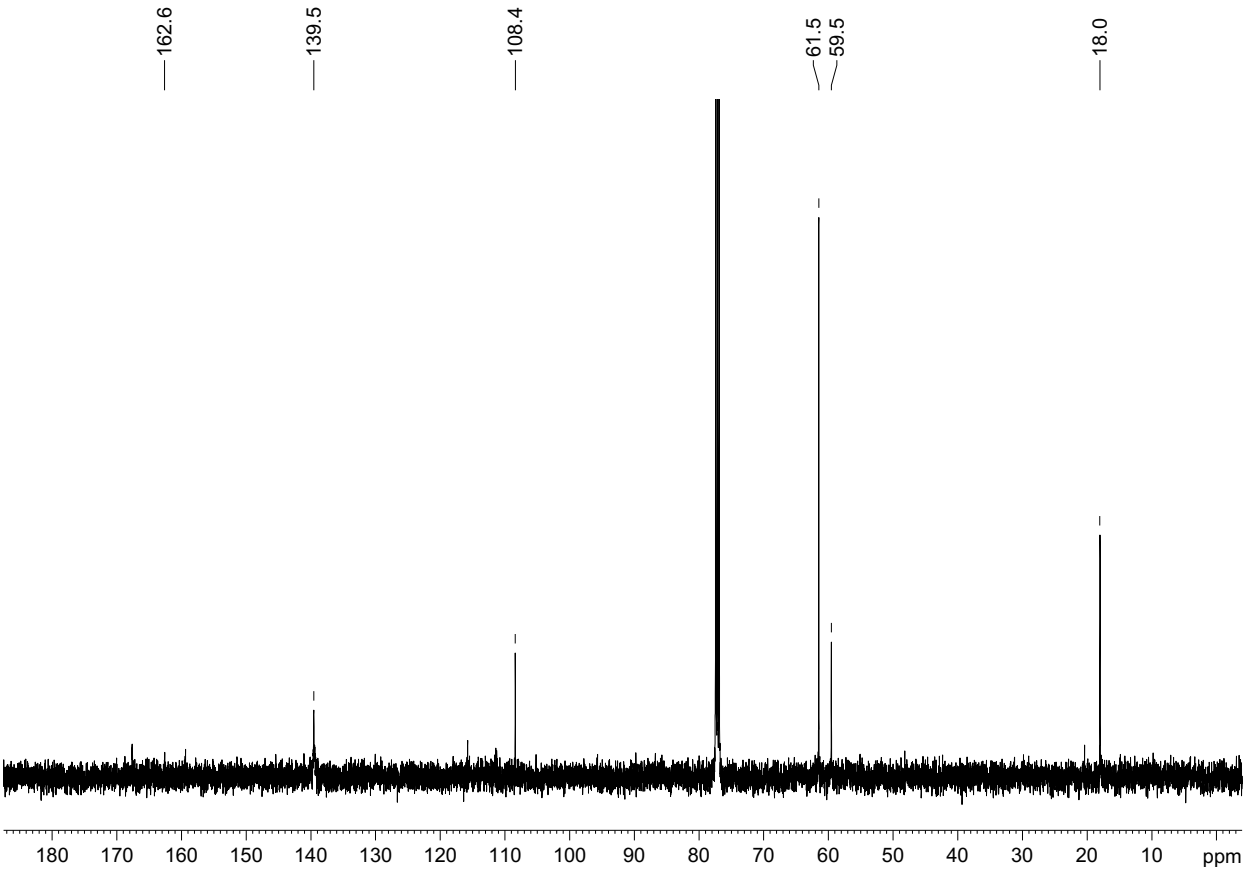
162.6
139.5
108.4
61.5
59.5
18.0
180
170
160
150
140
130
120
110
100
90
80
70
60
50
40
30
20
10
ppm

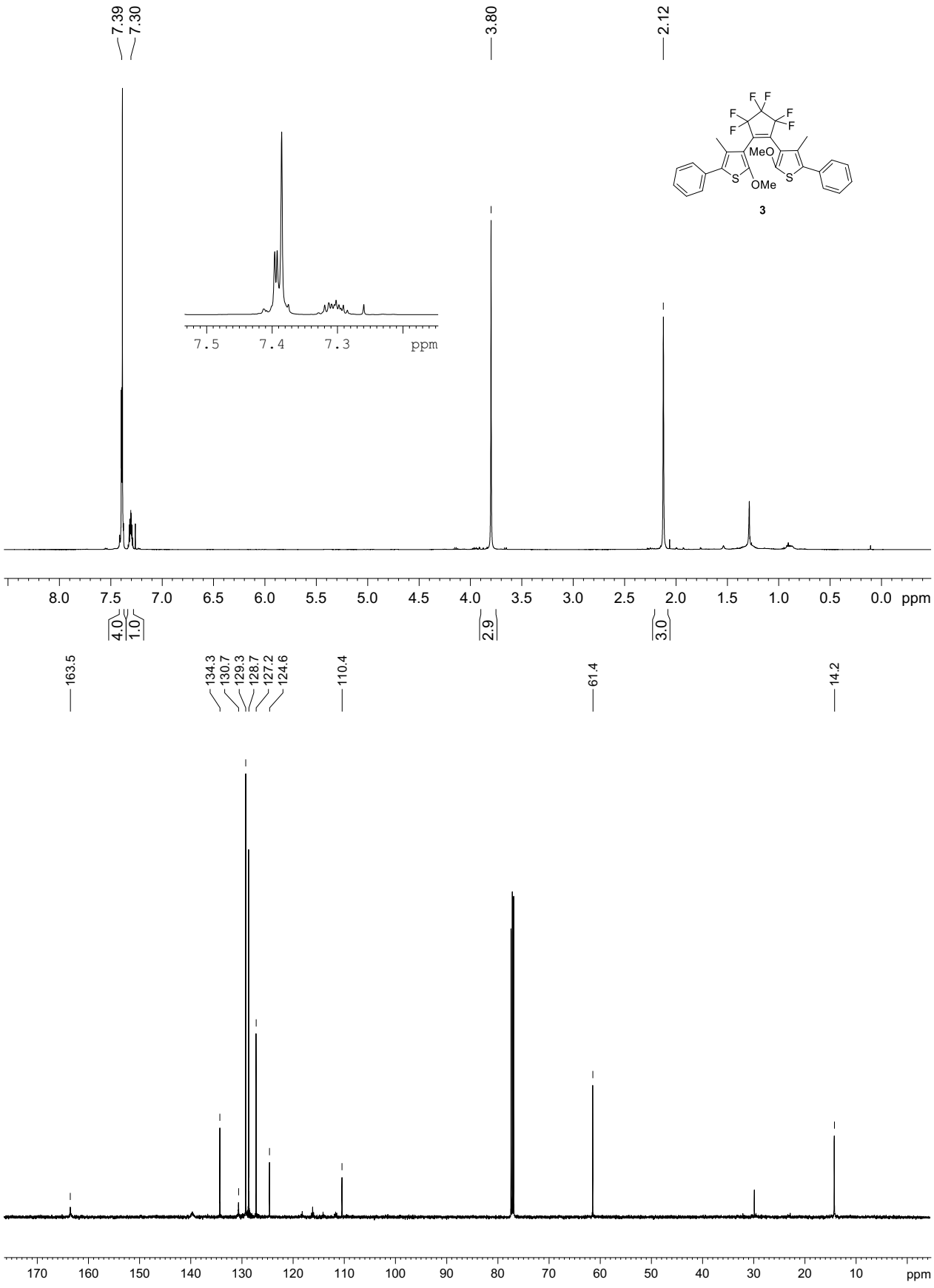
7.39
7.30
3.80
2.12
F F
F
F
F
F
MeO
S
OMe
S
3
7.5
7.4
7.3
ppm
8.0 7.5 7.0 6.5 6.0 5.5 5.0 4.5 4.0 3.5 3.0 2.5 2.0 1.5 1.0 0.5 0.0 ppm
4.0
1.0
2.9
3.0
163.5
134.3
130.7
129.3
128.7
127.2
124.6
110.4
61.4
14.2
170 160 150 140 130 120 110 100 90 80 70 60 50 40 30 20 10 ppm

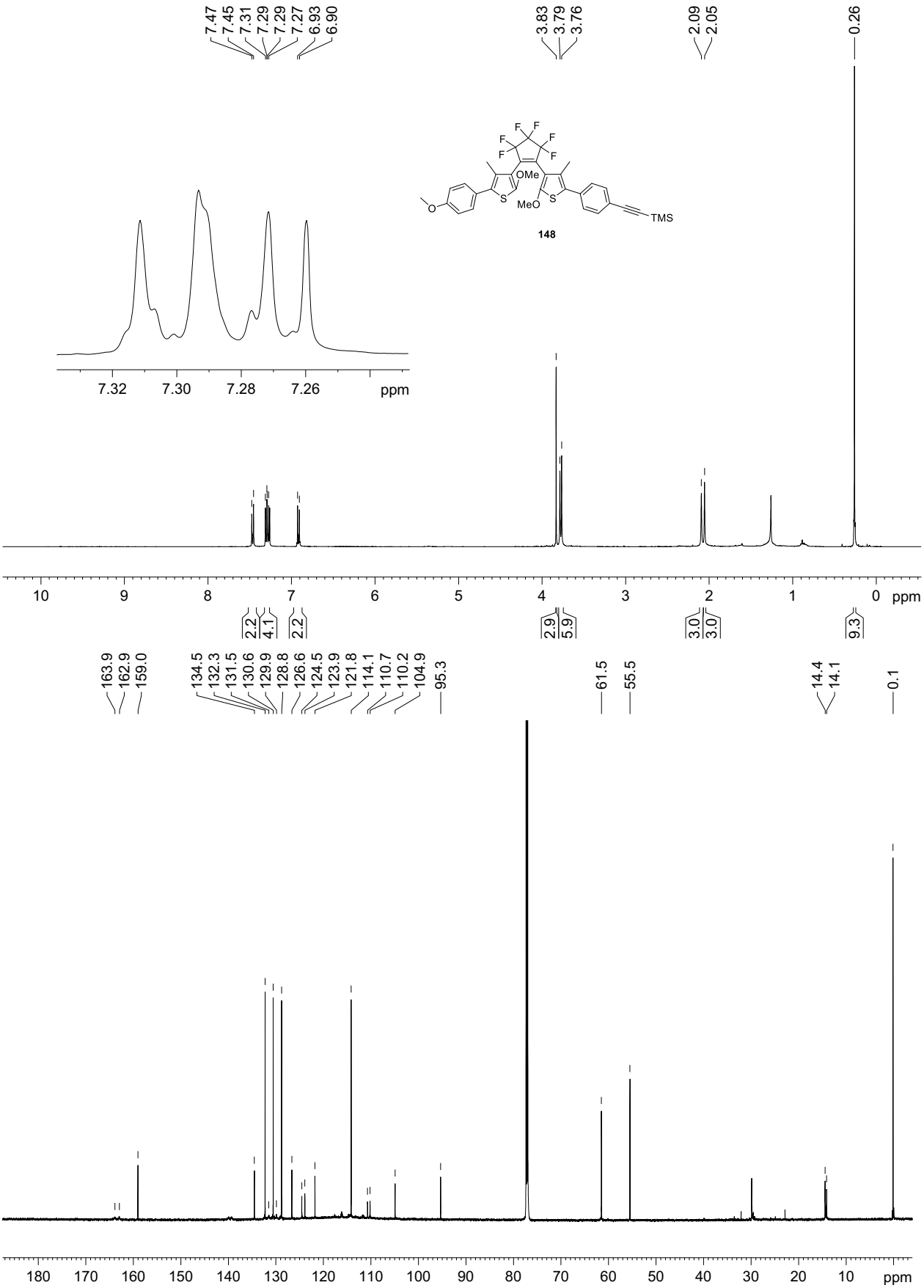
7.47
7.45
7.31
7.29
7.29
7.27
6.93
6.90
3.83
3.79
3.76
2.09
2.05
0.26
F
F
F
F
F
F
OMe
MeO
S
S
O
TMS
148
7.32
7.30
7.28
7.26
ppm
10
9
8
7
6
5
4
3
2
1
0
ppm
2.2
4.1
2.2
2.9
5.9
3.0
3.0
9.3
163.9
162.9
159.0
134.5
132.3
131.5
130.6
129.9
128.8
126.6
124.5
123.9
121.8
114.1
110.7
110.2
104.9
95.3
61.5
55.5
14.4
14.1
0.1
180
170
160
150
140
130
120
110
100
90
80
70
60
50
40
30
20
10
ppm

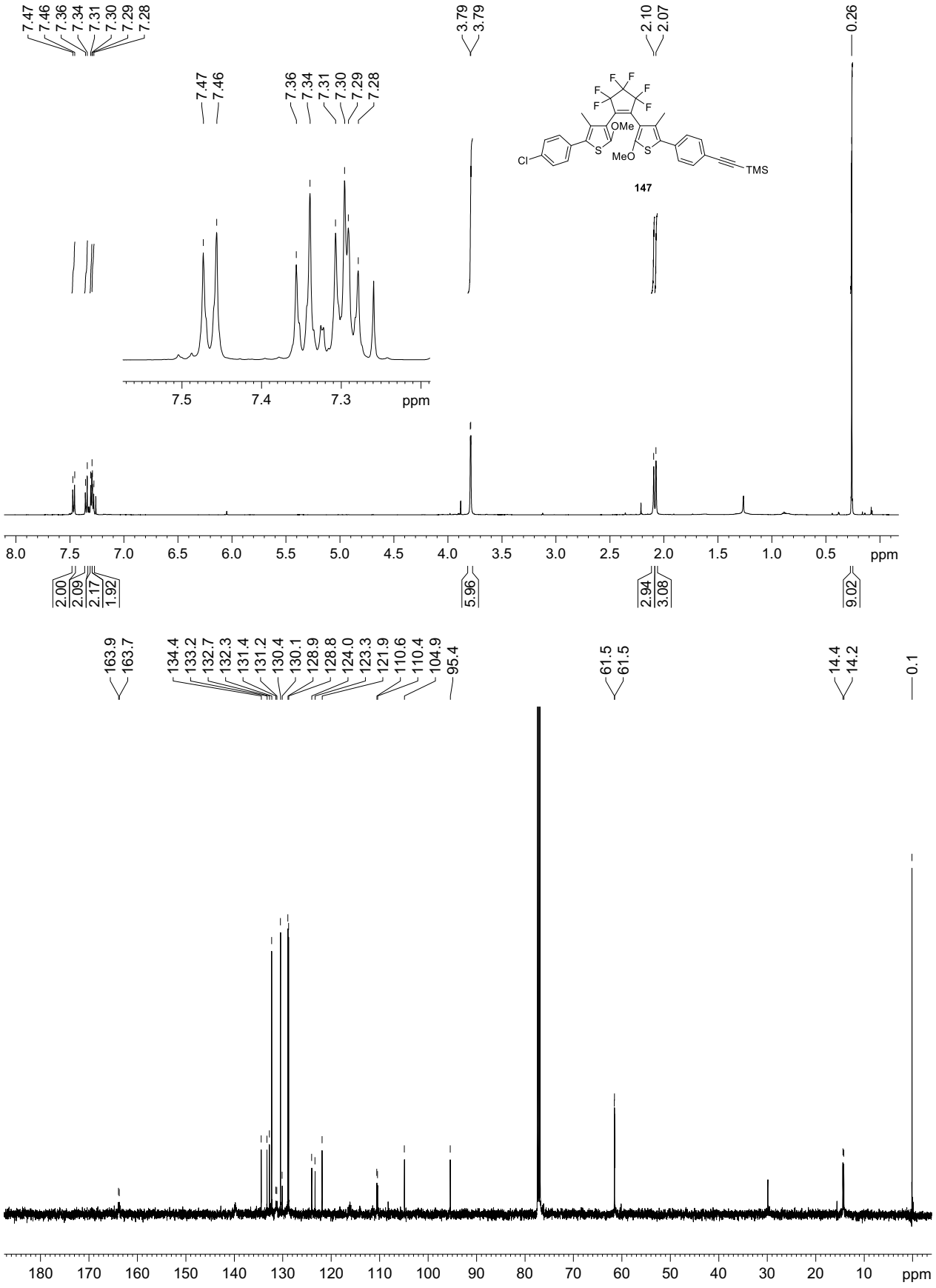
7.47
7.46
7.36
7.34
7.31
7.30
7.29
7.28
3.79
3.79
2.10
2.07
0.26
147
ppm
2.00
2.09
2.17
1.92
5.96
2.94
3.08
9.02
163.9
163.7
134.4
133.2
132.7
132.3
131.4
131.2
130.4
130.1
128.9
128.8
124.0
123.3
121.9
110.6
110.4
104.9
95.4
61.5
61.5
14.4
14.2
0.1

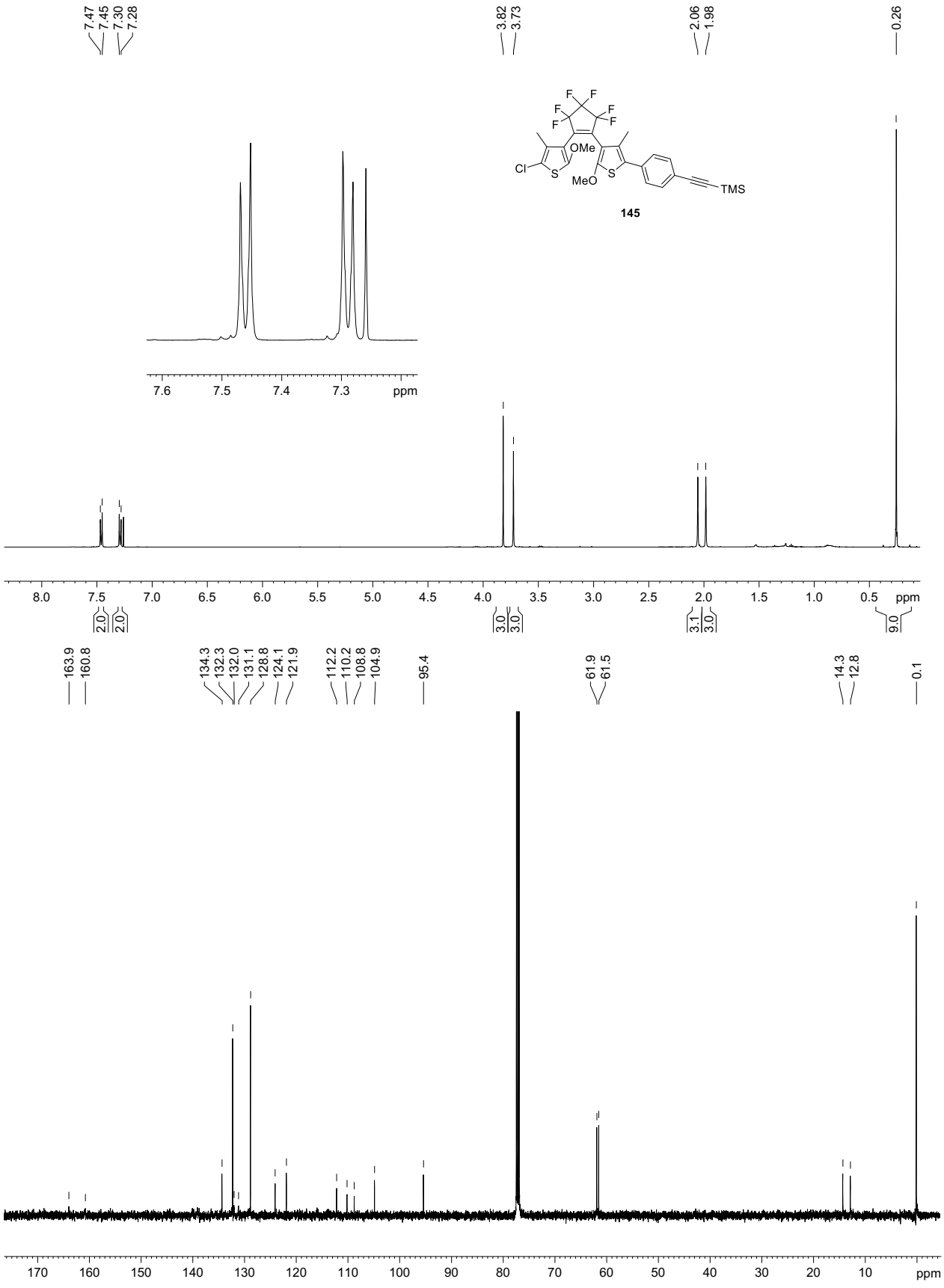
7.47
7.45
7.30
7.28
3.82
3.73
2.06
1.98
0.26
F
F
F
F
F
F
OMe
Cl
S
MeO
S
TMS
145
7.6
7.5
7.4
7.3
ppm
8.0
7.5
7.0
6.5
6.0
5.5
5.0
4.5
4.0
3.5
3.0
2.5
2.0
1.5
1.0
0.5
ppm
2.0
2.0
3.0
3.0
3.1
3.0
9.0
163.9
160.8
134.3
132.3
132.0
131.1
128.8
124.1
121.9
112.2
110.2
108.8
104.9
95.4
61.9
61.5
14.3
12.8
0.1
170
160
150
140
130
120
110
100
90
80
70
60
50
40
30
20
10
ppm

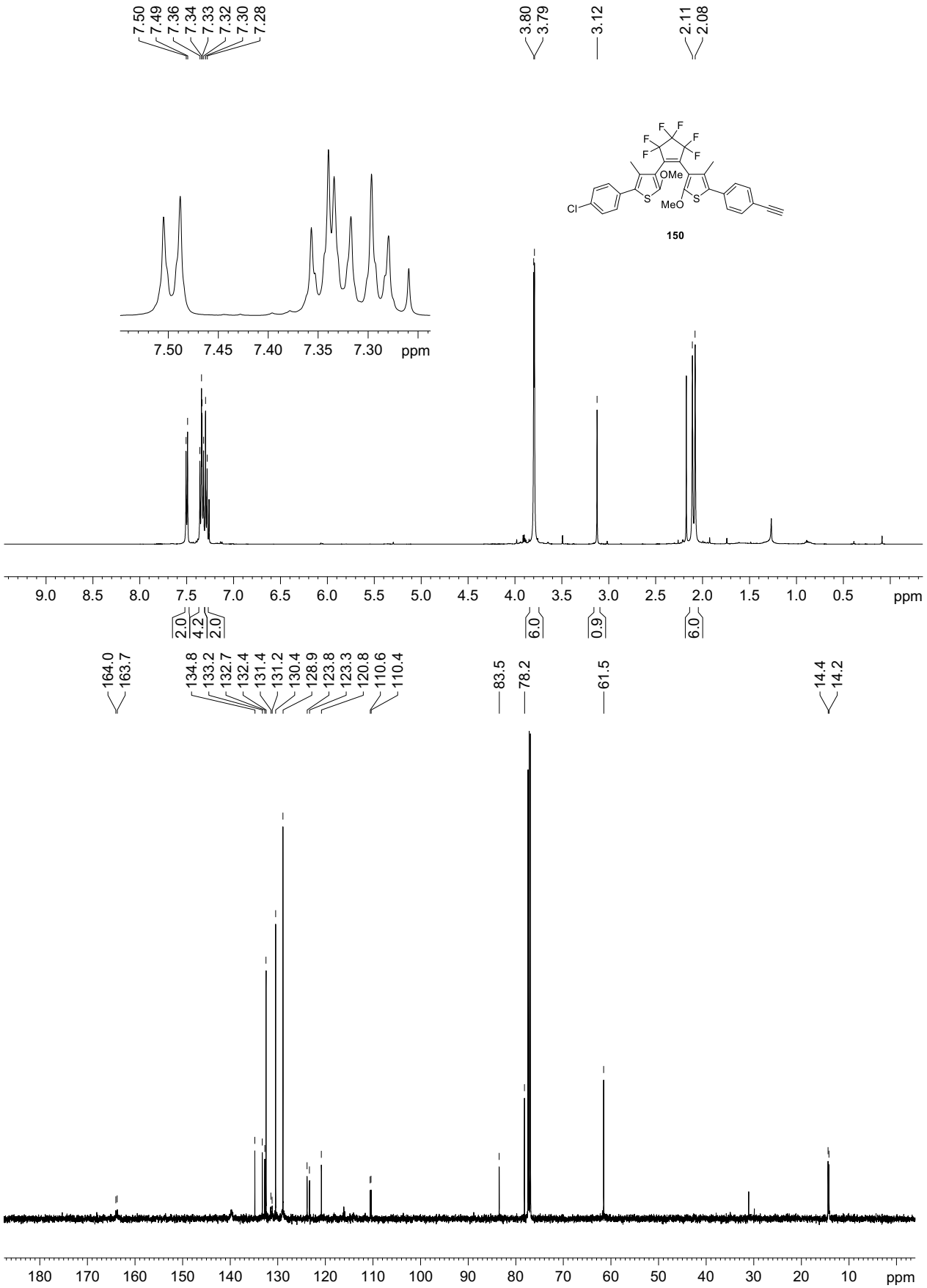
7.50
7.49
7.36
7.34
7.33
7.32
7.30
7.28
3.80
3.79
3.12
2.11
2.08
F
F
F
F
F
F
OMe
MeO
S
S
Cl
150
7.50 7.45 7.40 7.35 7.30 ppm
9.0 8.5 8.0 7.5 7.0 6.5 6.0 5.5 5.0 4.5 4.0 3.5 3.0 2.5 2.0 1.5 1.0 0.5 ppm
2.0
4.2
2.0
6.0
0.9
6.0
164.0
163.7
134.8
133.2
132.7
132.4
131.4
131.2
130.4
128.9
123.8
123.3
120.8
110.6
110.4
83.5
78.2
61.5
14.4
14.2
180 170 160 150 140 130 120 110 100 90 80 70 60 50 40 30 20 10 ppm

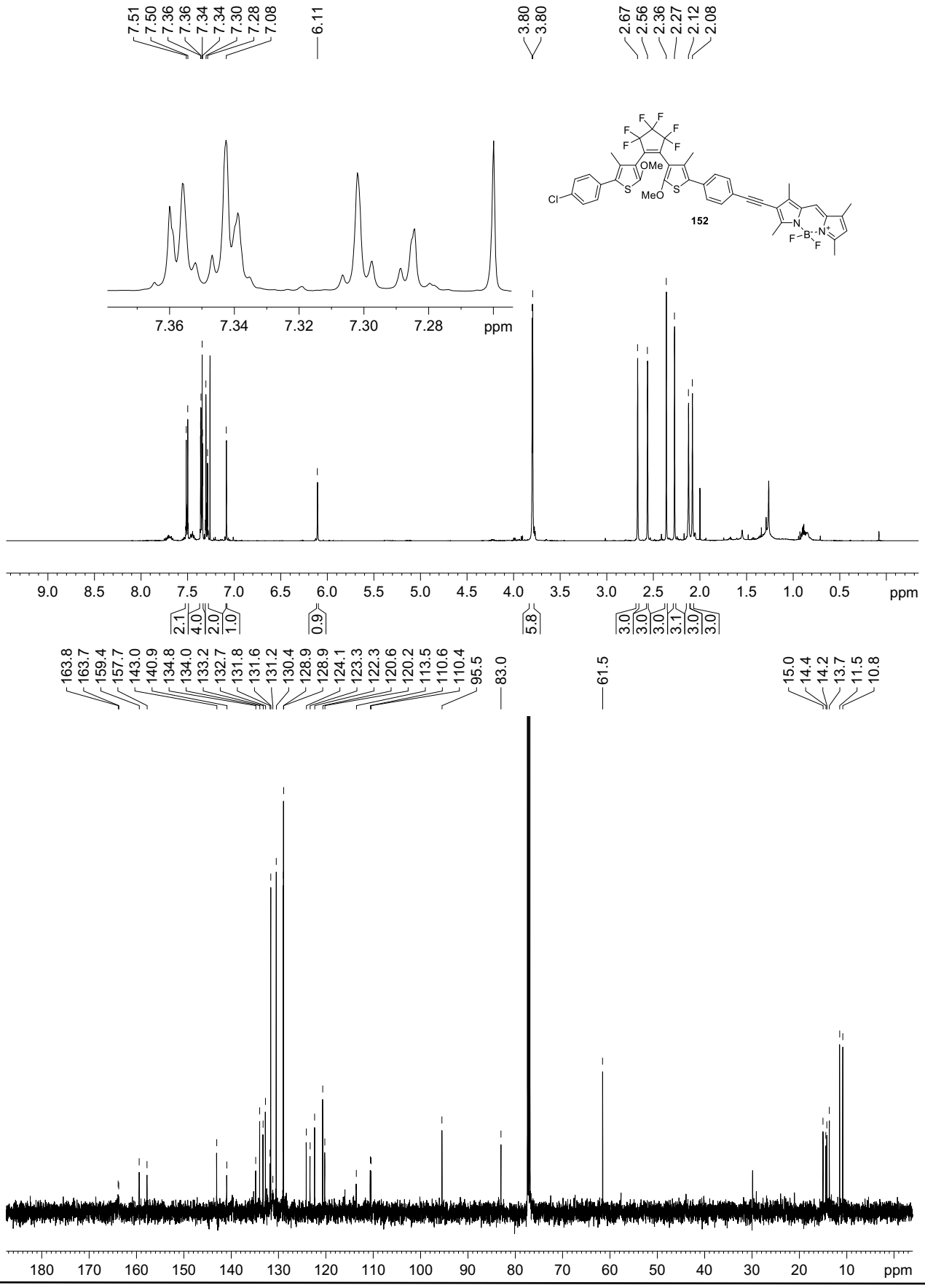
7.51
7.50
7.36
7.36
7.34
7.34
7.30
7.28
7.08
6.11
3.80
3.80
2.67
2.56
2.36
2.27
2.12
2.08
152
7.36
7.34
7.32
7.30
7.28
ppm
9.0
8.5
8.0
7.5
7.0
6.5
6.0
5.5
5.0
4.5
4.0
3.5
3.0
2.5
2.0
1.5
1.0
0.5
ppm
2.1
4.0
2.0
1.0
0.9
5.8
3.0
3.0
3.0
3.1
3.0
3.0
163.8
163.7
159.4
157.7
143.0
140.9
134.8
134.0
133.2
132.7
131.8
131.6
131.2
130.4
128.9
128.9
124.1
123.3
122.3
120.6
120.2
113.5
110.6
110.4
95.5
83.0
61.5
15.0
14.4
14.2
13.7
11.5
10.8
180
170
160
150
140
130
120
110
100
90
80
70
60
50
40
30
20
10
ppm

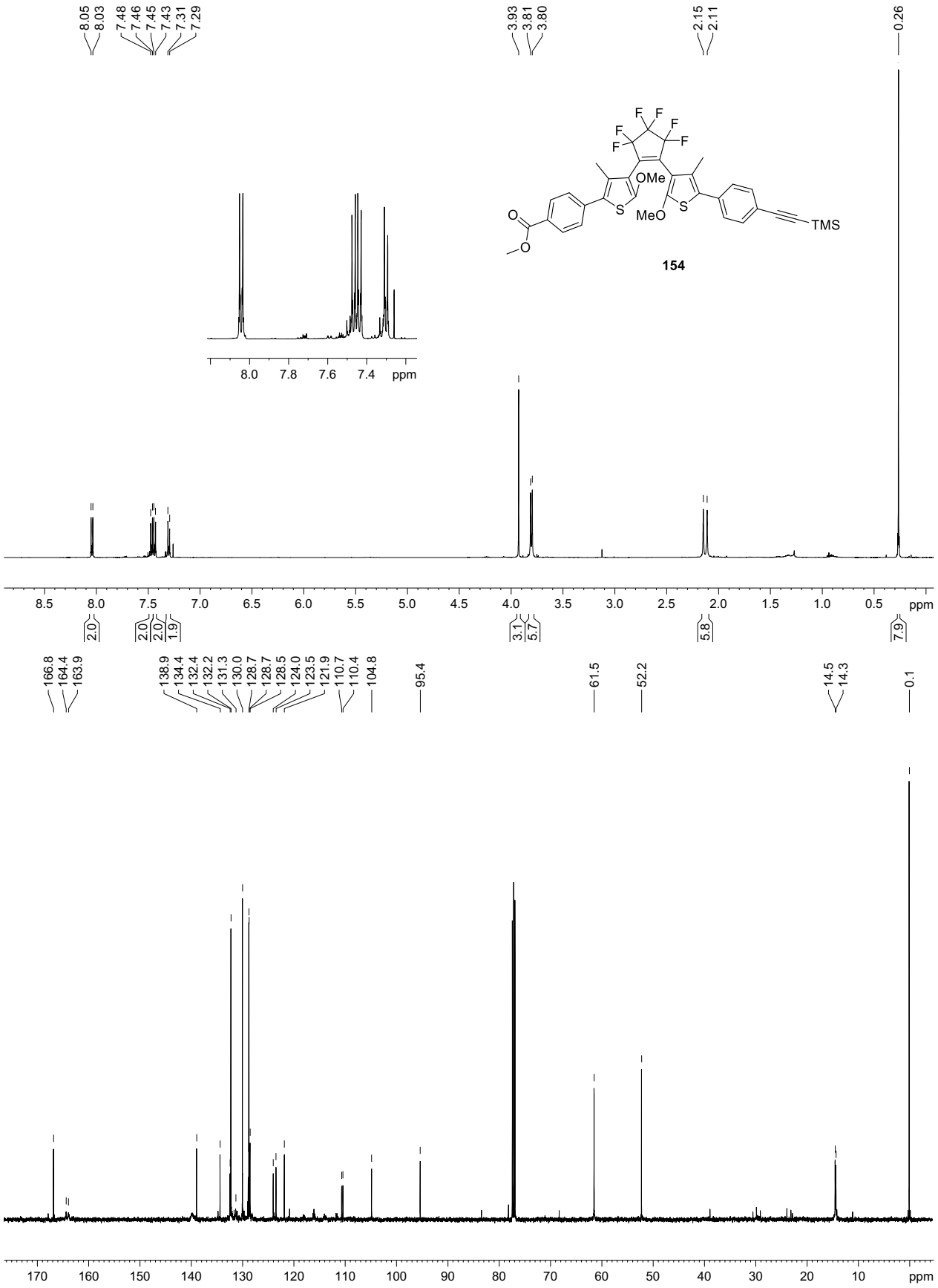
8.05
8.03
7.48
7.46
7.45
7.43
7.31
7.29
3.93
3.81
3.80
2.15
2.11
0.26
F
F
F
F
F
F
OMe
MeO
S
S
O
O
TMS
154
8.0
7.8
7.6
7.4
ppm
8.5
8.0
7.5
7.0
6.5
6.0
5.5
5.0
4.5
4.0
3.5
3.0
2.5
2.0
1.5
1.0
0.5
ppm
2.0
2.0
2.0
1.9
3.1
5.7
5.8
7.9
166.8
164.4
163.9
138.9
134.4
132.4
132.2
131.3
130.0
128.7
128.7
128.5
124.0
123.5
121.9
110.7
110.4
104.8
95.4
61.5
52.2
14.5
14.3
0.1
170
160
150
140
130
120
110
100
90
80
70
60
50
40
30
20
10
ppm

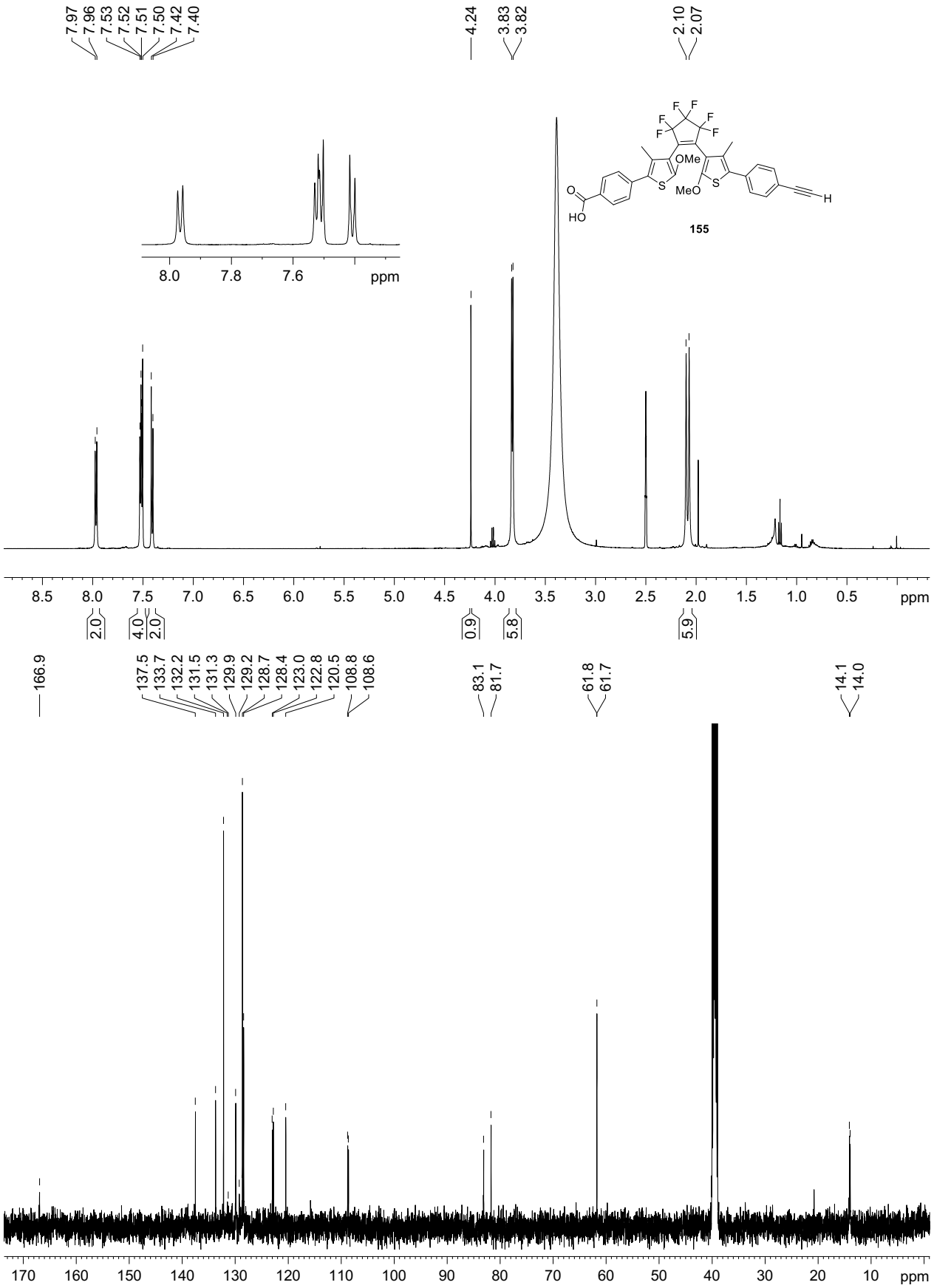
7.97
7.96
7.53
7.52
7.51
7.50
7.42
7.40
4.24
3.83
3.82
2.10
2.07
F
F
F
F
F
F
OMe
MeO
S
S
O
HO
H
155
8.0
7.8
7.6
ppm
8.5
8.0
7.5
7.0
6.5
6.0
5.5
5.0
4.5
4.0
3.5
3.0
2.5
2.0
1.5
1.0
0.5
ppm
2.0
4.0
2.0
0.9
5.8
5.9
166.9
137.5
133.7
132.2
131.5
131.3
129.9
129.2
128.7
128.4
123.0
122.8
120.5
108.8
108.6
83.1
81.7
61.8
61.7
14.1
14.0
170
160
150
140
130
120
110
100
90
80
70
60
50
40
30
20
10
ppm

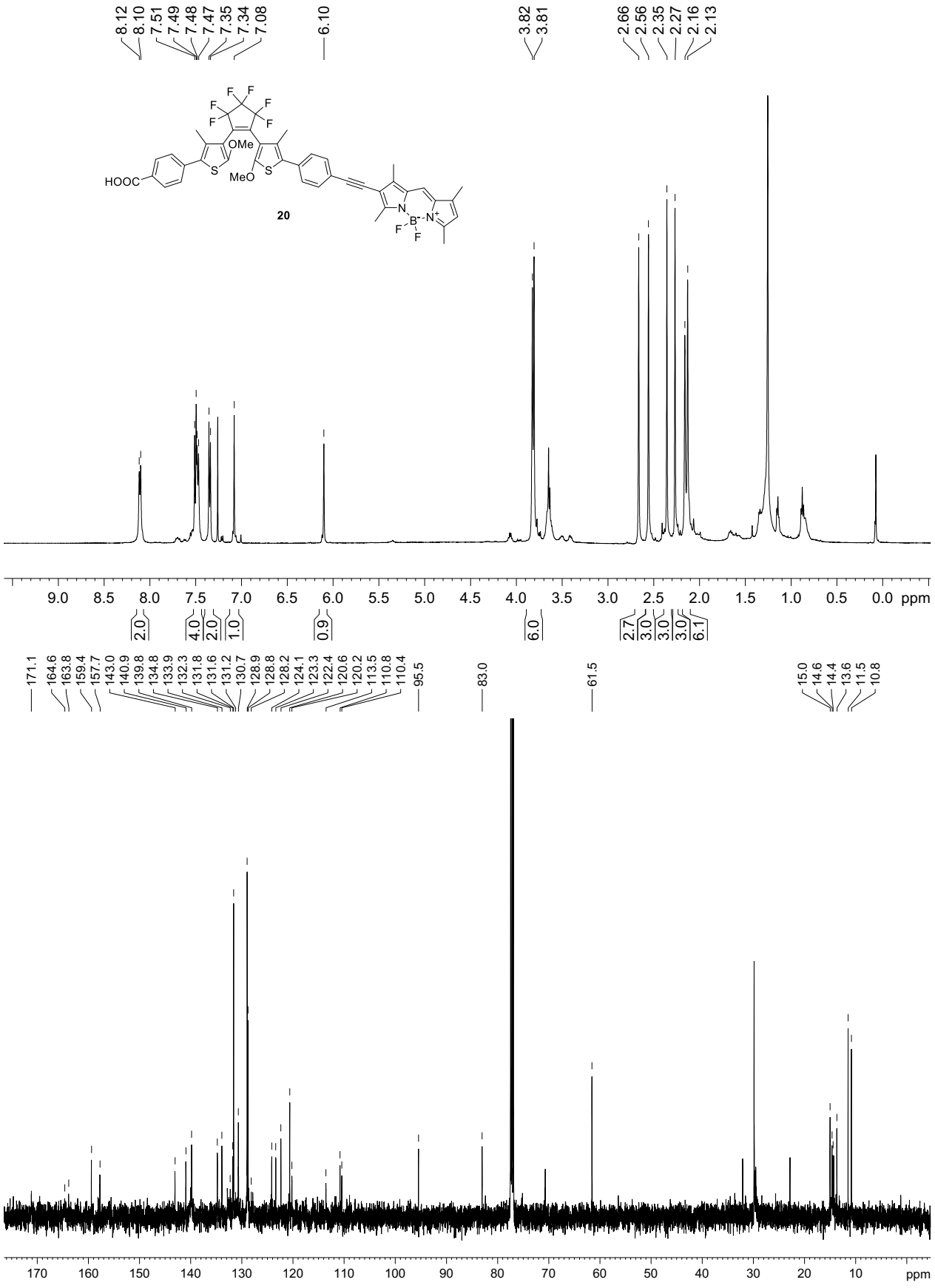
8.12
8.10
7.51
7.49
7.48
7.47
7.35
7.34
7.08
6.10
3.82
3.81
2.66
2.56
2.35
2.27
2.16
2.13
HOOC
OMe
MeO
S
S
F
N
B
N+
20
9.0 8.5 8.0 7.5 7.0 6.5 6.0 5.5 5.0 4.5 4.0 3.5 3.0 2.5 2.0 1.5 1.0 0.5 0.0 ppm
2.0
4.0
2.0
1.0
0.9
6.0
2.7
3.0
3.0
3.0
6.1
171.1
164.6
163.8
159.4
157.7
143.0
140.9
139.8
134.8
133.9
132.3
131.8
131.6
131.2
130.7
128.9
128.8
128.2
124.1
123.3
122.4
120.6
120.2
113.5
110.8
110.4
95.5
83.0
61.5
15.0
14.6
14.4
13.6
11.5
10.8
170 160 150 140 130 120 110 100 90 80 70 60 50 40 30 20 10 ppm

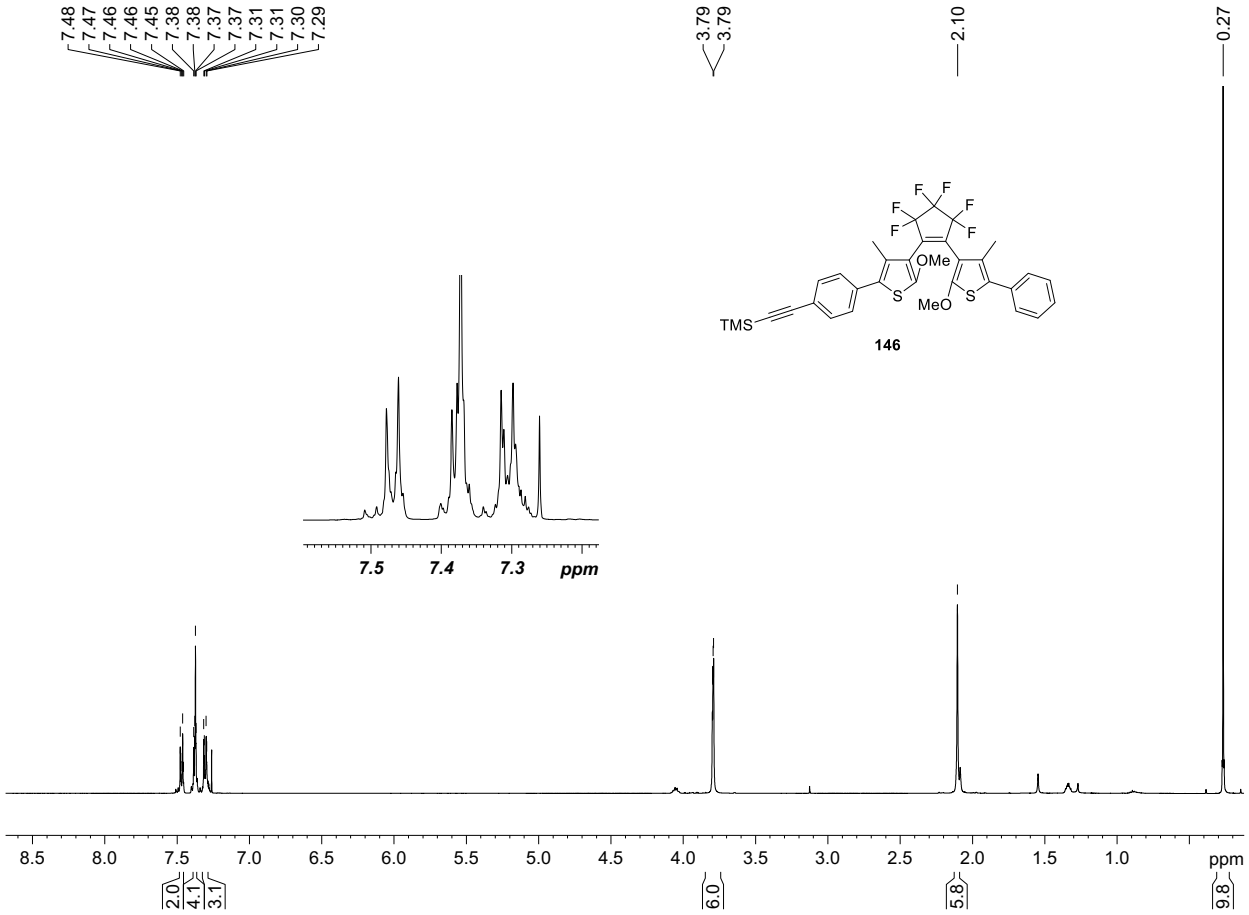
7.48
7.47
7.46
7.46
7.45
7.38
7.38
7.37
7.37
7.31
7.31
7.30
7.29
3.79
3.79
2.10
0.27
F
F
F
F
F
F
OMe
MeO
S
S
TMS
146
7.5
7.4
7.3
ppm
8.5
8.0
7.5
7.0
6.5
6.0
5.5
5.0
4.5
4.0
3.5
3.0
2.5
2.0
1.5
1.0
ppm
2.0
4.1
3.1
6.0
5.8
9.8

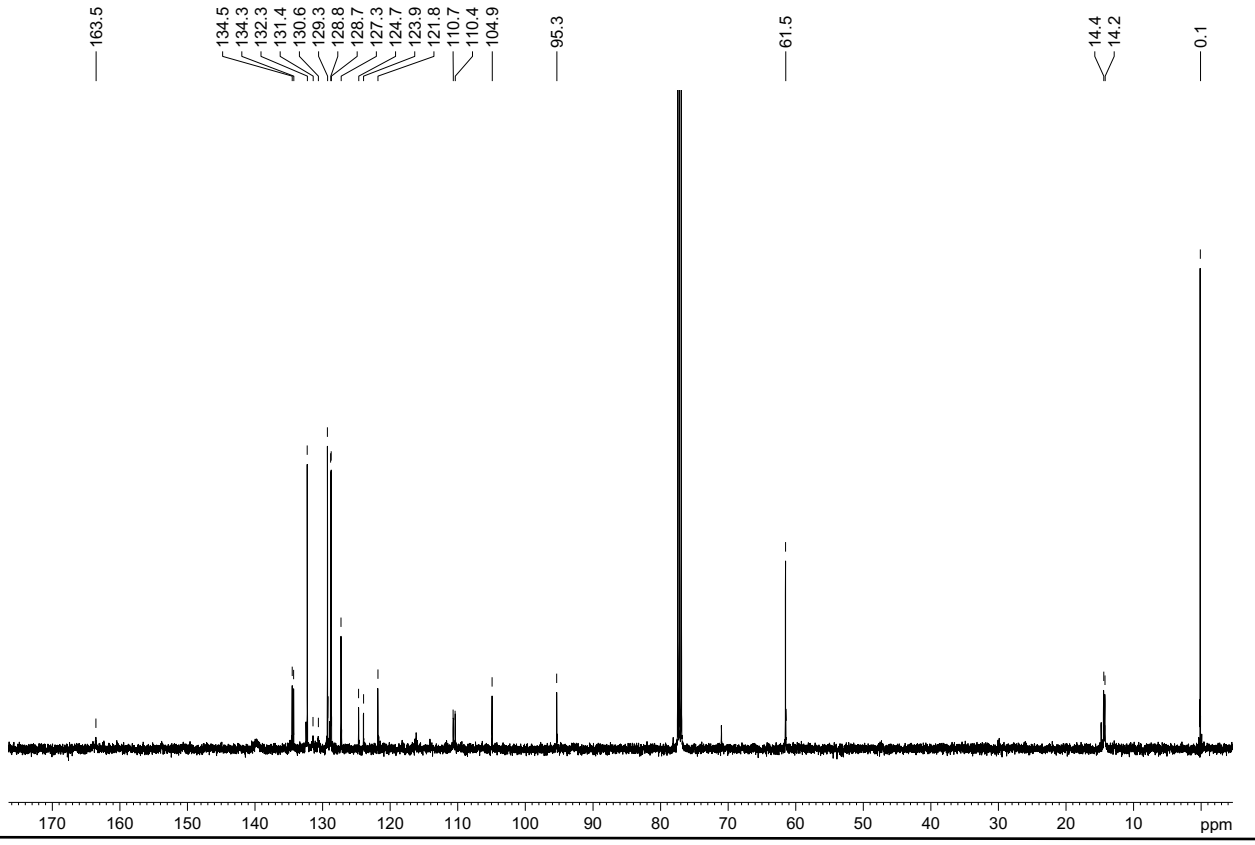
163.5
134.5
134.3
132.3
131.4
130.6
129.3
128.8
128.7
127.3
124.7
123.9
121.8
110.7
110.4
104.9
95.3
61.5
14.4
14.2
0.1
170
160
150
140
130
120
110
100
90
80
70
60
50
40
30
20
10
ppm

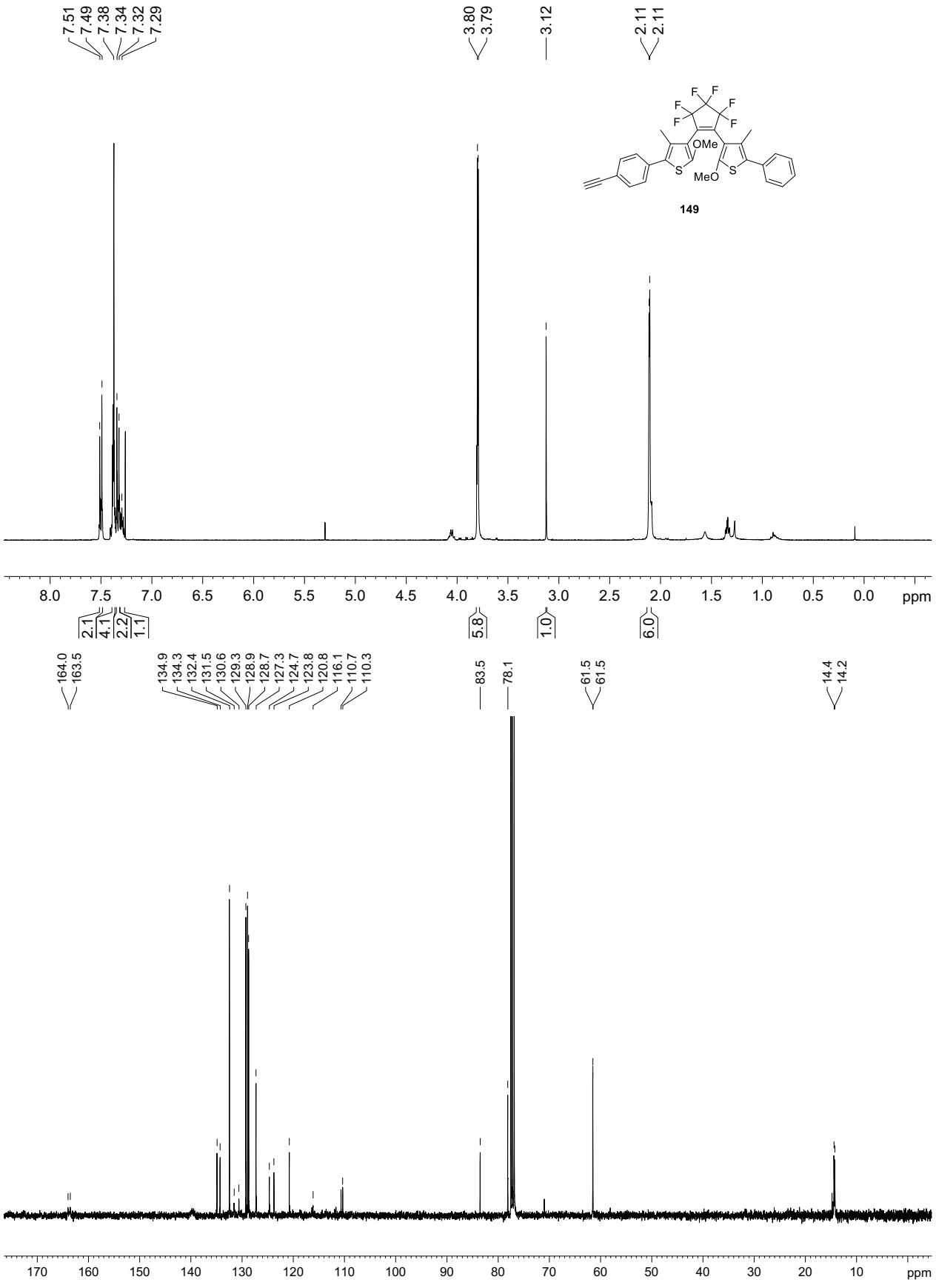
7.51
7.49
7.38
7.34
7.32
7.29
3.80
3.79
3.12
2.11
2.11
F
F
F
F
F
F
OMe
MeO
S
S
149
8.0
7.5
7.0
6.5
6.0
5.5
5.0
4.5
4.0
3.5
3.0
2.5
2.0
1.5
1.0
0.5
0.0
ppm
2.1
4.1
2.2
1.1
5.8
1.0
6.0
164.0
163.5
134.9
134.3
132.4
131.5
130.6
129.3
128.9
128.7
127.3
124.7
123.8
120.8
116.1
110.7
110.3
83.5
78.1
61.5
61.5
14.4
14.2
170
160
150
140
130
120
110
100
90
80
70
60
50
40
30
20
10
ppm

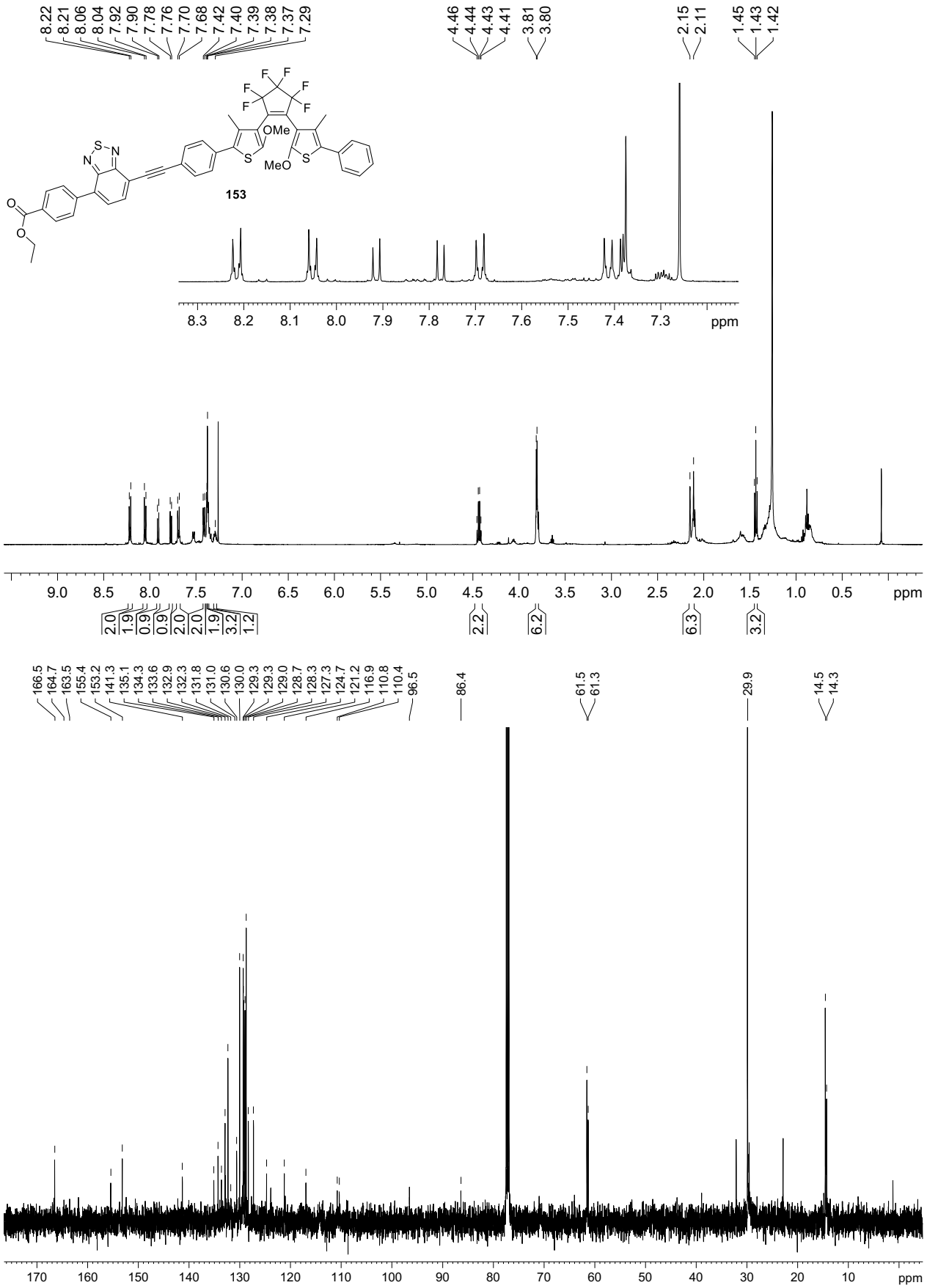
8.22
8.21
8.06
8.04
7.92
7.90
7.78
7.76
7.70
7.68
7.42
7.40
7.39
7.38
7.37
7.29
4.46
4.44
4.43
4.41
3.81
3.80
2.15
2.11
1.45
1.43
1.42
153
ppm
2.0
1.9
0.9
0.9
2.0
2.0
1.9
3.2
1.2
2.2
6.2
6.3
3.2
166.5
164.7
163.5
155.4
153.2
141.3
135.1
134.3
133.6
132.9
132.3
131.8
131.0
130.6
130.0
129.3
129.3
129.0
128.7
128.3
127.3
124.7
121.2
116.9
110.8
110.4
96.5
86.4
61.5
61.3
29.9
14.5
14.3

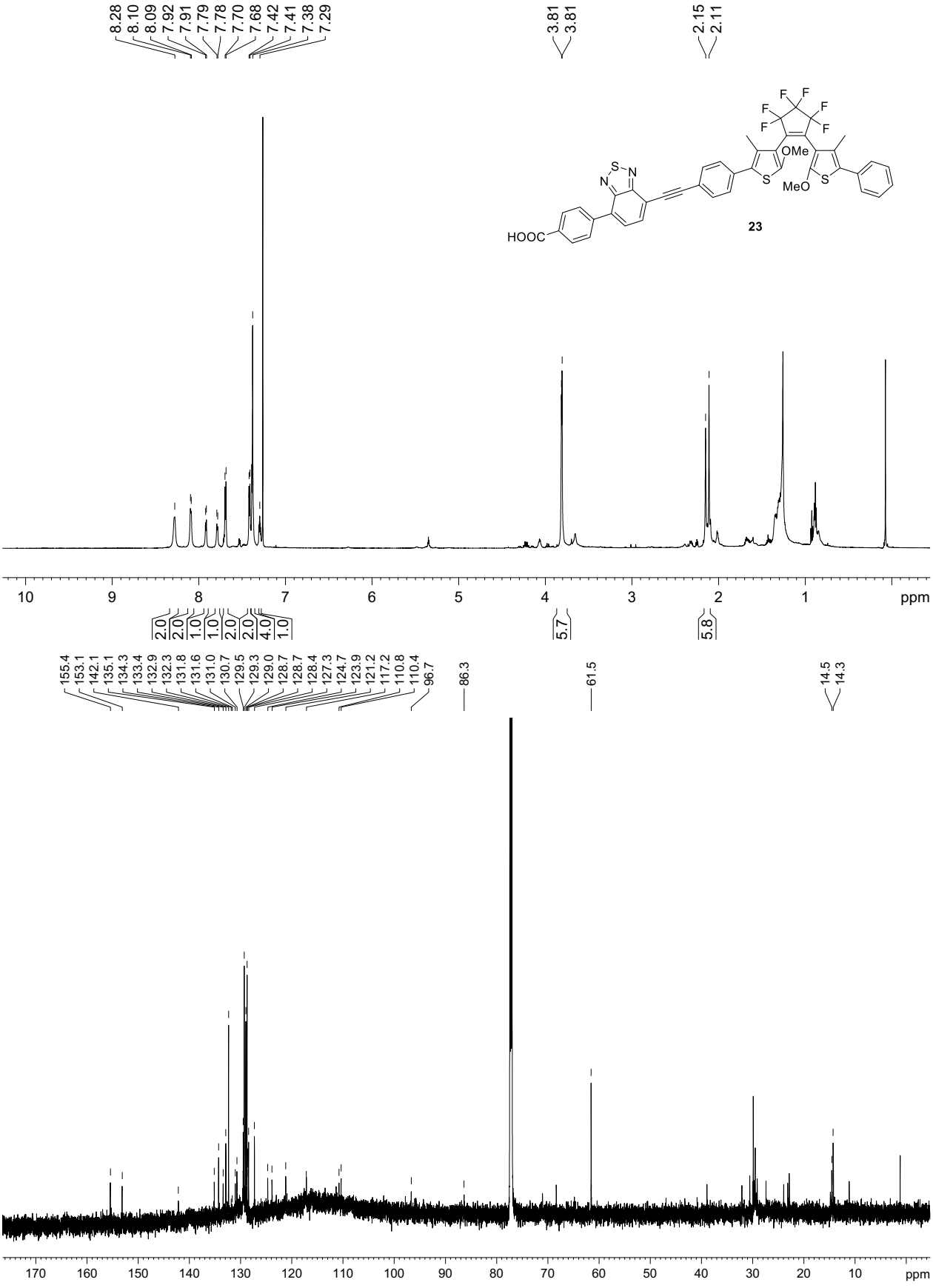
8.28
8.10
8.09
7.92
7.91
7.79
7.78
7.70
7.68
7.42
7.41
7.38
7.29
3.81
3.81
2.15
2.11
HOOC
23
ppm
2.0
2.0
1.0
1.0
2.0
2.0
4.0
1.0
5.7
5.8
155.4
153.1
142.1
135.1
134.3
133.4
132.9
132.3
131.8
131.6
131.0
130.7
129.5
129.3
129.0
128.7
128.7
128.4
127.3
124.7
123.9
121.2
117.2
110.8
110.4
96.7
86.3
61.5
14.5
14.3
ppm

5.2 Absorption-, Emission- and LCMS-Spectra

5.2.1 General

The determination of the pss was done with DTE(OMe) photoswitches irradiated with 345 nm LED in degassed solvents. A sample without irradiation, after short time irradiation and in the pss (proved by UV/Vis-spectra) was taken and investigated in LC-MS (ESI). The used column is a Grom-Sil-120-ODS-4-HE (Grace), length 50 mm, ID 2 mm, 3 µm. All peaks of the UV/Vis-trace at the isosbestic point of the DTE(OMe)s are shown. The determination of DTE(OMe) OF, DTE(OMe) CF and their dimers was done by comparison of the absorption spectra with the literature.[29] The dimers were assigned using the following hints: a) they show identical UV/Vis spectra to their monomers, b) they are less polar than their monomers, c) they are switchable.

5.2.1.1 Diiodo-DTE(OMe) 29

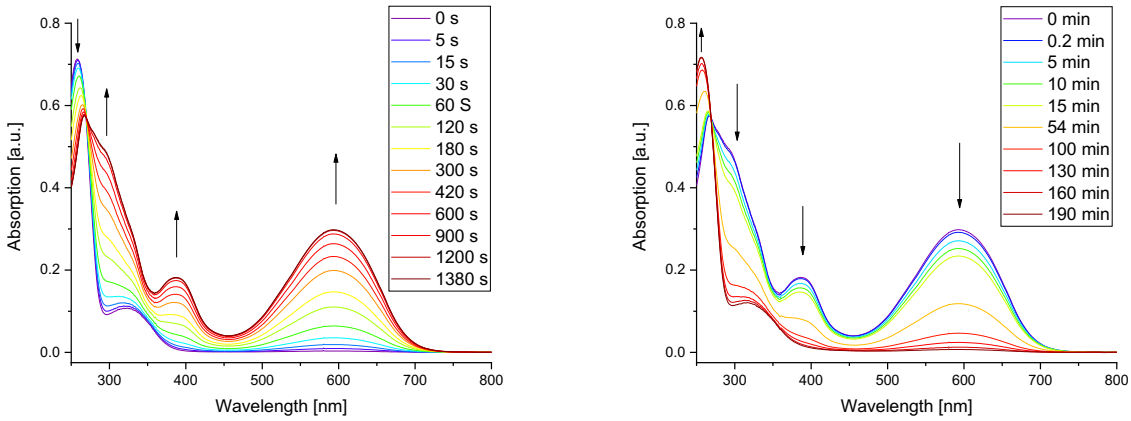

*Figure 159: Diiodo-DTE(OMe) **29** with 4.0*10^{-5} M in MeCN; left: OF irradiation with HBO 200 W, 326 nm-filter, HW: 1 nm, 2.0 mW/cm^2, right: CF irradiation with Xe-lamp 1000 W, 500 nm edge-filter, 8.3 mW/cm^2 until pss was reached.*

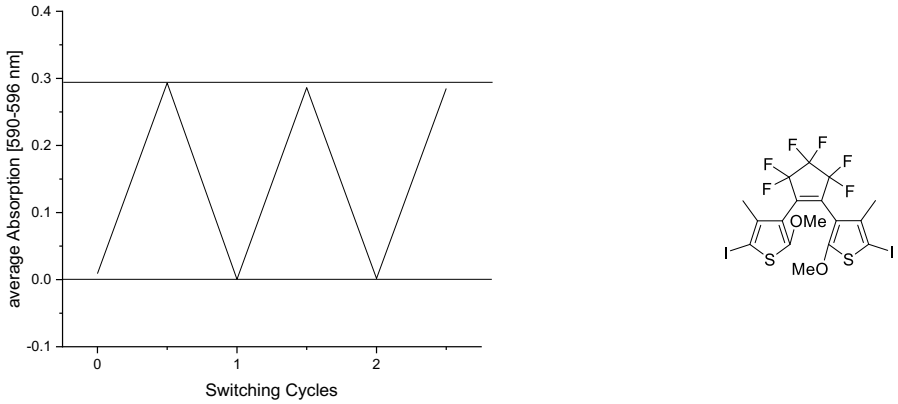

*Figure 160: switching cycles of diphenyl-DTE(OMe) **3** with alternating 345 nm and 632 nm LED in MeCN with average absorption at the maximum at 590-596 nm.*

5.2.1.2 IR measurement of 29 in MeCN under 365 nm LED irradiation.

The IR measurement in solution was recorded on a Bruker Vertex70v ATR-FTIR spectrometer, using the deuterated Lanthanum α-alanine doped triglycine sulphate (DLaTGS) detector. The sample compartment was kept under nitrogen. The measurement was carried out in a standard cuvette (two NaCl slides, 21 mm × 14 mm). The irradiation was carried out with a set-up equipped with LED diodes (λ_{irr} = 365 nm), which were directly attached to the cuvette. The spectral range between 370 and 4000 cm^{-1} was investigated, with 4 cm^{-1} resolution. IR data were analyzed using the software OPUS 6.5 (Bruker).

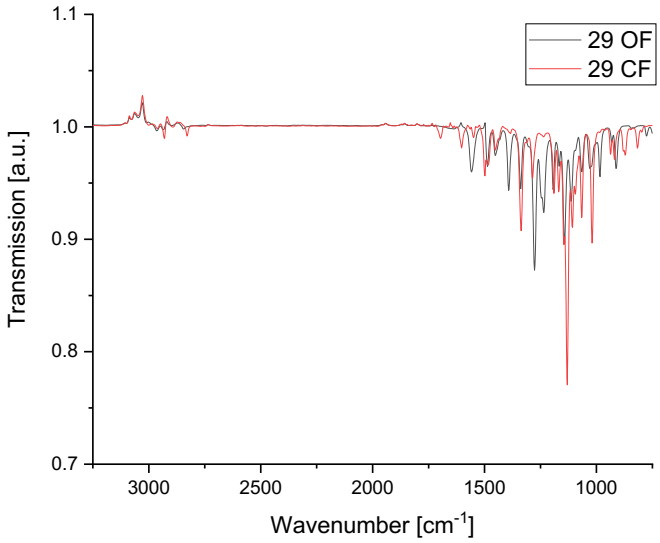

*Figure 161: IR-spectra of diiodo-DTE(OMe) **29** (4.1*10^{-5} M) OF (black), CF (red) in MeCN after irradiation with 365 nm LED.*

5.2.1.3 Diphenyl-DTE(OMe) 3

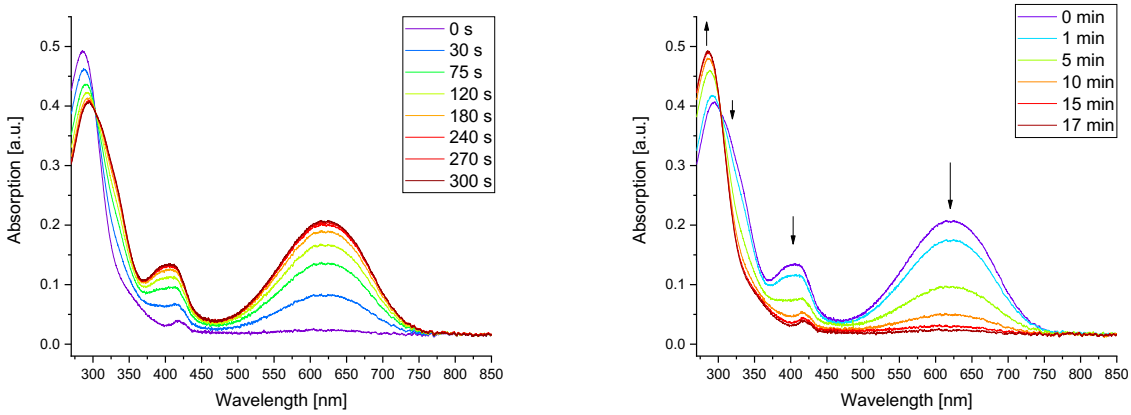

*Figure 162: Diphenyl-DTE(OMe) **3** with 1.8*10^{-5} M in MeCN, left: OF irradiation with 345 nm LED, HW 11 nm, 2.0 mW/cm^2, right: CF irradiation with 632 nm LED, HW 18 nm, 250 mW/cm^2 until pss was reached.*

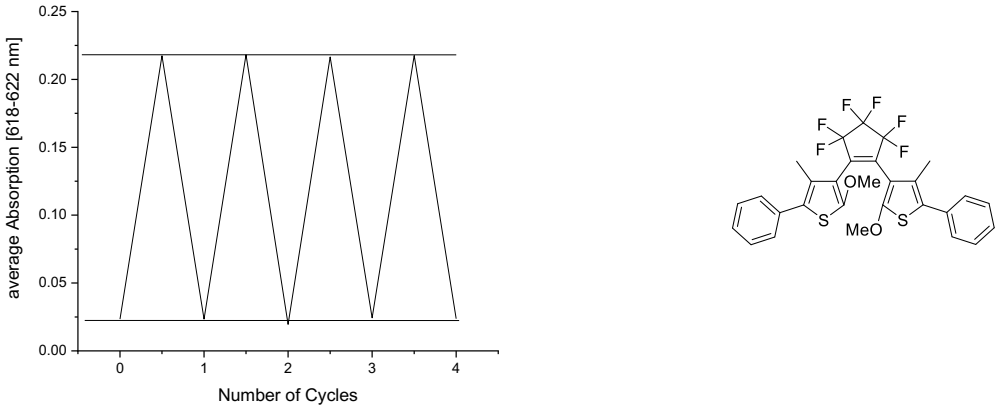

*Figure 163: left: switching cycles of diphenyl-DTE(OMe) **3** with alternating 345 nm and 632 nm LED in MeCN with average absorption at the maximum at 618-622 nm, right: structure of diphenyl-DTE(OMe) **3**.*

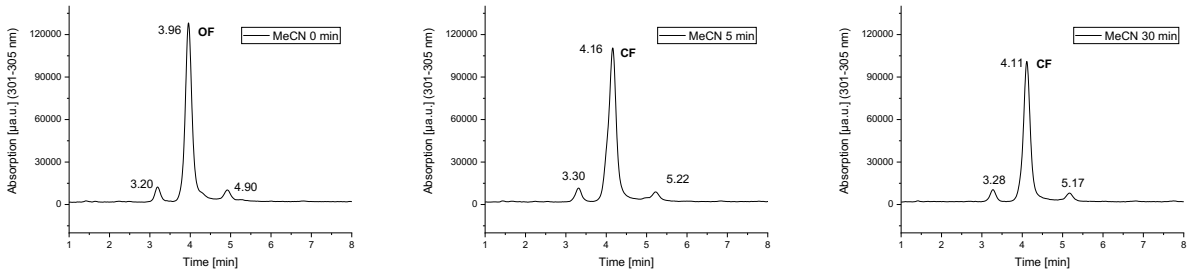

*Figure 164: left: start spectra of diphenyl-DTE(OMe) **3** ($1.8 \cdot 10^{-5}$ M in MeCN) (RT: 3.96 min), middle: after 5 min irradiation (RT: 4.16 min); right: after 0.5 min irradiation (RT: 4.11 min); MeCN/H_2O (+0.1% HCOOH) 90:10 to 100:0 in 10 min, 0.3 mL/min, detection wavelength 335-339 nm, irradiated with 345 nm LED.*

No diphenyl-DTE(OMe) 3 OF visible after 30 min -> 100:0 of compound **3** CF to OF in the pss under 345 nm LED in MeCN.

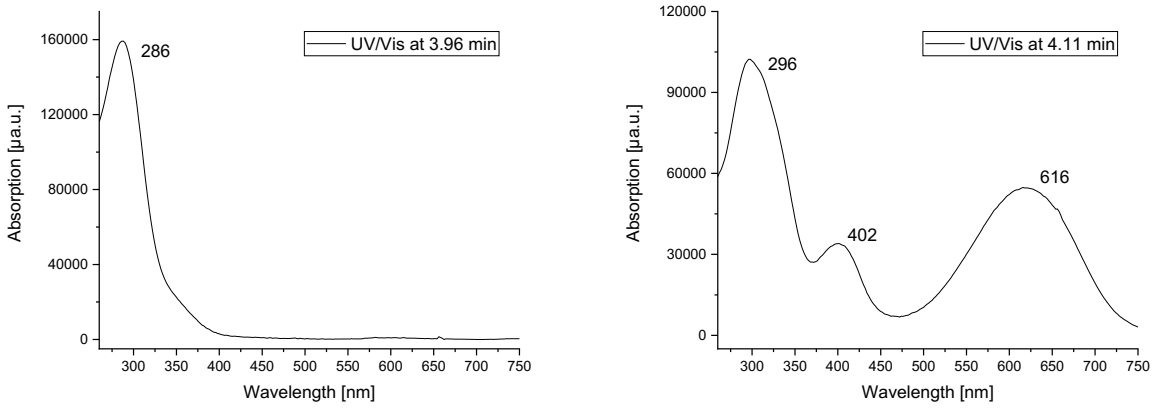

Figure 165: UV/Vis-spectra via diode-array detector in HPLC, left: 0 min irradiation with 345 nm LED, (RT: 3.96 min), right: 30 min irradiation with 345 nm LED in MeCN (RT: 4.11 min).

5.2.1.4 Chloro-DTE(OMe) 145

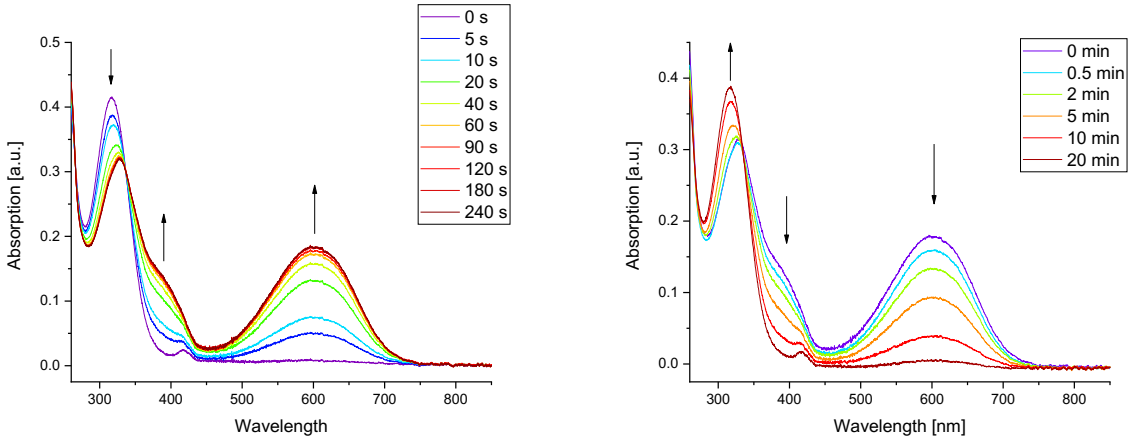

*Figure 166: chloro-DTE(OMe) **145** with 1.8*10^{-5} M in MeCN, left: OF irradiation with 345 nm LED, HW 11 nm, 2.0 mW/cm^2, right: CF irradiation with 632 nm LED, HW 18 nm, 250 mW/cm^2 until pss was reached.*

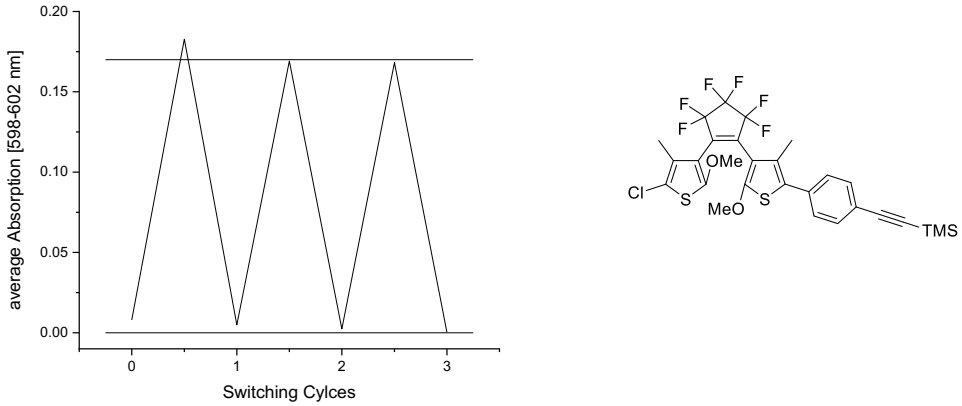

Figure 167: left: switching cycles of chloro-DTE(OMe) ***145*** *with alternating 345 nm and 632 nm LED in MeCN with average absorption at the maximum at 598-602 nm, right: structure of chloro-DTE(OMe)* ***145****.*

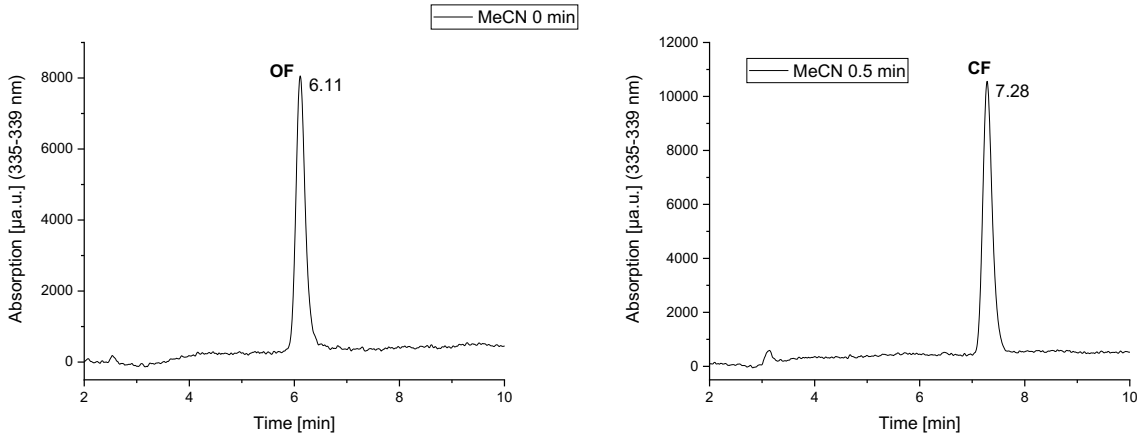

Figure 168: left: start spectra of chloro-DTE(OMe) ***145*** *(1.8·10^{-5} M in MeCN) (RT: 6.11 min), right: after 0.5 min irradiation (RT: 7.28 min); MeCN/H_2O (+0.1% HCOOH) 80:20 to 100:0 in 10 min, 0.3 mL/min, detection wavelength 335-339 nm, irradiated with 345 nm LED.*

No chloro-DTE(OMe) 145 OF visible after 0.5 min -> 100:0 145 CF to OF in the pss under 345 nm LED in MeCN.

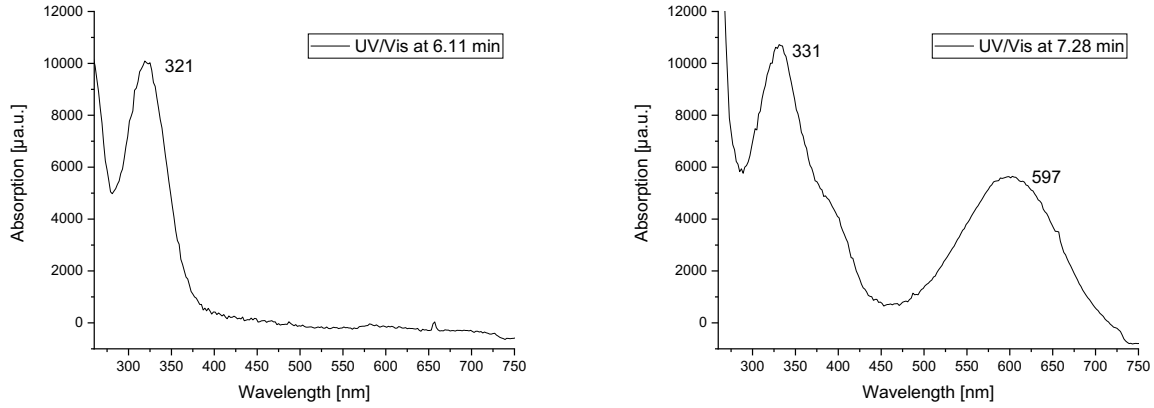

*Figure 169: UV/Vis-spectra of chloro-DTE(OMe) **145** via diode-array detector in HPLC, left: 0 min irradiation with 345 nm LED, (RT: 6.11 min), right: 30 min irradiation with 345 nm LED (RT: 7.28 min).*

5.2.1.5 Benzoic acid-DTE(OMe) 155

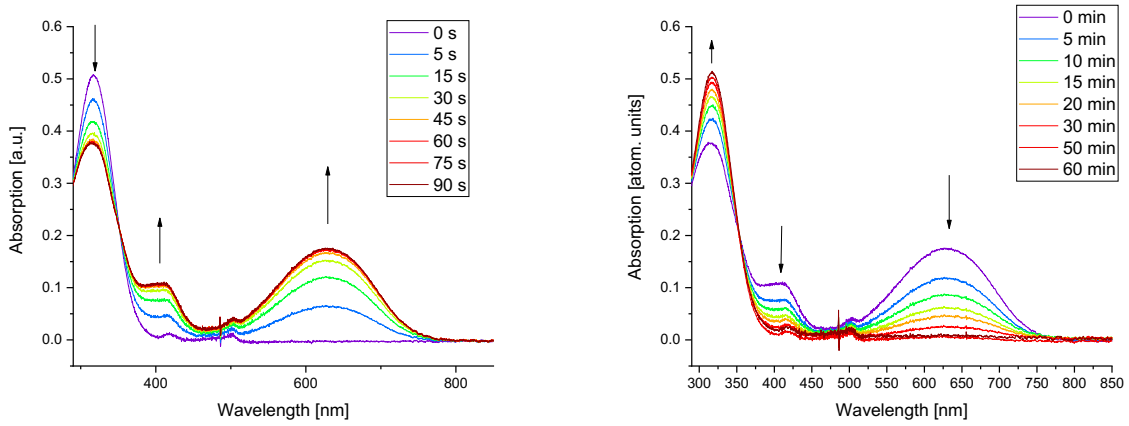

*Figure 170: benzoic acid-DTE(OMe) **155** with 1.8*10^{-5} M in MeCN, left: OF irradiation with 345 nm LED, HW 11 nm, 2.0 mW/cm^2, right: CF irradiation with 632 nm LED, HW 18 nm, 250 mW/cm^2 until pss was reached.*

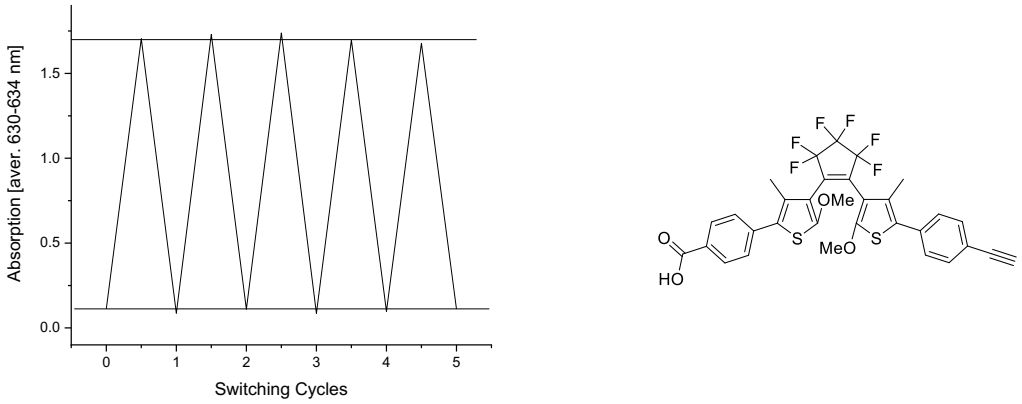

*Figure 171: left: switching cycles of benzoic acid-DTE(OMe) **155** with alternating 345 nm and 632 nm LED in MeCN with average absorption at the maximum at 630-634 nm, right: structure of benzoic acid-DTE(OMe) **155**.*

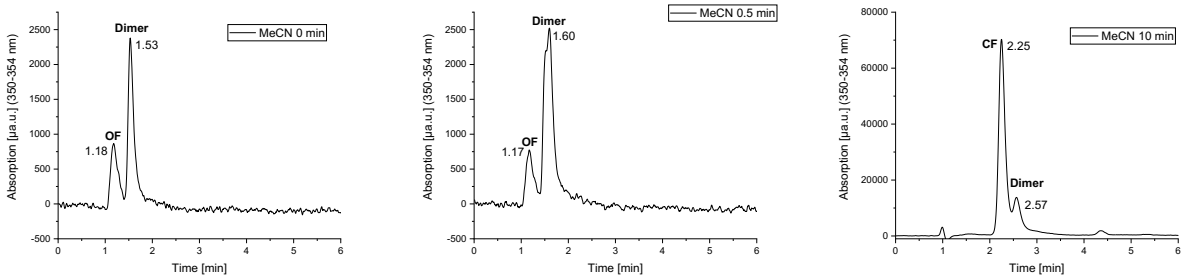

*Figure 172: left: start spectra of benzoic acid-DTE(OMe) **155** ($1.8 \cdot 10^{-5}$ M in MeCN) (RT: 1.18 and 1.53 min), middle: after 0.5 min irradiation (RT: 1.11 and 1.60 min); right: after 10 min irradiation (RT: 2.25 and 2.51 min); MeCN/H_2O (+0.1% HCOOH) 92:8 to 100:0 in 10 min, 0.2 mL/min, detection wavelength 350-354 nm, irradiated with 345 nm LED.*

No benzoic acid-DTE(OMe) **155** OF visible after 10 min -> 100:0 of compound **155** CF to OF in the pss under 345 nm LED in MeCN.

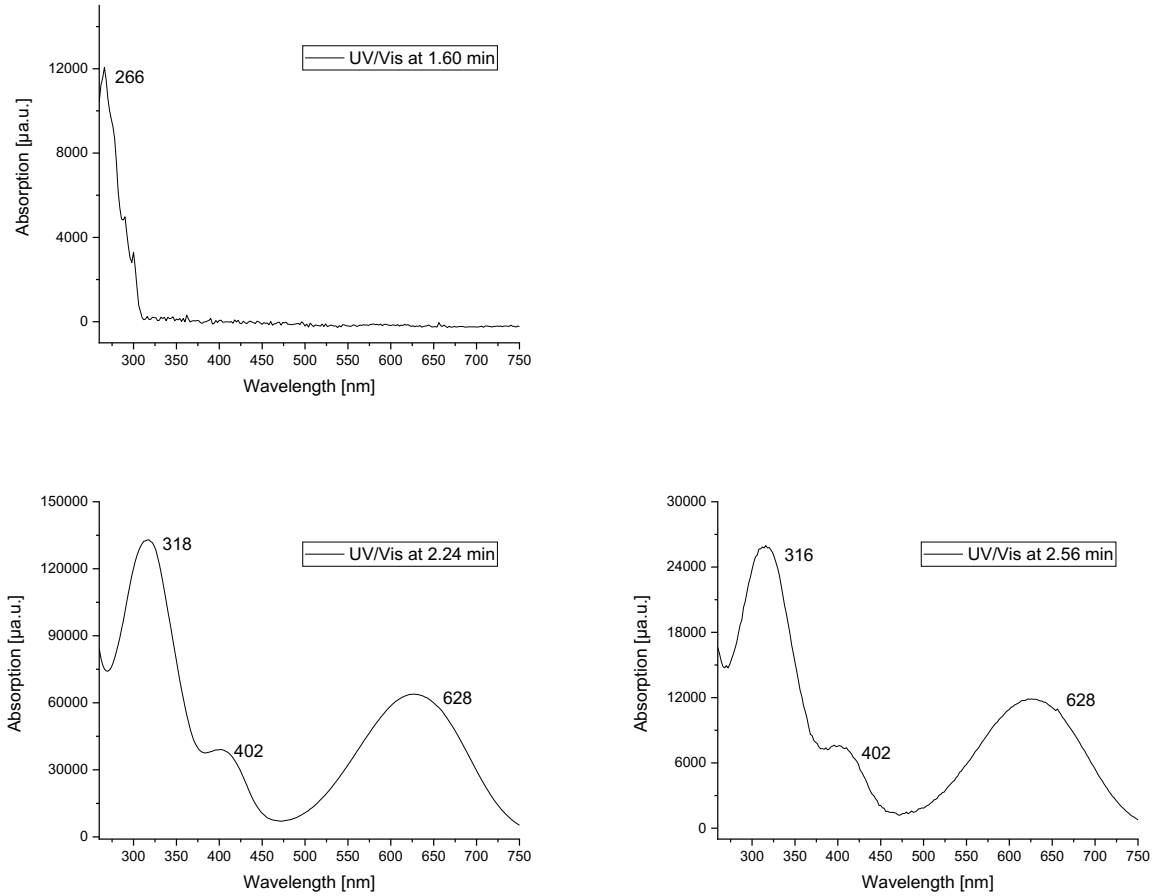

*Figure 173: UV/Vis-spectra via diode-array detector of benzoic acid-DTE(OMe) **155** in HPLC, top: 0 min irradiation with 345 nm LED in MeCN, (RT: 1.60 min), bottom: left: 10 min irradiation with 345 nm LED in MeCN, (RT: 2.24 min), right: 10 min irradiation with 345 nm LED in MeCN (RT: 2.56 min).*

5.2.1.6 Chlorophenyl-DTE(OMe) 147

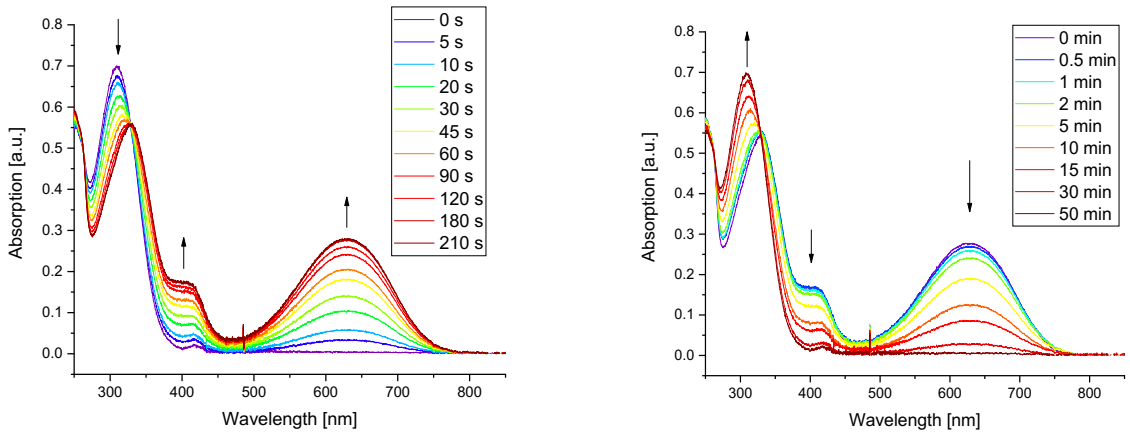

*Figure 174: chlorophenyl-DTE(OMe) **147** with 1.8*10^{-5} M in MeCN, left: OF irradiation with 345 nm LED, HW 11 nm, 2.0 mW/cm^2, right: CF irradiation with 632 nm LED , HW 18 nm, 250 mW/cm^2 until pss was reached.*

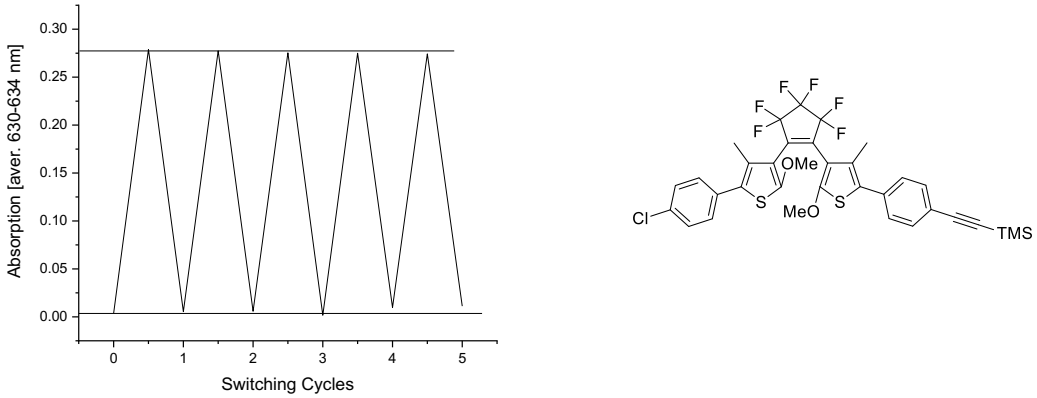

*Figure 175: left: switching cycles of chlorophenyl-DTE(OMe) **147** with alternating 345 nm and 632 nm LED with average absorption at the maximum at 630-634 nm, right: structure of chlorophenyl-DTE(OMe) **147**.*

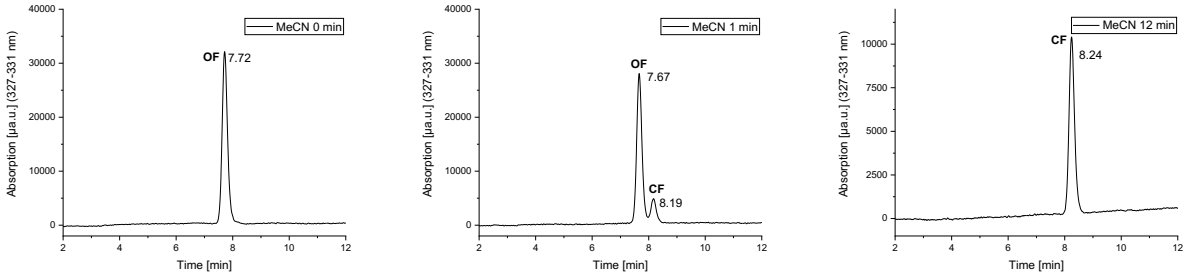

*Figure 176: left: start spectra of chlorophenyl-DTE(OMe) **147** ($1.8 \cdot 10^{-5}$ M in MeCN) (RT: 7.72 min), middle: after 1 min irradiation (RT: 7.67 and 8.19 min); right: after 12 min irradiation (RT: 8.24 min); MeCN/H_2O (+0.1% HCOOH) 90:10 to 100:0 in 10 min, 0.3 mL/min, detection wavelength 327-331 nm, irradiated with 345 nm LED.*

No chlorophenyl-DTE(OMe) **147** OF visible after 12 min -> 100:0 of compound **147** CF to OF in the pss under 345 nm LED in MeCN.

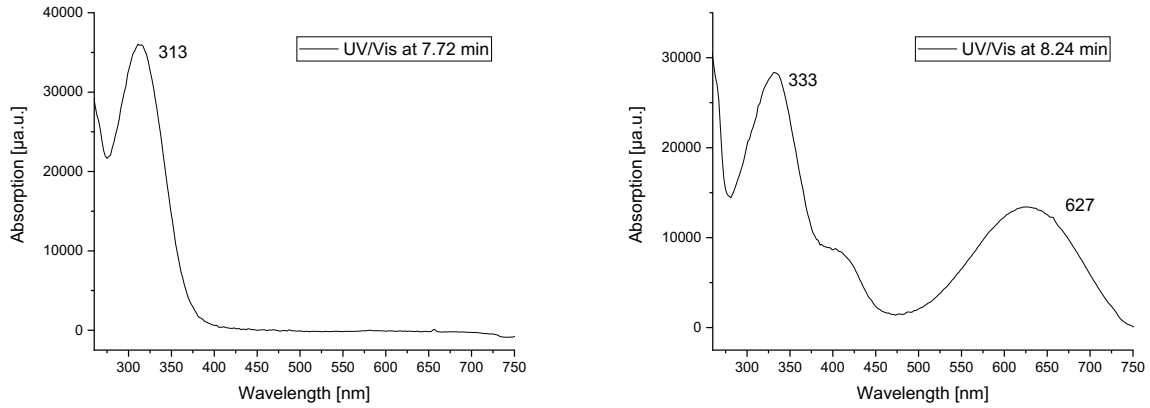

*Figure 177: UV/Vis-spectra via diode-array detector of chlorophenyl-DTE(OMe) **147** in HPLC, left: 0 min irradiation with 345 nm LED in MeCN, (RT: 7.72 min), right: 12 min irradiation with 345 nm LED in MeCN (RT: 8.24 min).*

5.2.1.7 Methoxyphenyl-DTE(OMe) 148

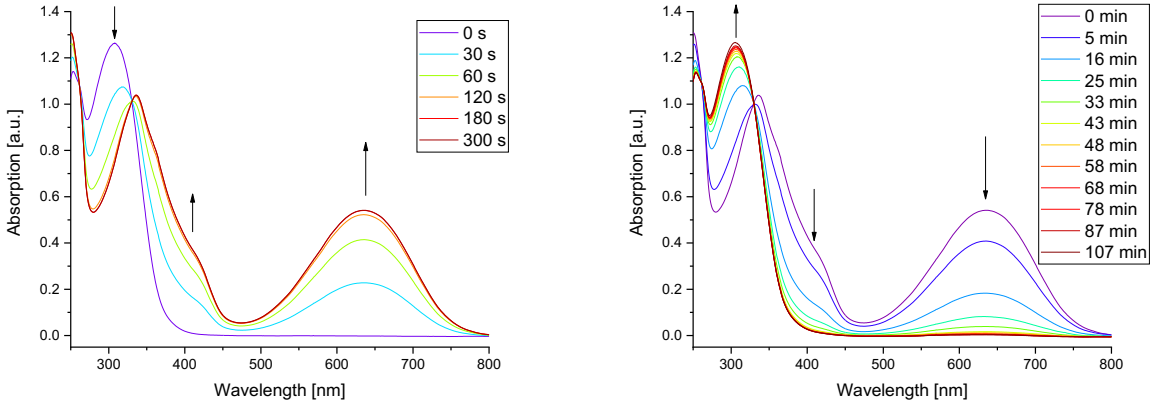

*Figure 178: methoxyphenyl-DTE(OMe) **148** with 4.1*10^{-5} M in MeCN, left: 148 OF irradiation with 326 nm mercury lamp with filter, HW 10 nm, 2.0 mW/cm², right: 148 CF irradiation with >500 nm xenon lamp with edge filter, 8.3 mW/cm² until pss was reached.*

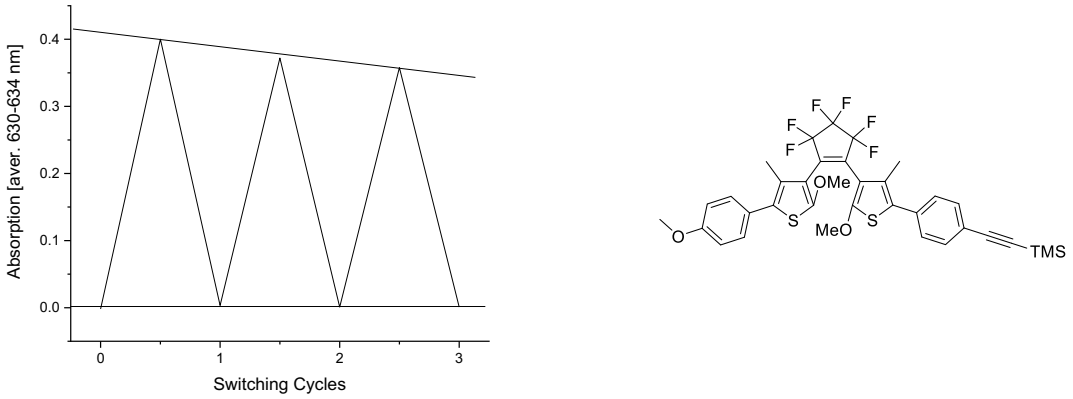

*Figure 179: left: switching cycles of methoxyphenyl-DTE(OMe) **148** with alternating 326 and >500 nm irradiation with average absorption at the maximum at 630-634 nm, right: structure of methoxyphenyl-DTE(OMe) **148**.*

5.2.1.8 NMR in situ irradiation of DTE(OMe) 148

Methoxyphenyl-DTE(OMe) **148** was dissolved in $CDCl_3$ and irradiated with 345 nm LED (7 µW/cm^2) for 120 min in a NMR-spectrometer (set-up see 2.4.2). The spectra were recorded each 5 min in a *Bruker* AvanceIII 500 MHz spectrometer and processed with *Bruker* TopSpin 3.5pl7 software.

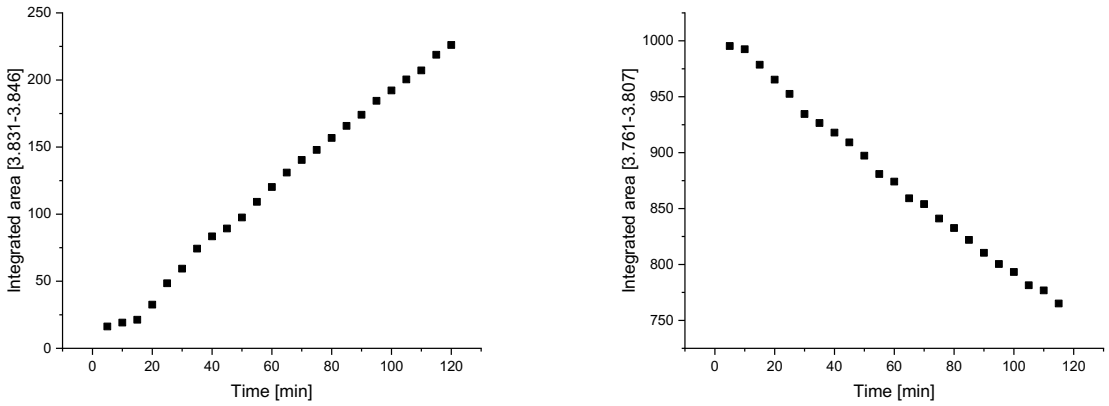

*Figure 180: change of the integrated area between left: 3.81-3.85 ppm; right: 3.76-3.81 ppm in the NMR spectra of DTE(OMe) **148** (1.7·10^{-4} M in $CDCl_3$) under 345 nm LED irradiation (without reaching pss).*

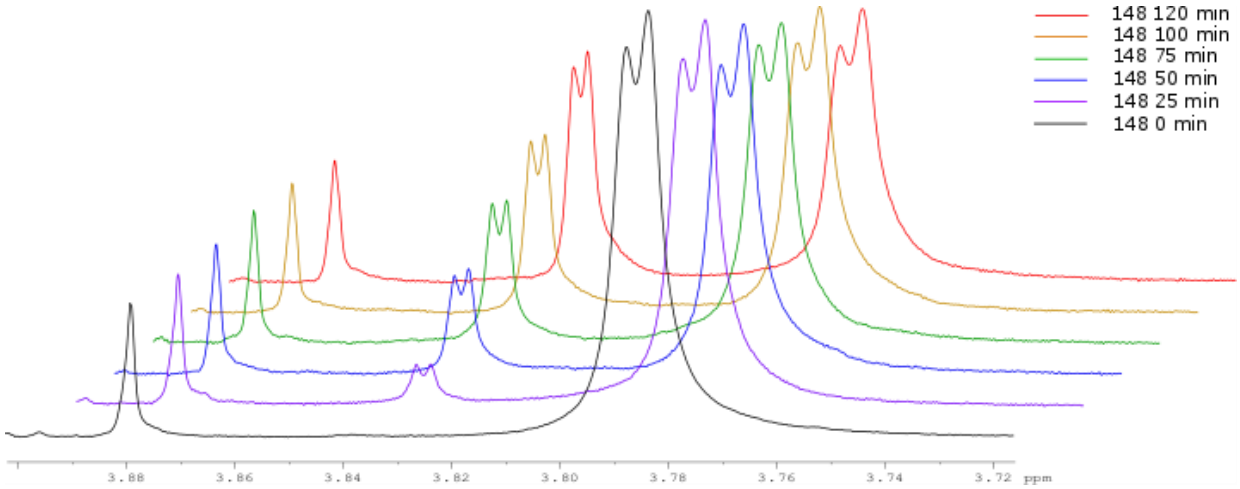

*Figure 181: NMR spectra (3.72-3.90 ppm) change of DTE(OMe) **148** (1.7·10^{-4} M in $CDCl_3$) under 345 nm LED irradiation (without reaching pss). The peak at 3.88 ppm is an inpurity.*

5.2.1.9 Phenyl-DTE(OMe) 149

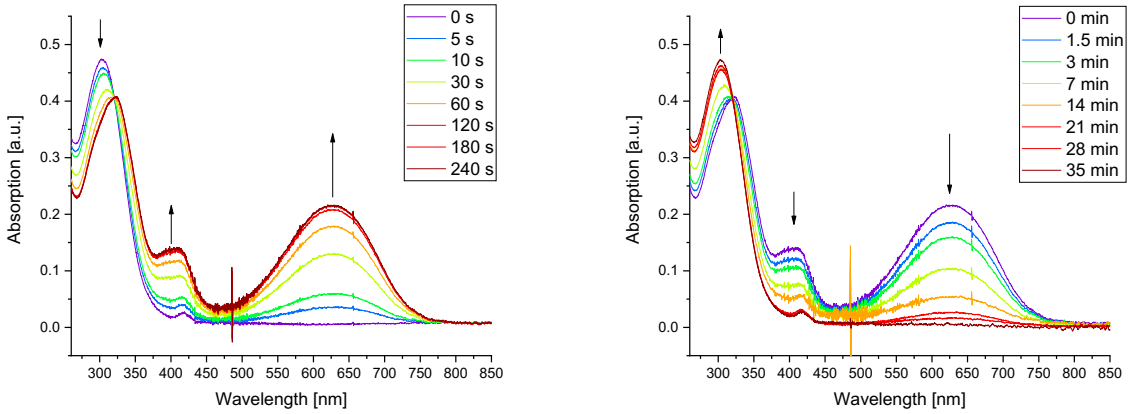

*Figure 182: Phenyl-DTE(OMe) **149** with 1.8*10^{-5} M in MeCN, left:**149** OF irradiation with 345 nm LED, HW 11 nm, 2.0 mW/cm^2, right: **149** CF irradiation with 632 nm LED until pss was reached, HW 18 nm, 250 mW/cm^2.*

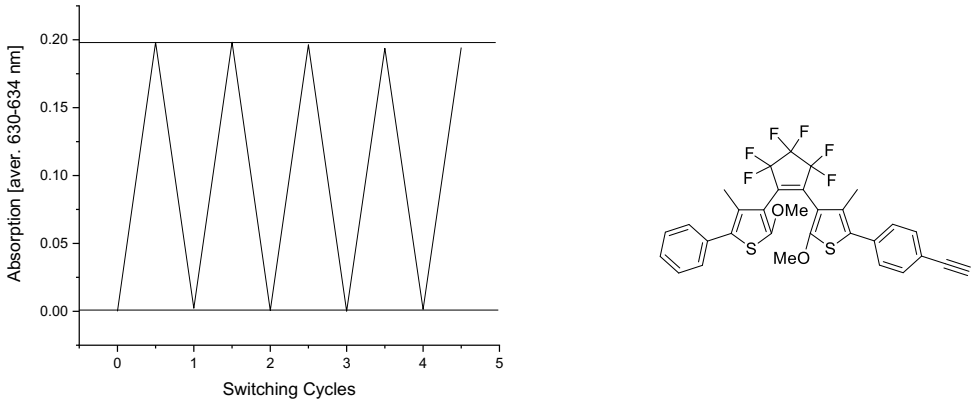

*Figure 183: left: switching cycles of phenyl-DTE(OMe) **149** with alternating 345 nm and 632 nm LED with average absorption at the maximum at 630-634 nm, right: structure of methoxyphenyl-DTE(OMe) **149**.*

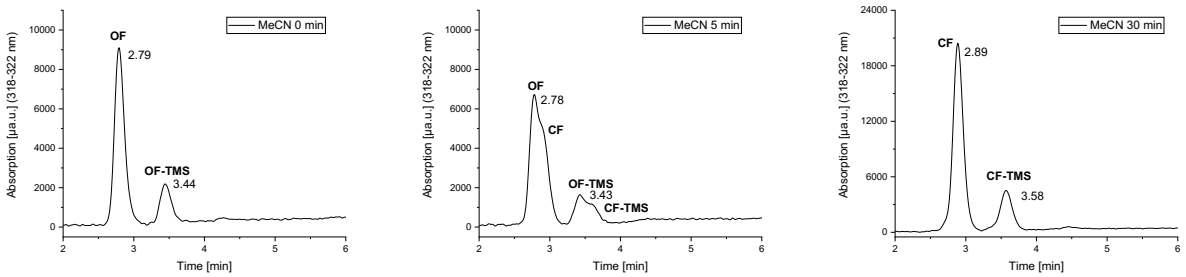

*Figure 184: left: start spectra of phenyl-DTE(OMe) **149** ($1.8 \cdot 10^{-5}$ M in MeCN) (RT: 7.72 min), middle: after 1 min irradiation (RT: 7.67 and 8.19 min); right: after 12 min irradiation (RT: 8.24 min); MeCN/H_2O (+0.1% HCOOH) 90:10 to 100:0 in 10 min, 0.3 mL/min, detection wavelength 318-332 nm, irradiated with 345 nm LED.*

No phenyl-DTE(OMe) **149** OF visible after 30 min -> 100:0 of compound **149** CF to OF in the pss under 345 nm LED in MeCN. The peaks for OF-TMS and CF-TMS show not full conversion of the reaction from DTE(OMe)-TMS **146** to DTE(OMe) **149**.

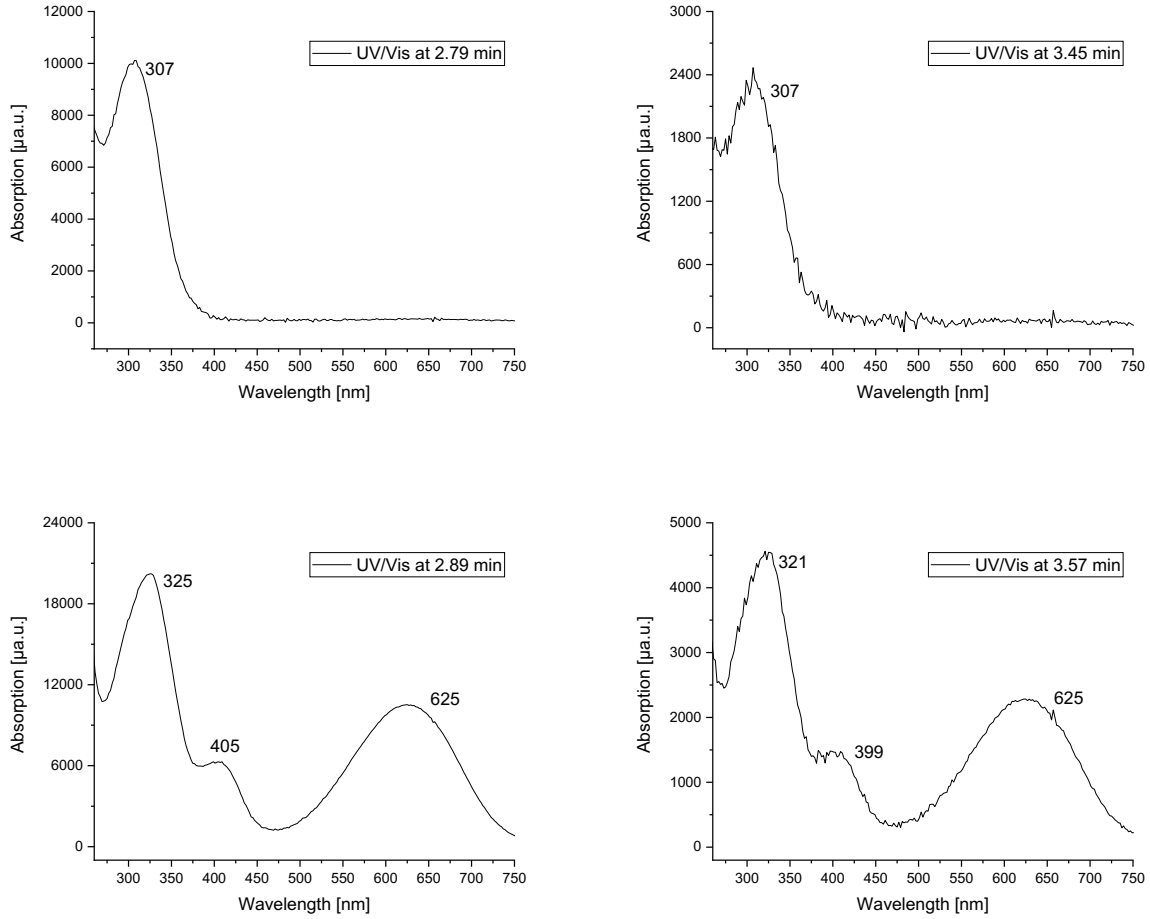

*Figure 185: UV/Vis-spectra via diode-array detector of benzoic acid-DTE(OMe) **149** in HPLC, top: left: 0 min irradiation with 345 nm LED in MeCN, (RT: 2.79 min), right: 0 min irradiation with 345 nm LED in MeCN, (RT: 3.45 min), bottom: left: 10 min irradiation with 345 nm LED in MeCN, (RT: 2.89 min), right: 10 min irradiation with 345 nm LED in MeCN (RT: 3.57 min).*

5.2.1.10 Chloro-DTE(OMe)-BODIPY 145

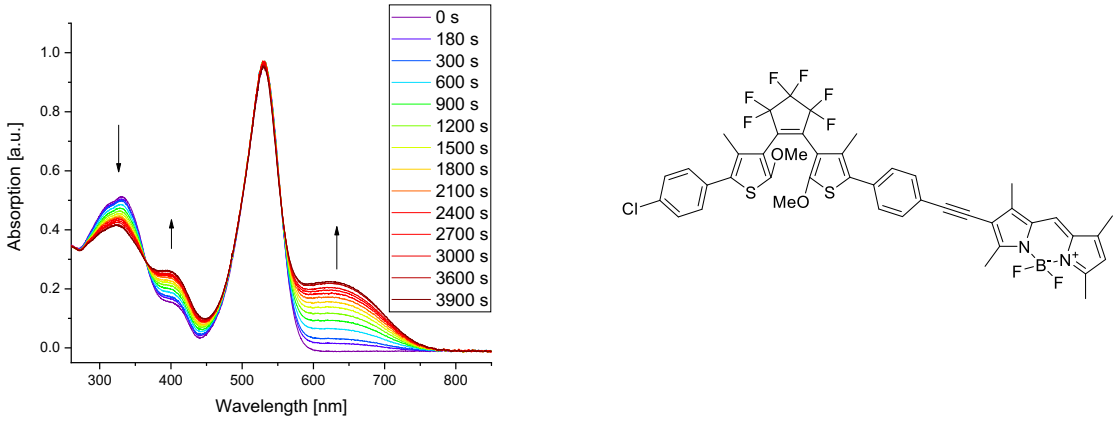

*Figure 186: chloro-DTE(OMe)-BODIPY **145** with 2.1*10^{-5} M in MeCN, left: OF irradiation with 345 nm LED, HW 11 nm, 2.0 mW/cm^2, right: CF irradiation with 632 nm LED until pss is reached, HW 18 nm, 250 mW/cm^2.*

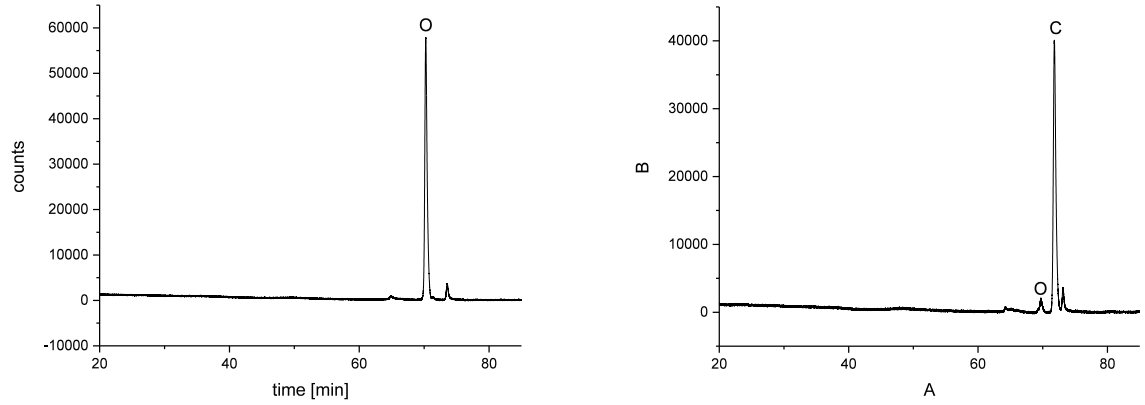

*Figure 187: HPLC condition: 50-100% MeCN/H_2O, then 100% MeCN isocratic, measured at 362 nm, LUNA C18, 1 mL/min, 10 µL injection volume, irradiated with 345 nm LED, 22 mW/cm^2: left: **145** OF, in MeCN with 6.44*10^{-4} M, right: **145** CF, pss$_\lambda$ at 362 nm in MeCN in 6.44*10^{-4} M.*

5.2.1.11 DTE(OMe)-BODIPY 20

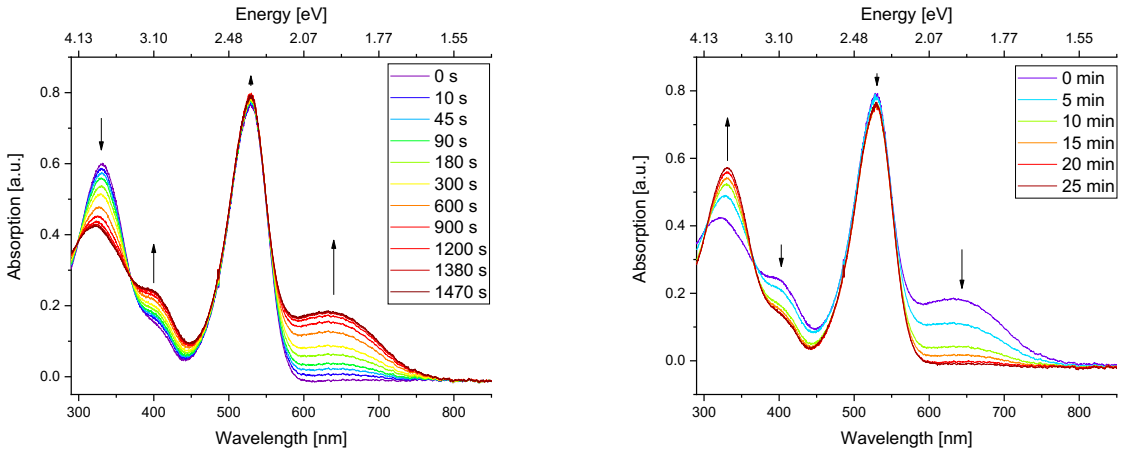

*Figure 188: DTE(OMe)-BODIPY **20** with 1.8*10^{-5} M in MeCN, left: OF irradiation with 345 nm LED, HW 11 nm, 2.0 mW/cm^2, right: CF irradiation with 632 nm LED until pss is reached, HW 18 nm, 250 mW/cm^2.*

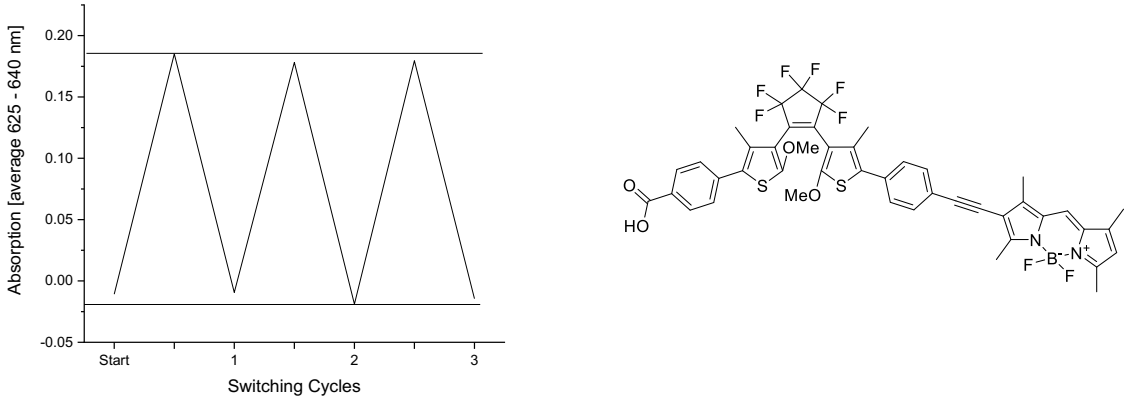

*Figure 189: left: switching cycles of DTE(OMe)-BODIPY **20** with alternating 345 nm and 632 nm LED with average absorption at the maximum at 630-634 nm, right: structure of DTE(OMe)-BODIPY **20**.*

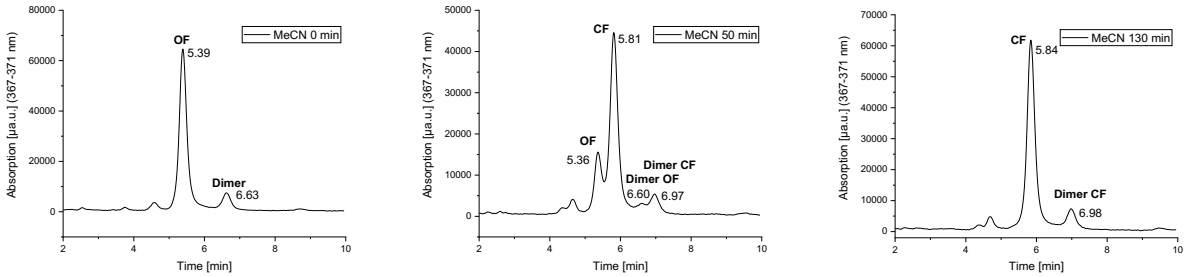

*Figure 190: left: start spectra of DTE(OMe)-BODIPY **20** ($1.8 \cdot 10^{-5}$ M in MeCN) (RT = 5.39 and 6.63 min), middle: after 50 min irradiation (RT: 5.36, 5.81, 6.60 and 6.97 min); right: after 130 min irradiation (RT: 5.84 and 6.98 min); MeCN/H_2O (+0.1% HCOOH) 92:8 isocratic, 0.2 mL/min, detection wavelength 367-371 nm, irradiated with 345 nm LED in MeCN.*

No DTE(OMe)-BODIPY **20** OF visible after 30 min -> 100:0 of compound **20** CF to OF in the pss under 345 nm LED in MeCN.

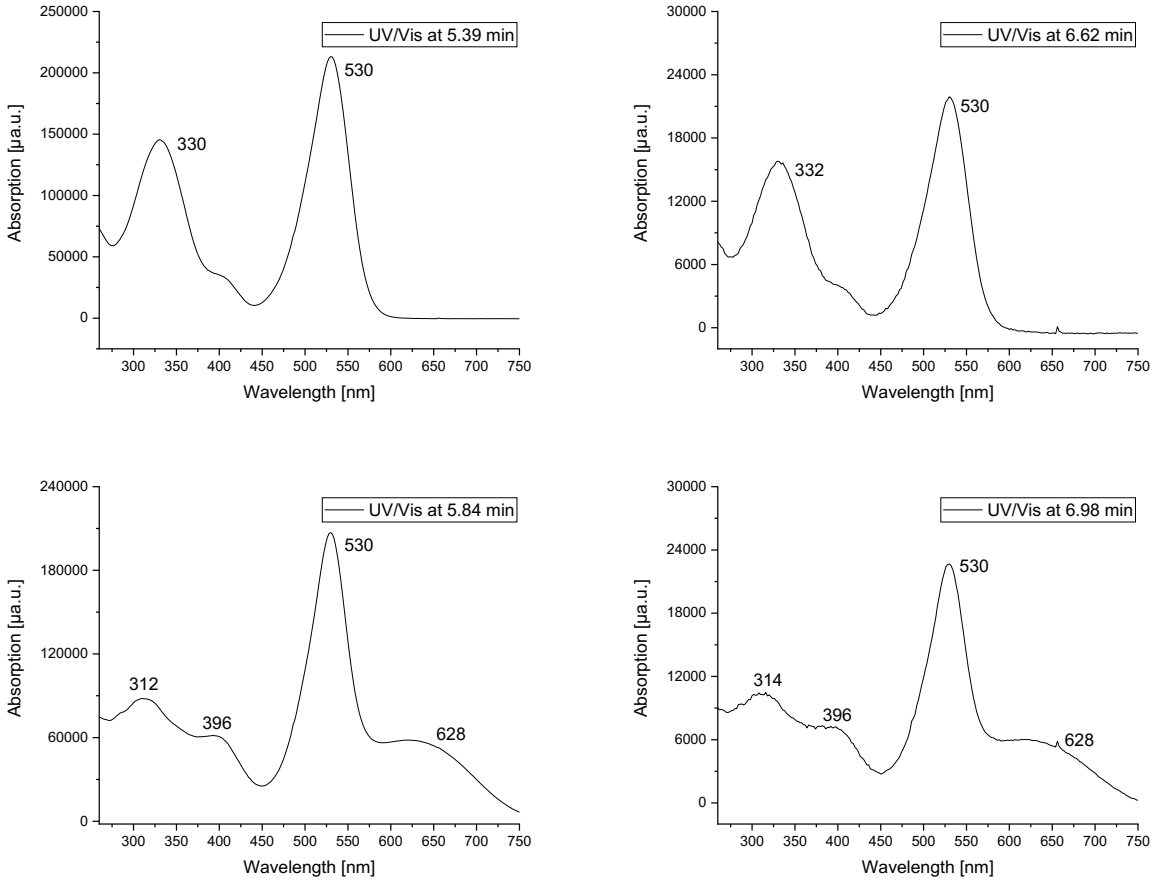

*Figure 191: UV/Vis-spectra via diode-array detector of DTE(OMe)-BODIPY **20** in HPLC, top: left: 0 min irradiation with 345 nm LED in MeCN, (RT: 5.39 min), right: 0 min irradiation with 345 nm LED in MeCN, (RT: 6.62 min), bottom: left: 130 min irradiation with 345 nm LED in MeCN, (RT: 5.84 min), right: 130 min irradiation with 345 nm LED in MeCN (RT: 6.98 min).*

5.2.1.12 Solvatochromism of DTE(OMe)-BODIPY 20

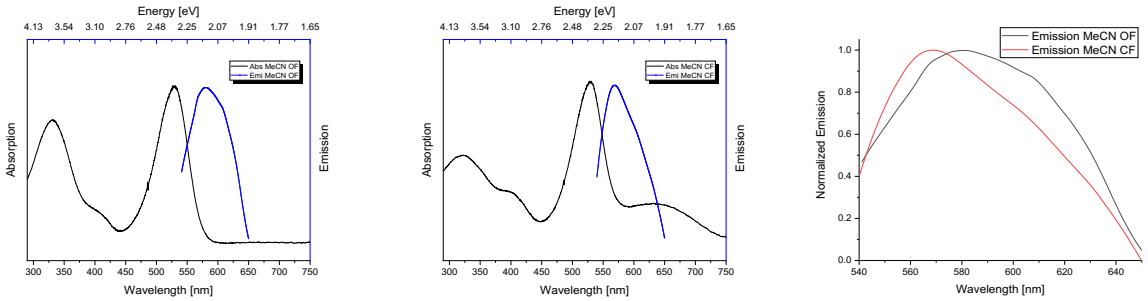

*Figure 192: absorption (black) and emission (blue) spectra of DTE(OMe)-BODIPY **20** in MeCN (1.8*10^{-5} M) of left: OF (λ_{Exc} 533 nm); middle: CF (λ_{Exc} 530 nm); right: stacked emission spectra of DTE(OMe)-BODIPY **20** OF (black) and CF (red).*

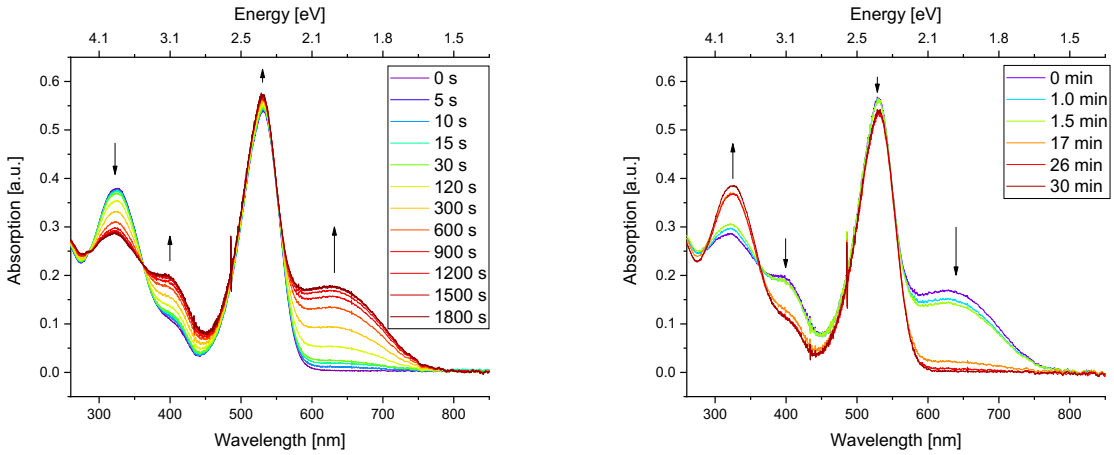

*Figure 193: absorption spectra of DTE(OMe)-BODIPY **20** in MeOH (1.8·10^{-5} M) after different irradiation times of left: 345 nm; right: 632 nm LED until pss is reached.*

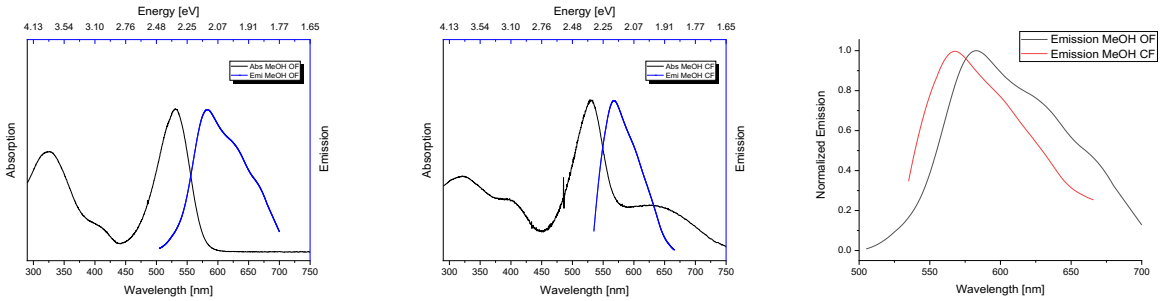

*Figure 194: absorption (black) and emission (blue) spectra of DTE(OMe)-BODIPY **20** in MeOH (1.8*10^{-5} M) of left: OF (λ_{Exc} 531 nm); middle: CF (λ_{Exc} 530 nm); right: stacked emission spectra of DTE(OMe)-BODIPY **20** OF (black) and CF (red).*

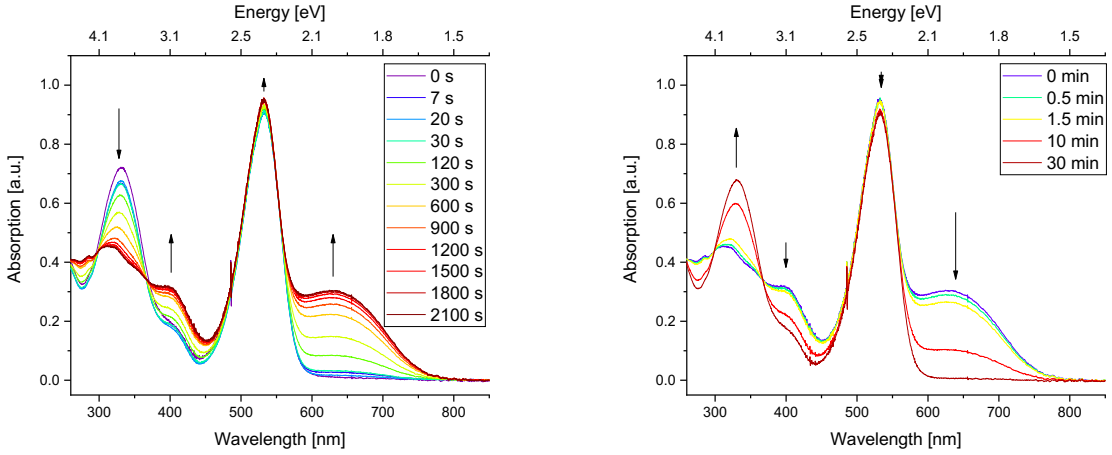

*Figure 195: absorption spectra of DTE(OMe)-BODIPY **20** in EtOAc (1.8·10^{-5} M) after different irradiation times of left: 345 nm; right: 632 nm LED until pss is reached.*

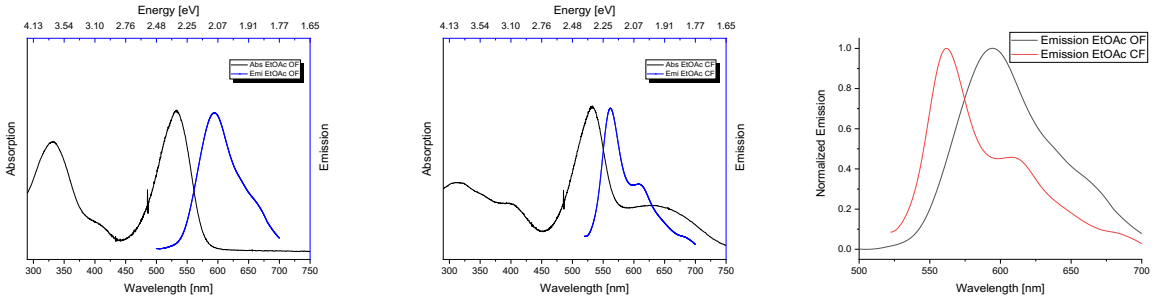

*Figure 196: absorption (black) and emission (blue) spectra of DTE(OMe)-BODIPY **20** in EtOAc (1.8·10^{-5} M) of left: OF (λ_{Exc} 532 nm); middle: CF (λ_{Exc} 532 nm); right: stacked emission spectra of DTE-BODIPY **20** OF (black) and CF (red).*

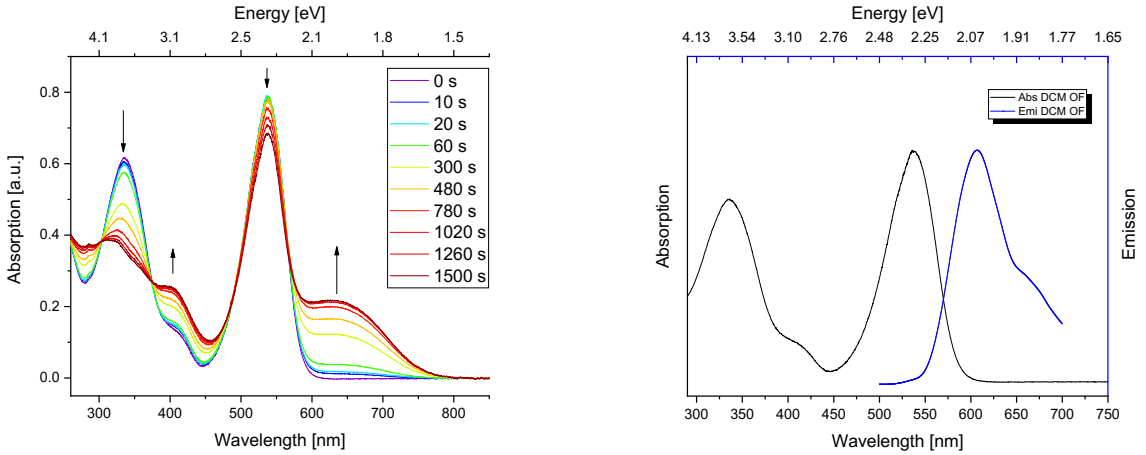

*Figure 197: left: absorption spectra of DTE(OMe)-BODIPY **20** in DCM ($1.8 \cdot 10^{-5}$ M) after different irradiation times of 345 nm LED; right: absorption (black) and emission (blue) spectra of DTE(OMe)-BODIPY **20** in DCM ($1.8 \cdot 10^{-5}$ M) of OF (λ_{Exc} 537 nm).*

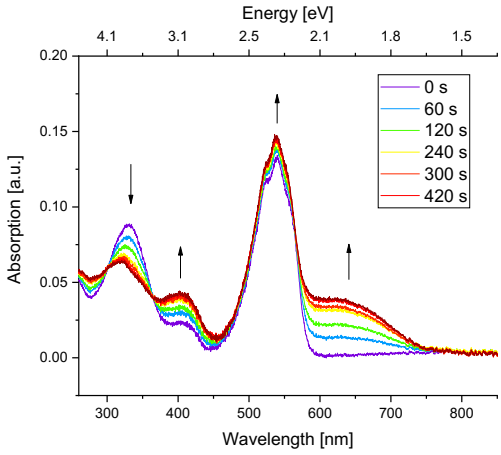

*Figure 198: absorption spectra of DTE(OMe)-BODIPY **20** in hexane (concentration not determined) after different irradiation times of 345 nm LED until pss is reached.*

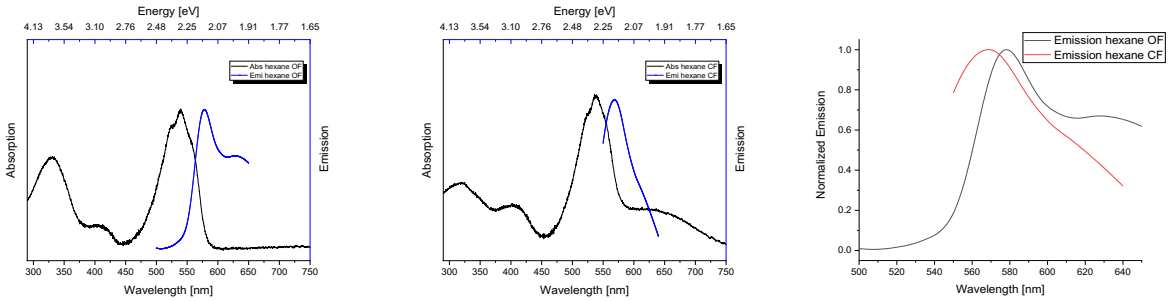

*Figure 199: absorption (black) and emission (blue) spectra of DTE(OMe)-BODIPY **20** in hexane (concentration not determined) of left: OF (λ_{Exc} 540 nm); middle: CF (λ_{Exc} 536 nm); right: stacked emission spectra of DTE-BODIPY **20** OF (black) and CF (red).*

5.2.1.13 BTD-DTE(OMe) 23

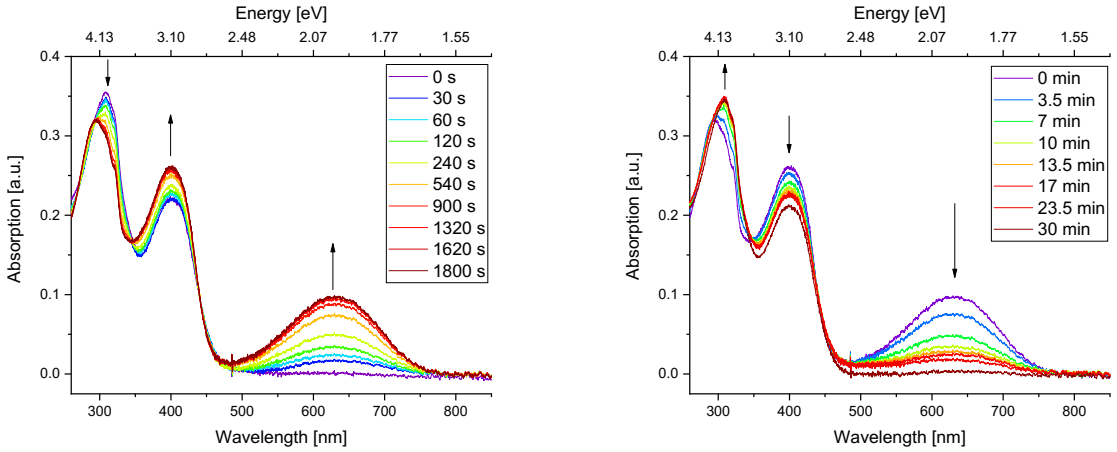

*Figure 200: BTD-DTE(OMe) **23** with 1.8*10^{-5} M in MeCN, left: OF irradiation with 345 nm LED, HW 11 nm, 2.0 mW/cm^2, right: CF irradiation with 632 nm LED until pss is reached, HW 18 nm, 250 mW/cm^2.*

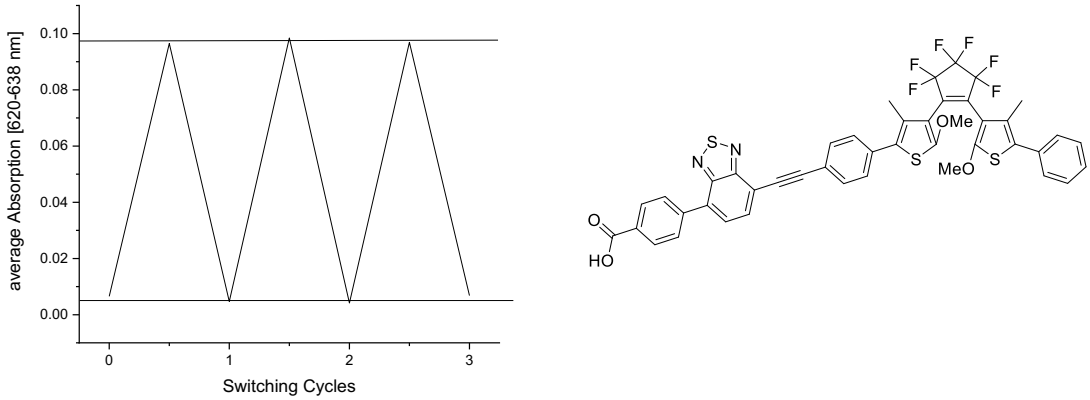

*Figure 201: left: switching cycles of BTD-DTE(OMe) **23** with alternating 345 nm and 632 nm LED with average absorption at the maximum at 620-638 nm, right: structure of BTD-DTE(OMe) **23**.*

5.2.1.14 Solvatochromism of BTD-DTE(OMe) 23

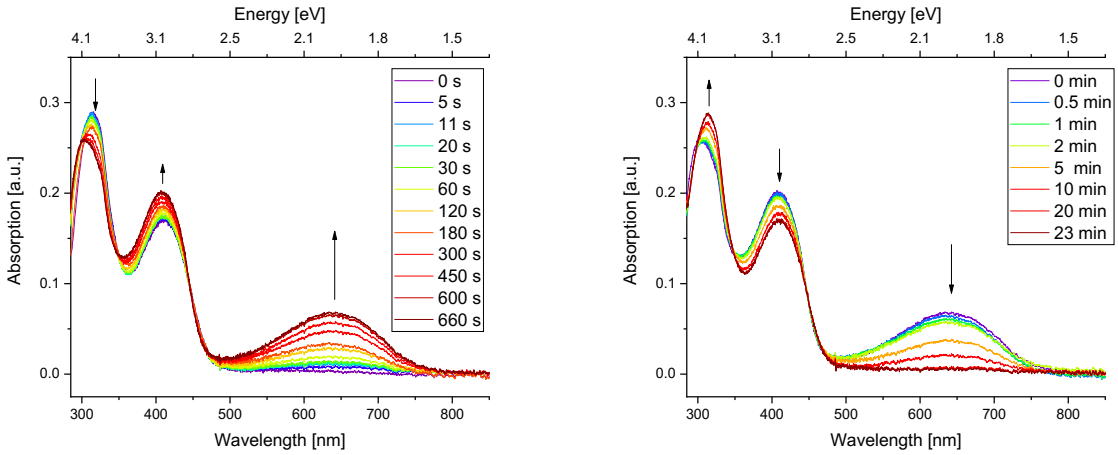

*Figure 202: absorption spectra of BTD-DTE(OMe) **23** in toluene ($9.0*10^{-6}$ M) after different irradiation times of left: 345 nm LED; right: 632 nm until pss is reached.*

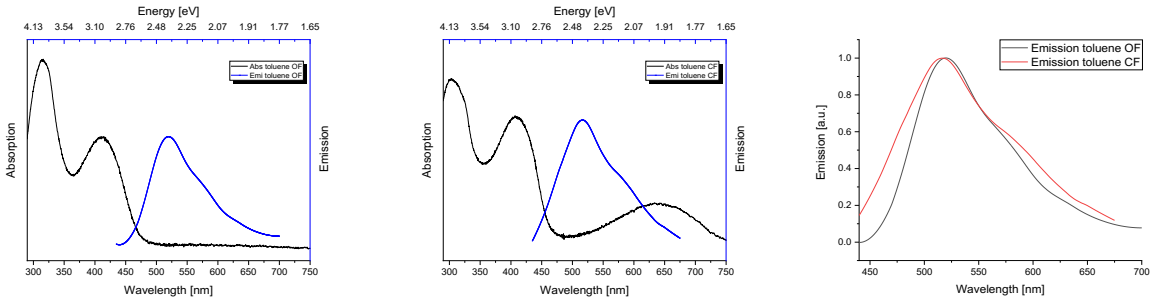

*Figure 203: absorption (black) and emission (blue) spectra of BTD-DTE(OMe) **23** in toluene (9.0*10^{-6} M) of left: OF (λ_{Exc} 412 nm); middle: CF (λ_{Exc} 408 nm); right: stacked emission spectra of BTD-DTE **23** OF (black) and CF (red).*

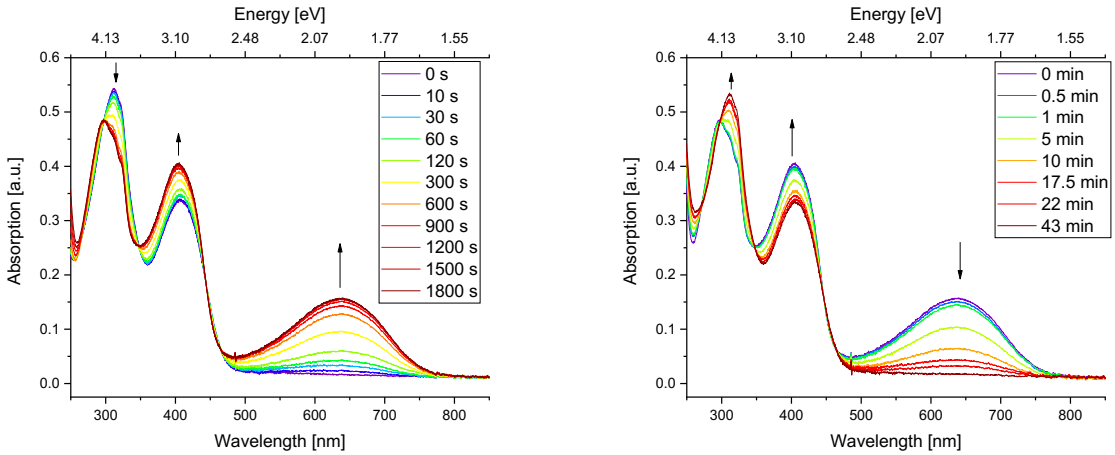

*Figure 204: absorption spectra of BTD-DTE(OMe) **23** in dioxane (1.8*10^{-5} M) after different irradiation times of left: 345 nm LED; right: 632 nm until pss is reached.*

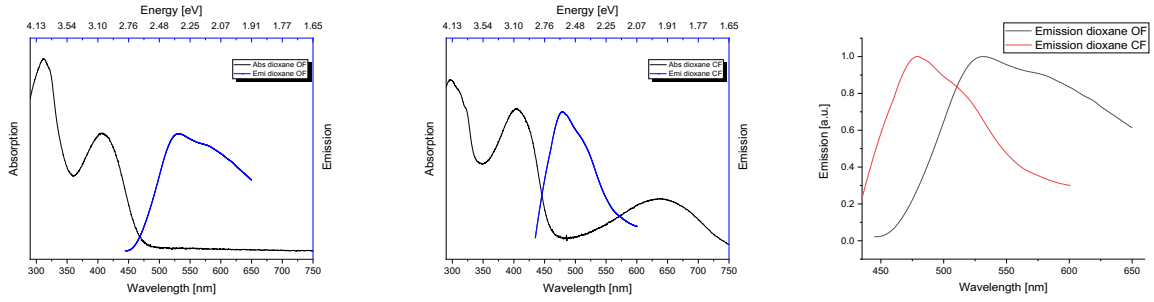

*Figure 205: absorption (black) and emission (blue) spectra of BTD-DTE(OMe) **23** in 1,4-dioxane (1.8*10^{-5} M) of left: OF (λ_{Exc} 407 nm); middle: CF (λ_{Exc} 404 nm); right: stacked emission spectra of BTD-DTE(OMe) **23** OF (black) and CF (red).*

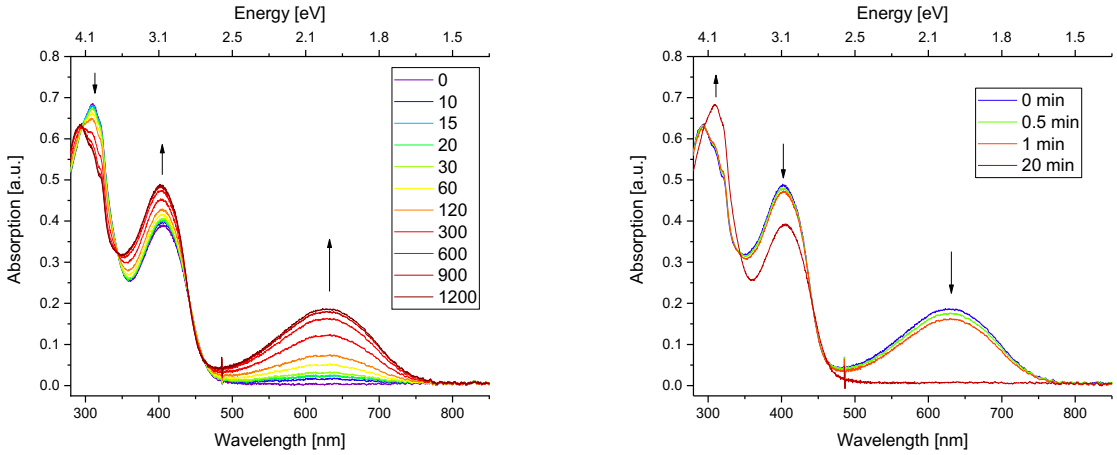

*Figure 206: absorption spectra of BTD-DTE(OMe) **23** in MTBE (1.8*10^{-5} M) after different irradiation times of left: 345 nm LED; right: 632 nm until pss is reached.*

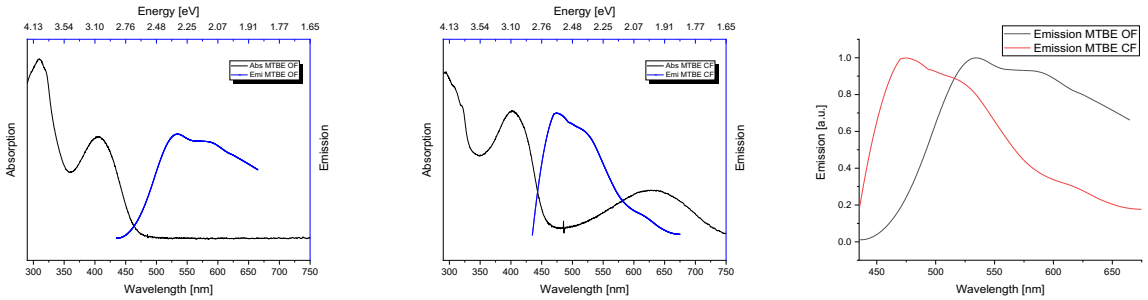

*Figure 207: absorption (black) and emission (blue) spectra of BTD-DTE(OMe) **23** in MTBE (1.8*10^{-5} M) of left: OF (λ_{Exc} 405 nm); middle: CF (λ_{Exc} 404 nm); right: stacked emission spectra of BTD-DTE(OMe) **23** OF (black) and CF (red).*

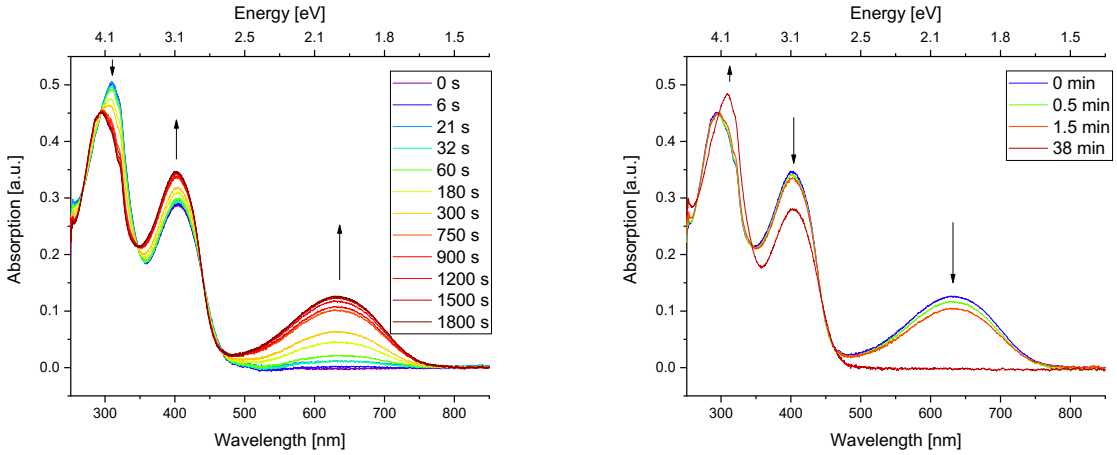

*Figure 208: absorption spectra of BTD-DTE(OMe) **23** in EtOAc ($1.8*10^{-5}$ M) after different irradiation times of left: 345 nm LED; right: 632 nm until pss is reached.*

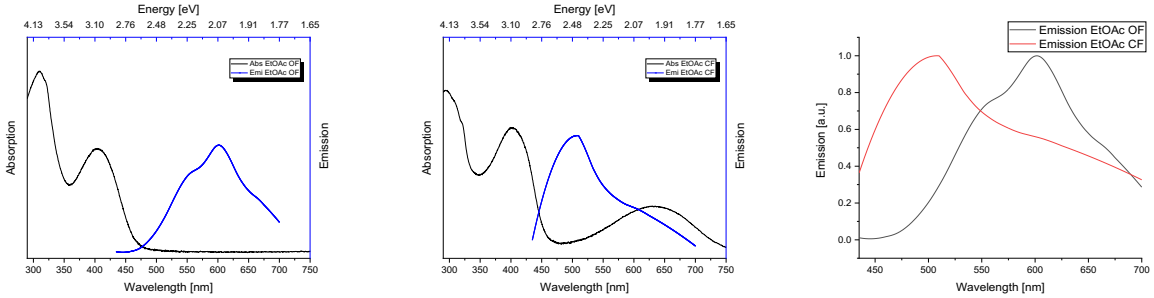

*Figure 209: absorption (black) and emission (blue) spectra of BTD-DTE(OMe) **23** in EtOAc ($1.8*10^{-5}$ M) of left: OF (λ_{Exc} 405 nm); middle: CF (λ_{Exc} 401 nm); right: stacked emission spectra of BTD-DTE(OMe) **23** OF (black) and CF (red).*

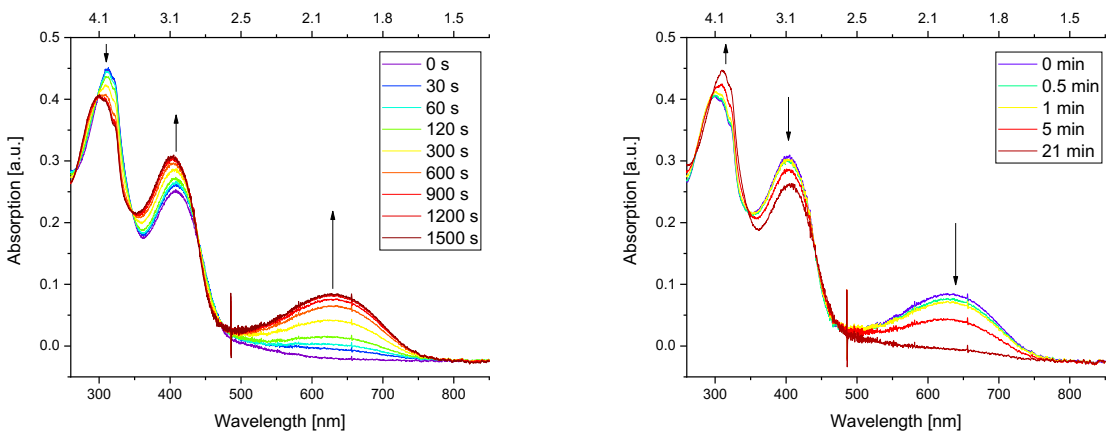

*Figure 210: absorption spectra of BTD-DTE(OMe) **23** in DCM (1.8*10^{-5} M) after different irradiation times of left: 345 nm LED; right: 632 nm until pss is reached.*

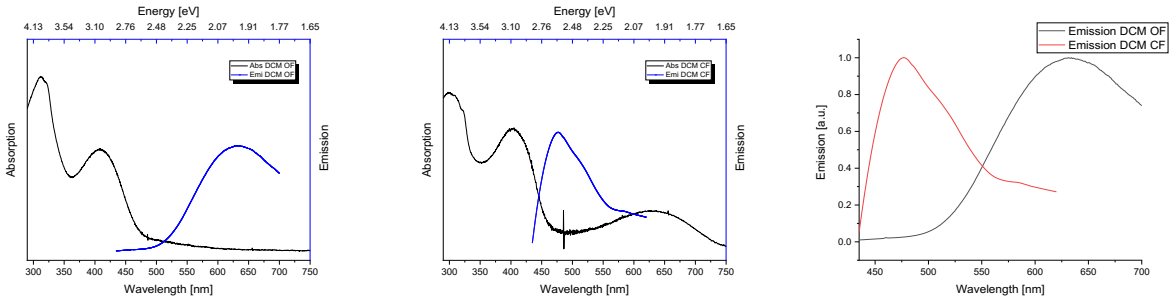

*Figure 211: absorption (black) and emission (blue) spectra of BTD-DTE(OMe) **23** in DCM (1.8*10^{-5} M) of left: OF (λ_{Exc} 407 nm); middle: CF (λ_{Exc} 403 nm); right: stacked emission spectra of BTD-DTE(OMe) **23** OF (black) and CF (red).*

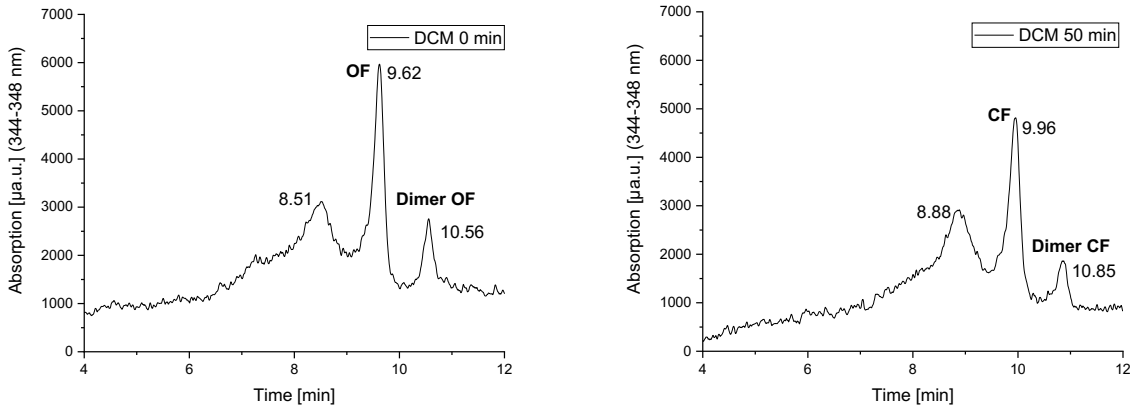

*Figure 212: start spectra of BTD-DTE(OMe) **23** ($2.2 \cdot 10^{-5}$ M in MeCN) (RT: 8.51, 9.62 and 10.56 min), right: after 50 min irradiation (RT: 8.88, 9.96 and 10.85 min); MeCN/H_2O (+0.1% HCOOH) 90:10 to 100:0 in 10 min, 0.3 mL/min, detection wavelength 345-349 nm, irradiated with 345 nm LED.*

No DTE(OMe)-BODIPY **23** OF visible after 50 min -> 100:0 of compound **23** CF to OF in the pss under 345 nm LED in MeCN. The peaks at 8.51 after 0 min irradiation and 8.88 min after 50 min irradiation show the same absorption spectra, as **23** OF and CF (see Figure 213). It can be assumed, that the separation in the LCMS of a sample dissolved in DCM is difficult.

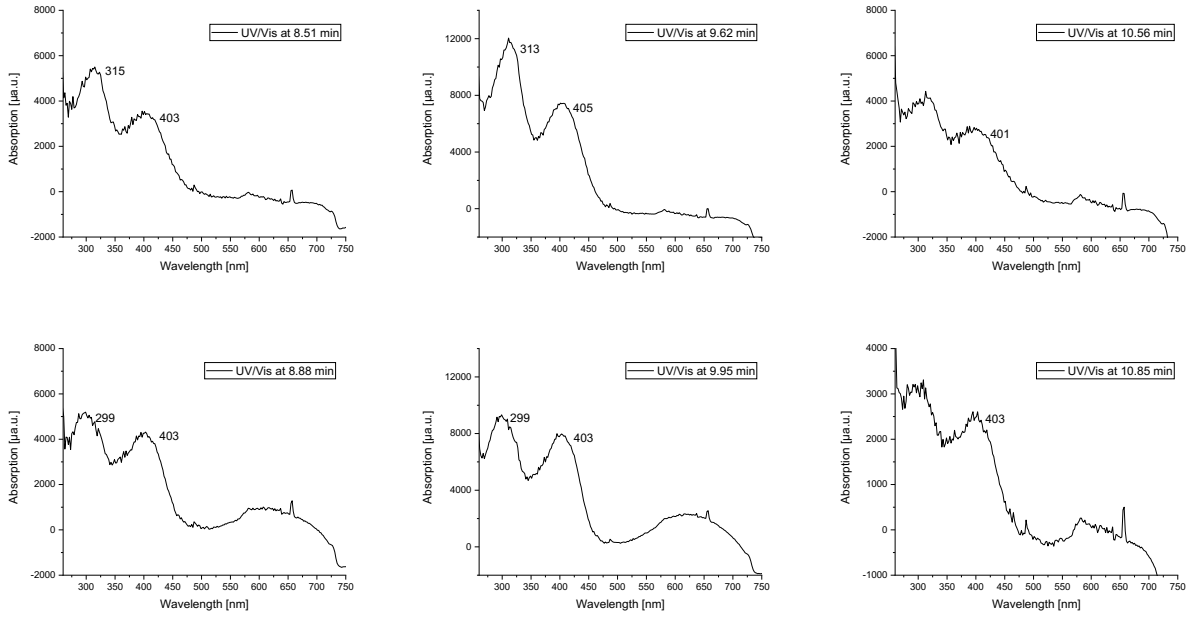

*Figure 213: UV/Vis-spectra via diode-array detector of BTD-DTE(OMe) **23** in HPLC, top left: 0 min irradiation with 345 nm LED in MeCN, (RT: 8.51 min), middle: 0 min irradiation with 345 nm LED in MeCN, (RT: 9.62 min), right: 0 min irradiation with 345 nm LED in MeCN, (RT: 10.56 min), bottom left: 50 min irradiation with 345 nm LED in MeCN, (RT: 8.88 min), middle: 50 min irradiation with 345 nm LED in MeCN, (RT: 9.95 min), right: 130 min irradiation with 345 nm LED in MeCN (RT: 10.85 min).*

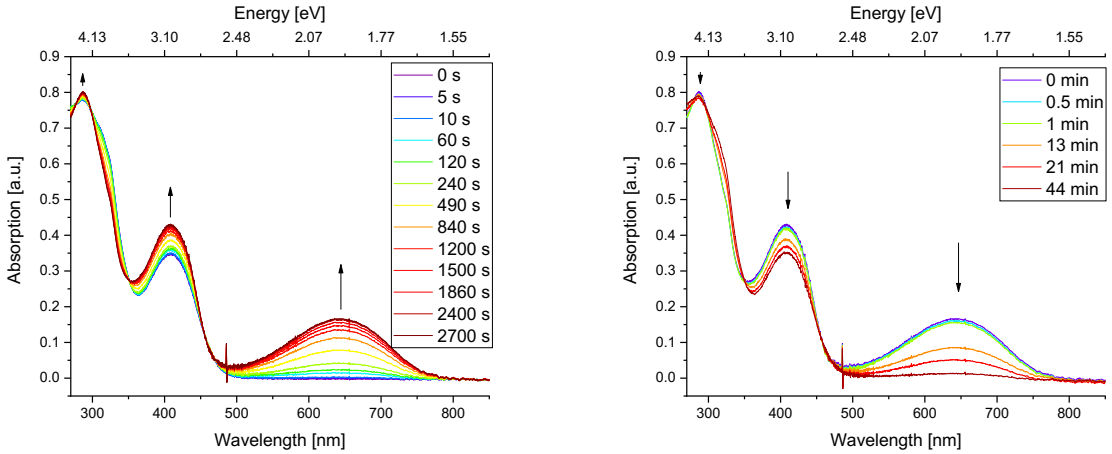

*Figure 214: absorption spectra of BTD-DTE(OMe) **23** in DMSO ($1.8*10^{-5}$ M) after different irradiation times of left: 345 nm LED; right: 632 nm until pss is reached.*

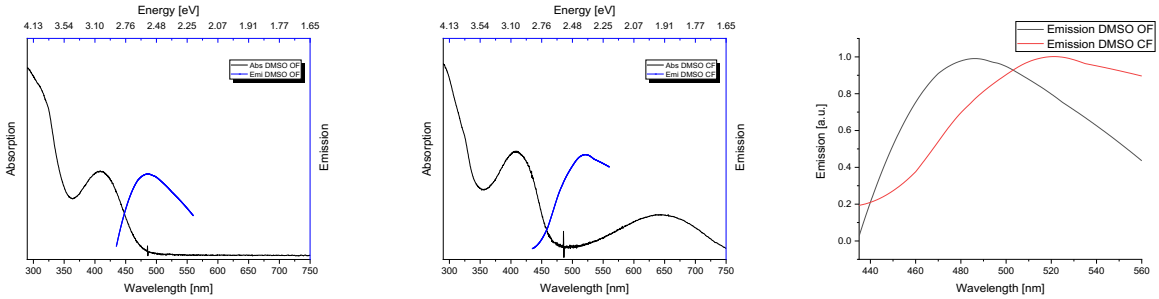

*Figure 215: absorption (black) and emission (blue) spectra of BTD-DTE(OMe) **23** in DMSO ($1.8*10^{-5}$ M) of left: OF (λ_{Exc} 408 nm); middle: CF (λ_{Exc} 407 nm); right: stacked emission spectra of BTD-DTE(OMe) **23** OF (black) and CF (red).*

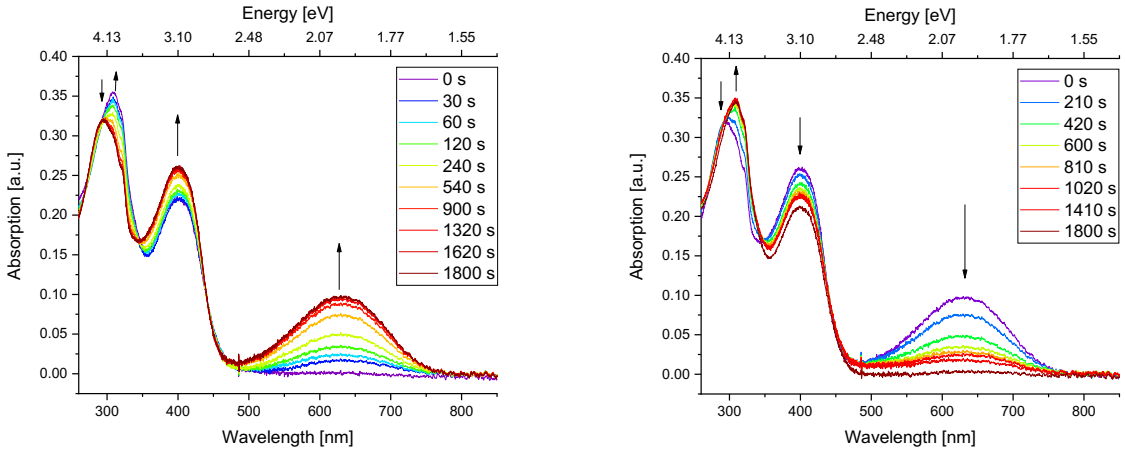

*Figure 216: absorption spectra of BTD-DTE(OMe) **23** in MeCN (1.8*10^{-5} M) after different irradiation times of left: 345 nm LED; right: 632 nm until pss is reached.*

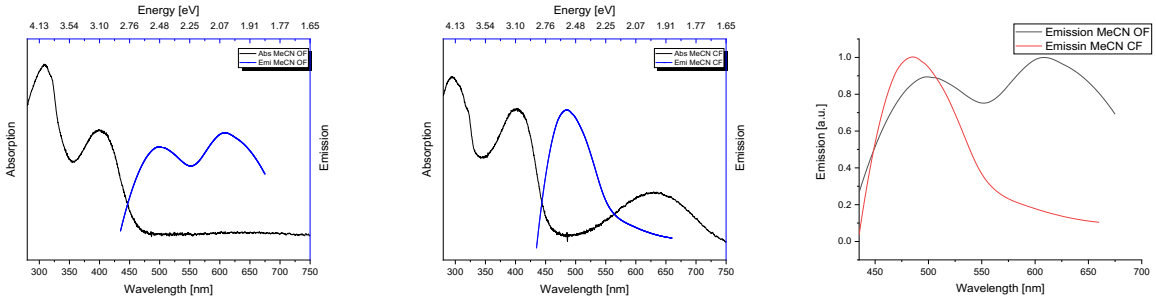

*Figure 217: absorption (black) and emission (blue) spectra of BTD-DTE(OMe) **23** in MeCN (1.8*10^{-5} M) of left: OF (λ_{Exc} 405 nm); middle: CF (λ_{Exc} 403 nm); right: stacked emission spectra of BTD-DTE(OMe) **23** OF (black) and CF (red).*

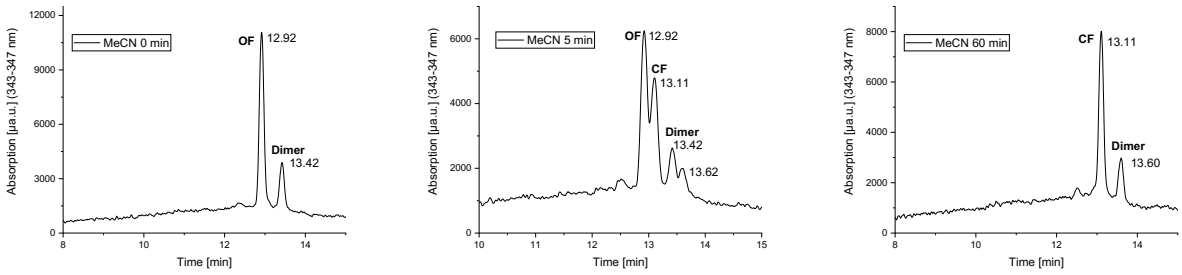

*Figure 218: left: start spectra of BTD-DTE(OMe) **23** (1.8·10^{-5} M in MeCN) (RT: 12.92 and 13.42 min), middle: after 5 min irradiation (RT: 12.92, 13.11, 13.42 and 13.62 min); right: after 60 min irradiation (RT: 13.11 and 13.60 min); MeCN/H_2O (+0.1% HCOOH) 90:10 to 100:0 in 10 min, 0.3 mL/min, detection wavelength 345-349 nm, irradiated with 345 nm LED in MeCN.*

RT [min]	Start RT [min]	End RT [min]	Area	%Area
12.93	12.83	12.93	1.392.811	1.87
13.11	12.94	13.31	59.374.196	79.56
13.6	13.48	13.72	13.864.772	18.58

➔ 98:2 CF: OF in MeCN in pss

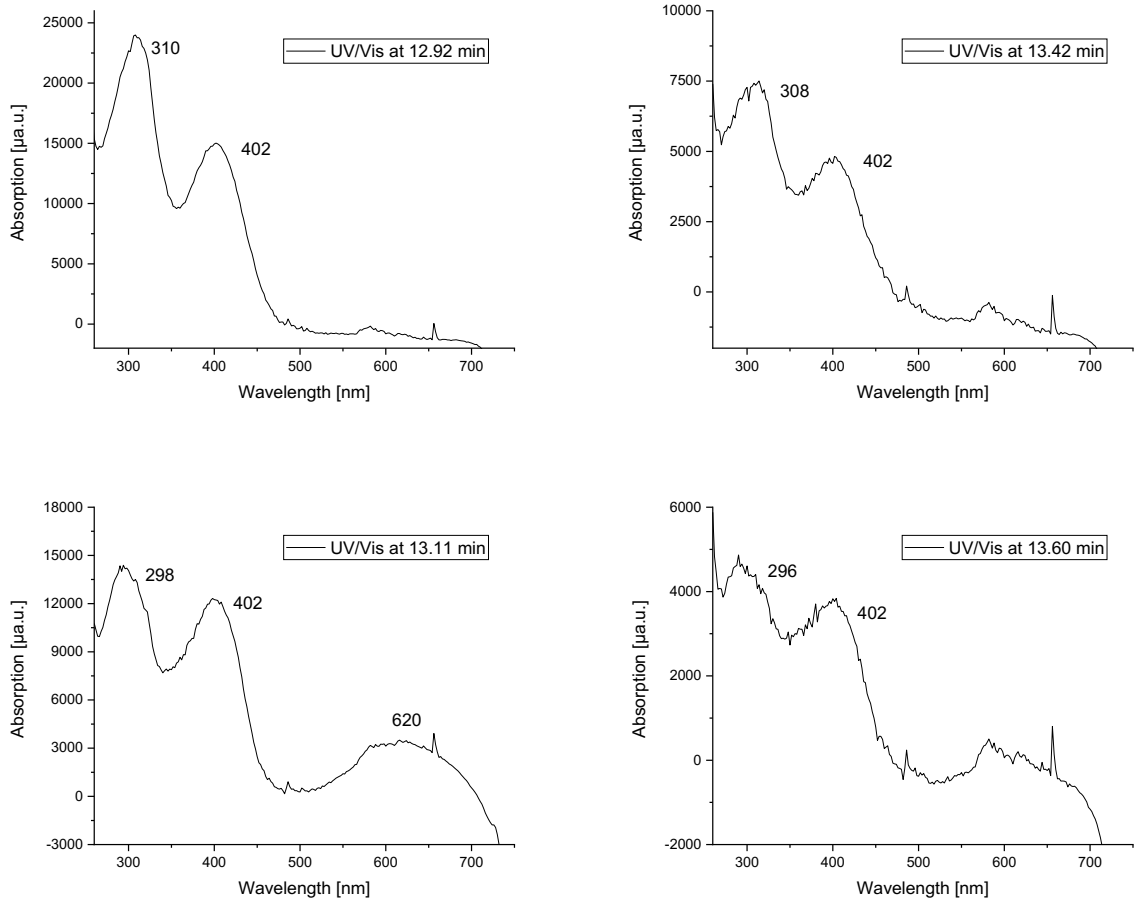

*Figure 219: UV/Vis-spectra via diode-array detector of BTD-DTE(OMe) **23** in HPLC, top: left: 0 min irradiation with 345 nm LED in MeCN, (RT: 12.92 min), right: 0 min irradiation with 345 nm LED in MeCN, (RT: 13.42 min), bottom: left: 130 min irradiation with 345 nm LED in MeCN, (RT: 13.11 min), right: 130 min irradiation with 345 nm LED in MeCN (RT: 13.60 min).*

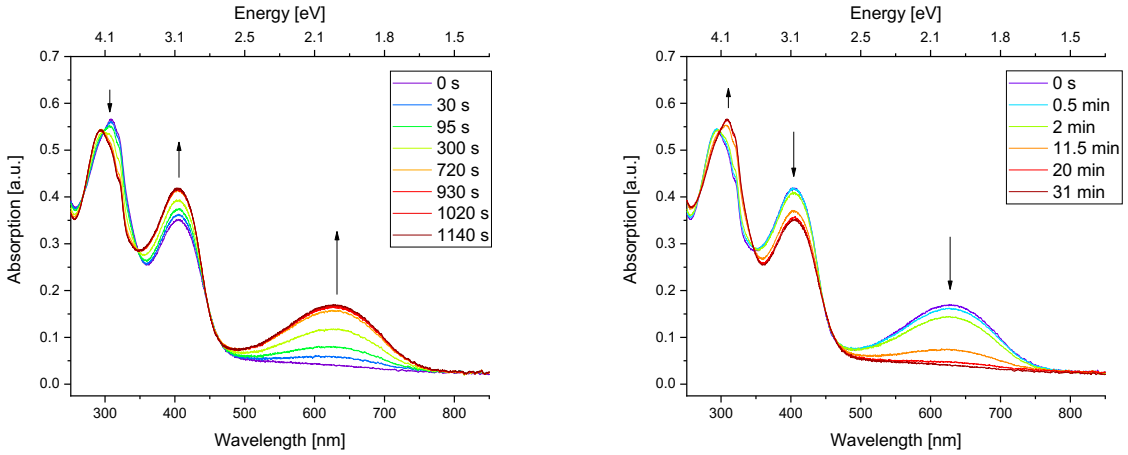

*Figure 220: absorption spectra of BTD-DTE(OMe) **23** in MeOH ($1.8*10^{-5}$ M) after different irradiation times of left: 345 nm LED; right: 632 nm until pss was reached.*

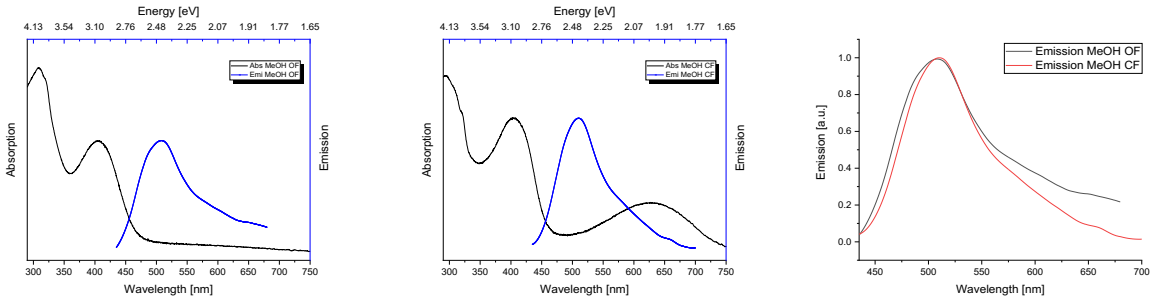

*Figure 221: absorption (black) and emission (blue) spectra of BTD-DTE(OMe) **23** in MeOH ($1.8*10^{-5}$ M)) of left: OF (λ_{Exc} 405 nm); middle: CF (λ_{Exc} 404 nm); right: stacked emission spectra of BTD-DTE(OMe) **23** OF (black) and CF (red).*

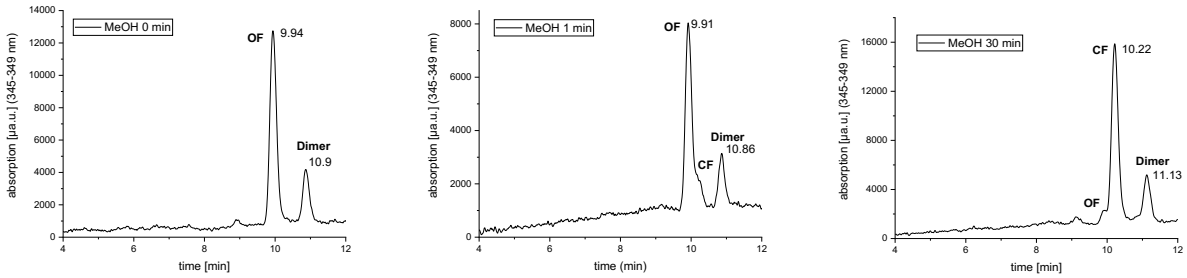

Figure 222: left: start spectra of BTD-DTE(OMe) ***23*** *($2.0 \cdot 10^{-5}$ M in MeCN) (RT: 9.94 and 10.9 min), middle: after 1 min irradiation (RT: 9.91 and 10.86 min); right: after 30 min irradiation (RT: 10.22 and 11.13 min); MeCN/H_2O (+0.1% HCOOH) 90:10 to 100:0 in 10 min, 0.3 mL/min, detection wavelength 345-349 nm, irradiated with 345 nm LED in MeOH.*

RT [min]	Start RT [min]	End RT [min]	Area	%Area
9.95	9.75	9.98	13.488.482	4.64
10.22	9.98	10.53	217.518.224	74.76
11.13	10.91	11.35	59.940.608	20.6

➔ 94:6 CF: OF in MeOH in pss

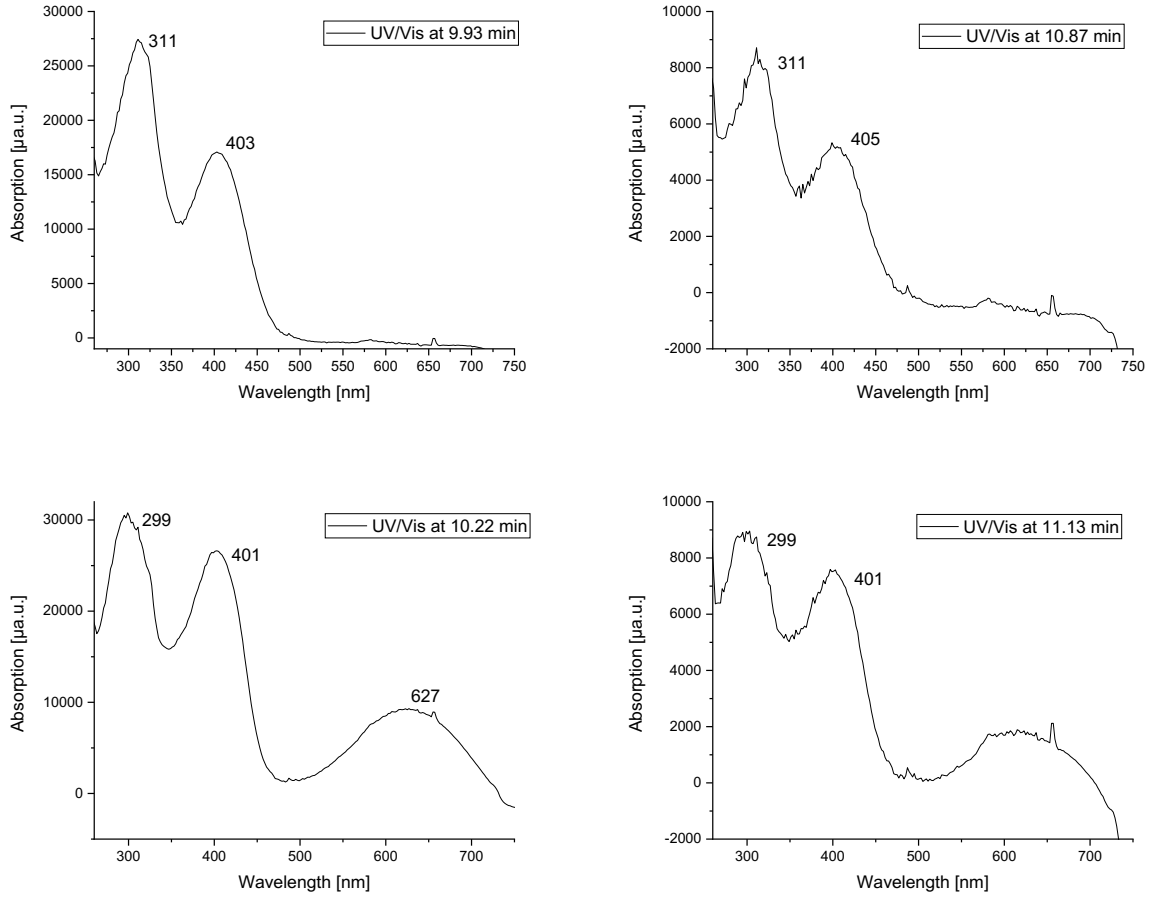

*Figure 223: UV/Vis-spectra via diode-array detector of BTD-DTE(OMe) **23** in HPLC, top: left: 0 min irradiation with 345 nm LED in MeOH, (RT: 9.93 min), right: 0 min irradiation with 345 nm LED in MeOH, (RT: 10.87 min), bottom: left: 130 min irradiation with 345 nm LED in MeOH, (RT: 10.22 min), right: 130 min irradiation with 345 nm LED in MeOH (RT: 11.13 min).*

5.3 CALCULATIONS

5.3.1.1 Quantum yields for Cyclization and Cycloreversion

Compound	$1000 I_0\left(1-10^{-A'(0)}\right) * \varepsilon_B^{obs}$	$\frac{dA^{obs}(t)}{dt}$	Φ_X
145 MeCN OF	10^3*3.473*10^{15}*(1-$10^{-1.21*1.8*0.1}$)*1.05*10^4 / 6.022*10^{23} = 2.39*10^{-2}	6.00*10^{-3}	2.25*10^{-1}
145 MeCN CF	10^3*7.954*10^{17}*(1-$10^{-1.8*1.05*0.1}$)*1.05*10^4 / 6.022*10^{23} = 5.453	3.87*10^{-4}	7.10*10^{-5}
155 MeCN OF	10^3*3.473*10^{15}*(1-$10^{-1.59*1.8*0.1}$)*9.72*10^3 / 6.022*10^{23} = 2.71*10^{-2}	3.90*10^{-3}	1.14*10^{-1}
155 MeCN CF	10^3*7.954*10^{17}*(1-$10^{-1.8*9.72*0.01}$)*9.72*10^3 / 6.022*10^{23} = 4.257	1.87*10^{-4}	4.39*10^{-5}
147 MeCN OF	10^3*3.473*10^{15}*(1-$10^{-1.74*1.8*0.1}$)*1.54*10^4 / 6.022*10^{23} = 4.56*10^{-2}	5.39*10^{-3}	1.18*10^{-1}
147 MeCN CF	10^3*7.954*10^{17}*(1-$10^{-1.8*1.54*0.1}$)*1.54*10^4 / 6.022*10^{23} = 9.597	2.98*10^{-4}	3.11*10^{-5}
149 MeCN OF	10^3*3.473*10^{15}*(1-$10^{-9.65*1.8*0.01}$)*1.13*10^4 / 6.022*10^{23} = 2.15*10^{-2}	4.09*10^{-3}	1.90*10^{-1}
149 MeCN CF	10^3*7.954*10^{17}*(1-$10^{-1.8*1.13*0.1}$)*1.13*10^4 / 6.022*10^{23} = 5.581	3.12*10^{-4}	5.59*10^{-5}
3 MeCN OF	10^3*3.473*10^{15}*(1-$10^{-5.35*1.8*0.01}$)*1.13*10^4 / 6.022*10^{23} = 1.32*10^{-2}	1.94*10^{-3}	1.49*10^{-1}
3 MeCN CF	10^3*7.954*10^{17}*(1-$10^{-1.8*1.13*0.1}$)*1.13*10^4 / 6.022*10^{23} = 5.581	6.348*10^{-4}	1.13*10^{-4}
20 MeCN OF	10^3*3.473*10^{15}*(1-$10^{-1.8*2.86*0.1}$)*1.02*10^4 / 6.022*10^{23} = 4.08*10^{-2}	5.44±0.63*10^{-4}	1.33*10^{-2}
20 MeCN CF	10^3*7.954*10^{17}*(1-$10^{-1.02*1.8*0.1}$)*1.02*10^4 / 6.022*10^{23} = 4.652	2.36*10^{-4}	5.07*10^{-5}
20 MeOH OF	10^3*3.473*10^{15}*(1-$10^{-1.8*1.68*0.1}$)*9.54*10^3 / 6.022*10^{23} = 2.76*10^{-2}	6.98±1.30*10^{-4}	2.53*10^{-2}
20 MeOH CF	10^3*7.954*10^{17}*(1-$10^{-9.54*1.8*0.01}$)*9.54*10^3 / 6.022*10^{23} = 4.12	2.76±0.09*10^{-4}	6.70*10^{-5}

20 EtOAc OF	$10^3*3.473*10^{15}*(1-10^{-1.8*3.62*0.1})*1.58*10^4$ / $6.022*10^{23}$ = $1.15*10^{-2}$	$9.94\pm1.98*10^{-4}$	$8.64*10^{-2}$
20 EtOAc CF	$10^3*7.954*10^{17}*(1-10^{-1.58*1.8*0.1})*1.58*10^4$ / $6.022*10^{23}$ = 10.02	$5.98\pm1.26*10^{-4}$	$5.97*10^{-5}$
23 MeOH OF	$10^3*3.473*10^{15}*(1-10^{-1.42*1.8*0.1})*7.61*10^3$ / $6.022*10^{23}$ = $1.93*10^{-2}$	$5.07\pm0.47*10^{-4}$	$2.63*10^{-2}$
23 MeOH CF	$10^3*7.954*10^{17}*(1-10^{-7.61*1.8*0.01})*7.61*10^3$ / $6.022*10^{23}$ = 2.719	$2.094\pm0.13*10^{-4}$	$7.70*10^{-5}$
23 MeCN OF	$10^3*3.473*10^{15}*(1-10^{-1.8*9.7*0.01})*5.6*10^3$ / $6.022*10^{23}$ = $1.07*10^{-2}$	$3.56*10^{-4}$	$3.33*10^{-2}$
23 MeCN CF	$10^3*7.954*10^{17}*(1-10^{-5.6*1.8*0.01})*5.6*10^3$ / $6.022*10^{23}$ = 1.63	$1.26*10^{-4}$	$7.73*10^{-5}$
23 EtOAc OF	$10^3*3.473*10^{15}*(1-10^{-1.23*1.8*0.1})*7.07*10^3$ / $6.022*10^{23}$ = $1.628*10^{-2}$	$4.34\pm0.41*10^{-4}$	$2.67*10^{-2}$
23 EtOAc CF	$10^3*7.954*10^{17}*(1-10^{-7.07*1.8*0.01})*7.07*10^3$ / $6.022*10^{23}$ = 2.37	$2.32\pm0.13*10^{-4}$	$9.80*10^{-5}$
23 Dioxane OF	$10^3*3.473*10^{15}*(1-10^{-1.33*1.8*0.1})*6.75*10^3$ / $6.022*10^{23}$ = $1.64*10^{-2}$	$6.82*10^{-4}$	$4.16*10^{-2}$
23 Dioxane CF	$10^3*7.954*10^{17}*(1-10^{-6.75*1.8*0.01})*6.75*10^3$ / $6.022*10^{23}$ = 2.18	$1.97\pm0.07*10^{-4}$	$9.04*10^{-5}$
23 DMSO OF	$10^3*3.473*10^{15}*(1-10^{-1.74*1.8*0.1})*9.25*10^3$ / $6.022*10^{23}$ = $2.74*10^{-2}$	$2.32*10^{-4}$	$8.47*10^{-3}$
23 DMSO CF	$10^3*7.954*10^{17}*(1-10^{-9.25*1.8*0.01})*9.25*10^3$ / $6.022*10^{23}$ = 3.90	$1.71\pm0.03*10^{-4}$	$4.38*10^{-5}$
23 DCM OF	$10^3*3.473*10^{15}*(1-10^{-1.09*1.8*0.1})*3.88*10^3$ / $6.022*10^{23}$ = $8.06*10^{-3}$	$3.76\pm0.73*10^{-4}$	$4.67*10^{-2}$
23 DCM CF	$10^3*7.954*10^{17}*(1-10^{-3.88*1.8*0.01})*3.88*10^3$ / $6.022*10^{23}$ = $7.63*10^{-1}$	$2.10\pm0.30*10^{-4}$	$2.75*10^{-4}$
23 Toluene OF	$10^3*3.473*10^{15}*(1-10^{-1.13*0.9*0.1})*5.97*10^3$ / $6.022*10^{23}$ = $7.19*10^{-3}$	$6.85\pm1.18*10^{-4}$	
23 Toluene CF	$10^3*7.954*10^{17}*(1-10^{-5.97*0.9*0.01})*5.97*10^3$ / $6.022*10^{23}$ = $9.18*10^{-1}$	$8.84\pm1.31*10^{-5}$	$9.63*10^{-5}$
23 MTBE OF	$10^3*3.473*10^{15}*(1-10^{-1.16*1.8*0.1})*1.11*10^4$ / $6.022*10^{23}$ = $6.40*10^{-2}$	$1.28\pm0.01*10^{-3}$	$2.00*10^{-2}$
23 MTBE CF	$10^3*7.954*10^{17}*(1-10^{-1.11*1.8*0.1})*1.11*10^4$ / $6.022*10^{23}$ = 7.17	$2.39\pm0.01*10^{-4}$	$3.33*10^{-5}$

5.3.1.2 Fluorescence Quantum yields

DTE(OMe)-BODIPY (20)

solvent	n	I (conc)	OD	$Q_R \frac{I}{I_R}\frac{OD_R}{OD}\frac{n^2}{n_R^2}$	Q	ΔQ
MeCN OF	1.3442			$0.95 * \frac{1.01*10^5}{5.14*10^6}\frac{1.807}{1.807}$	1.87*10^{-2}	-
CF				$0.95 * \frac{7.10*10^4}{5.14*10^6}\frac{1.807}{1.807}$	1.31*10^{-2}	0.70
MeOH OF	1.3288	163685 (1.8E-5)	0.522	$0.95 * \frac{3.14*10^5}{1.30*10^9}\frac{1.766}{1.807}$	2.24*10^{-4}	-
CF		55041 (1.8E-5)	0.5454	$0.95 * \frac{1.01*10^5}{1.30*10^9}\frac{1.766}{1.807}$	7.21*10^{-5}	0.32
EtOAc OF	1.3723	357513 (1.8E-5)	0.9234	$0.95 * \frac{3.87*10^5}{4.08*10^7}\frac{1.883}{1.807}$	9.39*10^{-3}	-
CF		158546 (1.8E-5)	0.9432	$0.95 * \frac{1.68*10^5}{4.08*10^7}\frac{1.883}{1.807}$	4.08*10^{-3}	0.43
Hexane OF	1.3749	49011	0.1566	$0.95 * \frac{3.13*10^5}{4.08*10^7}\frac{1.890}{1.807}$	7.62*10^{-3}	-
CF		27779	0.1243	$0.95 * \frac{2.23*10^5}{1.30*10^9}\frac{1.890}{1.807}$	1.70*10^{-4}	0.022
DCM OF	1.4242	417304 (1.8E-5)	0.9306	$0.95 * \frac{4.48*10^5}{4.08*10^7}\frac{2.028}{1.807}$	1.17*10^{-2}	-

BTD-DTE(OMe) (23)

solvent	n	I (conc)	OD	$Q_R \frac{I}{I_R}\frac{OD_R}{OD}\frac{n^2}{n_R^2}$	Q	ΔQ
MeCN OF	1.3442	14975 (9E-6)	0.0901	$0.95 * \frac{1.66*10^5}{1.71*10^{10}}\frac{1.807}{1.807}$	9.22*10^{-6}	
CF		228530 (9E-6)	0.1445	$0.95 * \frac{1.58*10^6}{1.71*10^{10}}\frac{1.807}{1.807}$	8.78*10^{-5}	9.52
MeOH OF	1.3288	90231 (1.8E-5)	0.352	$0.95 * \frac{2.56*10^5}{1.30*10^9} * \frac{1.766}{1.807}$	1.82*10^{-4}	-
CF		122603 (1.8E-5)	0.419	$0.95 * \frac{2.93*10^5}{1.30*10^9} * \frac{1.766}{1.807}$	2.09*10^{-4}	1.15
EtOAc OF	1.3723	699470 (9E-6)	0.143	$1.0 * \frac{4.89*10^6}{1.36*10^7}\frac{1.883}{1.766}$	0.38	-
CF		143685 (9E-6)	0.174	$0.95 * \frac{8.25*10^5}{1.30*10^9}\frac{1.883}{1.807}$	6.28*10^{-4}	0.0017
Toluene OF	1.4961	753304 (1to1)	0.079	$0.95 * \frac{9.54*10^6}{1.30*10^9} * \frac{2.238}{1.807}$	8.63*10^{-3}	
CF		65191 (1)	0.203	$0.95 * \frac{3.21*10^5}{1.30*10^9} * \frac{2.238}{1.807}$	2.91*10^{-4}	0.034

Dioxane OF	1.4224	33600 (9E-6)	0.163	$1.0 * \frac{2.06 * 10^5}{2.94 * 10^5} * \frac{2.023}{1.766}$	0.80	-
CF		8845 (9E-6)	0.209	$0.95 * \frac{4.23 * 10^4}{4.08 * 10^7} * \frac{2.023}{1.807}$	1.10*10^{-3}	0.0014
MTBE OF	1.3664	64519 (1.8E-5)	0.395	$1.0 * \frac{1.62 * 10^5}{2.94 * 10^5} * \frac{1.867}{1.766}$	0.58	-
CF		12289 (1.8E-5)	0.486	$0.95 * \frac{2.53 * 10^4}{4.08 * 10^7} * \frac{1.867}{1.807}$	6.09*10^{-4}	0.0011
DMSO OF	1.4790	10754 (1.8E-5)	0.344	$0.95 * \frac{3.13 * 10^4}{1.30 * 10^9} * \frac{2.187}{1.807}$	2.77*10^{-5}	-
CF		252988 (9E-6)	0.216	$0.95 * \frac{1.17 * 10^6}{1.30 * 10^9} * \frac{2.187}{1.807}$	1.03*10^{-3}	37.2
DCM OF	1.4242	9343 (9E-6)	0.137	$1.0 * \frac{6.82 * 10^4}{2.94 * 10^5} * \frac{2.028}{1.766}$	0.27	-
CF		16128 (9E-6)	0.167	$0.95 * \frac{9.66 * 10^4}{4.08 * 10^7} * \frac{2.028}{1.807}$	2.52*10^{-3}	0.009

BODIPY 62 and 22

solvent	n	I (conc)	OD	$\boldsymbol{Q_R \frac{I}{I_R} \frac{OD_R}{OD} \frac{n^2}{n_R^2}}$	Q
62 in MeCN	1.3442	20441	1.31	$0.95 * \frac{1.56 * 10^4}{4.08 * 10^7} \frac{1.807}{1.807}$	3.63*10^{-4}
22 in MeCN	1.3442	209961	0.23	$0.95 * \frac{9.13 * 10^5}{4.08 * 10^7} * \frac{1.807}{1.807}$	2.13*10^{-2}

6 Literature

[1] H. Dürr, *Angew. Chem.* **2004**, *116*, 3404.

[2] Y. Hirshberg, *Hebd. Seances Acad. Sci* **1950**, *203*.

[3] M. Irie, W. Schnabel, *Eur. Polym. J.* **1982**, *18*, 15.

[4] M. Irie, M. Mohri, *J. Org. Chem.* **1988**, *53*, 803.

[5] M. Morimoto, Y. Takagi, K. Hioki, T. Nagasaka, H. Sotome, S. Ito, H. Miyasaka, M. Irie, *Dyes Pigment.* **2018**, *153*, 144.

[6] M. Irie, T. Fukaminato, K. Matsuda, S. Kobatake, *Chem. Rev.* **2014**, *114*, 12174.

[7] H. Jean-Ruel, R. R. Cooney, M. Gao, C. Lu, M. A. Kochman, C. A. Morrison, R. J. D. Miller, *J. Phys. Chem. A* **2011**, *115*, 13158.

[8] Y. Tsuboi, R. Shimizu, T. Shoji, N. Kitamura, *J. Am. Chem. Soc.* **2009**, *131*, 12623.

[9] J. Finden, T. K. Kunz, N. R. Branda, M. O. Wolf, *Adv. Mater.* **2008**, *20*, 1998.

[10] S. Nakamura, S. Yokojima, K. Uchida, T. Tsujioka, A. Goldberg, A. Murakami, K. Shinoda, M. Mikami, T. Kobayashi, S. Kobatake et al., *J. Photoch. Photobio. A* **2008**, *200*, 10.

[11] S. Kobatake, Y. Matsumoto, M. Irie, *Angew. Chem.* **2005**, *117*, 2186.

[12] W.-L. Wang, X.-Y. Chen, Y. Gao, L.-X. Gao, L. Sheng, J. Zhu, L. Xu, Z.-Z. Ding, C. Zhang, J.-Y. Li et al., *Bioorg. Med. Chem. Lett.* **2017**, *27*, 5154.

[13] D. Wutz, C. Falenczyk, N. Kuzmanovic, B. König, *RSC Adv.* **2015**, *5*, 18075.

[14] T. Yamaguchi, K. Uchida, M. Irie, *J. Am. Chem. Soc.* **1997**, *119*, 6066.

[15] A. G. Lvov, A. M. Kavun, V. V. Kachala, Y. V. Nelyubina, A. V. Metelitsa, V. Z. Shirinian, *J. Org. Chem.* **2017**, *82*, 1477.

[16] T. Koshido, T. Kawai, K. Yoshino, *J. Phys. Chem.* **1995**, *99*, 6110.

[17] W. R. Browne, J. J. de Jong, T. Kudernac, M. Walko, L. N. Lucas, K. Uchida, J. H. van Esch, B. L. Feringa, *Chemistry* **2005**, *11*, 6430.

[18] H. Logtenberg, W. R. Browne, *Org. Biomol. Chem.* **2013**, *11*, 233.

[19] M. Boggio-Pasqua, M. Ravaglia, M. J. Bearpark, M. Garavelli, M. A. Robb, *J. Phys. Chem. A* **2003**, *107*, 11139.

[20] G. A. Worth, L. S. Cederbaum, *Annu. Rev. Phys. Chem.* **2004**, *55*, 127.

[21] L. S. Cederbaum, W. Domcke, H. Köppel, W. von Niessen, *Chem. Phys.* **1977**, *26*, 169.

[22] M. Takeshita, M. Yamada, N. Kato, M. Irie, *J. Chem. Soc. Perk. T. 2* **2000**, 619.

[23] M. Irie, K. Sakemura, M. Okinaka, K. Uchida, *J. Org. Chem.* **1995**, *60*, 8305.

[24] R. Hoffmann, R. B. Woodward, *J. Am. Chem. Soc.* **1965**, *87*, 2046.

[25] F. Nickel, M. Bernien, M. Herder, S. Wrzalek, P. Chittas, K. Kraffert, L. M. Arruda, L. Kipgen, D. Krüger, S. Hecht et al., *J. Phys. Condens. Matter.* **2017**, *29*, 374001.

[26] J. Wirth, N. Hatter, R. Drost, T. R. Umbach, S. Barja, M. Zastrow, K. Rück-Braun, J. I. Pascual, P. Saalfrank, K. J. Franke, *J. Phys. Chem. C* **2015**, *119*, 4874.

[27] K. Morimitsu, S. Kobatake, M. Irie, *Mol. Cryst. Liq. Cryst.* **2005**, *431*, 451.

[28] K. Morimitsu, S. Kobatake, S. Nakamura, M. Irie, *Chem. Lett.* **2003**, *32*, 858.

[29] A. de Meijere, L. Zhao, V. N. Belov, M. Bossi, M. Noltemeyer, S. W. Hell, *Chemistry* **2007**, *13*, 2503.

[30] Y. Ishibashi, K. Okuno, C. Ota, T. Umesato, T. Katayama, M. Murakami, S. Kobatake, M. Irie, H. Miyasaka, *Photochem. Photobiol. Sci.* **2010**, *9*, 172.

[31] T. Fukaminato, T. Sasaki, T. Kawai, N. Tamai, M. Irie, *J. Am. Chem. Soc.* **2004**, *126*, 14843.

[32] T. Fukaminato, T. Umemoto, Y. Iwata, S. Yokojima, M. Yoneyama, S. Nakamura, M. Irie, *J. Am. Chem. Soc.* **2007**, *129*, 5932.

[33] A. Treibs, F.-H. Kreuzer, *Liebigs Ann. Chem.* **1968**, *718*, 208.

[34] E. A. Jares-Erijman, T. M. Jovin, *Nat. Biotechnol.* **2003**, *21*, 1387.

[35] A. Schmitt, B. Hinkeldey, M. Wild, G. Jung, *J. Fluoresc.* **2009**, *19*, 755.

[36] A. Loudet, K. Burgess, *Chem. Rev.* **2007**, *107*, 4891.

[37] J. Killoran, L. Allen, J. F. Gallagher, W. M. Gallagher, D. F. O'Shea, *Chem. Commun.* **2002**, *24*, 1862.

[38] S. O. McDonnell, D. F. O'Shea, *Org. Lett.* **2006**, *8*, 3493.

[39] C. Slavov, N. Bellakbil, J. Wahl, K. Mayer, K. Ruck-Braun, I. Burghardt, J. Wachtveitl, M. Braun, *Phys. Chem. Chem. Phys.* **2015**, *17*, 14045.

[40] F. Schweighofer, L. Dworak, M. Braun, M. Zastrow, J. Wahl, I. Burghardt, K. Ruck-Braun, J. Wachtveitl, *Sci. Rep.* **2015**, *5*, 9368.

[41] F. Schweighöfer, I. Yüce, L. Dworak, P. Guo, M. Zastrow, K. Mayer, C. Barta, D. Liebmann, N. Ziebart, K. Rück-Braun et al., *J. Phys.: Condens. Matter* **2018**, *30*, 54001.

[42] B. A. D. Neto, A. A. M. Lapis, E. N. da Silva Júnior, J. Dupont, *Eur. J. Org. Chem.* **2013**, *2013*, 228.

[43] Y. Wu, W.-H. Zhu, S. M. Zakeeruddin, M. Grätzel, *ACS Appl. Mater. Interfaces* **2015**, *7*, 9307.

[44] D.-H. Roh, K. M. Kim, J. S. Nam, U.-Y. Kim, B.-M. Kim, J. S. Kim, T.-H. Kwon, *J. Phys. Chem. C* **2016**, *120*, 24655.

[45] P. Bouguer, *J. Röntgen Soc.* **1922**, *18*, 93.

[46] M. Hesse, H. Meier, B. Zeeh, *Spektroskopische Methoden in der organischen Chemie*. *102 Tabellen*, Thieme, Stuttgart, **2005**.

[47] C. W. Wan, A. Burghart, J. Chen, F. Bergstrom, L. B. Johansson, M. F. Wolford, T. G. Kim, M. R. Topp, R. M. Hochstrasser, K. Burgess, *Chemistry* **2003**, *9*, 4430.

[48] J. Zheng in *Biomedical Applications of Biophysics* (Ed.: T. Jue), Humana Press, Totowa, NJ, **2010**, pp. 119–136.

[49] J. R. Lakowicz, *Principles of Fluorescence Spectroscopy*, Springer US, Boston, MA, **2006**.

[50] L. Dworak, M. Zastrow, G. Zeyat, K. Ruck-Braun, J. Wachtveitl, *J. Phys. Condens. Matter.* **2012**, *24*, 394007.

[51] L. Dworak, A. J. Reuss, M. Zastrow, K. Ruck-Braun, J. Wachtveitl, *Nanoscale* **2014**, *6*, 14200.

[52] M. A. Fox, *Photochem Photobiol* **1990**, *52*, 617.

[53] W. Rettig, *Angew. Chem.* **1986**, *98*, 969.

[54] Z. R. Grabowski, K. Rotkiewicz, W. Rettig, *Chem. Rev.* **2003**, *103*, 3899.

[55] S. Sasaki, G. P. C. Drummen, G.-i. Konishi, *J. Mater. Chem. C* **2016**, *4*, 2731.

[56] F. B. Dias, S. Pollock, G. Hedley, L.-O. Pålsson, A. Monkman, I. I. Perepichka, I. F. Perepichka, M. Tavasli, M. R. Bryce, *J. Phys. Chem. B* **2006**, *110*, 19329.

[57] A. Pathak, K. R. Justin Thomas, M. Singh, J.-H. Jou, *J. Org. Chem.* **2017**, *82*, 11512.

[58] T. Higashino, Y. Fujimori, K. Sugiura, Y. Tsuji, S. Ito, H. Imahori, *Angew. Chem. Int. Ed. Engl.* **2015**, *54*, 9052.

[59] M. Irie, T. Lifka, K. Uchida, S. Kobatake, Y. Shindo, *Chem. Commun.* **1999**, 747.

[60] G. Consiglio, D. Spinelli, S. Gronowitz, A.-B. Hörnfeldt, B. Maltesson, R. Noto, *J. Chem. Soc., Perkin Trans. 2* **1982**, 625.

[61] H. L. Aalten, G. van Koten, D. M. Grove, T. Kuilman, O. G. Piekstra, L. A. Hulshof, R. A. Sheldon, *Tetrahedron* **1989**, *45*, 5565.

[62] S. Sivakamasundari, R. Ganesan, *Int. J. Chem. Kinet.* **1980**, *12*, 837.

[63] K. Orito, T. Hatakeyama, M. Takeo, H. Suginome, *Synthesis* **1995**, *1995*, 1273.

[64] A. Lembo, P. Tagliatesta, D. M. Guldi, M. Wielopolski, M. Nuccetelli, *J. Phys. Chem. A* **2009**, *113*, 1779.

[65] R. P. Hsung, C. E. D. Chidsey, L. R. Sita, *Organometallics* **1995**, *14*, 4808.

[66] K. Sonogashira, Y. Tohda, N. Hagihara, *Tetrahedron Lett.* **1975**, *16*, 4467.

[67] R. Bruckner, M. Harmata, *Organic Mechanisms*, Springer Berlin Heidelberg, Berlin, Heidelberg, **2010**.

[68] R. Chinchilla, C. Najera, *Chem Rev* **2007**, *107*, 874.

[69] M. Sekiya, K. Umezawa, A. Sato, D. Citterio, K. Suzuki, *Chem. Commun. (Camb)* **2009**, 3047.

[70] Y. Huang, Y. Zhang, Y. Yuan, W. Cao, *Tetrahedron* **2015**, *71*, 2124.

[71] A. Mariani, A. Bartoli, M. Atwal, K. C. Lee, C. A. Austin, R. Rodriguez, *J. Med. Chem.* **2015**, *58*, 4851.

[72] S. R. Sritharan, B. A. Hussein, D. D. Machin, M. A. El-Aooiti, J. A. Adjei, J. K. Singh, J. T. H. Pau, J. S. Dhindsa, A. J. Lough, B. D. Koivisto, *RSC Adv.* **2017**, *7*, 8922.

[73] N. Miyaura, A. Suzuki, *J. Chem. Soc., Chem. Commun.* **1979**, 866.

[74] S. S. Gujral, S. Khatri, P. Riyal, *Indo glob. j. pharm.* **2012**, *2*, 351.

[75] M. X. Yan, P. Shen, W. Zhang, J. D. Gong, C. Y. Yang, *Appl. Mech. Mater.* **2014**, *488-489*, 265.

[76] F. A. Carey, R. J. Sundberg, *Advanced organic chemistry, part A: Structure and mechanisms*, Springer, New York, NY, **2008**.

[77] R. Ghosh, D. K. Palit, *J. Phys. Chem. A* **2015**, *119*, 11128.

[78] H. Beecken, *Chem. Ber.* **1967**, *100*, 2170.

[79] K. Pilgram, M. Zupan, R. Skiles, *J. Heterocyclic. Chem.* **1970**, *7*, 629.

[80] L. Zheng, Q. Cao, J. Wang, Z. Chai, G. Cai, Z. Ma, H. Han, Q. Li, Z. Li, H. Chen, *ACS Omega* **2017**, *2*, 7048.

[81] A. Seegerer, P. Nitschke, R. M. Gschwind, *Angew. Chem. Int. Ed. Engl.* **2018**, *57*, 7493.

[82] C. Feldmeier, H. Bartling, E. Riedle, R. M. Gschwind, *J. Magn. Reson.* **2013**, *232*, 39.

[83] K. Stranius, K. Börjesson, *Sci. Rep.* **2017**, *7*, 41145.

[84] E. Kim, M. Kim, K. Kim, *Tetrahedron* **2006**, *62*, 6814.

[85] Cunha Dias de Rezende, Lucas, M. Menezes Vaidergorn, J. C. Biazzotto Moraes, F. da Silva Emery, *J. Fluoresc.* **2014**, *24*, 257.

[86] M. Taniguchi, J. S. Lindsey, *Photochem. Photobiol. (Photochemistry and Photobiology)* **2018**, *94*, 290.

[87] T. K. Khan, P. Sheokand, N. Agarwal, *Eur. J. Org. Chem.* **2014**, *2014*, 1416.

[88] B. Wang, H. Pan, J. Jia, Y.-Q. Ge, W.-Q. Cai, J.-W. Wang, C.-H. Zhao, *Tetrahedron* **2014**, *70*, 5488.

[89] B. R. Henry, J. D. Morrison, *J. Mol. Spectrosc.* **1975**, *55*, 311.

[90] A. Pazini, L. Maqueira, R. Stieler, R. Q. Aucélio, J. Limberger, *J. Mol. Struct.* **2017**, *1131*, 181.

[91] T. E. A. Frizon, J. C. Valdivia Martínez, J. L. Westrup, R. d. C. Duarte, E. Zapp, K. G. Domiciano, F. S. Rodembusch, A. G. Dal-Bó, *Dyes Pigments* **2016**, *135*, 26.

[92] T. Tachikawa, N. Wang, S. Yamashita, S.-C. Cui, T. Majima, *Angew Chem Int Ed Engl* **2010**, *49*, 8593.

[93] J.-B. Wang, X.-Q. Fang, X. Pan, S.-Y. Dai, Q.-H. Song, *Chem. Asian J.* **2012**, *7*, 696.

[94] C. A. Parker, W. T. Rees, *The Analyst* **1960**, *85*, 587.

[95] A. M. Brouwer, *Pure Appl. Chem.* **2011**, *83*, 2213.

[96] C. Würth, M. Grabolle, J. Pauli, M. Spieles, U. Resch-Genger, *Nat. Protoc.* **2013**, *8*, 1535.

[97] S. Rihn, M. Erdem, A. de Nicola, P. Retailleau, R. Ziessel, *Org. Lett.* **2011**, *13*, 1916.

[98] T.-B. Ren, W. Xu, W. Zhang, X.-X. Zhang, Z.-Y. Wang, Z. Xiang, L. Yuan, X.-B. Zhang, *J. Am. Chem. Soc.* **2018**, *140*, 7716.

[99] B. A. Neto, A. A. Lapis, F. S. Mancilha, I. B. Vasconcelos, C. Thum, L. A. Basso, D. S. Santos, J. Dupont, *Org. Lett.* **2007**, *9*, 4001.

[100] M. A. Rauf, J. P. Graham, S. B. Bukallah, M. A. S. Al-Saedi, *Spectrochim. Acta A Mol. Biomol. Spectrosc.* **2009**, *72*, 133.

[101] A. Marini, A. Muñoz-Losa, A. Biancardi, B. Mennucci, *J. Phys. Chem. B* **2010**, *114*, 17128.

[102] H. Miyasaka, T. Nobuto, M. Murakami, A. Itaya, N. Tamai, M. Irie, *J. Phys. Chem. A* **2002**, *106*, 8096.

[103] O. A. Kucherak, L. Richert, Y. Mély, A. S. Klymchenko, *Phys. Chem. Chem. Phys.* **2012**, *14*, 2292.

[104] D. C. Harris, C. A. Lucy, *Quantitative chemical analysis*, WH Freeman, New York, **2016**.

[105] J.-L. M. Abboud, R. Notari, *Pure Appl. Chem.* **1999**, *71*, 645.

[106] C. Reichardt, *Chem. Rev.* **1994**, *94*, 2319.

[107] N. Ziebart, F. Schroeder, K. Rueck-Braun, *ChemPhotoChem* **2019**, accepted, DOI: 10.1002/cptc.201800230.

[108] I. Hamdi, G. Buntinx, A. Perrier, O. Devos, N. Jaïdane, S. Delbaere, A. K. Tiwari, J. Dubois, M. Takeshita, Y. Wada et al., *Phys. Chem. Chem. Phys.* **2016**, *18*, 28091.

[109] N. Ziebart, P. Schroeer, K. Rueck-Braun, *Tetrahedron* **2018**, *74*, 5561.

[110] P. R. Hania, A. Pugzlys, L. N. Lucas, J. J. D. de Jong, B. L. Feringa, J. H. van Esch, H. T. Jonkman, K. Duppen, *J. Phys. Chem. A* **2005**, *109*, 9437.

[111] I. Ata, D. Popovic, M. Lindén, A. Mishra, P. Bäuerle, *Org. Chem. Front.* **2017**, *4*, 755.

[112] M. Irie, K. Sayo, *J. Phys. Chem.* **1992**, *96*, 7671.

[113] L. Gai, H. Lu, B. Zou, G. Lai, Z. Shen, Z. Li, *RSC Adv.* **2012**, *2*, 8840.

[114] D. Braun, W. Rettig, S. Delmond, J.-F. Létard, R. Lapouyade, *J. Phys. Chem. A* **1997**, *101*, 6836.

[115] B. A. DaSilveira Neto, A. S.'A. Lopes, G. Ebeling, R. S. Gonçalves, V. E. U. Costa, F. H. Quina, J. Dupont, *Tetrahedron* **2005**, *61*, 10975.

[116] M. A. Keegstra, T. H. A. Peters, L. Brandsma, *Tetrahedron* **1992**, *48*, 3633.